Exploring interactions between anions and kinetically stable lanthanide complexes in aqueous solution

Jack David Routledge

University College

University of Oxford

A thesis submitted in fulfilment of the requirements for

the degree of *Doctor of Philosophy*

Hilary Term 2016

Abstract

‘Exploring interactions between anions and kinetically stable lanthanide complexes in aqueous solution’
Jack Routledge, University College, University of Oxford.
DPhil Thesis, Hilary term, 2016.

This work utilises the interactions between lanthanide complexes and anions in solution to explore the nature of coordination chemistry in the *f*-elements, and to define fundamental behaviour in paramagnetic complexes, as well as investigating the factors responsible for ensuring high lanthanide luminescence quantum yields.
Chapter one describes characteristic lanthanide properties with a focus on luminescence and the current understanding of lanthanide complexes. Illustrating the response of luminescent lanthanide complexes to a range of analytes in aqueous solution.
Chapter two explores the factors affecting luminescence quantum yield in arylacylDO3A complexes as well studying the pH behaviour of these species, showing that the whole energy transfer cascade involved in sensitisation of lanthanide luminescence must be considered when optimising the properties of lanthanide complexes.
Chapter three describes the effect of fluoride binding in lanthanide tetra-amide complexes appended with fluorinated benzyl groups on the lanthanide crystal field, demonstrating that the effect of a strong axial donor on the overall ligand field can determine the nature of the magnetic anisotropy at the lanthanide centre. This in turn determines both the optical spectra and the NMR spectra of the complexes. The results obtained illustrate that the whole structure of the complex (and not just the donor set) need to be considered when defining the behaviour of the lanthanide complex.
Chapter four investigates the interaction between fluoride and lanthanide complexes of the Lehn cryptand. In this case, the relatively symmetric donor set associated with the cryptand, combined with exchange between isomers, gives rise to small observed anisotropies in the absence of fluoride that are dramatically enhanced by fluoride binding. A range of fluoride responsive behaviour has been identified.
Chapter five describes the synthesis and study of a group of halogenated phenacylDO3A lanthanide complexes. It is shown how such complexes respond to changes in cyanide concentration but are essentially inert towards fluoride as a consequence of the reduced residual charge on the lanthanide centre. The interaction with cyanide is assigned to the formation of a cyanohydrin which is assisted by the proximate lanthanide ion, which acts as a Lewis acid.
Chapter six draws together the work described in earlier chapters.
Chapter seven provides experimental procedures along with characterisation data for the compounds studied.

Table of contents

Contents

Abstract i

Table of contents ii

Publications vi

Acknowledgments vii

Abbreviations ix

1 Introduction 1

1.1 General properties of lanthanide ions 1

1.2 The macrocyclic effect and complex stability 2

1.2.1 Thermodynamic stability 3

1.2.2 Kinetic stability 6

1.3 Ligand types 9

1.4 General lanthanide photophysical properties 11

1.4.1 Eu(III), Tb(III) and Yb(III) luminescence 14

1.4.2 Sensitised lanthanide luminescence 16

1.4.3 Choice of sensitiser 18

1.4.4 Luminescence quenching 23

1.4.5 Energy transfer mechanisms 26

1.5 Sensing of analytes 27

1.6 Lanthanide NMR....32
1.7 Isomers of Ln(III) complexes....36
1.8 Project aims....39
1.9 References....40
2 Achieving high luminescence quantum yields with arylacylDO3A complexes....43
2.1 Introduction....43
2.2 Synthesis and characterisation....48
2.2.1 NMR characterisation....50
2.2.2 Photophysical properties....52
2.2.3 pH behaviour of complexes....60
2.3 Conclusions....67
2.4 References....69
3 Studying the effect of fluoride on lanthanide tetra-amide complexes....70
3.1 Introduction....70
3.2 Synthesis and characterisation....73
3.3 NMR studies of lanthanide complexes....74
3.4 Luminescence....85
3.5 Fluoride binding....87
3.6 Rates of exchange....89
3.7 Conclusions....92

3.8 References....93

4 Investigating the interaction of fluoride with lanthanide complexes of Lehn's cryptand....95

4.1 Introduction....95

4.2 Synthesis and characterisation....98

4.3 NMR studies of lanthanide complexes....99

4.4 Photophysical properties....104

4.5 Fluoride binding....106

4.6 Conclusions....109

4.6 References....110

5 Synthesis and study of halogenated phenacylDO3A complexes....111

5.1 Introduction....111

5.2 Synthesis and characterisation....113

5.3 Photophysical properties....117

5.4 Attempted synthesis of a tri-amide analogue of Ln.5.14....124

5.5 Fluoride binding....127

5.6 Cyanide binding studies....129

5.7 Conclusions....132

5.8 References....133

6 Conclusions and future perspectives....134

7 Experimental.....138

7.1 General procedures.....138

7.2 X-ray crystallography.....140

7.3 Titration methodology.....141

7.4 Dynafit.....142

7.7 Synthesis.....146

7.14 References.....183

Publications

1. J. D. Routledge, M. W. Jones, S. Faulkner and M. Tropiano, *Inorg. Chem.*, 2015, **54**, 3337-3345.

2. O. A. Blackburn, J. D. Routledge, L. B. Jennings, N. H. Rees, A. M. Kenwright, P. D. Beer and S. Faulkner, *Dalton Trans*., 2016, **45**, 3070-3077.

Acknowledgments

Firstly, I would like to thank my supervisor Steve Faulkner for taking me into his group and giving me the opportunity to experience Oxford teaching and lab demonstrating. Thank you for being a constant source of optimism, joy and most of all knowledge. You are a great mentor.

I am very grateful to all the staff at the Chemistry Research Laboratory for the support and analytical services provided. In particular, I would like to thank Dr. Nick Rees for his support in all things NMR. I would also like to thank the mass spectrometry service for recording accurate mass spectra.

I have met some great people over my time in Oxford and I would like to thank past and present members of the group for all of their help and encouragement. I would not be the chemist I am today without Prof Stephen Faulkner, Dr. Manuel Tropiano, Dr. Michael Jones and Dr. Octavia Blackburn.

I would like to thank Manuel for teaching me all things luminescence and the ways of the lanthanides. You have been a great friend over my time in Oxford, I have always cherished my time spent with you, whether in be in lab, the pub or attempting to play squash and cricket. Thank you for being you and for teaching me some Italian ways and sayings.

I would like to thank Mike for trying to teach me the ways of a crystallographer and for providing me with endless synthetic tips. Meeting you has been one of the best things about coming to Oxford, you have always been there for me whatever the situation and I would like to thank you for introducing me to foraging, Squash, cricket and proper bike maintenance. Your range of chat is exquisite and you have provided me

with so much comedy gold over the years as well as providing a saying for most situations; ‘low yield is better than no yield’ and ‘T in B’ are my particular favorites.

I would like to thank Octavia for passing on her extensive knowledge of all things NMR and fluoride, your help has been invaluable. You are a fountain of knowledge; the group would be lost without you. When you and Manuel took me to the KA the first time we met and you had faggots I knew I would enjoy my time in the group. You have been a great friend and I’m glad that I have someone to talk to about northern life.

Outside the lab, I would like to thank all of the friends I have made. In particular, I would like to thank Ieuan, Matt and Nate for being there for me in my times of need and boredom as well as being great friends.

Finally, I would like to thank my family for always being there for me and providing me with lots of support, encouragement and happiness. In particular, I want to thank my mum and dad for the endless love and support they have given me, you are so proud of everything I have achieved and are always there for me. If I could be a fraction of the people you are then I will be happy.

Abbreviations

a.u.	arbitrary units
BET	back energy transfer
Bn	benzyl
cbz	benzylchloroformate
CT	charge transfer
Cyclen	1,4,7,10-tetrazacyclododecane
d	days
DCM	dichloromethane
DMF	dimethylformamide
DMSO	dimethylsulfoxide
DO2A	1,4,7,10-Tetraazacyclododecane-1,7-diacetic acid
DO3A	1,4,7,10-Tetraazacyclododecane-1,4,7-triacetic acid
DOTA	1,4,7,10-Tetraazacyclododecane-1,4,7,10-tetraacetic acid
DOTAM	1,4,7,10-Tetraazacyclododecane-1,4,7,10-tetraacetamide
DTPA	diethylenetriaminepentaacetic acid
EDTA	ethylenediaminetetraacetic acid
EI	electron ionisation
ES	electrospray
eT	electron transfer
ET	energy transfer
EtOAc	ethyl acetate
EtOH	ethanol

EXSY	exchange spectroscopy
FI	flame ionisation
h	hours
HPLC	high performance liquid chromatography
HRMS	high resolution mass spectrometry
IC	internal conversion
ILCT	intra-ligand charge transfer
IR	infrared
ISC	inter-system crossing
LIS	lanthanide induced shift
LMCT	ligand to metal charge transfer
Ln	lanthanide
LRMS	low resolution mass spectrometry
m	minutes
MALDI	matrix-assisted laser desorption ionisation
Me	methyl
MeCN	acetonitrile
MeOH	methanol
MLCT	metal to ligand charge transfer
MRI	magnetic resonance imaging
MWCO	molecular weight cut-off
NEt_3	triethylamine
NHE	normal hydrogen electrode

NIR	near infrared
NMR	nuclear magnetic resonance
NOTA	1,4,7-triazacyclononane-1,4,7-triacetic acid
ORTEP	oak ridge thermal ellipsoid plot
OTf	trifluoromethansulfonate (triflate)
PeT	photoelectron transfer
Ph	phenyl
RT	room temperature
S	singlet state
SAP	square anti-prism
T	triplet state
TETA	1,4,8,11-tetraazacyclotetradecane-1,4,8,11-tetraacetic acid
TFA	trifluoroacetic acid
THF	tetrahydrofuran
TLC	thin layer chromatography
TOF	time of flight
TSAP	twisted square anti-prism
UV	ultraviolet
UV-Vis	ultraviolet-visible

1 Introduction

In this thesis, the interactions between lanthanide complexes and anions are used to explore the nature of the coordination chemistry of the *f*-elements, with a particular emphasis on the photophysical and spectroscopic properties of these systems. The results outlined later in this work show how relatively small changes in local environment (and particularly in the crystal field) can have dramatic effects. This chapter outlines the current understanding of lanthanide behaviour using examples to illustrate key concepts.

1.1 General properties of lanthanide ions

The most common oxidation state of lanthanide ions is 3+ with the notable exceptions of Eu and Yb which can be found in the 2+ oxidation state (with standard electrode potentials of -0.35 and -1.05 V vs. NHE respectively)[1] whilst Ce and Tb can be found in the 4+ oxidation state. Lanthanide ions are hard Lewis acids causing them to preferentially bind to hard Lewis bases such as N, O and F. Trivalent lanthanide ions have similar chemical properties and this is derived from the nature of the electronic configuration of these ions. The 4*f* orbitals of trivalent lanthanide ions are partially filled apart from lanthanum ($4f^0$) and lutetium ($4f^{14}$); these orbitals penetrate the atomic core more than the completely filled 5*s* and 5*p* orbitals, resulting in the shielding of the 4*f* orbitals. This results in negligible overlap of the 4*f* orbitals with ligand orbitals causing the interaction to be essentially electrostatic in nature giving rise to small crystal field contributions [ca. 10^2 cm^{-1}]; crystal field splitting is generally considered to be small relative to spin orbit coupling. Lanthanide complexes therefore typically have a low degree of covalency and their coordination chemistry is largely

dictated by the size of the ions and electrostatics. As a result of the poor orbital overlap then multidentate ligands are required to form kinetically and thermodynamically stable species with coordination numbers usually ranging from 8 to 10 in aqueous media.

Lanthanide ions can mimic calcium coordination chemistry;[2] they possess a higher charge than calcium but they have similar atomic radii meaning that lanthanide ions have a high affinity for Ca(II) sites in biological molecules. Therefore, it is essential that highly kinetically and thermodynamically stable lanthanide species are employed for use *in vivo* to avoid free lanthanide ions being present.

1.2 The macrocyclic effect and complex stability

Thermodynamic and kinetic stabilities of lanthanide complexes are critical parameters to consider when designing ligands for lanthanide encapsulation. Lanthanide complexes are typically thermodynamically stable if there are a suitable number of hard donor atoms within the ligand backbone and if the ligand is suitably arranged for coordination to the lanthanide ion. Many chelating arms are required to decrease the lability of the lanthanide ion and to reduce the likelihood of demetallation. Multidentate ligands are far superior to mono and bidentate ligands when considering complex stability e.g. **[Ln.DTPA]$^{2-}$** complexes are ca. 20 orders of magnitude more stable than lanthanide acetate complexes.[3]

1.2.1 Thermodynamic stability

The thermodynamic stability constants of representative lanthanide complexes are shown in Table 1. 1 and the structures of the complexes discussed in this section are shown in Figure 1. 1.

Table 1. 1 Thermodynamic stability constants (Log*K*) of linear and macrocyclic polyaminocarboxylate complexes of Ln (III) ions (298 K, 0.1 M NaCl, H_2O).

Ln(III)	**EDTA[4]**	**DTPA[4]**	**DOTA[5]**	**NOTA[5]**	**TETA[6]**
La(III)	15.5	19.5	22.9	13.5	11.6
Eu(III)	17.3	22.5	23.5	13.9	14.0
Gd(III)	17.4	22.5	24.7	14.3	13.8
Tb(III)	17.9	22.7	24.2	14.5	14.8
Lu(III)	19.9	22.4	25.4	15.9	-

There is a linear increase in stability across the lanthanide series for complexes of **EDTA**, this is due to an increase in the charge density of the lanthanide centre resulting in a stronger electrostatic interaction with the ligand. **[Ln.DTPA]$^{2-}$** complexes also show an increase in stability across the lanthanide series, however the maximum stability is reached around Tb(III) and Ho(III). This is due to **DTPA** being less flexible than **EDTA** which results in **DTPA** being less capable of enveloping the smaller lanthanides at the end of the series. **DTPA** lanthanide complexes are more stable than **EDTA** complexes due to the former having a higher denticity.

DOTA complexes of lanthanides are more stable than the corresponding **[Ln.DTPA]$^{2-}$** complexes. The enhanced stability of **[Ln.DOTA]$^{-}$** complexes is largely due to entropic reasons, with the free ligand, **DOTA** being pre-organised for complexation so only a small ligand rearrangement needs to occur upon complexation, though reduced

solvation of the inner surface of the macrocycle also plays an enthalpic role.[7] This is a classic example of the macrocyclic effect.

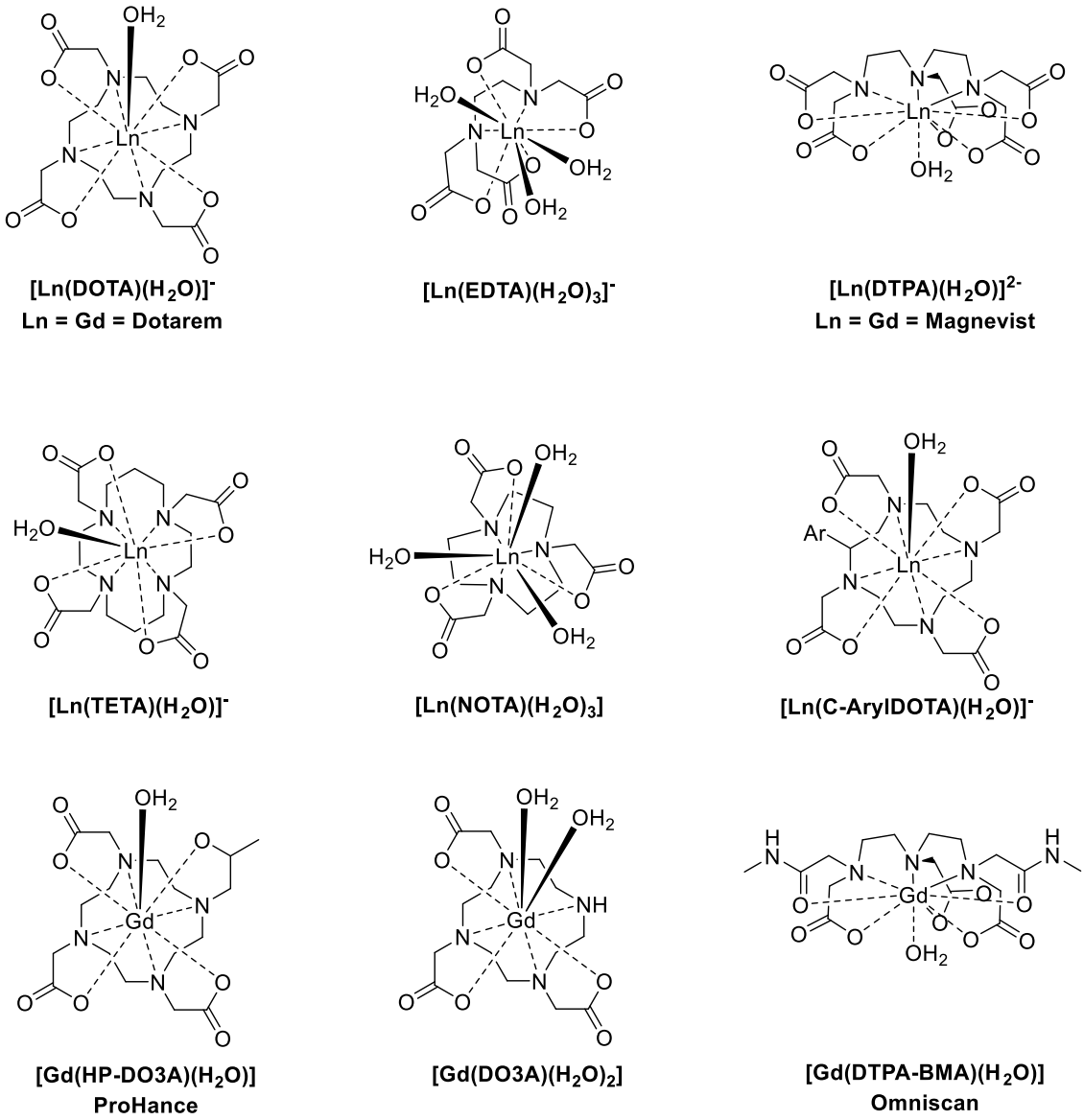


Figure 1. 1 Chemical structures of lanthanide complexes discussed in this section.

The lower stabilities of **[Ln.TETA]**$^{-}$ complexes as compared to those of **[Ln.DOTA]**$^{-}$, reflect the fact that **[Ln.TETA]**$^{-}$ complexes adopt a dodecahedral geometry which has higher repulsion energy than in the square antiprism (SAP) conformation found in **[Ln.DOTA]**$^{-}$ complexes. Also the larger chelate rings formed with the Ln(III) ion in

[Ln.TETA]$^{-}$ complexes are more sterically crowded than the smaller rings in **[Ln.DOTA]**$^{-}$ complexes.[8]

[Ln.NOTA] complexes are significantly less stable compared to the corresponding **[Ln.EDTA]**$^{-}$ complexes; this is likely due to the smaller size of the cavity in the **NOTA** ligand. The stability constants of lanthanide **NOTA** complexes are similar for the first five lanthanides (La(III)-Sm(III)) with an increase in stability for the later lanthanides as the cation size decreases.

A variety of C-aryl monosubstituted analogues of **DOTA** have been synthesised *via* iron templation (Figure 1. 1, **[Ln.C-ArylDOTA]**$^{-}$).[9] The solution behaviour of the Eu(III) and Tb(III) complexes of the phenyl substituted species are analogous to those of the corresponding **[Ln.DOTA]**$^{-}$ species with each having one bound water molecule. Upon exposure to **EDTA** a decrease in observed luminescence lifetimes in D_2O and H_2O was observed which is consistent with the decomplexation of the C-aryl species and the competitive formation of the lanthanide **EDTA** complex. This behaviour is consistent with the fact that the aryl species are less kinetically stable than their **DOTA** analogues, this implies the thermodynamic stability of the aryl species is much less than that of their **DOTA** analogues ($\beta_{ML} < 10^{10}$ compared to 10^{25} for **DOTA**). It was postulated that the lack of stability may be due to the unfavorable steric interaction between the aryl group on the macrocycle ring and the adjacent methyl protons on the ring, this interaction could prevent the complex from taking up the favourable square antiprismatic form. Also the presence of an aryl ring on the backbone may rigidify the macrocycle preventing it forming an appropriate conformation to form a stable complex.

1.2.2 Kinetic stability

The kinetic stability of Gd(III) lanthanide complexes has been extensively studied due to their use as MRI contrast agents. The rate at which the complex forms depends on many factors including the pH, temperature, concentration and the nature of the ligand. The structures of the examples discussed in this section are in Figure 1. 1. Open chain ligands such as **DTPA** form complexes with Gd(III) faster than macrocyclic ligands such as **DOTA**. Initially the Gd(III) ion is electrostatically attracted to the carboxylate groups in **DTPA**, the ligand is conformationally flexible which allows the ligand to rapidly wrap around the Gd(III) ion displacing all but one bound H_2O molecules. The **[Gd.DTPA]$^{2-}$** complex is typically formed in the ms-s range. Again the first step for macrocyclic ligands such as **DOTA** involves the Gd(III) ion being electrostatically attracted to the carboxylate groups. However the ligand is conformationally rigid so it takes longer for the Gd(III) ion to be fully encapsulated by the ligand, also macrocyclic amines tend to be more basic than open chain analogues which means that a proton within the cavity must dissociate before Gd(III) can enter. **[Gd.DOTA]$^{-}$** is typically formed within the min-hour range.[10] The rate of dissociation of Gd(III) complexes *in vivo* is arguably one of the most important factors in determining the toxicity of the compounds. The principle of microscopic reversibility states that the forward and reverse mechanism for a reaction must be identical, thus it is likely that Gd(III) will be able to dissociate from **DTPA** more quickly than from **DOTA**. Table 1. 2 shows dissociation kinetics data for a variety of Gd(III) complexes, this clearly shows that macrocyclic chelates are more kinetically stable compared to open chain analogues.

Brücher et al.[11, 12] showed that the rate of exchange of lanthanide ions has pH dependent and pH independent terms:

$$k_{obs} = k_{ind} + k_{dep}[H^+]$$

It is common that authors speed up the rate of dissociation by measuring them at low pH where the pH dependent term is dominant. From the above equation and data in Table 1. 2 it is clear that the pH independent term will be dominant a physiological pH. The pH dependent pathway will only dominate for **[Gd.DOTA]**$^-$ at pH < 2 whilst for **[Gd.HP-DO3A]** the pH dependent pathway plays an important role up until pH 6,[13] these results show that ligand pK_a significantly effects dissociation kinetics.

Table 1. 2 Dissociation kinetic data for a series of Gd(III) complexes.

Compound	**k_{ind} / s^{-1}**	**k_{dep} / $M^{-1}s^{-1}$**	**k_{obs} (pH 1)**	**$T_{1/2}$[14]**	**Ref**
[Gd.DOTA]$^-$	$<5x10^{-8}$	$5x10^{-6}$	$>3x10^{-7}$	> month	12
[Gd.DTPA]$^{2-}$	-	-	$1.2x10^{-3}$	10 min	10
[Gd.DTPA-BMA]	-	-	$>2x10^{-2}$	35 sec	10
[Gd.DO3A]	-	-	$2.3x10^{-3}$	5 min	14
[Gd.HP-DO3A]	$-7(\pm20)x10^{-10}$	$2.6x10^{-4}$	$2.6x10^{-5}$	3 hrs	12

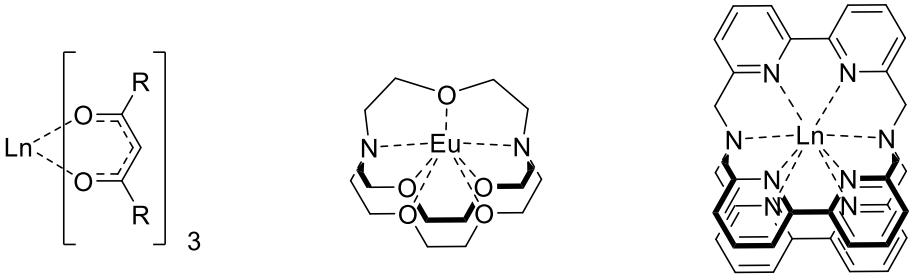
Transmetallation is important to consider when investigating the kinetic stability of lanthanide chelates, attention has been focussed on the potential of Zn(II) to displace Gd(III) from the ligand scaffold due to its relatively high concentration in serum (50 µM). For complexes of acyclic ligands such as **[Gd.DTPA]**$^{2-}$ the rate of transmetallation is directly proportional to the concentration of Zn(II) or Cu(II) which suggests that transmetallation occurs *via* direct attack of these endogenous ions on **[Gd.DTPA]**$^{2-}$.[11, 15] Transmetallation in macrocyclic complexes such a **[Gd.DOTA]**$^-$ however is independent of Zn(II) concentration, Muller et al.[16] observed no reaction of **[Gd.DOTA]**$^-$ after four

days in the presence of 2.5 mM $ZnCl_2$. Transmetallation in macrocyclic species depends on the rate of proton-assisted dissociation of the complex which is very slow at physiological pH. Brücher et al.[17] investigated the exchange reactions of Gd(III) complexes with Cu(II) in the presence of endogenous species such as citrate, carbonate and phosphate. Open chain analogues such as **[Gd.DTPA]$^{2-}$** showed dissociation kinetics that were accelerated by the presence of endogenous ions at physiological pH whilst the macrocyclic species such as **[Gd.DOTA]$^{-}$** showed no dependence on the presence of these ions.

More recently Caravan et al.[18] investigated the stability of a range of **DO3A** analogues in the presence of Zn(II). It was noted that the choice of the third pendant arm of the macrocycle (the other two are carboxylates) has a profound effect on the kinetic inertness of Gd(III) chelates. The kinetic inertness of the chelates does not necessarily correlate with the ligand coordination number and the third arm needs to coordinate strongly to the Gd(III) centre to decrease lability. It was also noted the N-alkylation of the fourth cyclen nitrogen with a bulky aromatic group significantly lowers the kinetic stability of the chelates. It was suggested that this was due to the steric strain introduced which causes the macrocycle to be a less efficient at encapsulating the Gd(III) centre. This hypothesis was supported by broad resonances being observed in the ^{1}H NMR spectra of analogous Eu(III) complexes which indicates a fluxional complex structure.

1.3 Ligand types

A wide variety of ligands have been exploited to bind to lanthanide ions, these typically are multidentate ligands with nitrogen and oxygen donors. This section will briefly cover some examples of non **DOTA/DO3A/DTPA** type ligand architectures employed in lanthanide chemistry.



Ln.1.1 **$[Eu.1.2]^{3+}$** **$[Ln.(bipy)_3]^{3+}$**

Figure 1. 2 Examples of lanthanide β-diketonates and cryptand lanthanide complexes.

There are many reports of lanthanide β-diketonates (e.g. **Ln.1.1**); the terminal substituents can be aliphatic or aromatic.[19-21] The substituents can affect the properties of the complexes such as stability, solubility and also sensitising groups can be incorporated to increase quantum yields of emission. The presence of two carbonyl groups means that the α-proton is particularly acidic, and its pK_a can be tuned by varying the electronic properties of the substituents. The stability of the lanthanide complexes decreases as the acidity of the β-diketonate ligand increases. Lanthanide β-diketonate complexes are kinetically labile[22] with many different species present in solution due to the fast exchange of ligands, limiting their use in aqueous media. Despite this kinetic lability lanthanide β-diketonates have been widely used as NMR shift reagents.[23]

[Eu.1.2]$^{3+}$ was one of the first examples of a lanthanide complex were the ligand is preorganised for coordination.[24] Despite the absence of a chromophore, weak LMCT bands were observed in the UV-Vis spectrum as a consequence of energy transfer from essentially non-bonding electrons on the oxygen donor atoms. The Eu(III) emissive lifetimes were temperature dependent which suggests that thermally populated deactivation of the $^5D_0$ state was occurring through a low lying LMCT state. There was an increase in the radiative lifetime of **[Eu.1.2]$^{3+}$** upon the addition of fluoride, which corresponds to fluoride displacing lanthanide bound solvent and thus removing a quenching pathway. Displacement of bound solvent by fluoride was also found to increase the energy of the LMCT state, rendering it less efficient at quenching the $^5D_0$ state.[25]

Lehn et al.[26] increased the intensity of lanthanide emission by incorporating strongly absorbing 2,2'-bipyridine groups into the cryptand scaffold to form the first strongly absorbing cryptand, **[Ln.(bpy)$_3$]$^{3+}$**. These species however still had low quantum yields, the high number of bound solvent molecules have a large role to play in deactivating the emissive states. There have been many subsequent reports of symmetric and unsymmetric lanthanide complexes of cryptands based on 2,2'-bipyridine;[27-29] cryptands are characterised by their high stability and selectivity as well as slow exchange rates which has led to them being used in biochemical applications.[30]

1.4 General lanthanide photophysical properties

Luminescence from lanthanide(III) species occurs from *f*-centred states. All lanthanide(III) ions are luminescent apart from La(III) and Lu(III); their emission covers a wide spectral range, from NIR (e.g. Nd(III), Er(III), Yb(III)) to visible (e.g. Eu(III), Tb(III)) to UV (e.g. Gd(III)). Lanthanides can be either fluorescent ($\Delta S = 0$) or phosphorescent ($\Delta S \neq 0$), and the term luminescence is generally used to cover both processes. The 4*f* orbitals are shielded by the 5*s* and 5*p* orbitals which mean that their overlap with ligand orbitals is small which results in small ligand field splitting. The presence of a ligand field results in Stark splitting of the J-levels in m_J components, and the nature of this splitting depends of the local symmetry around the lanthanide ion.[31] The contracted nature of 4*f* orbitals results in sharp line-like emission bands due to the post-transition molecular rearrangement being minimal, thus meaning that the intramolecular distances remain similar in the ground and excited states. This minimal molecular change results in very small Stokes' shifts upon direct lanthanide excitation. The *f-f* transitions responsible for most lanthanide luminescence are Laporte and spin forbidden which leads to long emissive lifetimes ranging from milliseconds to microseconds.[32] This has implications in medical imaging; time-gated luminescence allows short-lived background luminescence to be entirely removed whilst only the long-lived lanthanide based luminescence is detected.[33] This allows concentrations of lanthanide-based probe as low as femtomolar to be used due to an improved signal to noise ratio. Time gated imaging is performed by applying a delay time after the excitation pulse during which no signal is detected, this allows the short-lived species to decay before detection is started (Figure 1. 3).

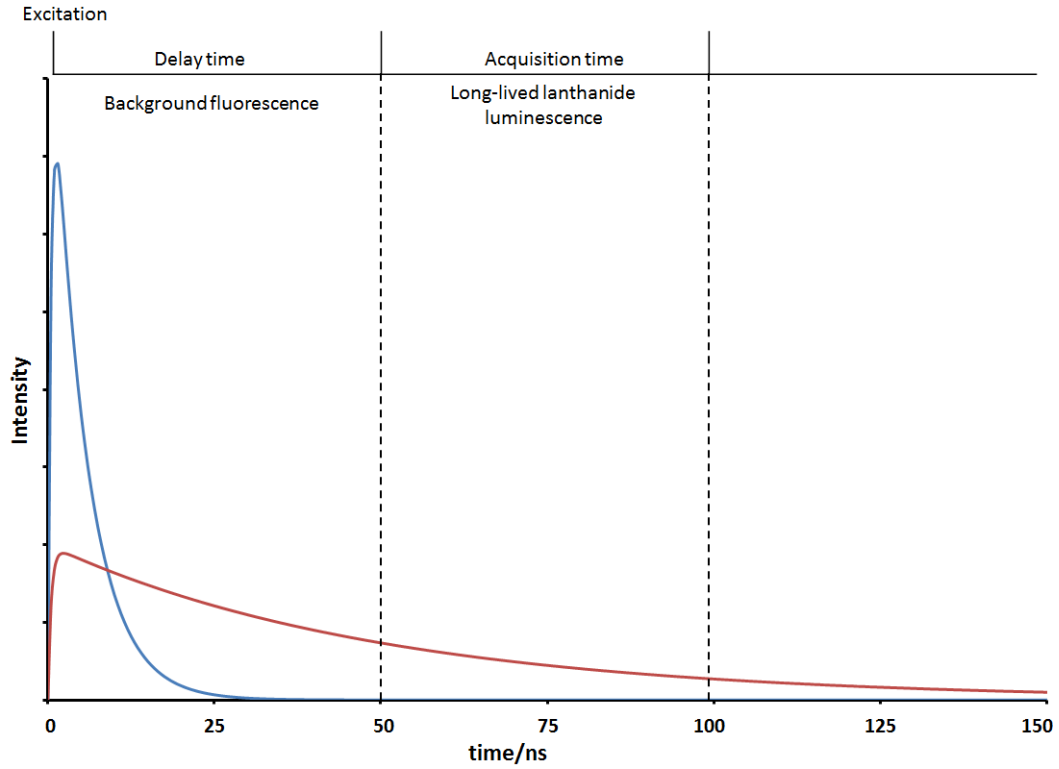


Figure 1. 3 Schematic showing how time gated imaging is performed. Blue: endogenous fluorescence, Red: lanthanide luminescence

There are three main types of electronic transition that occur in lanthanide species: these are electric dipole (ED), magnetic dipole (MD) and electric quadrupolar (EQ). These transitions are governed by selection rules, for example the Laporte selection rule (or parity selection rule) forbids ED transitions between levels of the same parity ($\Delta L = \pm 1$). ED and MD transitions are both observable whilst EQ transitions are much weaker and are typically not observable.[34] The selection rules for transitions in lanthanide ions, assuming that they obey the Russell-Saunders coupling scheme, are shown in Table 1. 3.

Table 1. 3 selection rules for transitions that occur in lanthanide ions adapted from reference.[35]

Transition type	**ΔS**	**ΔL**	**ΔJ[a]**	**Parity**
ED	0	≤6	≤6 (2,4,6 if J or J' = 0)	Opposite
MD	0	0	0, ±1	Same
EQ	0	0, ±1, ±2	0, ±1, ±2	Same

[a]J = 0 to J' = 0 transitions are always forbidden.

The selection rules are not always strictly followed, for example the presence of a ligand field allows the mixing of states of opposite parity into the 4*f* wavefunction which relaxes the selection rules thus making the transitions more allowed (i.e. induced ED). Hypersensitive transitions are commonly observed in lanthanide species and are prevalent in Eu(III), Ho(III) and Nd(III) species. These transitions show substantial variation of intensity, wavelength and splitting in emission spectra upon changes in the local lanthanide environment. Theoretical studies[36] attribute hypersensitivity to the enhancement in quadrupole transitions by dielectric inhomogeneity in media i.e. the intensity of (usually weak) quadrupole transitions are particularly affected by dielectric inhomogeneity. Judd[37] also suggested that the hypersensitive transitions are affected by changes in the symmetry of the lanthanide ion ligand field. Judd[38] and Ofelt[39] simultaneously published independent expressions for explaining the intensities of induced electric dipole transitions within the 4*f* manifold, this is referred to as the Judd-Ofelt theory. Judd-Ofelt theory is widely used due to its ability to predict oscillator strengths in absorption and luminescence spectra of lanthanide species.

1.4.1 Eu(III), Tb(III) and Yb(III) luminescence

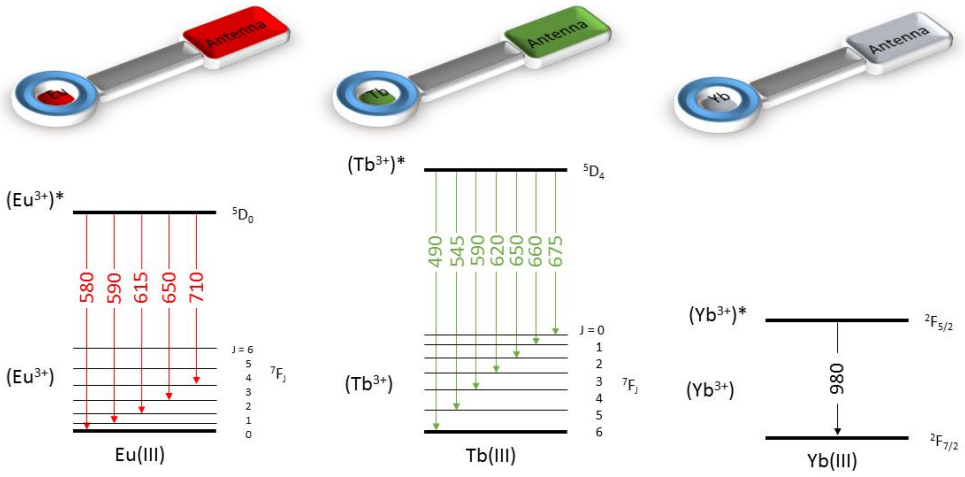


Figure 1. 4 Luminescent transitions in Eu(III), Tb(III) and Yb(III) complexes with common emission wavelengths (nm).

Energy level diagrams showing the characteristic transitions of Eu(III), Tb(III) and Yb(III) according to Russell-Saunders coupling are shown in Figure 1. 4, the characteristic properties of these bands are given in Table 1. 4.

The emission bands in Eu(III) complexes are regularly used to probe the symmetry of the lanthanide coordination environment. The $^5D_0$-$^7F_0$ transition can be used to determine the number of distinct lanthanide environments due to the $^5D_0$ and $^7F_0$ states each being non-degenerate. Richardson et al.[40, 41] noticed that the intensity ratio of the $^5D_0$-$^7F_2$ and the $^5D_0$-$^7F_1$ emission bands can be used to measure the local symmetry of the Eu(III) ion. In a centrosymmetric system the $^5D_0$-$^7F_1$ transition dominates whilst when the symmetry around the Eu(III) centre is distorted then there is a significant increase in intensity of the hypersensitive $^5D_0$-$^7F_2$ transition. The $^5D_4$-$^7F_5$ transition in Tb(III) is also hypersensitive to the metal environment but is not a reliable probe for determining the symmetry of the lanthanide environment. Only one emission band is observed for Yb(III) corresponding to the $^2F_{5/2}$-$^2F_{7/2}$ transition at 980

nm. The small energy gap between the ground and excited state of Yb(III) leads to very short luminescence lifetimes due to significant quenching by high frequency oscillators.

Table 1. 4 The characteristic properties of Eu(III), Tb(III) and Yb(III) ions in aqueous solution adapted from reference.[42]

Ion	Transition	Properties
Eu(III)	$^5D_0 \rightarrow {}^7F_0$	Weak intensity, Single sharp line, induced ED
	$^5D_0 \rightarrow {}^7F_1$	Strong intensity, Sharp, MD
	$^5D_0 \rightarrow {}^7F_2$	Strong intensity, hypersensitive, induced ED
	$^5D_0 \rightarrow {}^7F_3$	Weak intensity, induced ED
	$^5D_0 \rightarrow {}^7F_4$	Medium intensity, structure sensitive to ligand environment, induced ED
Tb(III)	$^5D_4 \rightarrow {}^7F_6$	Medium intensity, Moderate sensitivity to ligand environment
	$^5D_4 \rightarrow {}^7F_5$	Strong intensity, Hypersensitive
	$^5D_4 \rightarrow {}^7F_4$	Medium intensity, Moderately sensitive to ligand environment
	$^5D_4 \rightarrow {}^7F_3$	Strong intensity, Structured at high resolution
	$^5D_4 \rightarrow {}^7F_2$	Weak intensity, Moderately sensitive to ligand environment
Yb(III)	$^2F_{5/2} \rightarrow {}^2F_{7/2}$	Weak intensity, prone to quenching due to small ΔE

1.4.2 Sensitised lanthanide luminescence

Direct excitation into the 4*f* excited states of lanthanide ions is formally forbidden, this coupled with the lack of significant interaction between the 4*f* orbitals and their environment gives extinction coefficients in the order of 1 M^{-1} cm^{-1}. The Laporte selection rule is responsible for the long luminescence lifetimes of lanthanide species. Due to the weak direct excitation of lanthanides it is often necessary to employ a sensitiser (antenna)[43] to transfer energy to the lanthanide excited states, this was first observed by Weissman in a Eu(III) complex[44] and is often referred to as the 'antenna effect' (a schematic is shown in Figure 1. 5).

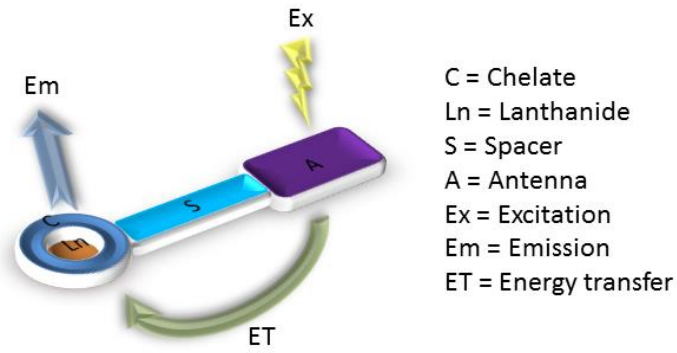


Figure 1. 5 Schematic representation of sensitisation in lanthanide complexes.

The mechanism of the sensitisation process proposed by Crosby and Whan[45-47] is summarised in Figure 1. 6. Excitation of the organic sensitiser *via* single or multi-photon[48, 49] absorption and subsequent internal conversion (IC) leads to the population of a singlet excited state, S_1. This excited state can then undergo radiative (fluorescence) or non-radiative decay to the ground state or it can undergo intersystem crossing (ISC) from S_1 to an excited state triplet state, T_1. Energy transfer from T_1 to the lanthanide acceptor state can occur *via* Förster or Dexter mechanisms, or again radiative (phosphorescence) or non-radiative decay can occur, deactivating

the T_1 excited state. Energy transfer from the sensitiser based triplet state to the lanthanide excited state is most efficient when the energy gap between the two states is around 2000 cm^{-1} as this ensures that back energy transfer to the sensitiser is minimised.[50] Sensitisation directly from the antenna singlet state to the lanthanide emissive state has been shown to play a role in the energy transfer cascade and is particularly prevalent when intra ligand charge transfer states are present.[51, 52]

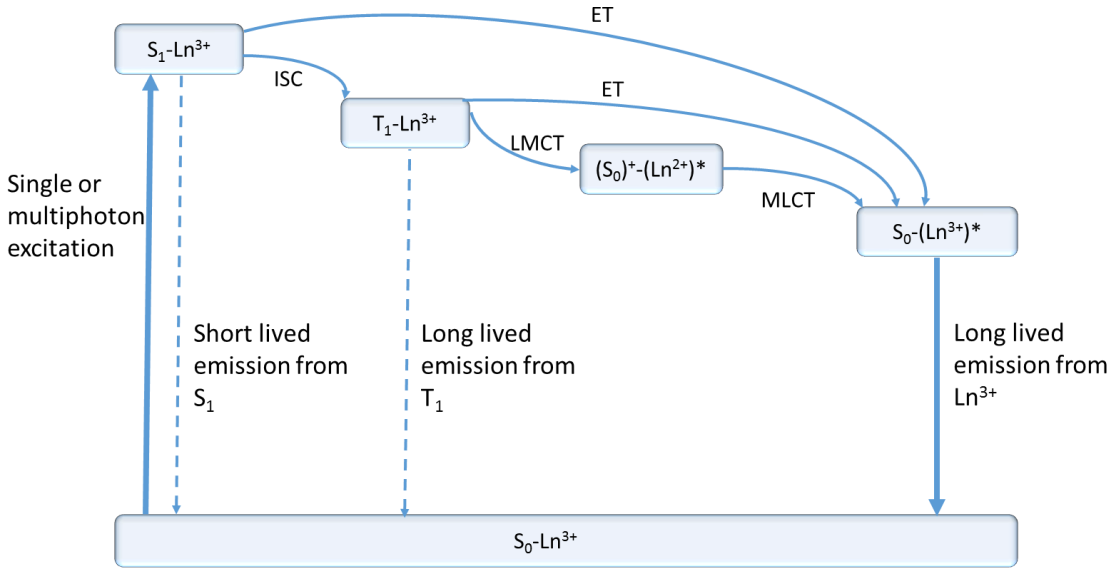


Figure 1. 6 Simplified Jablonski diagram showing the main energy transfer pathways in sensitised lanthanide emission.

The excited *f*-centred states can either undergo radiative decay leading to characteristic lanthanide emission or they can be quenched, commonly by high frequency oscillators (XH, XD and CH) *via* a Förster mechanism. Furthermore, resonant energy transfer from a lanthanide to an acceptor chromophore is generally likely to be more efficient than energy transfer to the lanthanide from a donor chromophore (on the basis of improved spectral overlap when the lanthanide acts as a donor). The antenna based singlet states can undergo collisional quenching through photoelectron

transfer (PeT) from for example halide lone pairs,[53] whilst the triplet states of the antenna can be quenched by O_2.[54]

Charge transfer states (CT) have also been shown to play a role in the energy transfer cascade. They are allowed, have high energies and are most commonly singlet in nature. Charge transfer processes have been shown to be particularly important in Yb(III) complexes due to the accessibility of the Yb(II) state.[55] A double electron transfer sensitisation mechanism is feasible for Yb(III) complexes bearing electron rich ligands due to the emissive $^2F_{5/2}$ state of Yb(III) being generally lower than the LMCT state. The formation of an LMCT Yb(II) state populates the emissive $^2F_{5/2}$ state of Yb(III) following MLCT back electron transfer leading to emission (Figure 1. 6).[56] This process was first suggested by Horrocks et al.[57] and explains why sensitised Yb(III) emission is still observed even when spectral overlap between the sensitiser and Yb(III) is negligible. LMCT states can also be involved in energy transfer cascades in Eu(III) and Tb(III) complexes, however their formation typically precludes lanthanide emission due to the LMCT states being generally lower in energy than the lanthanide emissive states.

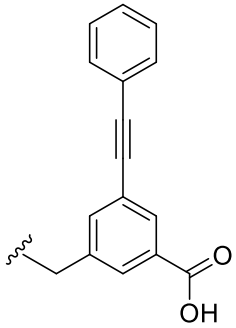
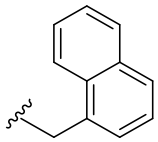
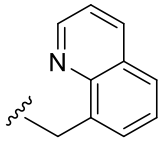
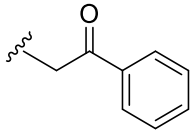
1.4.3 Choice of sensitiser

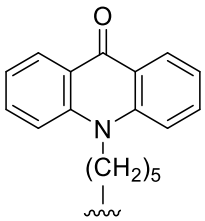
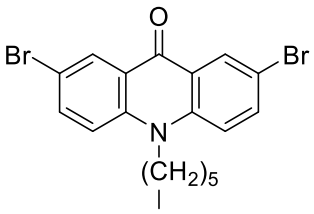
The choice of sensitiser used is often dictated by the nature of the lanthanide, with organic sensitisers typically employed for visibly emitting lanthanides such as Eu(III) and Tb(III), whilst for NIR emitting lanthanides such as Yb(III) inorganic based sensitisers can be utilised.

A wide variety of organic chromophores have been shown to sensitise lanthanide emission. Latva et al.[58] undertook a comprehensive study of the correlations between

the chromophore triplet state energy and the lanthanide luminescence quantum yield for a variety of pyridyl based chromophores; the authors showed that the excited state energy of the chromophore has a profound effect on its ability to sensitise lanthanide emission. A few examples of chromophore structures with their associated triplet energies are shown in Table 1. 5 along with the lanthanides they are capable of sensitising. Many of these examples as well as other examples of lanthanide complexes bearing organic chromophores will be discussed throughout this thesis.

Table 1. 5 Examples of organic chromophores used for lanthanide sensitisation.

Chromophore	**E_T / cm^{-1}**	**Lanthanide(III) ions sensitised**	**Reference**
	21640	Eu, Tb	[58]
	21320	Eu, Tb	[59]
	21740	Eu, Tb	[59]
	25600	Eu, Tb	[50]

	21500	Eu, Tb (not studied)	[60]
	19800	Eu, Tb (not studied)	[60]

A number of lanthanide complexes bearing inorganic containing chromophores (*d-f* hybrids) are shown in Figure 1. 7.

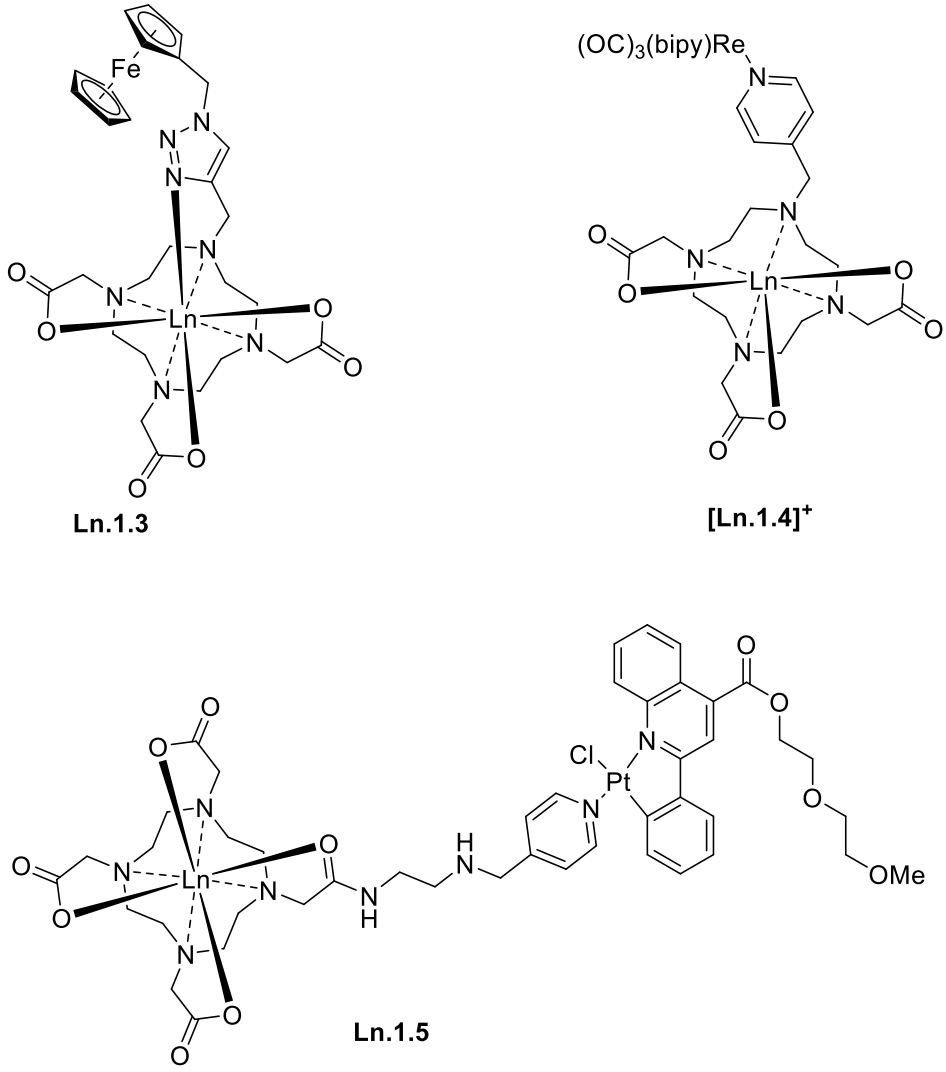


Figure 1. 7 Examples of lanthanide complexes bearing inorganic based sensitisers.

Tropiano et al.[61] developed a lanthanide ferrocene dyad utilising 'click' chemistry (**Ln.1.3**, Figure 1. 7); the photophysics of these systems could be modulated by altering the ferrocene redox state. Oxidation of ferrocene caused a decrease in intensity of lanthanide centred emission in both **Eu.1.3** and **Yb.1.3**; this process was found to be fully reversible over a number of cycles. Only the triazole triplet state (23000 cm^{-1}) was observed when studying **Gd.1.3**, the absence of the ferrocene centred triplet state

suggests that sensitisation occurs through the triazole triplet state or, in the case of **Yb.1.3**, a charge transfer mechanism is feasible. It is likely that the observed mechanism of quenching of lanthanide emission is due to the non-radiative energy transfer from triazole states to ferrocenium excited states which are lower in energy that the Ln(III) emissive states.

[Ln.1.4]$^{+}$ was developed as a prototype for a single molecule dual imaging agent (optical and magnetic resonance imaging).[62] The ^{3}MLCT state of the Re(I) chromophore was unable to sensitise **[Eu.1.4]**$^{+}$ lanthanide emission due to a mismatch in energy, whilst **[Yb.1.4]**$^{+}$ did exhibit sensitised emission. The replacement of chloride in Re(bipy)$(CO)_3$Cl with the pyridine moiety from the parent lanthanide complex (to form **[Ln.1.4]**$^{+}$) resulted in a significant increase in the ^{3}MLCT lifetime of the Re(I) moiety (<10 ns to 0.24 μs in **[Gd.1.4]**$^{+}$) due to the removal of the efficient chloride PeT quencher; this lifetime is long enough to allow time gating and exclude signal from endogenous species. **[Gd.1.4]**$^{+}$ gave high proton relaxivity in aqueous media which shows the potential of these species to be employed as dual imaging agents.

More recently, Pope et al.[63] developed a water soluble Pt(II)-Ln(III) dyad (**Ln.1.5**, Figure 1. 7); **Gd.1.5** and **Yb.1.5** both display complex absorption in the UV region with absorption extending well into the visible region, with **Gd.1.5** exhibiting broad structureless Pt(II) based emission at 617 nm upon excitation at 425 nm. **Yb.1.5** also displayed this Pt(II) based emission as well as characteristic Yb(III) based emission at 980 nm upon excitation at 425 nm; absorption at 425 nm is dominated by the Pt(II) sensitiser which suggests that Yb(III) is being sensitised through the Pt(II) containing chromophore. The *q* value of **Yb.1.5** was found to be 0.8 which supports the coordination of the amide carbonyl to Yb(III), giving an octadentate species. Upon

coupling of the Gd(III) pyridyl species to the Pt(II) cyclometalated complex an 86% increase in proton relaxivity was observed which was attributed to the increase in molecular weight of the species. Preliminary confocal microscopy studies using **Gd.1.5** revealed characteristic Pt(II) based red emission from cells showing the potential of these species to be utilised as dual modal imaging agents. However the cytotoxicity of this class of species needs to be established before future studies can occur.

1.4.4 Luminescence quenching

The *f-f* excited states are prone to quenching by NH, OH and CH oscillators whose vibrational harmonics are similar in energy to the *f-f* transition energy; the energy of the excited *f*-centred states can be readily transferred to the vibrational manifold.[64] This is a non-radiative pathway thus there is a decrease in the intensity of lanthanide emission. The corresponding ND, OD and CD oscillators have lower stretching frequencies which means that energy matching is only possible with higher vibrational harmonics (which have reduced Franck Condon overlap) and these are less efficient quenchers.[65] This is due the decrease in the overlap integral between the excited *f-f* state and the corresponding vibrational overtone. The C=O stretching frequencies are also capable of quenching lanthanide emission but they are less efficient than XH oscillators.[66] The degree of quenching by water molecules is inversely proportional to the energy gap between the emissive excited and ground *f*-centred states (Figure 1. 8). This means that Ln(III) ions with the largest excited to ground state energy gaps, such as Eu(III) and Tb(III), are less prone to quenching (due to a smaller Franck Condon overlap) than species such as Nd(III) and Er(III) with smaller energy gaps. This difference in quenching ability also has a large effect on the emissive state lifetimes of

the lanthanides across the series, for instance Eu(III) and Tb(III) species have lifetimes in the order of ms whilst lower energy gap species such as Nd(III) and Er(III) have lifetimes typically of ns and below. Furthermore, vibrational manifolds can also bridge between the emissive state and a lower energy excited state, hence Nd(III) complexes have shorter lifetimes than Yb(III) complexes.

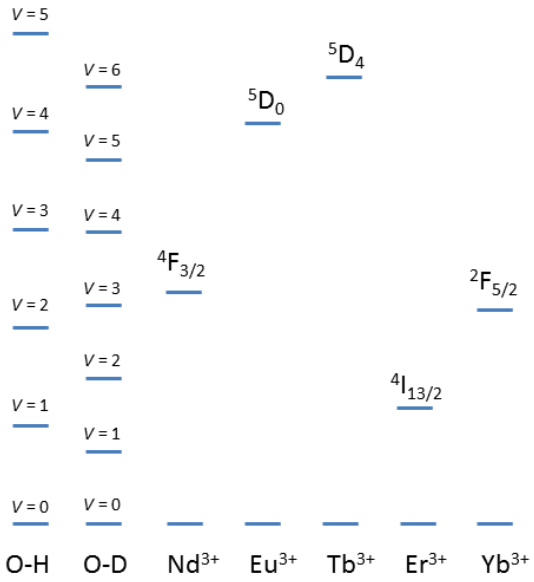


Figure 1. 8 Schematic energy level diagram of certain Ln(III) ions showing the energy of their ground and emissive excited states in comparison with the vibrational energy levels of OH and OD oscillators.

The number of water molecules bound to the lanthanide ion (q = inner sphere hydration number) can be calculated using the modified Horrocks equation.[64] This equation uses the rate of depopulation of the excited state in both H_2O (k_H) and D_2O (k_D) and assumes that the main mode of quenching in aqueous media is by OH/OD oscillators:

$$q = A\left(k_H - k_D - \mathrm{B}\right)$$

Where A is a proportionality constant which is specific to each lanthanide ion and describes the sensitivity of the lanthanide ion to coupling to OH oscillators. An empirical correction factor (B) is also needed to take into account that most lanthanide

species have other donors bound to them such as ligand bound carboxylate oxygen atoms and the fact that outer sphere solvent molecules can also quench. Amide NH oscillators on the ligand scaffold can also quench the lanthanide excited state, in the case of Eu(III) and additional correction factor needs to be applied to take this into account when determining *q*:

$$q_{Eu} = A\left(k_H \ - k_D \ - \mathrm{B} - 0.075\mathrm{x}\right)$$

Where x is the number of exchangeable amide NH protons in close proximity to the lanthanide centre. Table 1. 6 shows values of A and B for Eu(III), Tb(III) and Yb(III).

Table 1. 6 Table of A and B values for use in the Horrocks equation.

	A	**B**
Eu	1.2 ms	0.25 ms^{-1}
Tb	5 ms	0.06 ms^{-1}
Yb	1 µs	0.2 μs^{-1}

As XH oscillators are such good quenchers it is desired, for optical applications, that the ligand supplies many donor species so that the lanthanide ion is almost coordinatively saturated meaning fewer XH oscillators can bind.

Typically the energy transfer from the ligand triplet state to the lanthanide emissive state is rapid and irreversible which means that the luminescence intensity and lifetime are essentially independent of oxygen concentration. However in complexes where thermal repopulation of the sensitiser triplet state from the lanthanide emissive state is facile, the intensity and lifetimes of the lanthanide emission can be dependent on the concentration of oxygen in solution.[54] This is particularly prevalent in Tb(III) species[67] but can be observed for other lanthanides such as Eu(III).[68] In cases where energy transfer from the chromophore to the lanthanide is relatively slow, then the

signal is also found to be oxygen dependent, though the lifetime of the lanthanide emissive state is unaltered by pO_2.[69]

1.4.5 Energy transfer mechanisms

The two main energy transfer mechanisms in lanthanide luminescence are Förster (dipolar)[70] and Dexter (double electron exchange),[71] these mechanisms are represented schematically in Figure 1. 9. The Förster mechanism involves a through space interaction were the efficiency of energy transfer varies with separation (r) by r^{-6} and typically occurs over distances of up to 1000 pm. This mechanism also depends on donor-acceptor spectral overlap, though the narrow emission profiles of lanthanide species mean this mechanism is not particularly efficient. Dexter transfer is an electron exchange interaction were the efficiency of energy transfer varies with separation (r) according to e^{-r} and typically occurs at shorter distances up to 30-50 pm where orbital overlap is significant. However, coupling across much larger distances (up to at least 2 nm) can be observed where superexchange can occur through the ligand skeleton, as in the case of polyphenyl-derived structures.

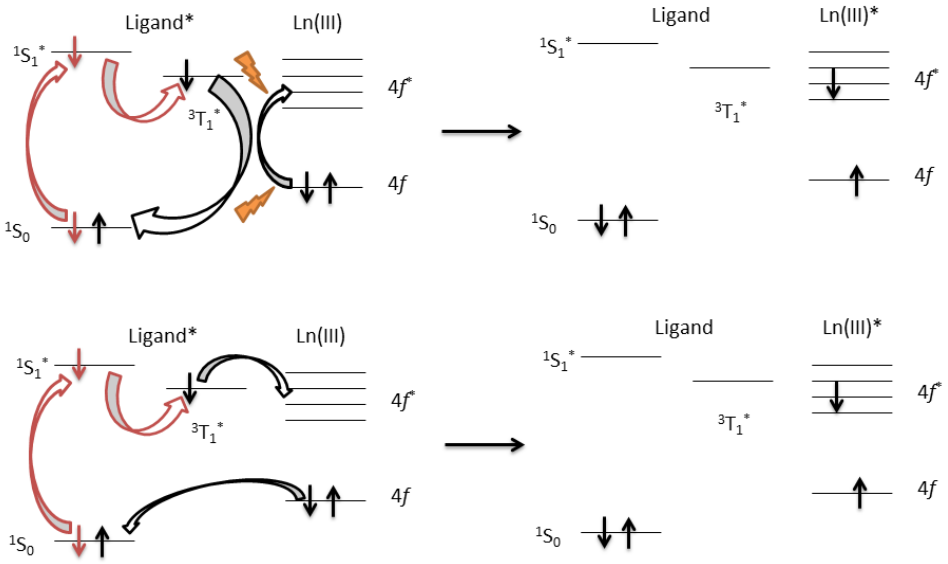


Figure 1. 9 Schematic representation of Förster (top) and Dexter (bottom) energy transfer mechanisms.

1.5 Sensing of analytes

An extensive review on the ability of lanthanide complexes to detect anions in aqueous media has been published recently by Parker et al.[72] Broadly speaking there are two main methods by which lanthanide complexes can sense analytes. Firstly, anions can reversibly bind to the lanthanide ion, displacing coordinated solvent,[73] or a ligand donor thus modulating emission.[74] If the anion contains a chromophore then sensitised lanthanide emission can be observed upon the chromophore binding to the lanthanide centre.[75] Secondly, both anions and cations can interact with the sensitising chromophore thus modulating emission, this interaction can take place *via* coordination to the chromophore, reaction with the chromophore or through a collisional interaction between the analyte and chromophore.

Examples of lanthanide complexes capable of sensing analytes through interaction with the sensitiser are shown in Figure 1. 10.

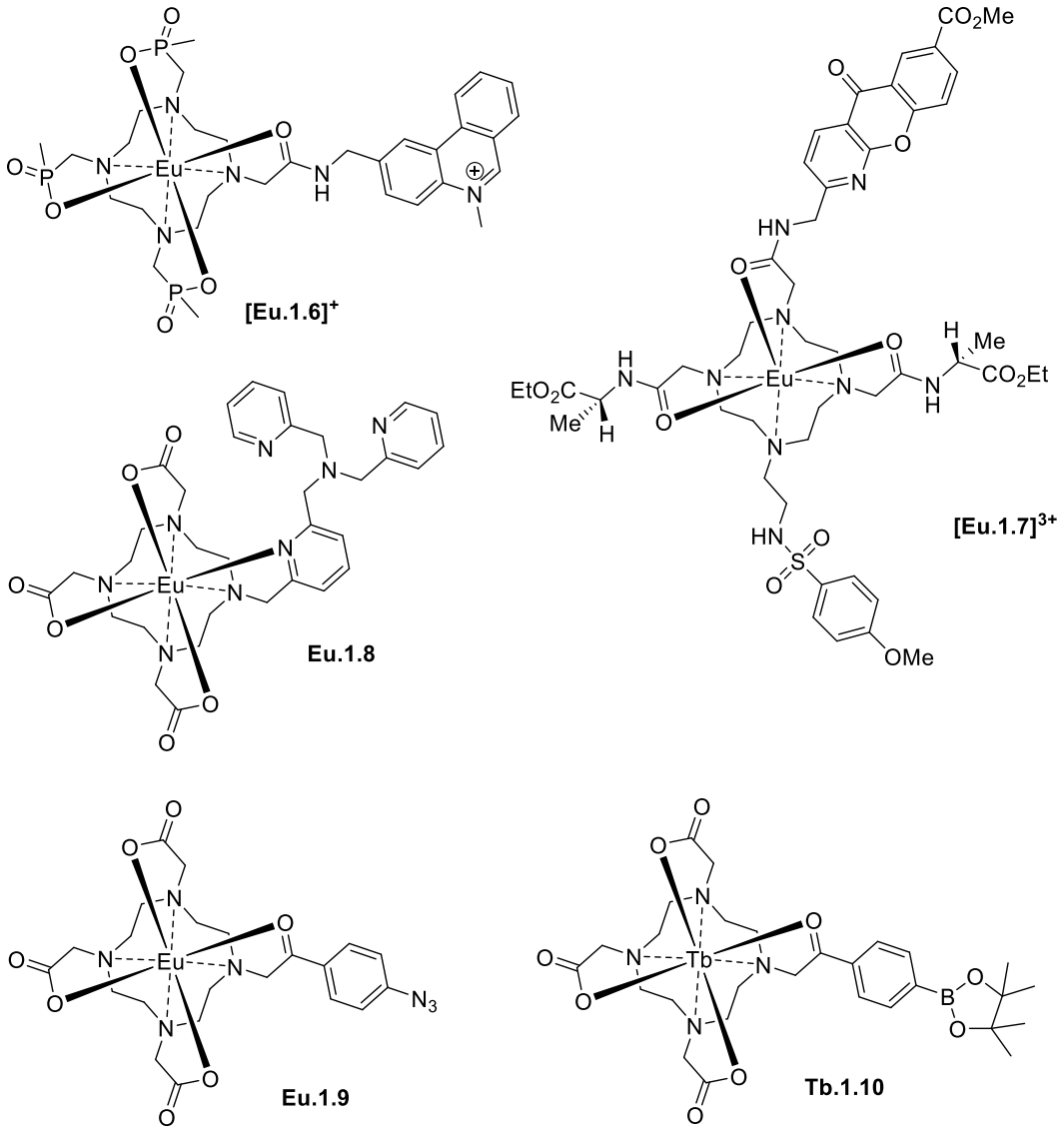


Figure 1. 10 Lanthanide complexes capable of sensing analytes through interaction with the sensitiser.

[Eu.1.6]$^{+}$ has been used to detect halides through a collisional interaction between the halide and the positively charged phenanthridine sensitiser.[76] The interaction between the halide and the sensitiser results in quenching of the excited singlet state (and a decrease in emission intensity) *via* photoelectron transfer, this quenching effect follows the order; $I^{-}>Br^{-}>Cl^{-}$ which is in line with the ease of oxidation of the halide.

[Eu.1.7]$^{3+}$ can monitor the pH of a solution through the sulfonamide moiety,[77] were the sulphonamide can reversibly coordinate to the lanthanide centre in response to changes in pH which results in changes in the spectral form and intensity. The

azaxanthone moiety promotes uptake of the probe into lysosomes. At high pH, the sulfonamide is deprotonated allowing the sulfonamide to coordinate to the lanthanide centre, reducing its hydration state. However, at low pH the sulfonamide is protonated, which reduces the likelihood of it being coordinated to the lanthanide and increases the hydration of the lanthanide. Interestingly the emission intensity increases as the pH decreases due to quenching of the europium $^5D_0$ state by intramolecular charge transfer occurring through the proximate electron rich *p*-methoxyphenylsulfonamide anion in the sulphonamide-bound form outweighing the reduced quenching by high frequency oscillators.

Eu.1.8[78] exploits a conformational change in the complex brought about by the geometric requirements of the Zn(II) target ion. In the absence of Zn(II) a pyridine nitrogen is coordinated to the lanthanide centre making the lanthanide eight coordinate (depicted in Figure 1. 10). Upon addition of $ZnCl_2$ a significant decrease in Eu(III) emission intensity was observed with *q* increasing from 0.2 to 2. This was attributed to an induced conformational change of the sensitiser required to accommodate the Zn(II) in a four coordinate pyridyl environment. This resulted in a change in the solvation of the lanthanide ion due to the pyridine no longer coordinating to the lanthanide centre.

Eu.1.9[79] and **Tb.1.10**[80] are reaction based probes, i.e. the chemical structure and properties of the probes are changed irreversibly upon reaction with the analyte. **Eu.1.9** utilises an aryl ketone sensitiser which have been shown to be efficient lanthanide sensitisers and the electron donating ability of substituents on such sensitisers has been shown to be linked with the sensitisation efficiency. The reduction of the azide group to an electron donating amino group occurred on addition of NaHS

to **Eu.1.9** in H_2O. This resulted in a 'turn-on' of emission due to an increase in the energy transfer efficiency to the lanthanide centre. This response was shown to be selective in the presence of a variety of biologically selective ions and reducing species. **Tb.1.10** is capable of detecting H_2O_2 *via* a 'turn-on' luminescence response. In the absence of H_2O_2 the boronate protected phenol acts as a poor sensitiser. Removal of the electron withdrawing boronate group by reaction with H_2O_2 results in the formation of an electron rich phenol which is capable of sensitising Tb(III) emission. This sensor can selectively detect H_2O_2 over a variety of other biologically reactive oxygen species.

For reaction based probes the kinetics of the reaction need to be fast enough to not limit the response and it is also important that any by-products formed during the reaction don't significantly interact with the probe under study. These systems can offer an advantage when developing probes with low detection limits.

Direct interaction of the anion with the lanthanide centre typically results in an increase in the emission intensity due to the displacement of high frequency oscillators from the lanthanides first coordination sphere; a change in spectral form is also common due to the nature of the donor species changing. The $^5D_0$-$^7F_2$ transition in Eu(III) is a hypersensitive electric dipole transition which is sensitive to the lanthanide environment; this transition undergoes greater change in intensity upon binding than the other characteristic Eu(III) bands. The ratios of the hypersensitive $^5D_0$-$^7F_2$ band *vs.* the other characteristic emission bands are often used to determine anion binding affinities in Eu(III) complexes. Examples of complexes where the analyte directly interacts with the lanthanide centre are shown in Figure 1. 11.

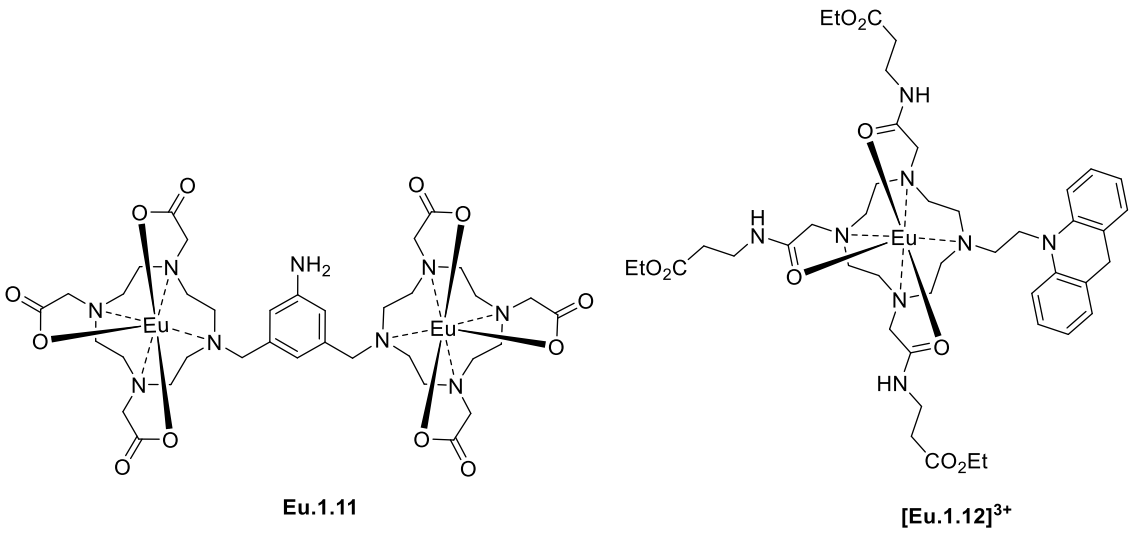


Figure 1. 11 Lanthanide complexes capable of sensing analytes through direct coordination to the Ln(III) ion.

Self-assembly between chromophores bearing carboxylates or phosphonates and lanthanide **DO3A** complexes has been exploited to quickly assess the ability of the chromophore to sensitise lanthanide emission.[81] The interaction between the lanthanide ion and the chromophore through displacement of bound solvent from the lanthanide allows the chromophore to be proximal to the lanthanide ion meaning that sensitisation can occur if there is a good overlap between the chromophore donor state and the lanthanide acceptor state. This approach has been used for both organic[82] and inorganic[83] sensitising chromophores.

Seven coordinate lanthanide complexes can accommodate bidentate anions assuming steric requirements are met whilst eight coordinate species prefer monodentate ions. Faulkner et al.[84-86] have studied the interaction of **Eu.1.11** with a variety of carboxylate species. The aminoaryl chromophore does not take part in the anion recognition event and simply acts as a rigid bridging unit. Binding of benzoic acid was shown to be significantly weaker than binding of bidentate phthalic acid derivatives, with isophthalic acid binding at least ten times stronger than terephthalic acid and

significantly stronger than phthalic acid. Isophthalic acid derivatives have been shown to effectively bridge the gap between the two lanthanide centres whilst binding simultaneously in a monodentate fashion to both lanthanide centres. The authors have also shown that the steric demand from remote substituents on the aromatic linker can have a profound effect on the conformational freedom of the lanthanide domains and thus the binding affinity of isophthalate.[87] Bulky substituents increase the binding affinity due to increased organisation of the complex resulting in a reduced loss of entropy upon binding, however it is possible to go too far and completely inhibit binding if the remote substituent is too large.

Parker et al.[88] investigated the interaction of **[Eu.1.12]$^{3+}$** and some of its derivatives (cationic, anionic and zwitterionic) with hydrogencarbonate in aqueous media. Addition of HCO_3^- to an aqueous solution of **[Eu.1.12]$^{3+}$** resulted in a decrease in *q* from 1 to 0 implying HCO_3^- has displaced the Eu(III) bound solvent. The positively charged lanthanide complexes bound HCO_3^- more strongly than the zwitterionic analogues, with the anionic analogues showing the weakest binding. This shows the strongly ionic nature of the interaction between the metal ion and the anion.

1.6 Lanthanide NMR

The presence of a paramagnetic lanthanide in a system containing NMR active nuclei results in an interaction between the nuclei and any unpaired electron spins. This interaction is only non-zero in the presence of an external magnetic field due to the degeneracy of the electronic spin states being removed. The result of this interaction is to change the chemical shift of the nuclei relative to their diamagnetic analogue; this is referred to as the lanthanide induced shift (LIS, Δ_ω). The LIS has contact shift (Δ_C) and

pseudocontact shift (Δ_p) contributions.[89] The contact shift contribution takes place directly on the resonating nucleus *via* Fermi coupling (through bond) whilst the pseudocontact shift is a through space dipole-dipole interaction between the electronic and magnetic dipole moments. The diamagnetic shifts (Δ_d) arise from the redistribution of electron density within the ligand scaffold upon binding to the metal. These shifts are typically small except for the metal bound nuclei and can be directly determined using diamagnetic lanthanide complexes such as La(III) and Lu(III).

The total shift observed is made up of the diamagnetic contribution (Δ_d) as well as the LIS contribution and is shown below:

$$\Delta = \Delta_d + \Delta_c + \Delta_p$$

The contact shifts occur due to through bond coupling between the unpaired electron spin on the lanthanide and the orbital centred on the resonating nucleus of interest. This contribution to the shift is often ignored as the overlap between the metal and the observed nucleus is only negligible unless directly bound to the metal. The contact shift contribution in paramagnetic lanthanide species is given by the following equation:[90]

$$\Delta_c = \langle S_z \rangle \frac{\mu_B}{3kT\gamma_I} \frac{A}{\hbar} 10^6$$

Where $\langle S_z \rangle$ is the reduced value of the average spin polarisation, μ_B is the Bohr magneton, $A/\hbar$ is the hyperfine coupling constant, T is the temperature, k is the Boltzmann constant, γ_I is the gyromagnetic ratio of the resonating nucleus and Δ_c is measured in ppm.

The pseudocontact shift has been used to entirely describe the NMR spectra of lanthanide complexes.[91, 92] Bleaney[89] derived an equation for the pseudocontact shifts

in lanthanide complexes assuming that the ligand field splitting for the lowest J state of the lanthanide is small compared to kT:

$$\Delta_p = \frac{2{\mu_B}^2 C_J}{60k^2T^2}\left(\frac{\langle r^2\rangle B_2^0(3cos^2\theta - 1)}{r^3} + \frac{\langle r^2\rangle B_2^2(sin^2\theta cos2\phi)}{r^3}\right)$$

$\langle r^2\rangle B_2^0$ and $\langle r^2\rangle B_2^2$ are crystal field coefficients, r, θ, ϕ are the spherical coordinates of the resonating nucleus with reference to the position of the lanthanide, C_J is a constant containing magnetic susceptibility factors (specific for each lanthanide) and μ_B is the Bohr magneton. In systems with axial symmetry the last term can be ignored and the equation simplifies. The pseudocontact shift is affected by the distance and angle between the lanthanide and the observed nucleus; this geometrical information is described using spherical coordinates as shown below in Figure 1. 12.

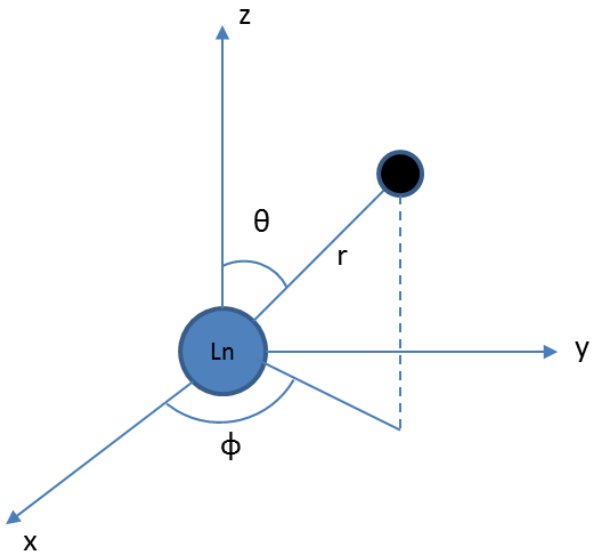


Figure 1. 12 Coordinate system used to describe the effect of a paramagnetic ion (blue sphere) on the observed nucleus (black sphere) with spherical coordinates ϕ, θ and r with the z axis aligned along the direction of the external magnetic field.

Parker et al.[93] have recently demonstrated the limitations of Bleaney's approach to the description of magnetic anisotropy. The Bleaney theory was applied to a number of lanthanide complexes with C_3, C_4 and lower symmetry utilising phosphinate, pyridyl

and carboxylates donor sets. They pointed out that many of the assumptions used in the theory do not always hold true:

- Firstly, Bleaney assumed ligand field splitting was less than kT however many compounds have B_0^2 values at least two times kT. Further, the contribution of higher order terms, B_q^k, to the overall crystal field are typically ignored and are usually important in low symmetry systems.- Secondly, Bleaney assumed that the lanthanide ion is a point charge and that relaxation is instantaneous. However it is more appropriate to consider the f electron distribution models which show that some Ln(III) ions possess prolate electron distributions whilst others have oblate electron distributions.[94]

- Thirdly, Bleaney assumed that the position of the principal magnetic axis doesn't vary across the lanthanide series. Sessoli et al.[95] demonstrated that the principal axis in complexes of **[Ln.DOTA]**$^-$ changes position across the lanthanide series. The principal axis approximately aligns with the C_4 axis for lanthanide ions with a prolate electron distribution and the principal axis rotates by up to 90° from Tb(III) to Yb(III). It must be noted that the measurements were conducted at very low temperature (2K) in the solid state so these observations may not transfer to solution behaviour at 298K.

- Finally, it is assumed that J is a good quantum number to define the spin-orbit coupling observed in lanthanide systems; J is used to determine the Bleaney constants (C_J). Russell-Saunders coupling to determine J might not always be appropriate for systems were the spin-orbit coupling energies are of the same order as the ligand field energies; these cases require the use of J mixing instead of Russell-Saunders coupling.

Despite the limitations of the Bleaney theory as noted above it remains an effective tool for rationalising the behaviour of cyclen based **DOTA**-tetraamide Yb(III) complexes as shown by Blackburn et al.[96, 97]

1.7 Isomers of Ln(III) complexes

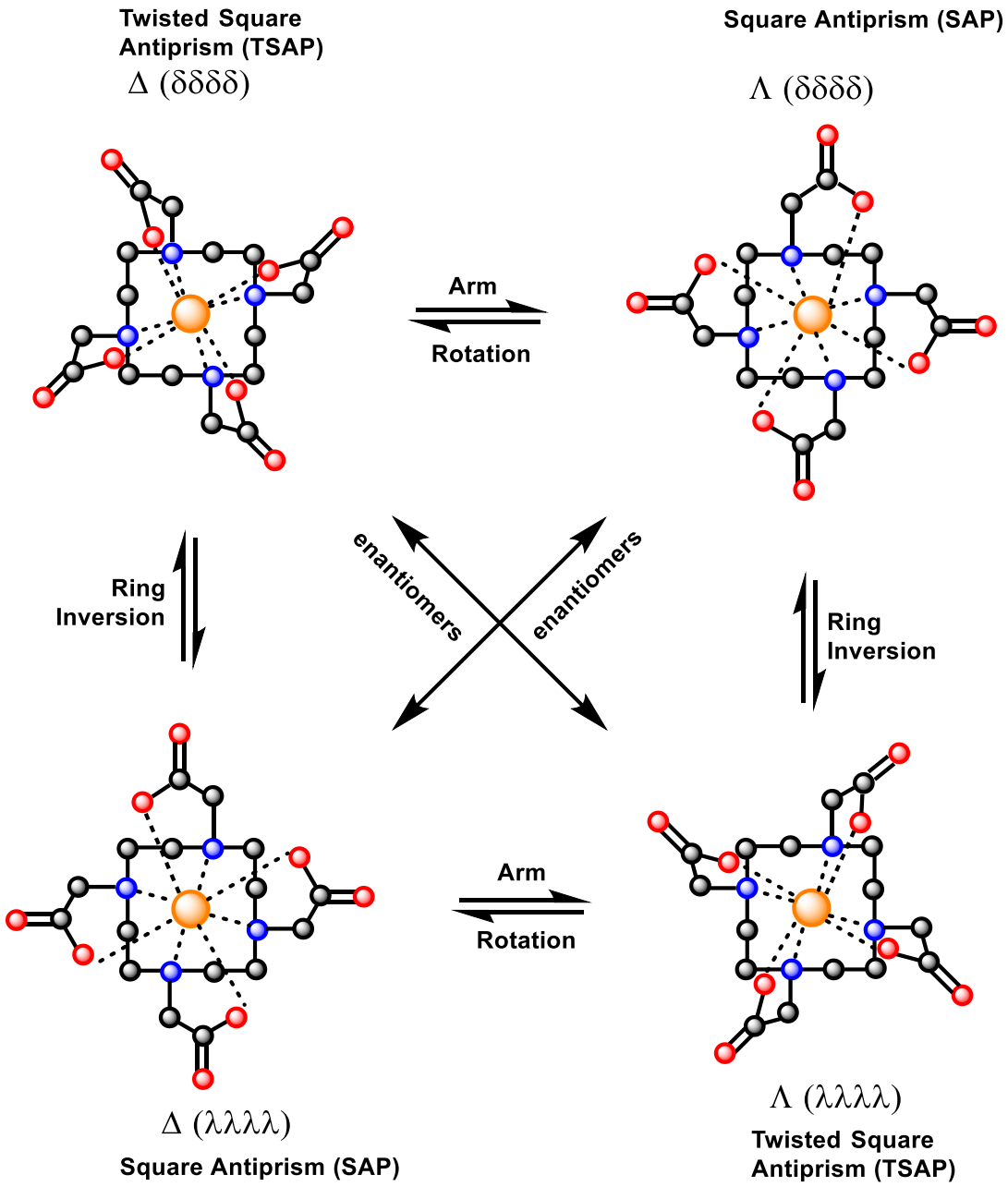


Figure 1. 13 Schematic diagram showing the possible isomers of **[Ln.DOTA]**$^{-}$ complexes.

In the solid state, Ln(III) complexes of **DOTA** and its derivatives generally contain four nitrogen donors in the basal plane of a square antiprism defined by four coplanar

oxygen donors forming the opposite and parallel face of the prism.[98] The two possible geometries are defined by the twist angle between the N_4 and O_4 planes; SAP with a twist angle of ca. 40° and TSAP with a twist angle of ca. 30° (Figure 1. 13). In the solid state **[Ln.DOTA]**$^-$ complexes (where Ln = Gd, Eu, Y and Ho) have the N_4O_4 environment with a capping H_2O molecule and the twist angle is indicative of the SAP geometry.[92] In solution the isomers can interconvert *via* ring inversion or acetate arm rotation in a single step (between SAP and TSAP diastereomers) or in two steps (between enantiomers). The barrier to interconversion is relatively high so these species are commonly in slow exchange on typical NMR timescales. Commonly in octadentate cyclen systems the SAP isomers dominate for the later lanthanides (Sm(III) to Lu(III)) and TSAP for the earlier lanthanides (La(III) to Pm(III)).[92] Heptadentate ligands such as **DO3A** have a lower barrier to arm rotation which means that the exchange between SAP and TSAP isomers can be fast on the NMR timescale and NMR spectra appear broad.[99] NMR spectroscopy is an excellent tool to determine the structure of lanthanide complexes and in the case of paramagnetic ions nearby nuclei are shifted with respect to their usual positions.[89] In the case of octadentate cyclen systems the most shifted proton will correspond to one of the axial ring protons and considering the solid state structures of **DOTA** species then a greater pseudo-shift contribution is expected for the SAP form as this subtends a smaller angle at the molecular axis. Also the rate of water exchange in the axial coordination site of the lanthanide is strongly dependent on which conformation the structure adopts, it has been shown that the exchange rate is ca. 50 times higher for the TSAP conformer than the SAP isomer.[100]

The NMR spectra of broken symmetry systems (e.g. **DO3A** based systems) are more difficult to analyse; the removal of the axial symmetry means that it is more difficult to

gain information about the ligand field due to the need to invoke higher order crystal field terms (B_q^k) which makes Bleaney analysis difficult. Full assignment of ^{1}H NMR of broken symmetry paramagnetic lanthanide systems isn't trivial, due to the need to use polar coordinates relative to a magnetic axis. However it is possible to discriminate between SAP and TSAP isomers by analogy with axial symmetric systems using the chemical shift range of the four axial cyclen ring protons. Resonances in the region between 25 and 40 ppm for Eu(III) **DO3A** type complexes correspond to the four axial cyclen ring protons and their chemical shift range suggests that the predominant isomer in solutions is SAP. The corresponding protons for the TSAP isomer give rise to less shifted, significantly broader resonances than those observed for SAP.

1.8 Project aims

This work explores the use of kinetically stable lanthanide complexes as responsive probes for anions. The following chapters describe the development of these ideas.

A key requirement in such systems is the development of brightly emissive complexes. We reasoned that this could be achieved by using chromophores that also act as donor groups to the lanthanide. Furthermore, changes to the ligand structure or metal coordination sphere can be exploited to determine analytes: we also set out to explore the fundamental physical properties of lanthanide ions that determine the effectiveness of such approaches.

1.9 References

1. A. J. Bard, R. Parsons and J. Jordan, *Standard Potentials in Aqueous Solution*, Taylor & Francis, 1985.
2. C. A. Barta, K. Sachs-Barrable, J. Jia, K. H. Thompson, K. M. Wasan and C. Orvig, *Dalton Trans.*, 2007, 5019-5030.
3. A. E. Martell and R. M. Smith, *Critical stability constants*, Springer, 1974.
4. R. M. Smith and A. E. Martell, *Sci. Total Environ.*, 1987, **64**, 125-147.
5. W. P. Cacheris, S. K. Nickle and A. D. Sherry, *Inorg. Chem.*, 1987, **26**, 958-960.
6. E. T. Clarke and A. E. Martell, *Inorg. Chim. Acta*, 1991, **190**, 37-46.
7. E. Constable, *Coordination chemistry of macrocyclic compounds*, Oxford University Press, 1999.
8. M. F. Loncin, J. F. Desreux and E. Merciny, *Inorg. Chem.*, 1986, **25**, 2646-2648.
9. C. D. Edlin, S. Faulkner, D. Parker, M. P. Wilkinson, M. Woods, J. Lin, E. Lasri, F. Neth and M. Port, *New J. Chem.*, 1998, **22**, 1359-1364.
10. A. D. Sherry, P. Caravan and R. E. Lenkinski, *J. Magn. Reson. Imaging*, 2009, **30**, 1240-1248.
11. L. Sarka, L. Burai and E. Brucher, *Chem. Eur. J.*, 2000, **6**, 719-724.
12. E. Toth, R. Kiraly, J. Platzek, B. Raduchel and E. Brucher, *Inorg. Chim. Acta*, 1996, **249**, 191-199.
13. S. Faulkner and O. A. Blackburn, in *The Chemistry of Molecular Imaging*, John Wiley & Sons, Inc, 2014, pp. 179-197.
14. J.-M. Idee, M. Port, I. Raynal, M. Schaefer, S. Le Greneur and C. Corot, *Fundam. Clin. Pharmacol.*, 2006, **20**, 563-576.
15. L. Sarka, L. Burai, R. Kiraly, L. Zekany and E. Brucher, *J. Inorg. Biochem.*, 2002, **91**, 320-326.
16. S. Laurent, L. V. Elst and R. N. Muller, *Contrast Media Mol. Imaging*, 2006, **1**, 128-137.
17. Z. Baranyai, Z. Palinkas, F. Uggeri, A. Maiocchi, S. Aime and E. Bruecher, *Chem. Eur. J.*, 2012, **18**, 16426-16435.
18. M. Polasek and P. Caravan, *Inorg. Chem.*, 2013, **52**, 4084-4096.
19. T. V. Usha Gangan and M. L. P. Reddy, *Dalton Trans.*, 2015, **44**, 15924-15937.
20. V. Divya, R. O. Freire and M. L. P. Reddy, *Dalton Trans.*, 2011, **40**, 3257-3268.
21. P. He, H. H. Wang, S. G. Liu, J. X. Shi, G. Wang and M. L. Gong, *Inorg. Chem.*, 2009, **48**, 11382-11387.
22. K. Binnemans, in *Handbook on the Physics and Chemistry of Rare Earths, Vol 35*, eds. K. A. Gschneidner, J. C. G. Bunzli and V. K. Pecharsky, 2005, vol. 35, pp. 107-272.
23. R. E. Rondeau and R. E. Sievers, *J. Am. Chem. Soc.*, 1971, **93**, 1522-&.
24. N. Sabbatini, S. Dellonte, M. Ciano, A. Bonazzi and V. Balzani, *Chem. Phys. Lett.*, 1984, **107**, 212-216.
25. N. Sabbatini, S. Perathoner, G. Lattanzi, S. Dellonte and V. Balzani, *J. Phys. Chem.*, 1987, **91**, 6136-6139.
26. B. Alpha, J. M. Lehn and G. Mathis, *Angew. Chem. Int. Ed.*, 1987, **26**, 266-267.
27. L. Prodi, M. Maestri, V. Balzani, J. M. Lehn and C. Roth, *Chem. Phys. Lett.*, 1991, **180**, 45-50.
28. J. Wahsner and M. Seitz, *Inorg. Chem.*, 2015, **54**, 9681-9683.
29. H. Autiero, H. Bazin and G. Mathis, *Journal*, 2006.
30. J. M. Zwier, H. Bazin, L. Lamarque and G. Mathis, *Inorg. Chem.*, 2014, **53**, 1854-1866.
31. G. Liu and B. Jacquier, *Spectroscopic Properties of Rare Earths in Optical Materials*, Springer Berlin Heidelberg, 2006.
32. J. C. G. Bunzli and C. Piguet, *Chem. Soc. Rev.*, 2005, **34**, 1048-1077.
33. S. Faulkner, S. J. A. Pope and B. P. Burton-Pye, *Appl. Spectrosc. Rev.*, 2005, **40**, 1-31.
34. J.-C. G. Bunzli, *Coord. Chem. Rev.*, 2015, **293**, 19-47.
35. S. V. Eliseeva and J.-C. G. Buenzli, *Chem. Soc. Rev.*, 2010, **39**, 189-227.
36. C. K. Jorgensen and B. R. Judd, *Mol. Phys.*, 1964, **8**, 281-&.
37. B. R. Judd, *J. Chem. Phys.*, 1966, **44**, 839-&.
38. B. R. Judd, *Physical Review*, 1962, **127**, 750-&.
39. G. S. Ofelt, *J. Chem. Phys.*, 1962, **37**, 511-&.
40. A. F. Kirby, D. Foster and F. S. Richardson, *Chem. Phys. Lett.*, 1983, **95**, 507-512.
41. A. F. Kirby and F. S. Richardson, *J. Phys. Chem.*, 1983, **87**, 2544-2556.
42. F. S. Richardson, *Chem. Rev.*, 1982, **82**, 541-552.

43. S. Pandya, J. Yu and D. Parker, *Dalton Trans.*, 2006, 2757-2766.
44. S. Weissman, *J. Chem. Phys.*, 1942, **10**, 214.
45. G. A. Crosby, R. M. Alire and R. E. Whan, *J. Chem. Phys.*, 1961, **34**, 743-&.
46. G. A. Crosby, R. E. Whan and J. J. Freeman, *J. Phys. Chem.*, 1962, **66**, 2493-&.
47. R. E. Whan and G. A. Crosby, *J. Mol. Spectrosc.*, 1962, **8**, 315-&.
48. T. J. Sorensen, O. A. Blackburn, M. Tropiano and S. Faulkner, *Chem. Phys. Lett.*, 2012, **541**, 16-20.
49. L.-O. Palsson, R. Pal, B. S. Murray, D. Parker and A. Beeby, *Dalton Trans.*, 2007, 5726-5734.
50. A. Beeby, L. M. Bushby, D. Maffeo and J. A. G. Williams, *J. Chem. Soc., Dalton Trans.*, 2002, 48-54.
51. A. D'Aleo, F. Pointillart, L. Ouahab, C. Andraud and O. Maury, *Coord. Chem. Rev.*, 2012, **256**, 1604-1620.
52. Kleinerm.M, *J. Chem. Phys.*, 1969, **51**, 2370-&.
53. C. Allain and S. Faulkner, *Future Med. Chem.*, 2010, **2**, 339-350.
54. D. Parker, *Coord. Chem. Rev.*, 2000, **205**, 109-130.
55. A. Beeby, S. Faulkner and J. A. G. Williams, *J. Chem. Soc., Dalton Trans.*, 2002, 1918-1922.
56. S. Faulkner, L. S. Natrajan, W. S. Perry and D. Sykes, *Dalton Trans.*, 2009, 3890-3899.
57. W. D. Horrocks, J. P. Bolender, W. D. Smith and R. M. Supkowski, *J. Am. Chem. Soc.*, 1997, **119**, 5972-5973.
58. M. Latva, H. Takalo, V. M. Mukkala, C. Matachescu, J. C. RodriguezUbis and J. Kankare, *J. Lumin.*, 1997, **75**, 149-169.
59. S. Quici, M. Cavazzini, M. C. Raffo, M. Botta, G. B. Giovenzana, B. Ventura, G. Accorsi and F. Barigelletti, *Inorg. Chim. Acta*, 2007, **360**, 2549-2557.
60. A. Dadabhoy, S. Faulkner and P. G. Sammes, *J. Chem. Soc., Perkin Trans. 2*, 2002, 348-357.
61. M. Tropiano, N. L. Kilah, M. Morten, H. Rahman, J. J. Davis, P. D. Beer and S. Faulkner, *J. Am. Chem. Soc.*, 2011, **133**, 11847-11849.
62. T. Koullourou, L. S. Natrajan, H. Bhavsar, S. J. A. Pope, J. Feng, J. Narvainen, R. Shaw, E. Scales, R. Kauppinen, A. M. Kenwright and S. Faulkner, *J. Am. Chem. Soc.*, 2008, **130**, 2178-+.
63. O. J. Stacey, A. J. Amoroso, J. A. Platts, P. N. Horton, S. J. Coles, D. Lloyd, C. F. Williams, A. J. Hayes, J. J. Dunsford and S. J. A. Pope, *Chem. Commun.*, 2015, **51**, 12305-12308.
64. A. Beeby, I. M. Clarkson, R. S. Dickins, S. Faulkner, D. Parker, L. Royle, A. S. de Sousa, J. A. G. Williams and M. Woods, *J. Chem. Soc., Perkin Trans. 2*, 1999, 493-503.
65. Y. Haas and G. Stein, *J. Phys. Chem.*, 1972, **76**, 1093-&.
66. J. L. Kropp and M. W. Windsor, *J. Chem. Phys.*, 1965, **42**, 1599-&.
67. G.-L. Law, R. Pal, L. O. Palsson, D. Parker and K.-L. Wong, *Chem. Commun.*, 2009, 7321-7323.
68. R. Hueting, M. Tropiano and S. Faulkner, *RSC Adv.*, 2014, **4**, 44162-44165.
69. A. Watkis, R. Hueting, T. J. Sorensen, M. Tropiano and S. Faulkner, *Chem. Commun.*, 2015, **51**, 15633-15636.
70. T. Forster, *Discuss. Faraday Soc.*, 1959, 7-17.
71. D. L. Dexter, *J. Chem. Phys.*, 1953, **21**, 836-850.
72. S. J. Butler and D. Parker, *Chem. Soc. Rev.*, 2013, **42**, 1652-1666.
73. R. S. Dickins, T. Gunnlaugsson, D. Parker and R. D. Peacock, *Chem. Commun.*, 1998, 1643-1644.
74. R. Carr, L. Di Bari, S. Lo Piano, D. Parker, R. D. Peacock and J. M. Sanderson, *Dalton Trans.*, 2012, **41**, 13154-13158.
75. M. P. Bailey, B. F. Rocks and C. Riley, *Anal. Chim. Acta*, 1987, **201**, 335-338.
76. D. Parker, P. K. Senanayake and J. A. G. Williams, *J. Chem. Soc., Perkin Trans. 2*, 1998, 2129-2139.
77. D. G. Smith, B. K. McMahon, R. Pal and D. Parker, *Chem. Commun.*, 2012, **48**, 8520-8522.
78. S. J. A. Pope and R. H. Laye, *Dalton Trans.*, 2006, 3108-3113.
79. M. Tropiano and S. Faulkner, *Chem. Commun.*, 2014, **50**, 4696-4698.
80. A. R. Lippert, T. Gschneidtner and C. J. Chang, *Chem. Commun.*, 2010, **46**, 7510-7512.
81. S. J. A. Pope, B. P. Burton-Pye, R. Berridge, T. Khan, P. J. Skabara and S. Faulkner, *Dalton Trans.*, 2006, 2907-2912.
82. S. Faulkner, B. P. Burton-Pye, T. Khan, L. R. Martin, S. D. Wray and P. J. Skabara, *Chem. Commun.*, 2002, 1668-1669.

83. S. J. A. Pope, B. J. Coe, S. Faulkner, E. V. Bichenkova, X. Yu and K. T. Douglas, *J. Am. Chem. Soc.*, 2004, **126**, 9490-9491.
84. J. A. Tilney, T. J. Sorensen, B. P. Burton-Pye and S. Faulkner, *Dalton Trans.*, 2011, **40**, 12063-12066.
85. G.-L. Davies, A. Brown, O. Blackburn, M. Tropiano, S. Faulkner, P. D. Beer and J. J. Davis, *Chem. Commun.*, 2015, **51**, 2918-2920.
86. L. R. Hill, O. A. Blackburn, M. W. Jones, M. Tropiano, T. J. Sorensen and S. Faulkner, *Dalton Trans.*, 2013, **42**, 16255-16258.
87. M. Tropiano, O. A. Blackburn, J. A. Tilney, L. R. Hill, M. P. Placidi, R. J. Aarons, D. Sykes, M. W. Jones, A. M. Kenwright, J. S. Snaith, T. J. Sorensen and S. Faulkner, *Chem. Eur. J.*, 2013, **19**, 16566-16571.
88. Y. Bretonniere, M. J. Cann, D. Parker and R. Slater, *Chem. Commun.*, 2002, 1930-1931.
89. B. Bleaney, *J. Magn. Reson.*, 1972, **8**, 91-&.
90. J. A. Peters, J. Huskens and D. J. Raber, *Prog. Nucl. Magn. Reson. Spectrosc.*, 1996, **28**, 283-350.
91. C. C. Bryden, C. N. Reilley and J. F. Desreux, *Anal. Chem.*, 1981, **53**, 1418-1425.
92. S. Aime, M. Botta, M. Fasano, M. P. M. Marques, C. Geraldes, D. Pubanz and A. E. Merbach, *Inorg. Chem.*, 1997, **36**, 2059-2068.
93. A. M. Funk, K.-L. N. A. Finney, P. Harvey, A. M. Kenwright, E. R. Neil, N. J. Rogers, P. Kanthi Senanayake and D. Parker, *Chem. Sci.*, 2015.
94. J. D. Rinehart and J. R. Long, *Chem. Sci.*, 2011, **2**, 2078-2085.
95. M.-E. Boulon, G. Cucinotta, J. Luzon, C. Degl'Innocenti, M. Perfetti, K. Bernot, G. Calvez, A. Caneschi and R. Sessoli, *Angew. Chem., Int. Ed.*, 2013, **52**, 350-354.
96. O. A. Blackburn, N. F. Chilton, K. Keller, C. E. Tait, W. K. Myers, E. J. L. McInnes, A. M. Kenwright, P. D. Beer, C. R. Timmel and S. Faulkner, *Angew. Chem., Int. Ed.*, 2015, **54**, 10783-10786.
97. O. A. Blackburn, A. M. Kenwright, P. D. Beer and S. Faulkner, *Dalton Trans.*, 2015.
98. S. Aime, M. Botta and G. Ermondi, *Inorg. Chem.*, 1992, **31**, 4291-4299.
99. M. P. Placidi, L. S. Natrajan, D. Sykes, A. M. Kenwright and S. Faulkner, *Helv. Chim. Acta*, 2009, **92**, 2427-2438.
100. S. Aime, A. Barge, M. Botta, A. S. De Sousa and D. Parker, *Angew. Chem., Int. Ed.*, 1998, **37**, 2673-2675.

2 Achieving high luminescence quantum yields with arylacylDO3A complexes[i]

2.1 Introduction

The unique properties of lanthanide ions have led to lanthanide complexes being used in a variety of imaging techniques such a magnetic resonance imaging (MRI)[1-3] and optical imaging.[4-6] The large Stokes' shifts, characteristic narrow emission lines and long emission lifetimes (μs-ms) which originate from the forbidden nature of *f-f* transitions make lanthanide complexes ideal candidates for applications in optical imaging. Long-lived lanthanide emission allows its selective detection in time-gated techniques which means that light scattering and interference from endogenous fluorescence can be avoided. To exploit these properties fully, the inherently inefficient direct excitation of lanthanides needs to be overcome by incorporating a sensitising chromophore on the ligand scaffold. Such chromophores must have high absorptivity with appropriate energy levels to allow efficient energy transfer to the lanthanide. Typically, organic chromophores are exploited due to them having appropriate energy to sensitise Eu(III) and Tb(III) which are commonly employed in luminescence imaging and bioassay techniques.

Figure 2. 1 shows the typical energy transfer cascade in sensitised lanthanide emission. The sensitiser chromophore absorbs a photon of appropriate energy (k_{abs}) to form an excited singlet state localised on the sensitiser (S_1-Ln), this then undergoes intersystem crossing (k_{ISC}) to produce an excited triplet state localised on the sensitiser (T_1-Ln). At this point, energy transfer (k_{ET}) takes place from the sensitiser triplet state to the

[i] Aspects of my work described in this chapter have already been published: see J. D. Routledge, M. W. Jones, S. Faulkner and M. Tropiano, *Inorg. Chem.*, 2015, **54**, 3337-3345.

lanthanide acceptor state (S_0-Ln*), followed by lanthanide centred emission (k_{em}). Each of the excited states in the pathway are prone to quenching; the S_1 sensitiser state can be quenched by fluorescence (k_{FI}), the T_1 sensitiser state can be quenched through collisional quenching with $^3O_2$ ($k_q[O_2]$) and the lanthanide excited state is prone to quenching by vibrational energy transfer to high frequency oscillators ($k_q[XH]$) e.g. OH and NH. In order to achieve the highest possible quantum yield k_{ISC} and k_{ET} need to be maximised whilst k_{FI}, $k_q[O_2]$ and $k_q[XH]$ need to be minimised. Furthermore, in order to maximise the brightness of the complexes the extinction coefficient of the sensitiser needs to be large.

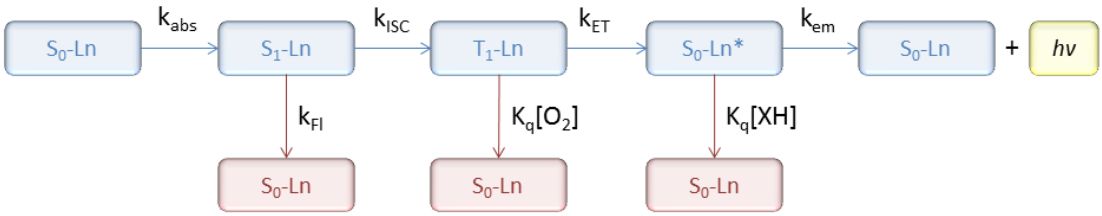


Figure 2. 1 Common energy transfer processes in sensitised lanthanide emission.

The first prerequisite for achieving high quantum yields in water is that the lanthanide is shielded from its environment in order to minimise the non-radiative deactivation of the lanthanide emissive state by high frequency solvent oscillators. It is also necessary that there is a high sensitisation efficiency which can be achieved by tuning the energy overlap between the states involved in the energy transfer cascade and by ensuring the close proximity of the sensitising group to the lanthanide. In the latter case, chromophores that are linked directly to the lanthanide have an enormous advantage, since energy transfer is facilitated by a Dexter exchange mechanism thanks to increased orbital overlap, as well as by proximity. In terms of relative energy, there is a clear correlation between the energy gap between the sensitising chromophore triplet

state and the emissive $^5D_0$ state of Eu(III), the optimal energy level of the sensitising chromophore triplet state is ca. 2000-5000 cm^{-1} above the Eu(III) $^5D_0$ state.[7] If this energy difference is larger than 5000 cm^{-1}, there will be poor overlap resulting in inefficient energy transfer, however if this gap is too small then thermally populated back energy transfer from the lanthanide excited state to the antenna centred state can occur, thus quenching the Eu(III) emissive state. Even with appropriate energy gaps, it is worth noting that an "ideal" energy gap still represents a substantial difference that needs to be bridged. This is generally referred to as phonon assistance, essentially meaning that the vibrational manifold of the ligand and solvent can be used to dissipate surplus energy. This has the unusual consequence of meaning that local oscillators in a bound water molecule can assist energy transfer, thereby increasing the efficiency of the overall process, while also increasing the efficiency of non-radiative quenching of the lanthanide excited state (which obviously reduces the efficiency of the overall process).

The optimisation of the sensitiser-lanthanide energy gap translates into using chromophores that have long absorption wavelengths (ca. 350 nm), this is advantageous for applications such as fluorescence light microscopy that utilise glass optics. For use *in vivo* it is essential that the lanthanide complex has high kinetic and thermodynamic stability as well as it being highly water soluble, this translates as using macrocyclic ligand scaffolds such as **DO3A** to encapsulate the lanthanide.

There are only a few examples of highly emissive Eu(III) complexes that can be excited in the spectral window consistent with the use of glass microscope optics (> 350 nm).[8, 9] Faulkner et al.[10, 11] reported the use of acridone (e.g. **2.1**, Figure 2. 2) to sensitise Eu(III) emission with excitation well above 400 nm. A modest quantum yield of 1.4%

was observed, which is presumably due to the relatively high energy of the acridone triplet state (21500 cm^{-1}) reducing the efficiency of energy transfer, the fact that Eu(III) has two bound solvent molecules and the large distance between the chromophore and Eu(III).

More recently Parker et al.[6, 12-14] have reported a variety of highly emissive Eu(III) compounds based on the triazacyclononane macrocycle (e.g. **2.2**, Figure 2. 2) which contain strongly absorbing pyridine based alkynyl chromophores on the ligand scaffold. The extended conjugation of the sensitising group leads to long absorption wavelengths with high absorptivities. The use of pyridyl carboxylate chromophores allows the exclusion of solvent from the Eu(III) coordination sphere as well as affording a complex with high rigidity; these reduce quenching of the Eu(III) emissive state thus aiding energy transfer efficiency and increasing the quantum yield. The modular synthesis of this class of species allows for easy modification of the aromatic R group to tune absorption wavelength, solubility and cellular uptake.[6]

A similar approach to that used in this chapter has been previously employed although lower emission quantum yields were observed (e.g. **2.3**, Figure 2. 2)[15] This complex fulfils many requirements to produce lanthanide complexes with high quantum yields;

- It has broken symmetry which reduces the natural lanthanide radiation lifetime, τ_{rad}, and hence maximises τ_{obs}/τ_{rad}.

- The sensitising chromophore is proximal to the lanthanide centre which will optimise energy transfer and minimise alternative pathways for quenching the ligand excited states.

- The sensitising chromophore has high extinction coefficients and absorption occurs at long wavelengths.

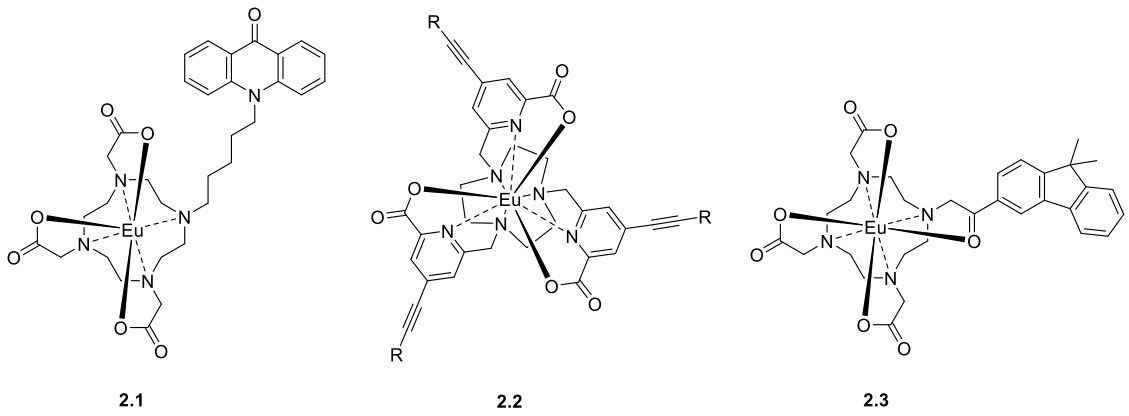


Figure 2. 2 Examples of highly emissive lanthanide complexes capable of being excited in the near visible region.

This chapter presents the synthesis and study of highly emissive, kinetically stable Eu(III) complexes based on the **DO3A** ligand scaffold. Aryl ketones were chosen as sensitiser chromophores due to their small singlet-triplet energy gap affording long excitation wavelengths whilst allowing triplet states of high enough energies to sensitise lanthanide emission. Further, aryl ketones offer a high yield of triplet formation and the potential to directly coordinate to the lanthanide centre through the ketone oxygen aiding sensitisation efficiency and reducing the number of bound solvent molecules. Previous work by Bushby et al.[16] confirmed the ability of aryl ketone chromophores to act as sensitisers for lanthanide emission so we reasoned that fine tuning of the chromophore could lead to enhanced luminescence properties.

2.2 Synthesis and characterisation

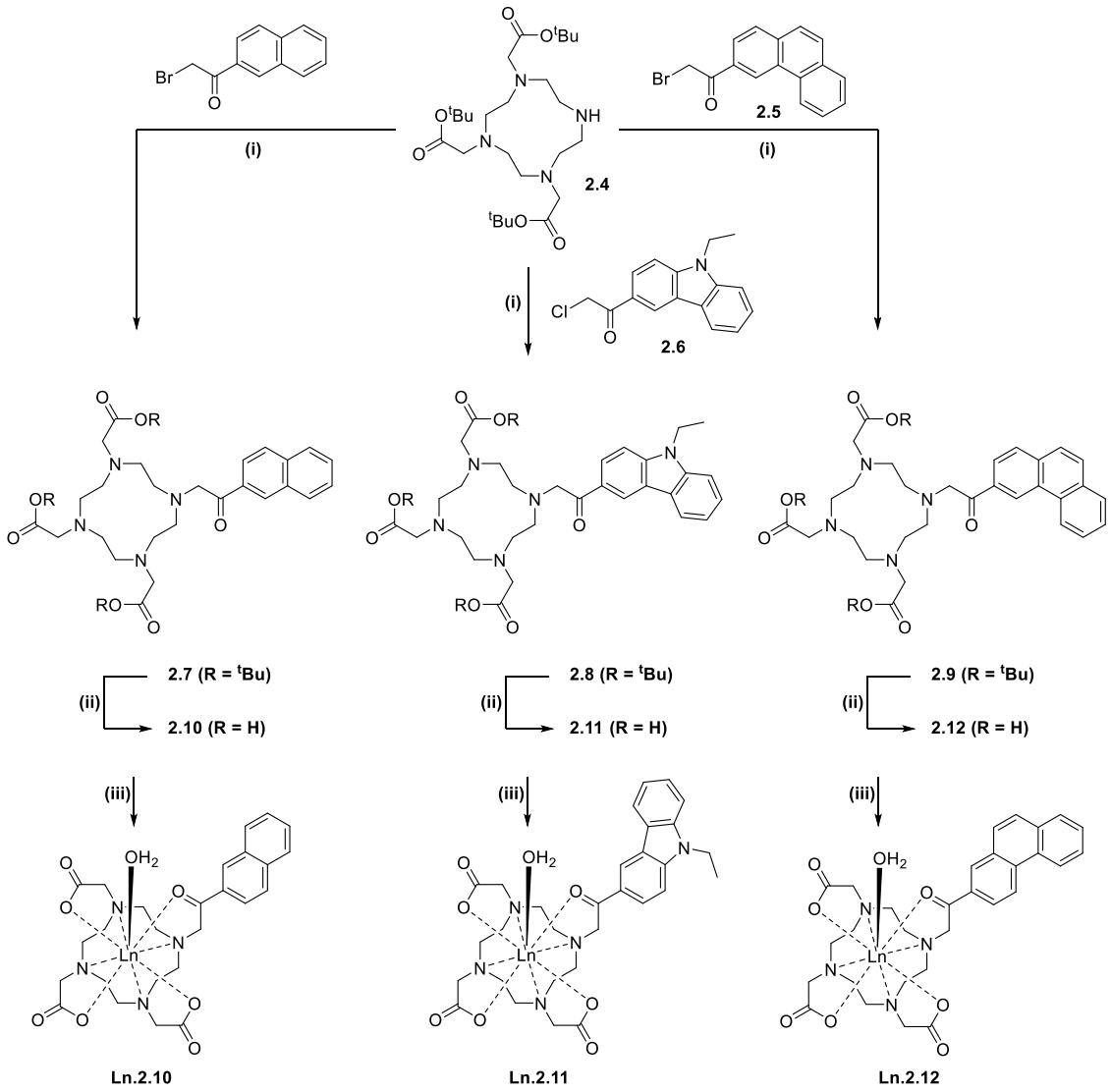


Figure 2. 3 Preparation of arylacylDO3A lanthanide complexes. (i) K_2CO_3, MeCN, RT, 18h; (ii) TFA, DCM, RT, 2d; (iii) $Ln(OTf)_3$, MeOH, 60°C, 2d.

The targets chosen, **Ln.2.10**, **Ln.2.11** and **Ln.2.12**, all combine an aryl ketone that is bound directly to the metal centre with an acylDO3A lanthanide binding domain thus fulfilling the need for an effective chromophore in direct proximity to the metal centre, and ensuring broken symmetry (*vide supra*). Synthesis of **2.6** was achieved by Friedel-Crafts acylation of carbazole using $AlCl_3$ as a Lewis acid catalyst; purification by silica gel column chromatography gave the desired species. Crystals were formed upon slow evaporation of a hexane:ethyl acetate solution, and the structure solved and

analysed by Dr. Michael Jones (Figure 2. 4). **2.5** was synthesised by the bromination of 3-acetylphenanthrene using liquid bromine and was subsequently purified by silica gel column chromatography whilst 2-bromo-2'-acetonaphthone is commercially available and was used without further purification.

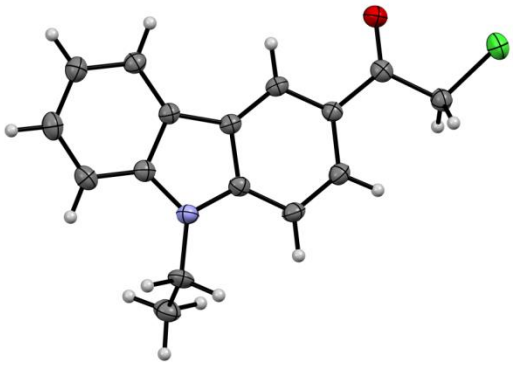


Figure 2. 4 ORTEP representation of the X-ray crystal structure of **2.6** with thermal ellipsoids at 50% probability.

The pro-ligands were synthesised by the alkylation of triester, **2.4** using standard literature conditions, these were isolated after purification by silica gel column chromatography. Subsequent deprotection of the *t*-butyl groups was achieved using TFA in DCM giving the desired ligands in quantitative yield. Lanthanide complexes were obtained by stirring the ligand and the corresponding lanthanide triflate salt in methanol at 60°C using a small excess of the lanthanide salt. Excess lanthanide was removed in the reaction work up by raising the pH (≈10) and precipitating it as its insoluble hydroxide which was removed by centrifuging and filtration. Semi-preparative HPLC was carried out on all Eu(III) complexes to obtain analytically pure samples for photophysical studies. Figure 2. 5 shows the accurate mass spectra obtained for these three europium complexes.

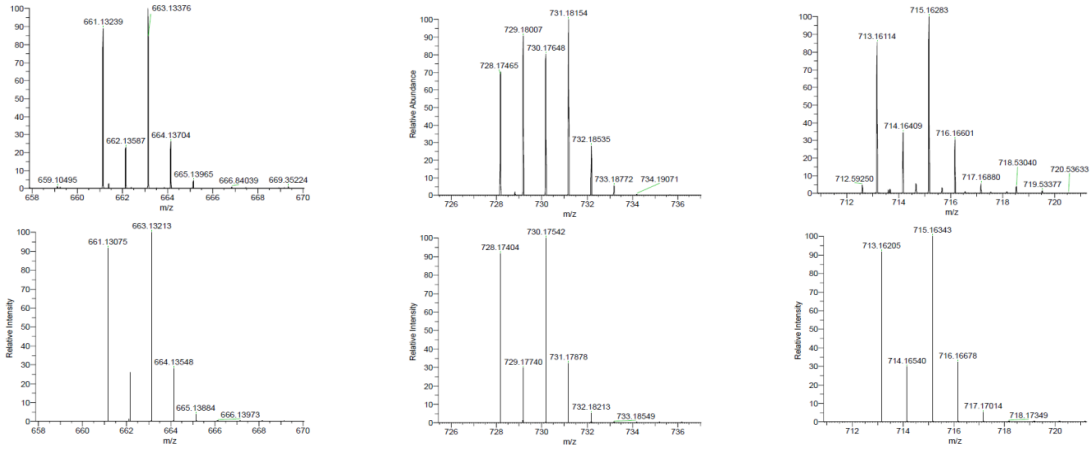


Figure 2. 5 Experimental (Top) and Theoretical (Bottom) high resolution mass spectra of **Eu.2.10** (left), **Eu.2.11** (middle) and **Eu.2.12** (right) as their $[M+H]^+$ adducts.

2.2.1 NMR characterisation

The ^{1}H NMR of the Eu(III) and Yb(III) complexes are shown in Figure 2. 6. The sharpness of the spectra indicates that the ketone oxygen atom is coordinating to the lanthanide centre, making it eight coordinate with the remaining axial sight occupied by a solvent molecule. The resonances in the region between 25 and 40 ppm for the Eu(III) complexes correspond to the four axial cyclen ring protons and their chemical shift range suggests that the predominant isomer in solutions is SAP. Trace amounts of the TSAP isomers are also present in solution and give rise to less shifted, significantly broader resonances than those observed for SAP. By contrast, only the SAP isomers are observed for the Yb(III) analogues which is similar behaviour to that reported for **[Ln.DOTA]**$^-$ complexes.[17]

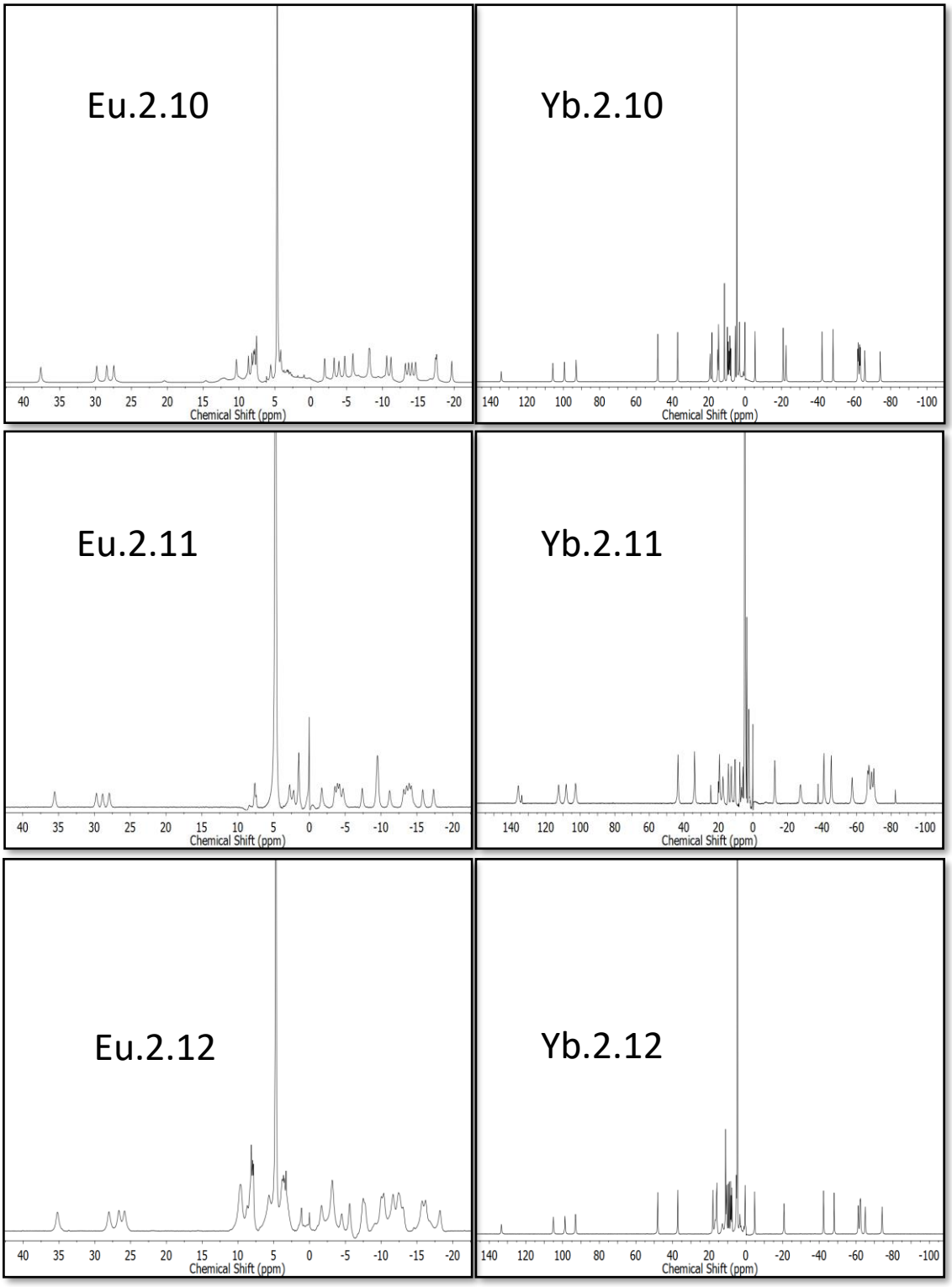


Figure 2. 6 ^{1}H NMR spectra of the paramagnetic complexes studied (298 K, D_2O, pH < 7).

2.2.2 Photophysical properties

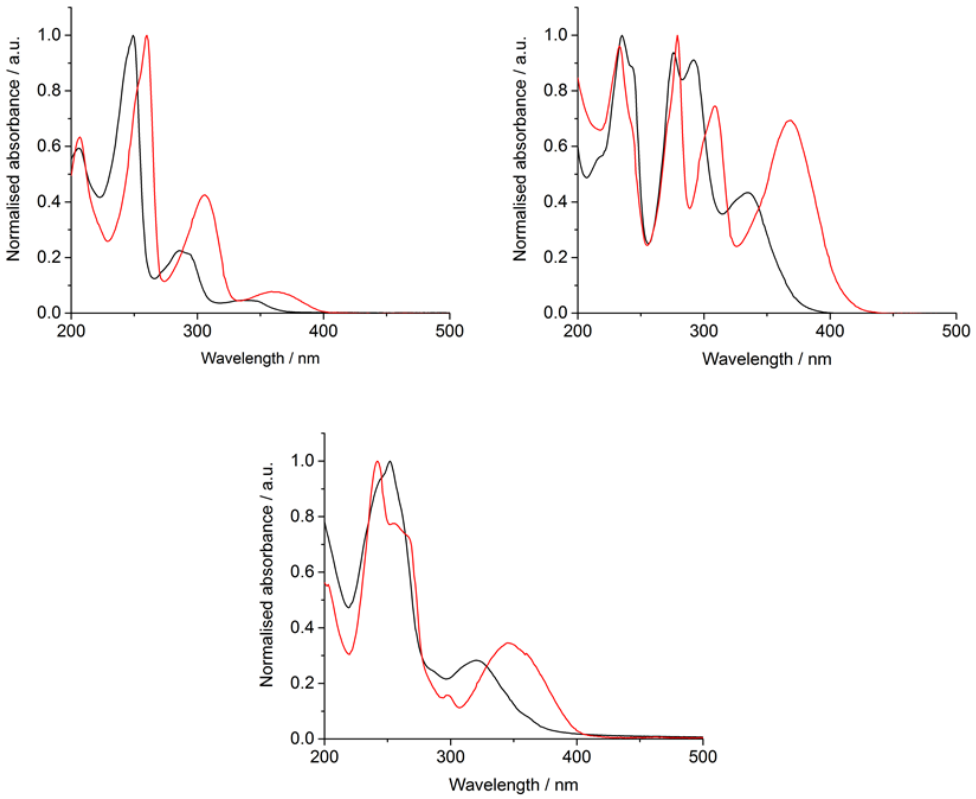


Figure 2. 7 Comparison of the UV-Vis absorption spectra of **Eu.2.10** (top left), **Eu.2.11** (top right) and **Eu.2.12** (bottom) with the spectra of their corresponding ligands recorded in H_2O. Ligand spectra (black) and complex spectra (red).

The UV-Vis absorption spectra of the ligands **2.10**, **2.11** and **2.12** along with their corresponding Eu(III) complexes are shown in Figure 2. 7. Upon complexation most of the absorption bands in all complexes are red shifted; this phenomenon is characteristic of the bands having significant charge transfer (CT) character and is indicative of a substantial interaction between the lanthanide ion and the carbonyl group on the sensitising chromophore. The presence of the Ln(III) ion in the macrocyclic cavity increases the polarisation of the carbonyl group which in turn stabilises the CT excited states, lowering their energy.

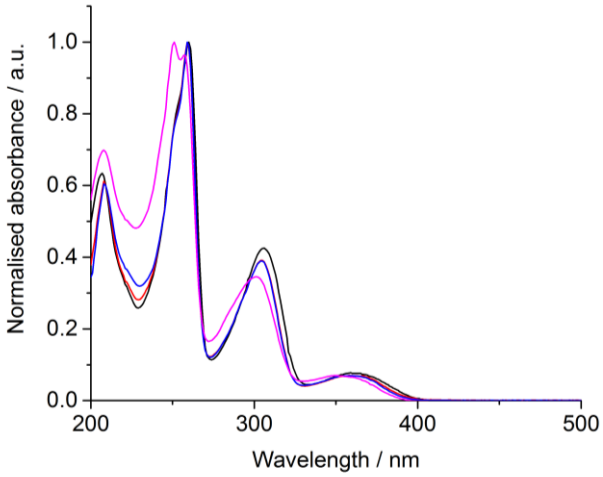


Figure 2. 8 UV-Vis absorption spectra of **Eu.2.10** in solvents of different polarity [H_2O (black), MeCN (purple), MeOH (red), EtOH (blue)].

Figure 2. 8 shows the UV-Vis absorption spectra of **Eu.2.10** in solvents of different polarities; due to the nature of lanthanide **DO3A** complexes only polar solvents were used in the study. The absorption band maxima of the two longest wavelength bands are red shifted upon the increase in solvent polarity, this is known as positive solvatochromism. This shift in wavelength is due to differences in the solvation energy of the ground and excited states as the solvent is changed. Typically, more polar solvents stabilise a more polar excited state - causing the wavelength of absorption to increase. The observation of solvent dependent behaviour of the absorption bands confirms their CT character.

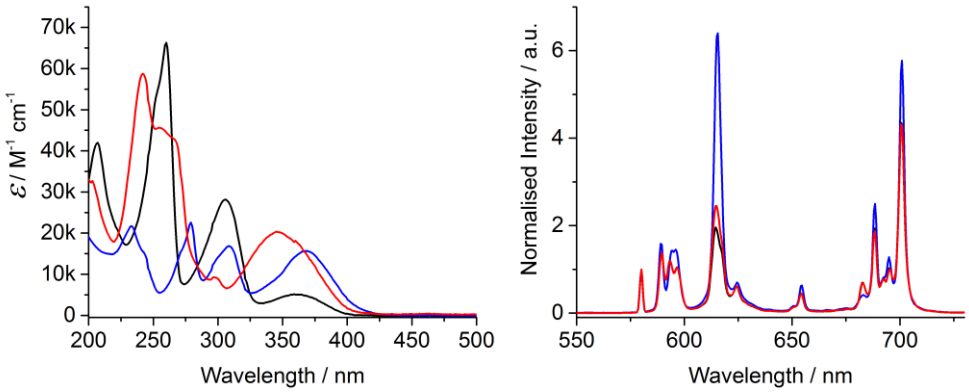


Figure 2. 9 UV-Vis absorption (left) and emission (right) spectra of **Eu.2.10** (black), **Eu.2.11** (blue) and **Eu.2.12** (red) upon excitation into the lowest energy absorption band in H_2O. Emission spectra are normalised to the intensity of the ΔJ=0 band.

The UV-Vis absorption and emission spectra of **Eu.2.10**, **Eu.2.11** and **Eu.2.12** are shown in Figure 2. 9. All complexes show significant absorption in the UV region with the lowest energy bands above 340 nm in all cases. The molar absorption coefficients for the lowest energy bands (Table 2. 1) are large, suggesting that these transitions are π-π* in nature with the expected n-π* bands presumably hidden under the more intense π-π* transitions. All species show absorption bands that extend into the visible region with **Eu.2.11** showing significant absorption in this region.

All of the Eu(III) compounds displayed characteristic emission upon excitation into the lowest energy absorption bands demonstrating that sensitisation is indeed occurring. Measurement of the excited state lifetimes in H_2O and D_2O allowed the determination of the inner sphere hydration number, q, using the modified Horrocks equation:

$$q_{Eu} = 1.2(k_H - k_D - 0.25)$$

Where k_H and k_D are the rates of depopulation of the lanthanide excited state in H_2O and D_2O respectively. In all cases q is close to one, this confirms the octadentate coordination of the ligand to the lanthanide and that only one solvent molecule is bound to the lanthanide. The direct coordination of the sensitiser to the lanthanide

enhances sensitisation efficiency. Taking into account the balance between non-radiative quenching and energy transfer rate, it is generally desirable that the lanthanide is coordinatively saturated to exclude high frequency oscillators from the first coordination sphere to remove this efficient quenching pathway, in this case however bound solvent does not preclude high quantum yields. **Eu.2.10** and **Eu.2.12** have quantum yields of 18% and 16% in H_2O respectively whilst **Eu.2.11** has a significantly smaller quantum yield of 1%. All of these values are significantly increased when measured in D_2O, due to OD oscillators being significantly weaker quenchers of the $^5D_0$ state of Eu(III) than OH oscillators.

Table 2. 1 Photophysical properties of **Eu.2.10**, **Eu.2.11** and **Eu.2.12**.

	Eu.2.10	**Eu.2.11**	**Eu.2.12**
λ_{ex} **/nm**	362	369	346
τ_{H2O} **/ms**[a]	0.58	0.52	0.55
τ_{D2O} **/ms**[a]	1.44	1.32	1.59
q	0.9	1.1	1.1
Φ_{H2O}[b]**/%**	18	1	16
Φ_{D2O}[b]**/%**	48	3	40
ε / M^{-1} cm^{-1}	5100	15600	19600
E_T / cm^{-1}	19900	21300	19500

[a]Uncertainty ±10%. [b]Uncertainty ±15%. All data obtained at 298K (5 < pH < 8).

Good energetic overlap between the donor (sensitiser) and acceptor (lanthanide) is essential to observe strong lanthanide based emission. The energy gap between these states can be determined by measuring the sensitiser centred triplet state and by using the known energy level of the $^5D_0$ state of Eu(III) which is 17200 cm^{-1}. Gd(III) analogues were synthesised to estimate the triplet state localised on the sensitiser.

Gd(III) was chosen as its lowest lying emissive state ($^6P_{7/2}$) lies much higher in energy (31750 cm^{-1}) than the organic sensitiser which prevents ligand to metal energy transfer meaning that any observed luminescence originates exclusively from the organic sensitiser. Another benefit of using Gd(III) is that it promotes the formation of the sensitiser centred triplet state by enhancing spin-orbit coupling whilst not quenching the sensitiser triplet state. The phosphorescence spectra for the Gd(III) complexes are shown in Figure 2. 10. **Gd.2.10** and **Gd.2.12** have similar phosphorescence profiles and the T_1-S_0 bands have similar 0-0 transition energies of 19900 and 19500 cm^{-1} respectively whilst **Gd.2.11** has significantly different profile with the 0-0 transition at 21300 cm^{-1}. It is clear that the energy difference between the $^5D_0$ emissive Eu(III) state and the triplet state located on the sensitiser plays an important role in the efficiency of energy transfer and hence the observed quantum yield. The largest quantum yields observed were for **Eu.2.10** and **Eu.2.12** which have triplet state energy gaps with the emissive $^5D_0$ state of 2700 and 2300 cm^{-1} respectively, the smaller energy difference and smaller quantum yield for **Eu.2.12** is likely due to an increase in back energy transfer from the $^5D_0$ emissive Eu(III) state to the sensitiser triplet state. A significantly larger triplet energy gap of 4100 cm^{-1} was observed for **Eu.2.11**, this corresponds to the lowest quantum yield due to the poor donor acceptor energy overlap meaning energy transfer is inefficient.

The emissive lifetimes of the triplet state localised on the sensitiser were determined to probe the nature of the emissive states. Lifetimes of 40, 5 and 21 ms were found for **Gd.2.10, Gd.2.11** and **Gd.2.12** respectively, this suggests that the phosphorescence occurs from a $^3(n\text{-}\pi^*)$ state for all of the Gd(III) species.[18] Emission from a $^3(\pi\text{-}\pi^*)$ triplet state in a simple aromatic chromophore would be expected to result in much

longer lifetimes - typically of the order of thousands of milliseconds.[19] Due to the weak nature of the $^1(n\text{-}\pi^*)$ absorption then it is likely that absorption occurs through the much stronger $^1(\pi\text{-}\pi^*)$ transition. This state then populates the $^1(n\text{-}\pi^*)$ state on the chromophore where rapid intersystem crossing occurs to the energetically close $^3(\pi\text{-}\pi^*)$ state which subsequently decays to the $^3(n\text{-}\pi^*)$ state. This state represents the lowest point in the triplet manifold, and cannot readily decay to the ground state, except by intersystem crossing (formally forbidden), intermolecular quenching or energy transfer to the lanthanide. In the case of Gd(III), energy transfer to the lanthanide is not thermodynamically feasible (the emissive state for Gd(III) is at 31750 cm^{-1}), and intermolecular quenching is unlikely as a consequence of the use of frozen solutions in these measurements. Intersystem crossing remains as a possible pathway for quenching the excited T_1 state, and will indeed be rendered more likely by the close proximity of the heavy Gd(III) ion causing classical selection rules to break down. Thus the observed short phosphorescence lifetimes are evidence in themselves for the nature of the emissive species.

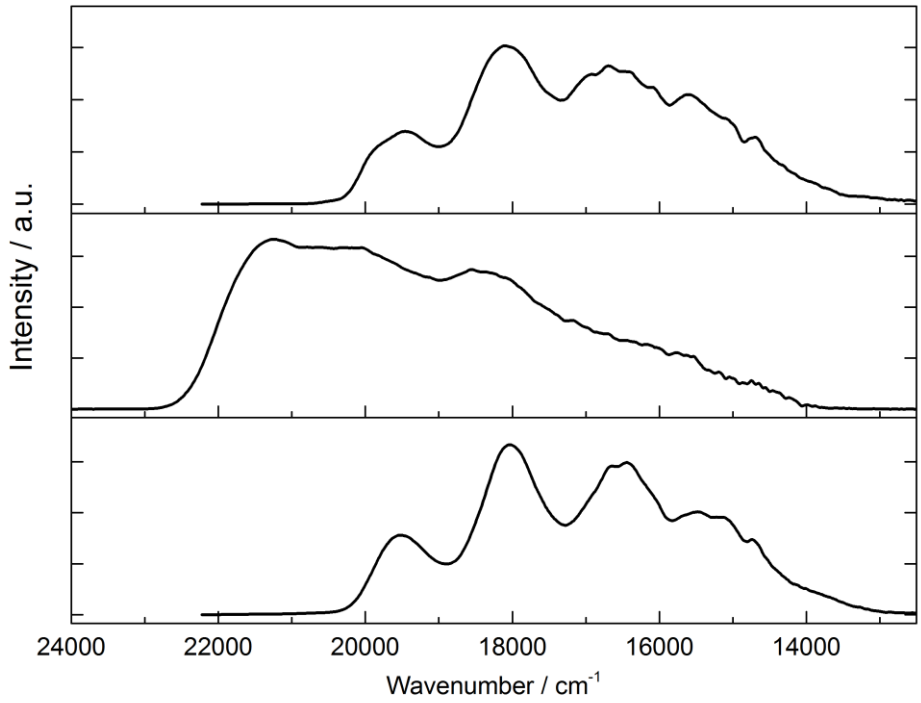


Figure 2. 10 Phosphorescence spectra of **Gd.2.10** (top), **Gd.2.11** (middle) and **Gd.2.12** (bottom) measured at 77K in an EtOH glass (excitation at 360, 370 and 345 nm respectively; delay time 0.5 ms, gate time 2 ms).

Information on the symmetry of Eu(III) can be determined through analysis of the emission spectra of the complexes. The presence of three peaks in the ΔJ = 1 transition is indicative of the Eu(III) ion being in a low symmetry environment. This splitting is similar for **Eu.2.10** and **Eu.2.12** suggesting that the Eu(III) ions have very similar coordination environments and experience a similar ligand field. Only two distinct peaks were observed in the fine structure of the ΔJ = 1 transition for **Eu.2.11** suggesting it experiences a slightly different ligand field which could be due to the strong electron donation ability of the carbazole chromophore altering the strength of the interaction between the Eu(III) ion and the carbonyl group on the sensitising chromophore. This difference in Eu(III) local symmetry is also apparent from the hypersensitive ΔJ = 2 transition, where for **Eu.2.11** this band displays significantly

stronger emission intensity compared to the corresponding transition for **Eu.2.10** and **Eu.2.12**.

Characteristic Yb(III) emission spectra were observed for each of the compounds studied upon excitation of the organic chromophores in D_2O solutions. Typically, Yb(III) emission is weak in the presence of OH oscillators due to its low lying excited $^2F_{5/2}$ state (ca. 10200 cm^{-1}) being particularly prone to quenching, D_2O was therefore chosen to maximise signal intensity. The emission spectra of all species display similar characteristic profiles suggesting that the Yb(III) ion in each case experiences a similar ligand field. The similarity of the Ln(III) environments in the case of the Yb(III) species compared to the Eu(III) species is likely to be due to the greater electrostatic interaction between the sensitiser carbonyl and the lanthanide for the Yb(III) species as a consequence of the lanthanide contraction.

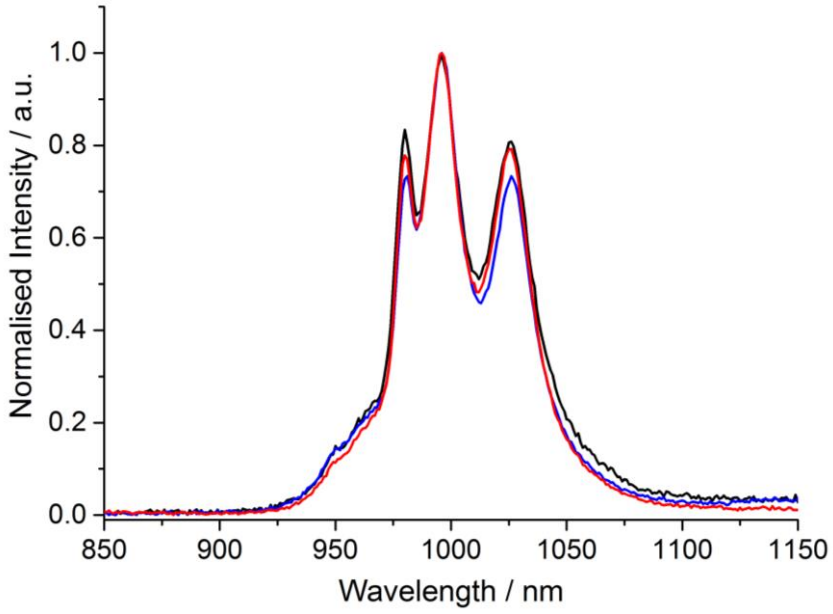


Figure 2. 11 Normalised emission spectra of **Yb.2.10** (black), **Yb.2.11** (blue) and **Yb.2.12** (red) recorded in D_2O upon excitation at 320 nm for **Yb.2.10** and **Yb.2.12** and 370 nm for **Yb.2.11** ($5 < pH < 8.5$).

The measurement of the excited state lifetimes in H_2O and D_2O allowed the determination of the inner sphere hydration number, *q,* using the modified Horrocks' equation:

$$q_{Yb} = (k_H - k_D - 0.1)$$

In all cases as with the corresponding Eu(III) complexes *q* is close to 1 for the Yb(III) species (Table 2. 2), this confirms the octadentate coordination of the ligand to the lanthanide and that only one solvent molecule is bound to the lanthanide. The values are smaller than those observed for the corresponding Eu(III) complexes due to the decrease in ionic radius across the lanthanide series causing the ligand to envelop the Ln(III) more effectively.

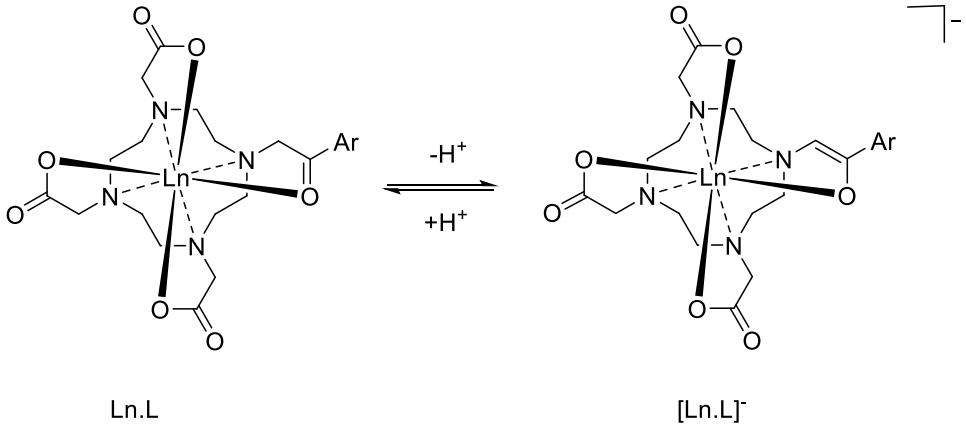
Table 2. 2 Emission lifetimes and hydration numbers of **Yb.2.10**, **Yb.2.11** and **Yb.2.12**.

	Yb.2.10	**Yb.2.11**	**Yb.2.12**
τ_{H2O} /µs[a]	1.23	1.01	1.00
τ_{D2O} /µs[a]	7.70	8.26	8.04
q	0.6	0.9	0.9

Uncertainty ±10%. All data obtained at 298K (pH < 7.5).

2.2.3 pH behaviour of complexes

The study of the pH behaviour of the arylacylDO3A complexes in aqueous solution was undertaken to understand the solution based structure of the complexes due to their high quantum yields and the potential of these complexes to be used in microscopy. It was envisaged that the direct coordination of the chromophore ketone oxygen to the electron withdrawing lanthanide would have a significant effect on the acid-base properties of the complexes and that an acid-base equilibrium as in Scheme 2. 1 could be observed.



Scheme 2. 1 Acid-base properties of arylacylDO3A lanthanide complexes.

Initially the pH dependent properties of the Eu(III) complexes were studied using UV-Vis absorption and luminescence techniques (Figure 2. 12). In the case of **Eu.2.10,** pH titrations revealed a pK_a of 10.5 ± 0.1 (0.1 M NaCl, 295 K). A decrease in emission intensity upon increasing the solution pH was observed. This suggests that only the ketone form of this complex is emissive with the formation of the non-emissive enolate species causing overall decrease in emission intensity. The emission spectral forms and emission lifetimes at pH 4.8 and pH 12 were identical supporting the fact that only one emissive species was present in solution. The non-emissive nature of the enolate complex is presumably due to the formation of an LMCT state which non-radiatively quenches the $^5D_0$ emissive state of Eu(III). A pK_a of 10.2 ± 0.1 (0.1 M NaCl, 295 K) was observed for **Eu.2.12**, this value is slightly lower than that observed for **Eu.2.10** which is likely due to the extended conjugation of the chromophore, stabilising the enolate species more effectively. The observed changes in the UV-Vis absorption spectra are consistent with the different electronic distribution expected for the ketone and enol tautomers. The UV-Vis absorption and emission spectra of **Eu.2.11** however showed no significant changes upon raising the pH of the solution, this is consistent with the strongly electron donating N-ethyl group on the carbazole

group resulting in a destabilised enolate state meaning that deprotonation is not observed in the pH range studied.

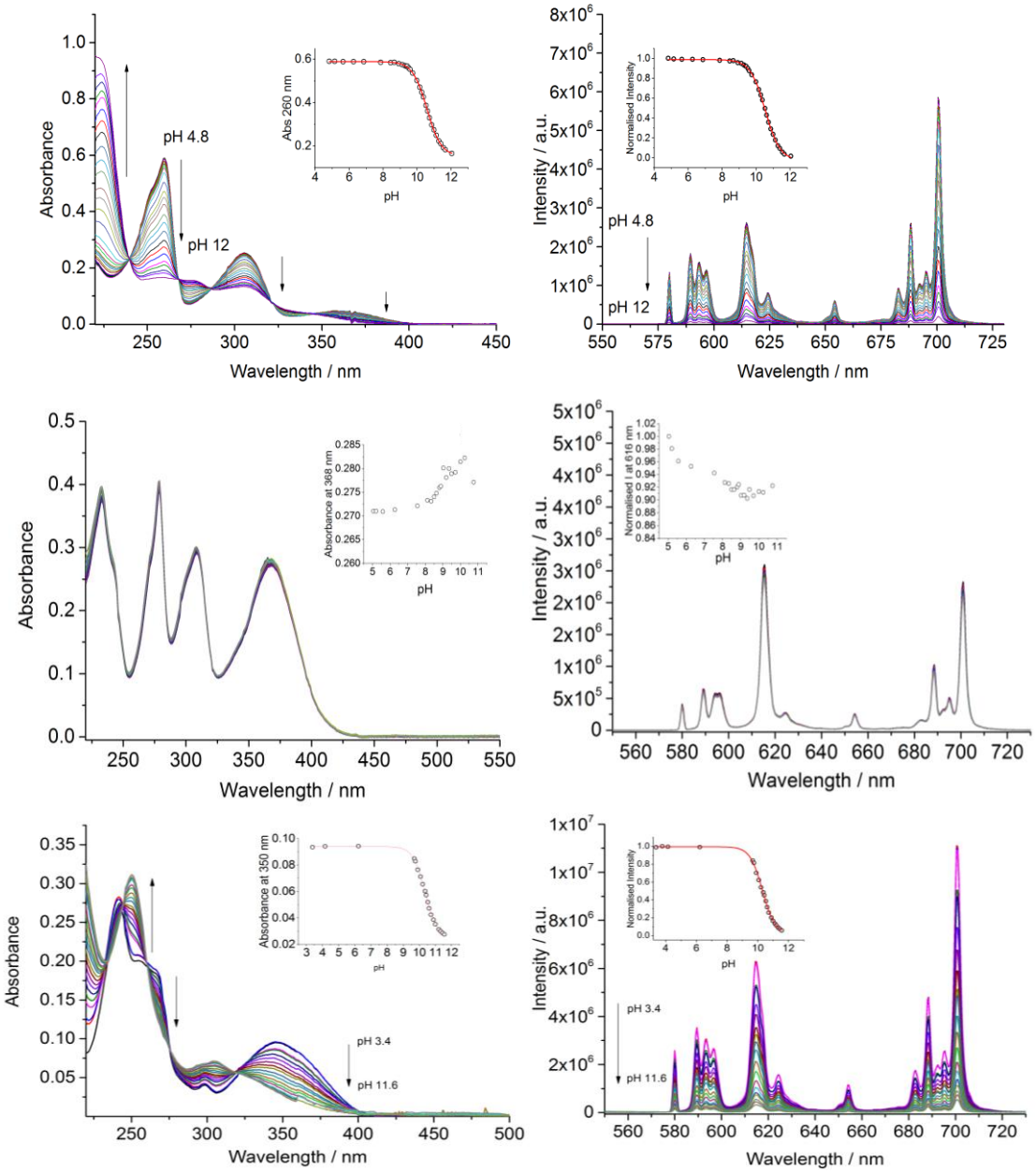


Figure 2. 12 UV-Vis absorption (left) and emission spectra (right) of **Eu.2.10** (top), **Eu.2.11** (middle) and **Eu.2.12** (bottom) upon increasing the pH of solution.

The nature of the chromophore based oxygen donor would change upon formation of the enolate species. The ketone and enolate donors would lead to different ligand fields experienced by the lanthanide which would have a profound effect on the Ln(III) emission spectra. In particular, a drastic change in the splitting pattern of the $^5D_0$-$^7F_1$

transition and the emission lifetime would be expected to be observed for Eu(III) upon changing the ligand field. Although this is expected to be the case, the non-emissive nature of the enolate species for Eu(III) complexes thwarted further luminescence studies on these species. In the case of Yb(III) the formation of a LMCT state would not quench the overall luminescence due to the emissive $^2F_{5/2}$ state being lower than the LMCT state. A double electron transfer sensitisation process is feasible for Yb(III) with the formation of an LMCT Yb(II) state which can populate the emissive $^2F_{5/2}$ state following MLCT back electron transfer leading to emission.[20] With this in mind, the photophysical properties in solution upon changing the pH were investigated in analogous Yb(III) complexes. Indeed, upon raising the pH of the solution for **Yb.2.10** (Figure 2. 13) a change in the shape of the emission spectrum was observed. This is due to the change in the metal coordination environment after deprotonation and the formation of the enolate species. Yb(III) excited state lifetimes increased substantially upon raising the pH of the H_2O solution and a lower hydration number was observed at higher pH; these both support a change in the lanthanide coordination environment and a change in the ligand field. Similar behaviour was observed for **Yb.2.12**; pK_a values for **Yb.2.10** and **Yb.2.12** are 10.5 ± 0.1 (0.1 M NaCl, 295 K) and 10.3 ± 0.1 (0.1 M NaCl, 295 K) respectively. As with **Eu.2.11** the analogous Yb(III) complex, **Yb.2.11** did not show any significant change in the UV-Vis absorption and emission spectra upon raising the pH.

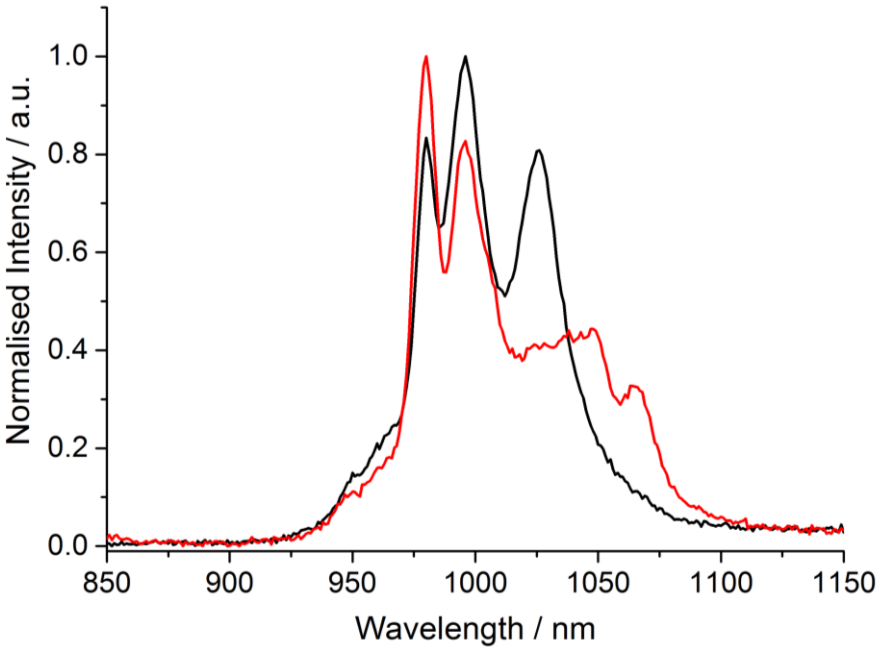


Figure 2. 13 Emission spectra of **Yb.2.10** (black) and **[Yb.2.10]**$^-$ (red) at pH 8 and 12.5 respectively (D_2O, 298 K).

The acid-base properties of the compounds were also investigated using ^{1}H NMR on paramagnetic and diamagnetic complexes. The deuterium exchange for the α-ketone proton due to the keto-enol tautomerisation was followed *via* ^{1}H NMR. A section of the ^{1}H NMR spectra for **Yb.2.10** is shown in Figure 2. 14, which shows a change in the fine structure of the $^2F_{5/2}$-$^2F_{7/2}$ transition - clearly revealing a change in the local crystal field at the lanthanide. The ketone α-protons (indicated with an *) have significantly different chemical shifts due to their difference in position relative to Yb(III). A decrease in the intensity of the α-proton resonances with time is observed due to deuterium exchange, this process is complete within 48h. The remaining proton resonances remain unchanged as there is no structure change in solution but deuterium exchange. Evidence of this keto-enol tautomerisation was also observed for **Eu.2.10**, **Eu.2.12** and **Yb.2.12**. Again **Eu.2.11** and **Yb.2.11** showed no pH-dependent

behaviour in the range studied with the ^{1}H NMR spectra showing no significant changes.

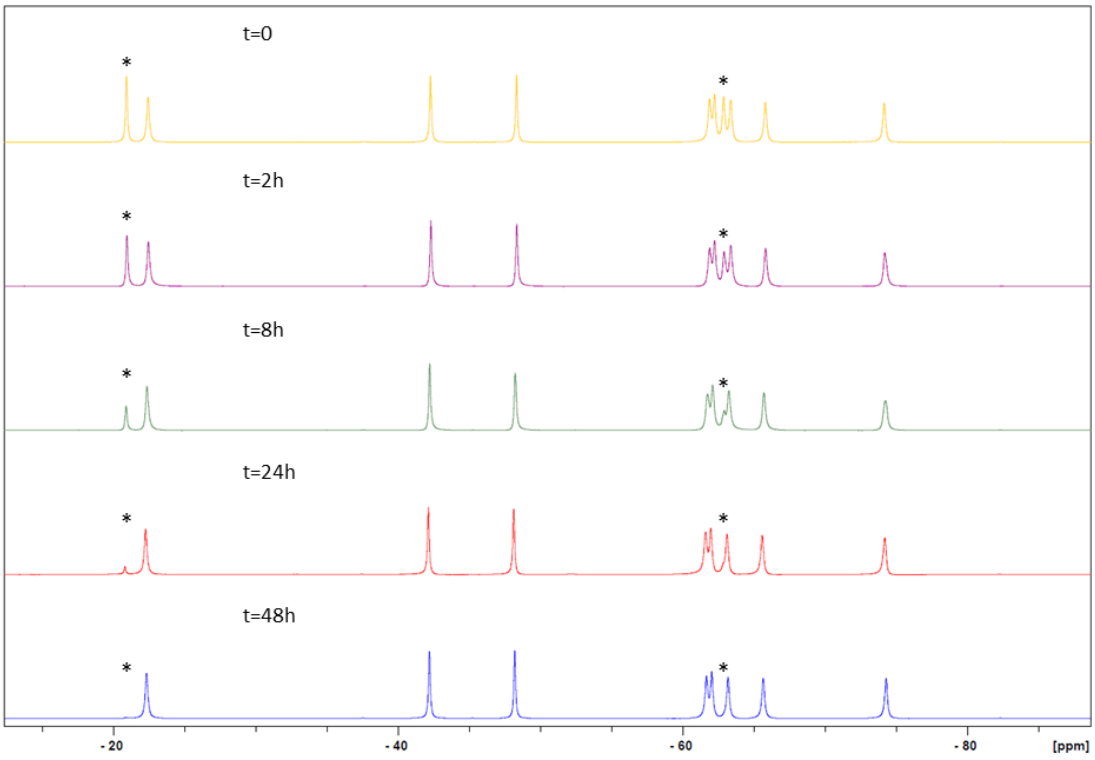


Figure 2. 14 Section of the ^{1}H NMR spectra of **Yb.2.10** at pH 5 taken over a period of 48h (298 K, D_2O). * indicates the ketone α-proton resonances.

Recording the ^{1}H NMR spectra of **Eu.2.10** (Figure 2. 15) and **Yb.2.10** at pH 12 where **[Eu.2.10]**$^{-}$ and **[Yb.2.10]**$^{-}$ dominate shows significantly different solution structure compared to when the ^{1}H NMR were recorded at lower pH (were the ketone form dominates). These enolate species are characterised by broad resonances due to the different lanthanide coordination environment as well as an increase in the LIS. Similar behaviour was observed when the ^{1}H NMR spectra of **Eu.2.12** and **Yb.2.12** were recorded at pH 12.

The pH-dependent behaviour of **Lu.2.10** was also studied by ^{1}H NMR (Figure 2. 15), upon an increase in pH from 5 to 12 significant changes in the form of the spectra were observed. At pH 5, the dominant species is the ketone form, **Lu.2.10**; deuterium

exchange of the α-ketone protons is observed while the other proton resonances remain unchanged. Changes in the macrocyclic and aromatic regions were observed as well as the disappearance of the α-ketone protons at pH 12. The domination of a new species, ascribed to the enolate form **[Lu.2.10]**$^{-}$, was observed at pH 12. A large change in the aromatic chemical shifts is observed as the pH increases, this is likely due to a change in the electronic distribution of the arylacyl moiety as a result of the formation of the enolate species. The broadening of the macrocyclic proton resonances is likely to be due to the structure becoming more fluxional as the pH is raised. This behaviour is completely reversible, with the NMR spectrum restored to its original appearance upon lowering the pH below 7, thus ruling out any possible reaction occurring in solution in the basic environment.

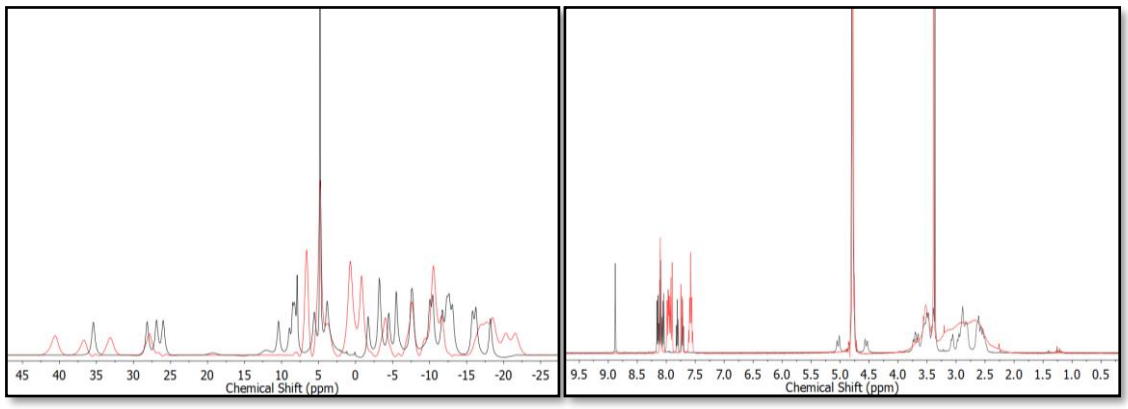


Figure 2. 15 Left: ^{1}H NMR spectra of **Eu.2.10** (black) and **[Eu.2.10]**$^{-}$ (red) at pH 5 and pH 12 respectively (298 K, D_2O). Right: ^{1}H NMR spectra of **Lu.2.10** (black) and **[Lu.2.10]**$^{-}$ (red) at pH 5 and pH 12 respectively (298 K, D_2O).

2.3 Conclusions

In this chapter it has been demonstrated that relatively simple chromophores such as aryl ketones can be used as sensitisers in **DO3A** based ligand scaffolds to afford highly emissive lanthanide complexes upon optimisation of the chromophore-to-lanthanide energy transfer cascade. This was possible due to the photophysical properties of the antenna chromophores chosen, in particular the high intersystem crossing yields and energy match with the Eu(III) accepting states. ^{1}H NMR and photophysical data confirms the aryl ketone oxygen is directly coordinated to the lanthanide centre which is a prerequisite for efficient energy transfer and for decreasing solvent quenching. Indeed, strong emission was observed upon excitation in the near visible region for Yb(III) and Eu(III) species of **2.10** and **2.12**; high quantum yields were observed for **Eu.2.10** and **Eu.2.12** in H_2O of 18% and 16% respectively increasing to a value close to 50% once the quenching effect of the solvent was reduced in D_2O. An anomalously low quantum yield (1%) was observed for **Eu.2.11** due to the large energy difference between the lanthanide emissive state and the chromophore centred triplet state. Furthermore, the pH dependent speciation was established by luminescence, UV-Vis and ^{1}H NMR spectroscopies for both the Eu(III) and Yb(III) complexes. Direct coordination of the aryl ketone oxygen to the lanthanide centre caused a change in the pK_a of the α-ketone proton allowing deuterium exchange. This was used to further confirm the change of speciation in solution. At high pH the dominance of the enolate form was apparent from both ^{1}H NMR and photophysical studies; ^{1}H NMR revealed a broadening and shifting of proton resonances upon raising pH as well as deuterium exchange of the α-ketone protons. Luminescence studies of **Yb.2.10** and **Yb.2.12**

revealed changes in the shape of the emission profile as pH is increased, this is due to a change in the Yb(III) coordination environment upon going from the ketone to the enolate species. This phenomenon was also observed for **Ln.2.10** and **Ln.2.12** demonstrating that the pH behaviour of arylacylDO3A species can be varied by tuning the electronic properties of the chromophore.

2.4 References

1. D. A. Fulton, E. M. Elemento, S. Aime, L. Chaabane, M. Botta and D. Parker, *Chem. Commun.*, 2006, 1064-1066.
2. J. Lee, M. J. Zylka, D. J. Anderson, J. E. Burdette, T. K. Woodruff and T. J. Meade, *J. Am. Chem. Soc.*, 2005, **127**, 13164-13166.
3. C. Li, Y. X. Li, G. L. Law, K. Man, W. T. Wong and H. Lei, *Bioconjugate Chem.*, 2006, **17**, 571-574.
4. L. Charbonniere, R. Ziessel, M. Guardigli, A. Roda, N. Sabbatini and M. Cesario, *J. Am. Chem. Soc.*, 2001, **123**, 2436-2437.
5. Z. Liao, M. Tropiano, K. Mantulnikovs, S. Faulkner, T. Vosch and T. J. Sorensen, *Chem. Commun.*, 2015, **51**, 2372-2375.
6. S. J. Butler, L. Lamarque, R. Pal and D. Parker, *Chem. Sci.*, 2014, **5**, 1750-1756.
7. M. Latva, H. Takalo, V. M. Mukkala, C. Matachescu, J. C. RodriguezUbis and J. Kankare, *J. Lumin.*, 1997, **75**, 149-169.
8. R. Pal and D. Parker, *Chem. Commun.*, 2007, 474-476.
9. E. Deiters, B. Song, A.-S. Chauvin, C. D. B. Vandevyver, F. Gumy and J.-C. G. Buenzli, *Chem. Eur. J.*, 2009, **15**, 885-900.
10. A. Dadabhoy, S. Faulkner and P. G. Sammes, *J. Chem. Soc., Perkin Trans. 2*, 2000, 2359-2360.
11. A. Dadabhoy, S. Faulkner and P. G. Sammes, *J. Chem. Soc., Perkin Trans. 2*, 2002, 348-357.
12. S. J. Butler, M. Delbianco, L. Lamarque, B. K. McMahon, E. R. Neil, R. Pal, D. Parker, J. W. Walton and J. M. Zwier, *Dalton Trans.*, 2015, **44**, 4791-4803.
13. M. Soulie, F. Latzko, E. Bourrier, V. Placide, S. J. Butler, R. Pal, J. W. Walton, P. L. Baldeck, B. Le Guennic, C. Andraud, J. M. Zwier, L. Lamarque, D. Parker and O. Maury, *Chem. Eur. J.*, 2014, **20**, 8636-8646.
14. E. R. Neil, A. M. Funk, D. S. Yufit and D. Parker, *Dalton Trans.*, 2014, **43**, 5490-5504.
15. G. Bottaro, F. Rizzo, M. Cavazzini, L. Armelao and S. Quici, *Chem. Eur. J.*, 2014, **20**, 4598-4607.
16. A. Beeby, L. M. Bushby, D. Maffeo and J. A. G. Williams, *J. Chem. Soc., Dalton Trans.*, 2002, 48-54.
17. S. Aime, M. Botta, M. Fasano, M. P. M. Marques, C. Geraldes, D. Pubanz and A. E. Merbach, *Inorg. Chem.*, 1997, **36**, 2059-2068.
18. G. Scharf and J. D. Winefordner, *Talanta*, 1986, **33**, 17-25.
19. N. J. Turro, V. Ramamurthy and J. C. Scaiano, *Modern Molecular Photochemistry of Organic Molecules*, University Science Books, 2010.
20. S. Faulkner, L. S. Natrajan, W. S. Perry and D. Sykes, *Dalton Trans.*, 2009, 3890-3899.

3 Studying the effect of fluoride on lanthanide tetra-amide complexes[ii]

3.1 Introduction

Fluoride has been shown to play an essential role in the maintenance and growth of healthy teeth and bones. However, overexposure to fluoride can cause severe health conditions such as fluorosis and kidney failure, and this has led the world health organisation (WHO) to recommend a maximum concentration of fluoride in drinking water of 4 mg L^{-1}. With this in mind, the development of convenient and quantitative analytical methods to detect fluoride in drinking water has become an important research area. The most common method of detecting fluoride in water uses ion selective electrodes;[1] while these offer excellent detection limits (20 ppb), analysis is often time consuming and requires expensive instrumentation (meaning onsite analysis is difficult). Fluoride detection by molecular probes in aqueous media is challenging due to both the high free energy of hydration of fluoride (ΔG^{o}_{hyd} = -465 kJ mol^{-1}) and to competition with other (more abundant) halides such as chloride. Lanthanide complexes offer the potential for fluoride specificity that can be combined with the inherent potential advantages associated with the long luminescent lifetimes of paramagnetic ions. Since only the Ln-F interaction can compete with the Ln-H_2O interaction, fluoride is unique among the halides in being able to bind to a lanthanide centre in aqueous solution. This in turn raises the prospect of a fluoride-specific probe based on a lanthanide complex.

[ii] Much of my work described in this chapter has already been published: see, O. A. Blackburn, J. D. Routledge, L. B. Jennings, N. H. Rees, A. M. Kenwright, P. D. Beer and S. Faulkner, *Dalton Trans*., 2016, **45**, 3070-3077.

Only a handful of probes are capable of detecting fluoride in aqueous media, most reported systems are only effective in organic solvents (e.g. MeCN, MeOH, DCM).[2-5] In recent years water soluble lanthanide based probes have been reported which have relatively weak binding affinities for fluoride ($\log K_a$ = 1.4 – 4.1).[6-10] Butler[8] reported a quinoline containing C_2 symmetric lanthanide complex (**[Eu.3.1]$^+$**, Figure 3. 1) that gave a $\log K_a$ = 3.5 based on a 1:1 binding model. The relatively strong binding was attributed to a synergistic effect of electrostatic binding of fluoride to the lanthanide centre combined with hydrogen bonding interactions with the electron deficient quinoline group.

An exception to these weak binding events has been reported by Charbonnière et al.,[11] who observed fluoride binding with $\log K_a$ = 13.0 (**[Eu.3.2]$^+$**, Figure 3. 1). The high strength of binding is attributed to the formation of a supramolecular dimer in which fluoride is encapsulated between two Eu(III) complexes, assisted by H-bonding and π-π stacking. This binding constant reflects binding at both centres with each individual stepwise binding constant being much lower (ca. $\log K_a$ = 6). Also it is worth noting that the K_a value obtained for this system has different units to others in literature due to 2:1 complex forming rather than a 1:1 complex which means that direct comparison is difficult.

Aime et al. noticed that addition of fluoride to **[Ln.DOTA]$^-$** complexes causes significant changes to their NMR spectra, in contrast to the effects of a variety of other anions, without commenting on the reasons for this.[12] More recently Blackburn et al.[9, 10] have explored the effect of the displacement of axially bound solvent in **[Ln.DTMA]$^{3+}$** species (Figure 3. 1) by fluoride. EPR measurements of **[Yb.DTMA]$^{3+}$** in the presence and absence of fluoride showed considerable differences with a reduction of the g

value anisotropy upon fluoride addition. Inversion of the g value was also observed; going from $g_{\parallel} > g_{\perp}$ for **[Yb.DTMA.OH$_2$]$^{3+}$** to $g_{\parallel} < g_{\perp}$ for **[Yb.DTMA.F]$^{2+}$**. Bleaney analysis of **[Yb.DTMA]$^{3+}$** in the presence and absence of fluoride reveals a reduction and inversion of the second order crystal field parameter, B_0^2 when going from **[Yb.DTMA.OH$_2$]$^{3+}$** to **[Yb.DTMA.F]$^{2+}$**. The Stark splitting of the $^7F_1$ state of Eu(III) can be determined from the fine structure in the $^5D_0$-$^7F_1$ transition (since the $^5D_0$ state has no Stark degeneracy), and the value obtained can be used as a direct measure of B_0^2. Upon addition of fluoride to **[Eu.DTMA.OH$_2$]$^{3+}$** the Stark splitting significantly decreases and the A and E components merge to form one apparent peak corresponding to the **[Eu.DTMA.F]$^{2+}$** species. These observations were interpreted in terms of a change of crystal field around the lanthanide centre, more specifically as a change in the anisotropy of the magnetic susceptibility tensor; going from a prolate distribution of electrons to an oblate distribution.

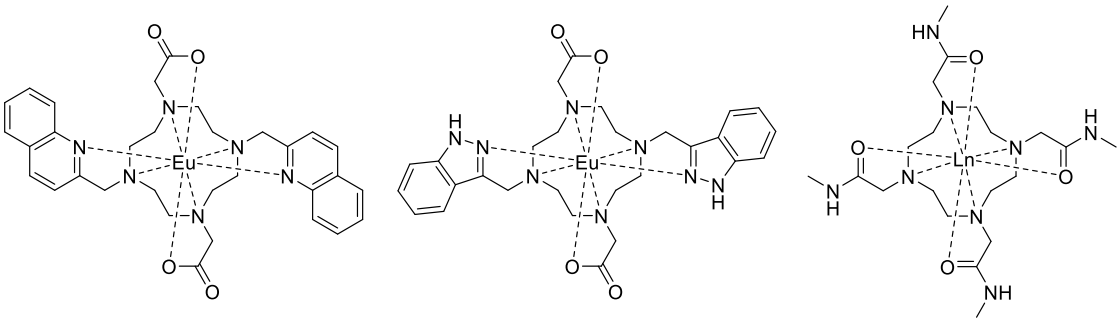


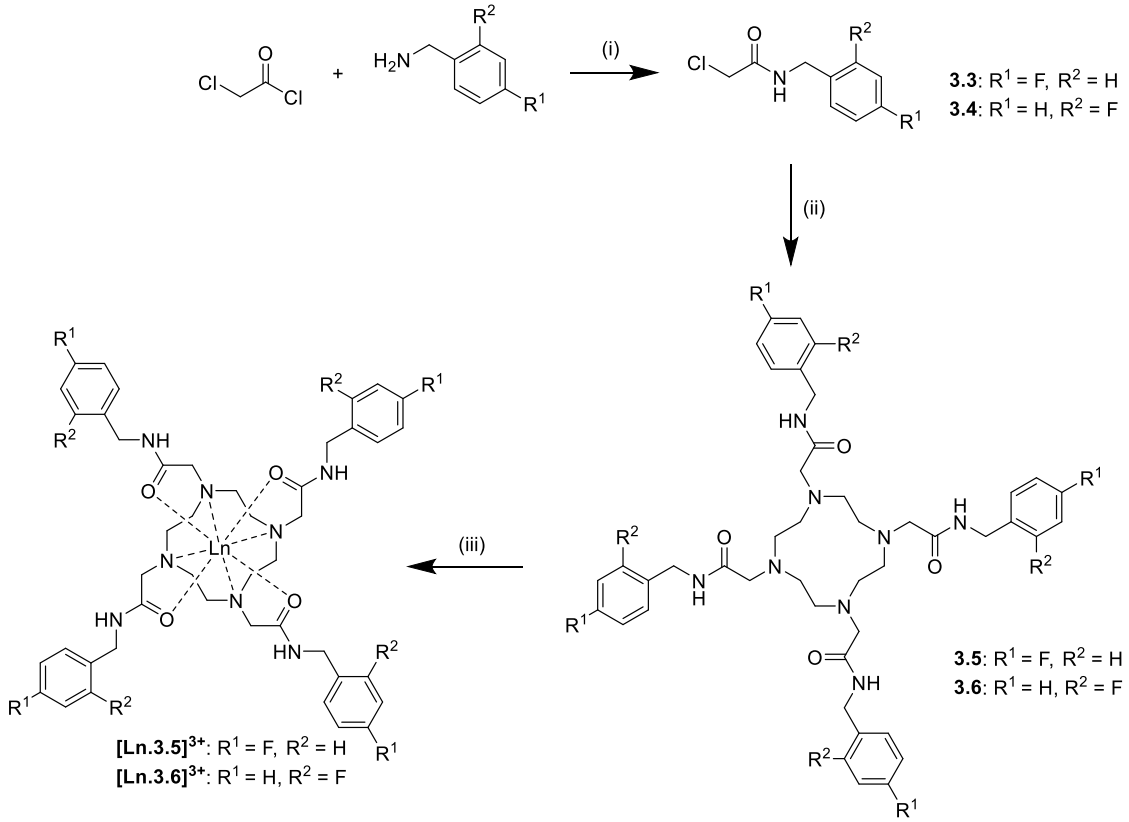
Figure 3. 1 Examples of lanthanide probes capable of detecting fluoride in aqueous media.

This chapter presents a study of the interaction between stable lanthanide complexes and fluoride ions in aqueous media, using NMR and luminescence techniques to explore the effects of fluoride binding to the axial site of a lanthanide complex. Ligands containing hydrophobic benzyl acetamide arms were used to investigate the changes in the nature of the binding event with respect to the less hydrophobic **[Ln.DTMA]$^{3+}$**

species (Figure 3. 1). It will be shown that covalently bound fluorine atoms on the ligand architecture can be used as useful probes in assessing the effects of fluoride binding to lanthanide centres.

3.2 Synthesis and characterisation

Two novel C_4 symmetric **DOTA**-tetraamide ligands bearing fluorine atoms on the benzylic periphery, **3.3** and **3.4**, were prepared as shown in Scheme 3. 1 by analogy with literature precedent for the unsubstituted benzyl system.[13]



Scheme 3. 1 Preparation of lanthanide tetraamide derivatives of cyclen. (i) NEt_3, DCM, RT, 18h; (ii) cyclen, NEt_3, DMF, 85°C, 2d; (iii) $Ln(OTf)_3$/$Y(OTf)_3$, MeCN, 70°C, 2d.

The appropriate benzylamine was reacted with chloroacetylchloride in the presence of triethylamine giving the chloroacetamides (**3.3** and **3.4**) in 50-60% yield after recrystallization from DCM/petroleum ether. The resulting acetamides were used to alkylate cyclen in the presence of excess triethylamine using DMF as a solvent; **3.5** and

3.6 were obtained by adding H_2O to the DMF solution causing them to precipitate. The precipitate was suspended in a mixture of DMF:H_2O and heated, the solids were filtered and washed. Figure 3. 2 shows the ^{1}H NMR of **3.6**, the high symmetry of the molecule is confirmed by the low number of observed resonances. The complexes **[Ln.3.5]$^{3+}$** and **[Ln.3.6]$^{3+}$** were obtained as colourless crystalline solids following reaction of the ligands with the corresponding lanthanide trifluoromethanesulfonate salt in acetonitrile for 2 days at 70°C. All complexes where characterised by ^{1}H NMR, ^{19}F NMR, mass spectrometry, and CHN analysis.

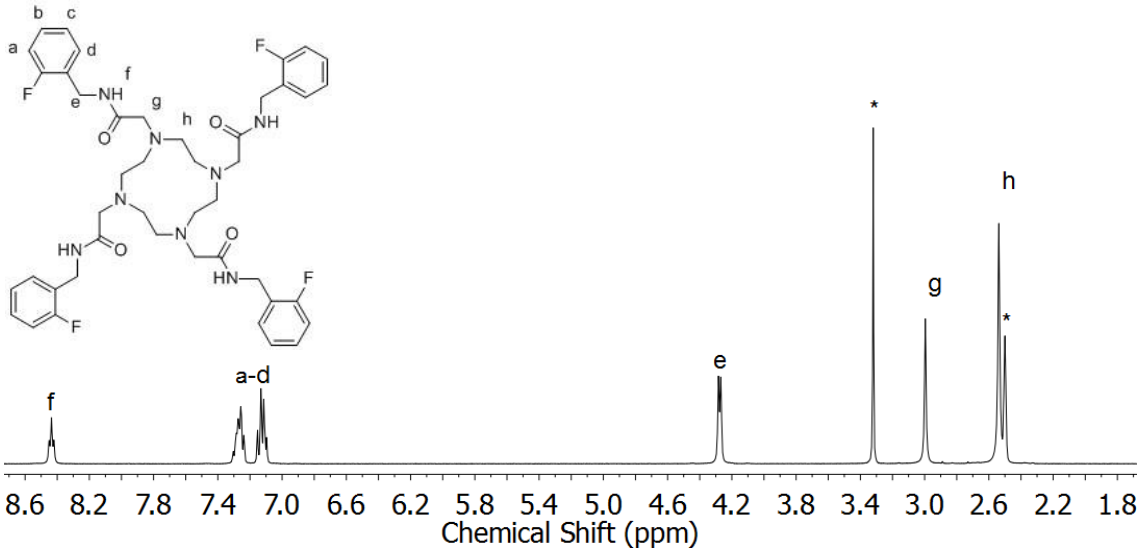


Figure 3. 2 ^{1}H NMR spectrum of **3.6** (DMSO-d_6, 298 K, 400 MHz). * indicates residual solvent signals.

3.3 NMR studies of lanthanide complexes

The ^{1}H NMR spectra of the complexes are similar to those found in literature for related compounds.[14] The crystal structures of related complexes in conjunction with literature precedent were used to assign the NMR resonances and subsequent Bleaney plots were used to validate the assignments due to the geometric factor dominating the observed chemical shift. The axial C_4 symmetry of the complexes leads to relatively simple NMR spectra (Figure 3. 3). The six outer peaks are due to the cyclen ring

protons and the acetamide arm NCH_2 protons whilst the aromatic and benzylic protons appear in the 0-10 ppm region due to them being further from the lanthanide ion and therefore feeling a relatively small lanthanide induced shift (LIS, see later). The SAP isomer predominates over TSAP for lanthanide complexes of **DOTA**-tetraamide ligands in the latter half of the series. The proportion of SAP increases as the series is traversed, and the spectra of **[Yb.3.5]$^{3+}$** and **[Yb.3.6]$^{3+}$** only show the presence of the SAP isomer. The ^{1}H NMR spectra of Yb(III) are easier to interpret than most lanthanides due to the effective absence of a contact contribution and hence the dominant pseudocontact contribution to the LIS. By contrast, the ^{1}H NMR spectra of Eu(III) complexes are more difficult to interpret quantitatively, due to the substantial contact contribution to the LIS and the significant Boltzmann population of the $^7F_1$ and $^7F_2$ states at room temperature.

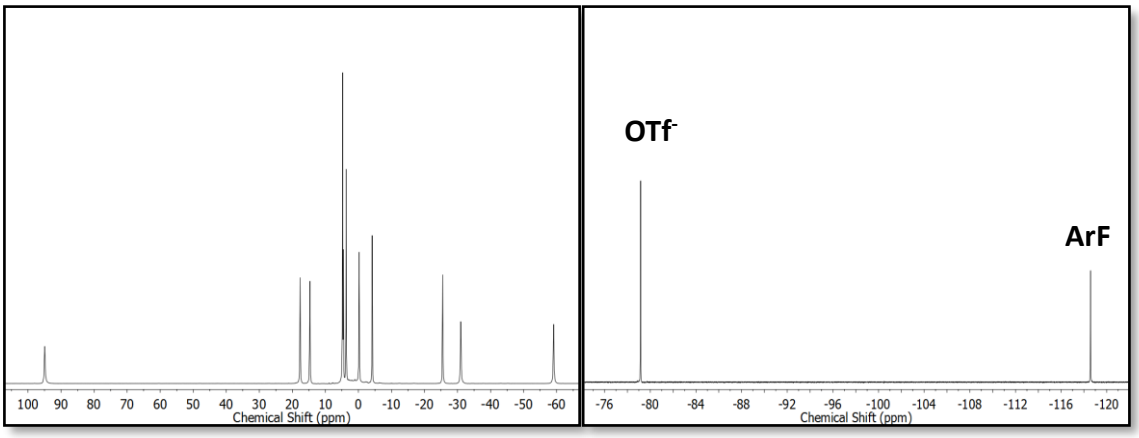


Figure 3. 3 Left: ^{1}H NMR spectrum of **[Yb.3.5]$^{3+}$** (D_2O, 298 K, 400 MHz). Right: $^{19}F\{^1H\}$ spectrum of **[Yb.3.5]$^{3+}$** (D_2O, 298 K, 376 MHz).

The fluorine atoms on the ligand skeleton provide a point of reference that can be used to probe fluoride binding; two ^{19}F resonances can be seen for complex **[Yb.3.5]$^{3+}$** (Figure 3. 3), one corresponding to the OTf^- counterion (-79.2 ppm) and one corresponding to the aromatic fluorine (ArF) on the ligand (-118.6 ppm). The presence

of one ArF resonance also supports the presence of only one isomer (SAP) in solution, consistent with the data in the ^{1}H NMR spectrum.

Upon addition of fluoride, three new resonances are observed in the ^{19}F NMR spectrum in addition to the resonances at -79.2 and -118.6 ppm (Figure 3. 4); one at -113.4 ppm corresponding to ArF on the ligand in the fluoride bound species, one at -123.1 ppm which corresponds to free fluoride and one at -1023 ppm corresponding to the Yb(III) bound fluoride (not shown). The chemical shift of the ArF resonance is different by 5 ppm in **[Yb.3.5.OD$_2$]$^{3+}$** compared with **[Yb.3.5.F]$^{2+}$**, this value is small due to the large distance between the lanthanide centre and the nuclei of interest. The ArF chemical shift of **[Yb.3.6]$^{3+}$** is more affected by the change in axial donor (Δ ^{19}F = 7 ppm) than in **[Yb.3.5]$^{3+}$** which is presumably a consequence of the closer distance between ArF and the lanthanide centre. The presence of free and bound fluoride as well as the observation of two ArF resonances upon fluoride addition indicates slow exchange on this timescale.

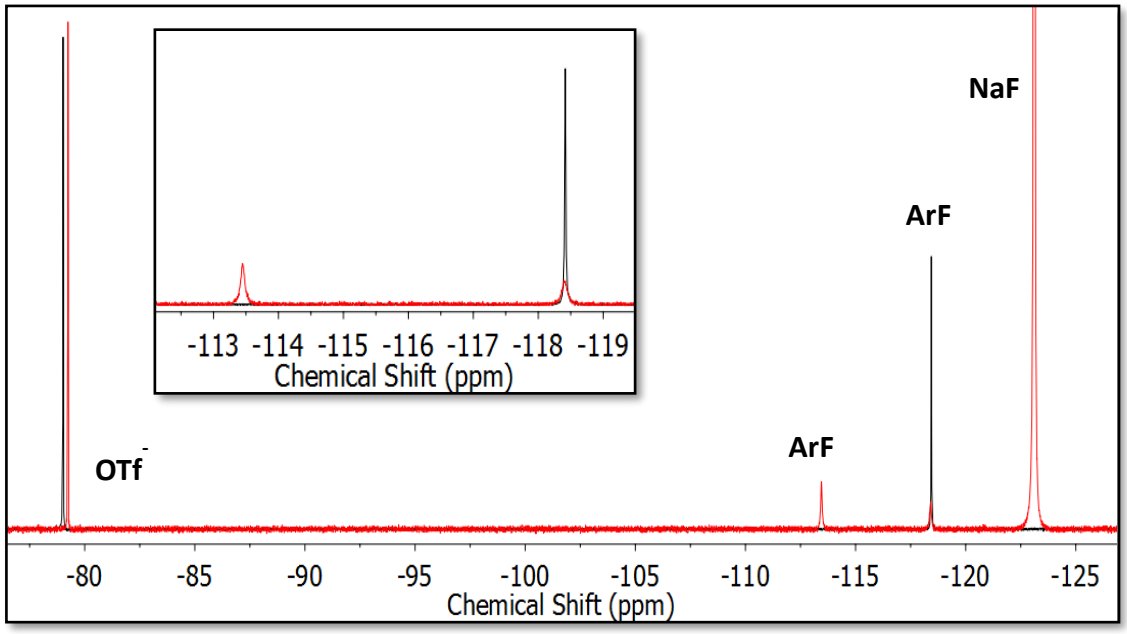


Figure 3. 4 ^{19}F NMR spectrum of **[Yb.3.5]$^{3+}$** without fluoride (black) and with fluoride (red) (D_2O, 298 K, 400 MHz). Inset: ArF resonances.

The chemical shifts of the bound fluoride resonances are shown in Table 3. 1. Eu(III) and Yb(III) complexes have significantly larger chemical shifts than Y(III) species due to the LIS associated with paramagnetic species. The Eu(III) complexes have similar bound fluoride chemical shifts. The LIS for Eu(III) is dominated by the contact shift which indicates that the contact contribution felt in all of these cases are similar and that the contact contribution is insensitive to the ligand substituents. However this is not the case for Yb(III) species, where there is a large variation in the bound fluoride chemical shift between the benzylic substituted species (**[Ln.3.5]$^{3+}$** and **[Ln.3.6]$^{3+}$**) vs. the aliphatic substituted species, **[Ln.DTMA]$^{3+}$**. This is due to the fact that the LIS for Yb(III) species is dominated by the pseudocontact contribution and will vary with the size of the crystal field (see later).

Table 3. 1 Chemical shifts of bound fluoride (D_2O, 298 K, 400 MHz).

	3.5 (ppm)	**3.6 (ppm)**	**DTMA (ppm)**
Eu	-482	-482	-481
Yb	-1023	-1047	-859
Y	-54 (d, J = 64 Hz)	-53 (d, J = 64 Hz)	-59 (d, J = 61 Hz)

Slow exchange is also observed in the ^{1}H NMR spectra (Figure 3. 5). Upon addition of fluoride a new set of peaks corresponding to the fluoride bound species, **[Yb.3.5.F]$^{2+}$** appear, and the resonances corresponding to **[Yb.3.5.OD$_2$]$^{3+}$** are also observed in the ^{1}H NMR spectrum but are diminished in intensity. The chemical shift range of the ^{1}H resonances in **[Yb.3.5.F]$^{2+}$** is significantly reduced compared to that in **[Yb.3.5.OD$_2$]$^{3+}$** (80 ppm compared to 160 ppm). This phenomenon was also observed for **[Yb.3.6]$^{3+}$**, the proton spectral ranges before and after fluoride addition are similar to those observed for **[Yb.3.5]$^{3+}$** due to the lanthanide environment not being significantly

affected by the change in fluorine substituent position. This phenomenon was also observed for **[Eu.3.5]$^{3+}$** and **[Eu.3.6]$^{3+}$**, where there is a reduction in the spectral width going from ca. 40 ppm in the solvent bound species to ca. 20 ppm in the fluoride bound species.

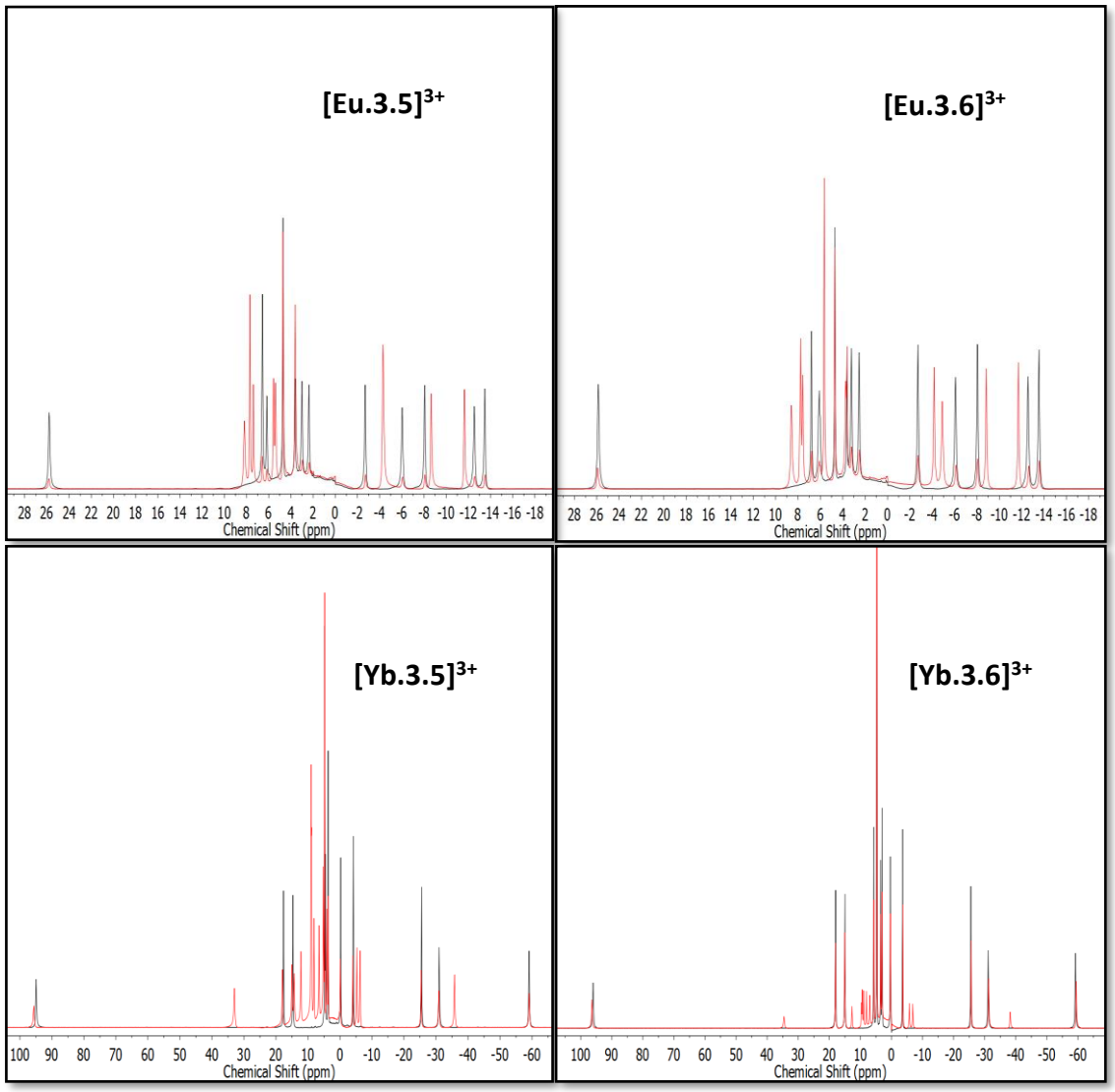


Figure 3. 5 ^{1}H NMR spectra of Eu(III) and Yb(III) complexes of **3.5** and **3.6** without fluoride (black) and with fluoride (red) (D_2O, 298 K, 400 MHz).

Bleaney's theory[15, 16] defines the observed chemical shift of a nucleus close to a lanthanide centre as the sum of the pseudocontact, contact and diamagnetic contributions, and is often used in the analysis of NMR spectra of lanthanide complexes. The pseudocontact component often dominates the LIS observed for

nuclei on ligand scaffolds since the contact shift is only significant for nuclei less than three bonds away, this is particularly true for Yb(III) where the contact contribution is negligible. For an axially symmetric system (> C_3) the pseudocontact contribution can be described by the Bleaney equation:

$$\Delta_{PC} = \frac{-2C_J{\mu_B}^2}{(kT)^2}\left(\frac{3cos^2\theta - 1}{r^3}\right)B_0^2$$

Where θ and r are the polar coordinates relative to the principal axis with the lanthanide at the origin, $C_J = g^2J(J + 1)(2J - 1)(2J + 3)\langle J|a|J'\rangle$, μ_B is the Bohr magneton and B_0^2 is the second order crystal field parameter (these assume that J is a good quantum number, and that higher order crystal field terms are not of importance). Plotting LIS vs. $(3cos^2\theta - 1/r^3)$ using nuclear coordinates taken from a closely related crystal structure[17] can be used to confirm the correct assignment of proton resonances and it can be used to assess changes in the second order crystal field parameter, B_0^2 which is proportional to the gradient of the line of best fit. The LIS is calculated by subtracting the diamagnetic contribution (δ_D) from the observed chemical shift (δ_{obs}). In this case 2.9 ppm was used as an estimate for δ_D of the aliphatic protons (representing an average value for NC*H* protons). Correct assignment of the proton spectra was confirmed by a linear Bleaney plot, while the assignment of the fluoride bound species is deduced from exchange correlation spectroscopy (EXSY), as shown in Figure 3. 6.

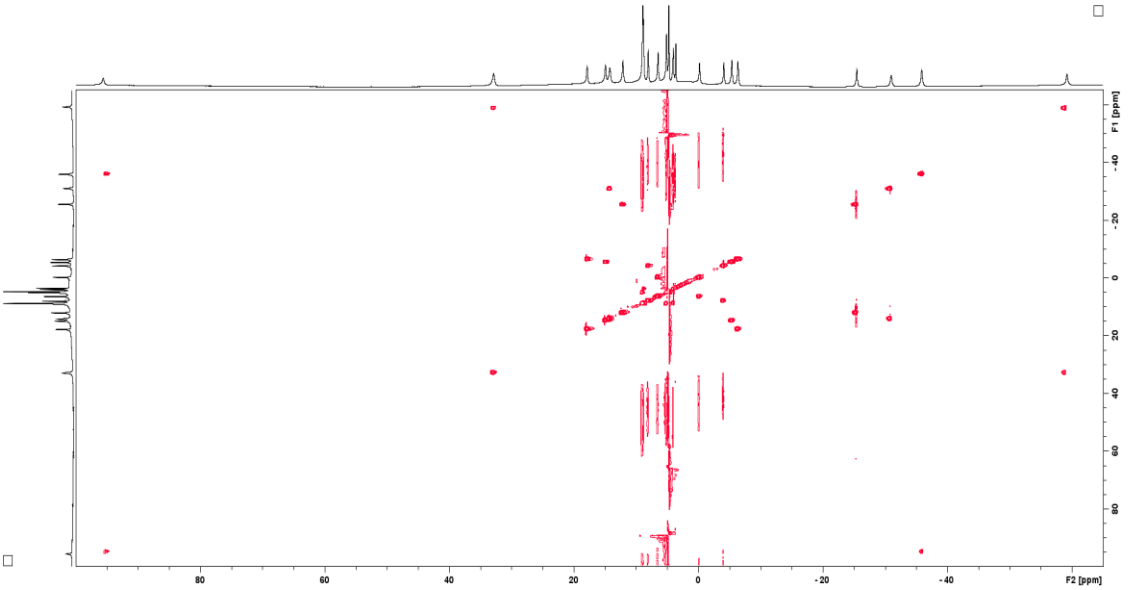


Figure 3. 6 ^{1}H EXSY spectrum of **[Yb.3.6]$^{3+}$** (D_2O, 298 K, 500 MHz).

Cross peaks observed in the EXSY spectra confirm that the new set of resonances is in exchange with the original peaks. The EXSY spectra also shows that upon fluoride binding the sign of each proton chemical shift changes which is due to a change in sign of B_0^2. The reduction of spectral width suggests a reduction in the magnitude of B_0^2.

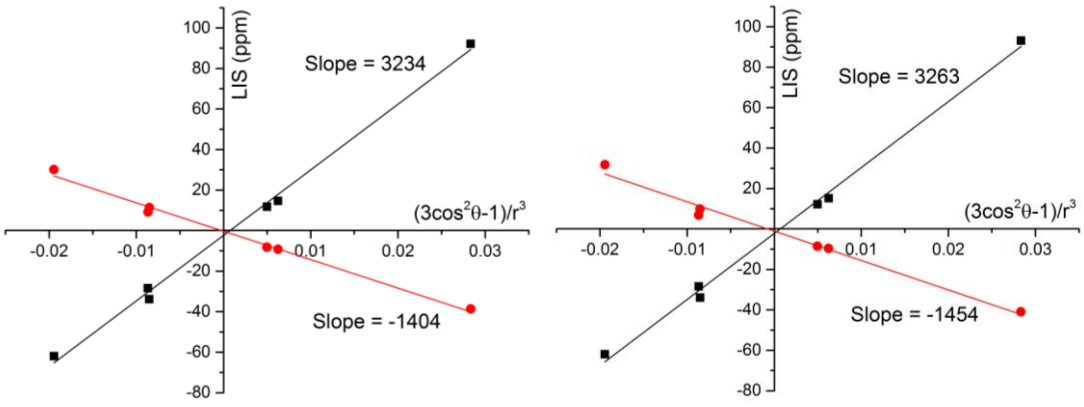


Figure 3. 7 Bleaney plots for **[Yb.3.5]$^{3+}$** (left) and **[Yb.3.6]$^{3+}$** (right) proton resonances in the absence (black) and presence (red) of an excess of NaF in D_2O using polar coordinates from the crystal structure of a related complex.[14]

The Bleaney plots (Figure 3. 7) confirm that B_0^2 is decreased in magnitude and its sign is reversed upon the binding of fluoride in the lanthanide axial site, replacing bound solvent. There is a reduction in magnitude of B_0^2 to 43% and 45% of the original values for **[Yb.3.5]$^{3+}$** and **[Yb.3.6]$^{3+}$** respectively, it is clear from this that the nature of the

axial donor plays an important role in determining the properties of lanthanide complexes. For **[Yb.DTMA]$^{3+}$** the gradient of the Bleaney plot in the absence of fluoride is 3216, and is -890 in the presence of fluoride, this corresponds to a reduction in magnitude of B_0^2 to 28% of its original value. For the hydrated species (**[Yb.3.5]$^{3+}$**, **[Yb.3.6]$^{3+}$** and **[Yb.DTMA]$^{3+}$**) the magnitudes of the Bleaney plot gradients fall within a narrow range, whilst for the fluoride bound species the benzyl substituted species have significantly more negative Bleaney plot gradients. The change in magnitude of the gradients upon fluoride binding are 4638, 4717 and 4106 for **[Yb.3.5]$^{3+}$**, **[Yb.3.6]$^{3+}$** and **[Yb.DTMA]$^{3+}$** respectively. This is a consequence of fluoride being a stronger donor in the benzyl substituted species due to the weaker solvation of fluoride in the binding cavity. The more negative Bleaney gradients in the benzyl substituted species correlates with the more negative bound fluoride chemical shifts observed (see Table 3. 1); the larger magnitudes of B_0^2 for **[Yb.3.5]$^{3+}$** and **[Yb.3.6]$^{3+}$** generate larger pseudocontact shifts compared with **[Yb.DTMA]$^{3+}$**. The ^{1}H NMR spectra of **[Yb.3.6]$^{3+}$** were obtained at pH 10 and pH 7, and used to assess whether pH affects the appearance of the ^{1}H NMR spectra. No change was observed upon raising the pH, confirming that the effects observed due to fluoride addition are not due to deprotonation of an acetamide N*H* or bound solvent.

Analogous diamagnetic complexes (**[Lu.3.5]$^{3+}$**, **[Lu.3.6]$^{3+}$**, **[Y.3.5]$^{3+}$** and **[Y.3.6]$^{3+}$**) were also studied in the presence and absence of fluoride. Addition of fluoride to Lu(III) complexes caused significant shifting and broadening of the resonances corresponding to the cyclen ring protons and the NCH_2 protons of the arms, and only one set of resonances was observed after fluoride addition (Figure 3. 8). The absence of a

paramagnetic centre means the fluoride bound and solvated species have very similar chemical shifts and there is no relaxation enhancement in the absence of unpaired electron spins, and so the observed set of broad resonances indicates that exchange between solvent bound and fluoride bound species is in an intermediate exchange regime on this NMR timescale.

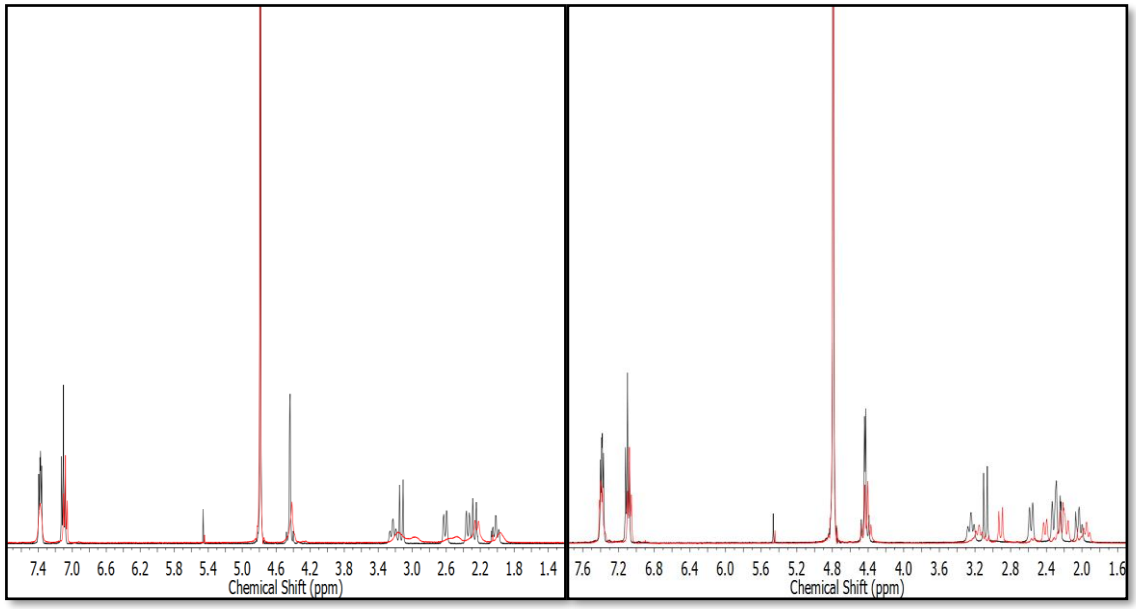


Figure 3. 8 ^{1}H NMR spectrum of **[Lu.3.5]$^{3+}$** (left) and **[Y.3.5]$^{3+}$** (right) without fluoride (black) and with fluoride (red) (D_2O, 298 K, 400 MHz).

Addition of fluoride to **[Y.3.5]$^{3+}$** and **[Y.3.6]$^{3+}$** resulted in the formation of a new species; a new set of ^{1}H peaks corresponding to the fluoride bound species and a decrease in intensity of the resonances of the solvent bound species was observed (Figure 3. 8). The exchange between these species is slow on the NMR timescale and sharp resonances are observed for fluoride and solvent bound species i.e. exchange is faster for Lu(III) species than Y(III) species. The ^{19}F NMR of **[Y.3.5]$^{3+}$** was very revealing, with a decrease in the intensity of the ArF resonance (-114.9 ppm) corresponding to the solvent bound species along with the emergence of a new ArF resonance (-115.3 ppm) corresponding to the fluoride bound species. Direct evidence of 1:1 fluoride

binding to ^{89}Y (I = ½) is observed in the ^{19}F NMR by the presence of a doublet at -54 ppm (J = 64 Hz); this behaviour is indicative of spin-spin coupling and significant orbital overlap between ^{89}Y(III) and ^{19}F. A doublet was also observed for **[Y.3.6]$^{3+}$** at -53 ppm (J = 64 Hz). The presence of the ^{89}Y(III) - ^{19}F doublet suggests that fluoride binding to Y(III) is appreciably slower than 64 Hz.

Reilley treatment can be used to separate the contact and pseudocontact contributions to the proton and fluorine shifts and therefore determine the change in these contributions upon fluoride binding.[18] The lanthanide induced shift can be described using the following equation:

$$LIS = \delta_c + \delta_p = \delta_{obs} - \delta_d = \langle S_z \rangle F + C_J \qquad \text{equation 1.}$$

Where <Sz> and C_J are characteristic of the lanthanide, and are tabulated in the literature,[19] and F and G are characteristic of the nucleus under observation. <Sz>F represents the contact contribution (δ_c) and C_JG represents the pseudocontact contribution (δ_p) to the chemical shift. This treatment makes assumptions about complexes across the lanthanide series: i) the complexes are isostructural, ii) the second order crystal field parameter, B_0^2 is constant and iii) the hyperfine coupling constant A/ħ is constant. Equation 1 can be rearranged to give two methods to determine F and G, these are shown below:

Method 1

$$\frac{LIS}{\langle S_Z \rangle} = \frac{C_J}{\langle S_Z \rangle} G + F$$

Method 2

$$\frac{LIS}{C_J} = \frac{\langle S_Z \rangle}{C_J} F + G$$

These equations can be used to produce plots using data from a series of lanthanide complexes to allow the extraction of F and G values for the nucleus in question, and the linearity of these plots offers an effective measure of the validity of the Bleaney treatment in a given family of complexes. Method 1 is preferred for pseudocontact dominated shifts whilst method 2 is preferred for contact dominated shifts.

The fluorine resonance on the ligand was chosen for Reilley analysis due to its ease of assignment; Reilley treatment of ring protons on **[Ln.DTMA]$^{3+}$** complexes has been done previously, and this approach has been extended to covalently bound fluorine.[9] For **[Ln.DTMA]$^{3+}$** species it was shown that proton G values (which define the pseudocontact contribution) change in sign and magnitude upon fluoride binding which was in agreement in the Bleaney treatment of **[Yb.DTMA]$^{3+}$**. However there was no clear pattern that defines the changes in the proton F values (which define the contact contribution) upon the addition of fluoride.

Reilley plots from the ^{19}F NMR data for **[Ln.3.5]$^{3+}$** in the presence (R^2 = 0.95) and absence (R^2 = 0.99) of fluoride obtained using method 1 are shown in Figure 3. 9. The G values obtained from the gradients of the lines of best fit change from -0.17 in the absence of fluoride to 0.08 in the presence of fluoride, which corresponds to G being reduced to 47% of its original value as a consequence to the reduction of the local magnetic anisotropy in the presence of ligated fluoride. This is in excellent agreement with the change observed by Bleaney treatment of **[Yb.3.5]$^{3+}$**, with the magnitude of B_0^2 being reduced to 43% of its original value upon fluoride binding: the two values are essentially within experimental error, suggesting that J is a good quantum number in this system. The F value goes from -7.6x10^{-4} in the absence of fluoride to 0.30 in the presence of fluoride, suggesting there is a significant increase in the magnitude of the

contact contribution to the ArF shift upon fluoride binding, as might be expected when paramagnetic anisotropy is moved into the equatorial plane (giving rise to an increased exchange integral).

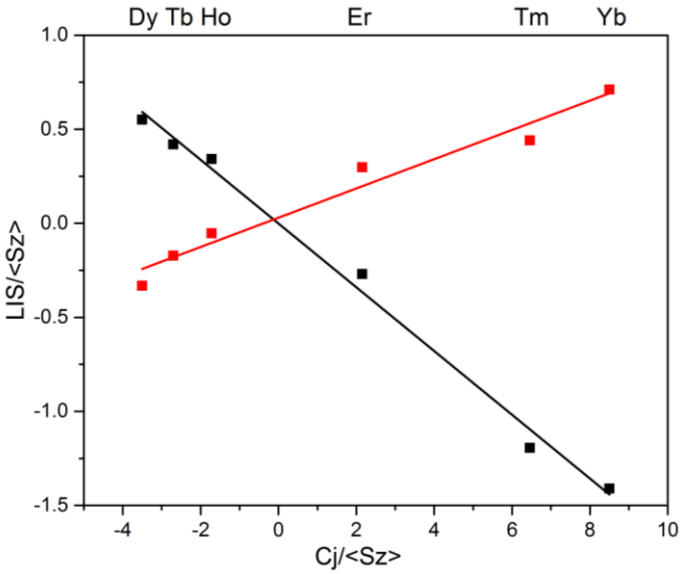


Figure 3. 9 Reilley plots (Method 1) for the aryl fluorine shifts of **[Ln.3.5]$^{3+}$** in the presence (red) and absence (black) of fluoride.

3.4 Luminescence

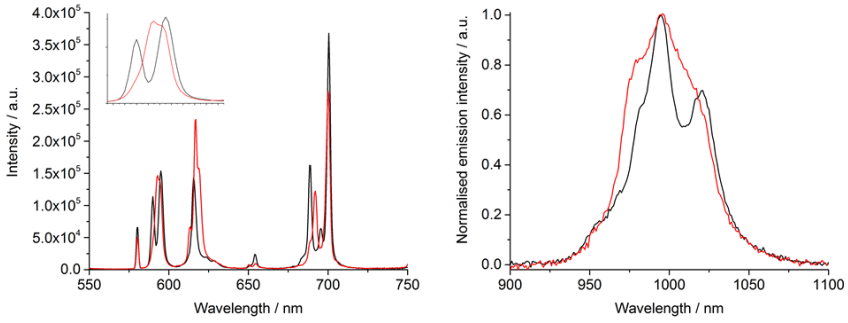


Figure 3. 10 Change in form of emission spectra with fluoride. Left: **[Eu.3.5]$^{3+}$** in D_2O (black) and with excess sodium fluoride (red), λ_{ex} = 395 nm, exit slits 1 nm (Inset: ΔJ = 1). Right: **[Yb.3.5]$^{3+}$** in D_2O (black) and with excess sodium fluoride (red), λ_{ex} = 265 nm, exit slits 5 nm.

The emission spectra of **[Eu.3.5]$^{3+}$**, **[Eu.3.6]$^{3+}$**, **[Yb.3.5]$^{3+}$** and **[Yb.3.6]$^{3+}$** were recorded in the presence and absence of fluoride (e.g. Figure 3. 10) following direct excitation at 395 nm. The ΔJ = 1 transition (ca. 590 nm) in the Eu(III) emission spectra can, in principle, be used to measure the magnitude of the second order crystal field

parameter, B_0^2 in axially symmetric systems. Addition of fluoride results in a decrease in the Stark splitting of the ΔJ = 1 transition indicating that B_0^2 has decreased in magnitude, the A and E components are much closer in energy and merge to form one apparent peak with fine structure (Figure 3. 11) - this is unsurprising for a molecular species in solution, where significant line widths contribute to the overlap between the two bands. However, this means that it is not possible to gain any quantitative information on a change in sign of B_0^2 from the luminescence spectra beyond observing how close in energy the A and E components are in the fluoride bound species. It is clear from the NMR data discussed previously that B_0^2 changes sign upon fluoride binding, and it can thus be inferred that the ordering of the Stark levels is in fact reversed by fluoride binding.[10] Changes in the shape of the Yb(III) emission spectra also support analogous changes in B_0^2, though analysis of Stark splitting is difficult due to the high J multiplicity of the ground ($^2F_{7/2}$) and excited ($^2F_{5/2}$) states of Yb(III).

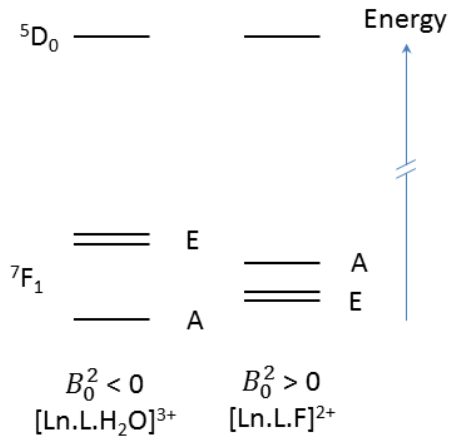


Figure 3. 11 Schematic representation of Stark splitting for ΔJ = 1 transition with and without fluoride.

The excited state lifetimes of the Eu(III) $^5D_0$ state in **[Eu.3.5]$^{3+}$** and **[Eu.3.6]$^{3+}$** were measured in H_2O and D_2O in the absence and presence of fluoride to determine the number of solvent molecules coordinated to the lanthanide centre, *q*. Lifetimes and *q*

values are tabulated in Table 3. 2; it can be seen that, in the absence of fluoride, the *q* values are close to 1 for both complexes which implies that a single solvent molecule is directly coordinated to the lanthanide in its axial site. Lifetimes were also measured upon the addition of fluoride to the point when there was no further change in luminescence spectra, in both cases *q* was calculated to be approximately 0. This indicates that the solvent molecule in the lanthanide inner coordination sphere has been replaced by fluoride. Luminescence quenching by OH and OD oscillators can occur through second and outer sphere solvent molecules which explains the difference in lifetimes in the deuterated and protonated lifetimes when fluoride is bound to the lanthanide.

3.5 Fluoride binding

The affinity of fluoride with **[Eu.3.5]$^{3+}$** and **[Eu.3.6]$^{3+}$** species was determined using NMR and luminescence spectroscopies. Dynafit®[20] was used to fit the changes observed during NMR and luminescence titrations; in all cases a 1:1 binding model was used. Association constants and confidence intervals are shown in Table 3. 2.

$$[LnL.D_2O]^{3+} + F^- \rightleftharpoons [LnL.F]^{2+} + D_2O$$

Since both **[Eu.3.5]$^{3+}$** and **[Eu.3.6]$^{3+}$** exhibit slow exchange of the ArF resonances upon addition of fluoride on the ^{19}F NMR timescale, integration of the signals corresponding to the ArF resonances in the fluoride bound and solvated species was used to establish the fluoride ion binding constants through a series of NMR titrations. In the case of luminescence titrations the changes in the intensity of the hypersensitive ΔJ = 2 transition were monitored relative to those of the ΔJ = 1 and ΔJ = 4 transitions to follow the change in the Eu(III) local coordination environment and hence assess binding. Representative fitted binding data is shown in Figure 3. 12 for **[Eu.3.5]$^{3+}$**.

Table 3. 2 Association constants, *K*, for lanthanide complexes with NaF in D_2O at 298K (95% confidence intervals in square brackets), lifetimes and *q* values. **[Eu.DTMA]$^{3+}$** from reference.[9]

	K/M^{-1}			No NaF			+ NaF		
	^{19}F NMR	Luminescence		τ_{H2O}	τ_{D2O}	*q*	τ_{H2O}	τ_{D2O}	*q*
[Eu.3.5]$^{3+}$	43.7 [37.8 – 50.7]	40.7 [37.9 – 43.9]		0.54	1.92	0.9	1.13	2.56	0
[Eu.3.6]$^{3+}$	30.1 [26.7 – 34.0]	26.1 [24.9 – 27.4]		0.55	2.22	1	1.13	2.61	0
[Eu.DTMA]$^{3+}$	47.4 [30.0 – 80.2]	78.9 [56.2 – 113.9]		0.54	1.72	0.8	1.07	2.41	0

$q = 1.2(\frac{1}{\tau_{H_2O}} - \frac{1}{\tau_{D_2O}} - 0.25 - 0.075x)$ Where x = number of exchangeable amide N*H* protons.

The binding constant values obtained by different methods are within error of each other, indicating that the changes observed by the different techniques corresponds to the same event, and giving weight to the reliability of both methods. The titration data shows that **[Eu.3.6]$^{3+}$** has a significantly lower fluoride affinity than **[Eu.3.5]$^{3+}$**, although these are of similar magnitude as each other as well as related species reported in literature in which electrostatics plays a major role in the binding affinity. However, a few examples have significantly higher binding affinities for fluoride in aqueous media.[8, 11] In these cases, supramolecular π-π interactions have been reported to play an important role. These systems are typically C_2 symmetric and contain large conjugated chromophores which assist the formation of supramolecular dimers which can encapsulate fluoride (see section 3.1).

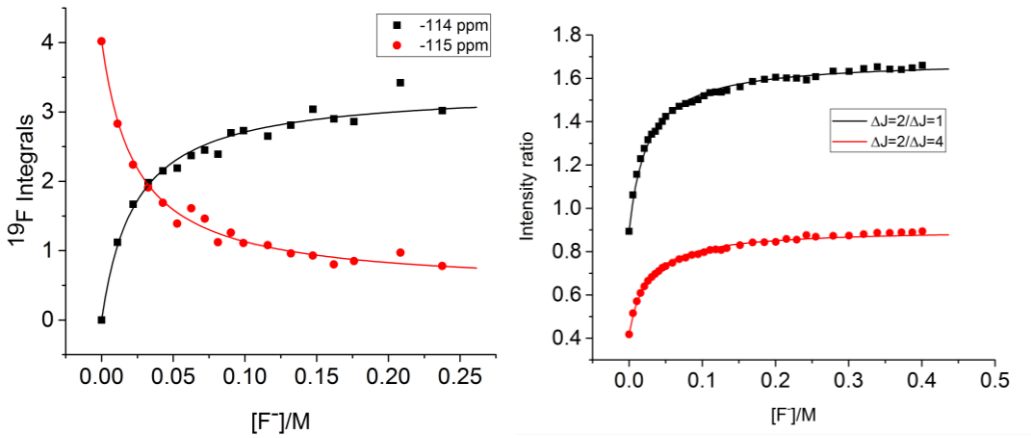


Figure 3. 12 Left: Binding isotherms and fits for titration of **[Eu.3.5]$^{3+}$** with NaF monitoring the ^{19}F NMR integrals of the new and old ArF peaks relative to the OTf^- peak. Right: Binding isotherms and fits for titration of **[Eu.3.5]$^{3+}$** with NaF using the intensity ratios ΔJ=2/ΔJ=1 and ΔJ=2/ΔJ=4.

Addition of chloride, bromide and iodide to **[Eu.3.5]$^{3+}$** resulted in no spectral changes – suggesting that there is no displacement of bound solvent; highlighting the fact that only the Ln-F interaction is strong enough to overcome the hydration enthalpy of the halide in aqueous media. The effect of pH on the emission spectra was also studied, and increasing pH resulted in an increase in the intensity of the characteristic Eu(III) emission bands with no change in the form of the bands. This suggests that the bound solvent is deprotonated which reduces the number of high frequency oscillators in close proximity to the lanthanide, so the Eu(III) excited state is less efficiently quenched.

3.6 Rates of exchange

NMR fluoride binding studies indicate that fluoride exchange is faster for **[Lu.3.5]$^{3+}$** and **[Lu.3.6]$^{3+}$** than their Y(III) analogues (see NMR discussion previously). The exchange rate of fluoride at a lanthanide centre can be probed for a system in slow exchange using a selective inversion NMR pulse sequence. Exchange between hydrated and fluoride-bound forms can be monitored in a sample that contains a

mixture of both species by monitoring the evolution of a pair of resonances after selective inversion of one of them. The evolution of their magnetisations after selective inversion is determined by the exchange rate (k) between the species and the spin lattice relaxation rates ($R_1 = 1/T_1$). Another experiment monitors the magnetisation after a non-selective inversion pulse is applied. The data from the selective and non-selective pulse experiments were then fitted using the CIFIT2 program[21] by varying k and R_1 until the values converge (conducted by Dr Blackburn). The ^{19}F resonances on the ligand backbone of **[Yb.3.5]$^{3+}$** where chosen to determine k since they are far enough away from the lanthanide to have reasonable R_1 values and the ^{19}F resonances don't overlap with any other signals. R_1 is very fast for nuclei close to paramagnetic centres; the methyl protons on **[Yb.DTMA]$^{3+}$** have much faster R_1 values than for ^{19}F on **[Yb.3.5]$^{3+}$** but they have a large enough exchange rate to compensate for this. Rates of exchange for fluoride and thermodynamic parameters as obtained from Eyring plots are in Table 3. 3.

Table 3. 3 Rates and thermodynamic parameters obtained from Eyring plots for the exchange between fluoride bound and solvent bound species.

	k at 298K (s^{-1})	**$\Delta H^{\ddagger}$ ($kJmol^{-1}$)**	**$\Delta S^{\ddagger}$ ($JK^{-1}mol^{-1}$)**	**$\Delta G^{\ddagger}$ at 298K ($kJmol^{-1}$)**
[Yb.DTMA]$^{3+}$	215.7 ± 3.0	47.2 ± 1.5	-41.8 ± 5.1	59.7 ± 3.0
[Yb.3.5]$^{3+}$	61.2 ± 3.6	45.5 ± 0.8	-58.1 ± 2.9	62.8 ± 1.7
[Eu.3.5]$^{3+}$	0.41 ± 0.01	-	-	-

It is immediately clear that the rate of fluoride exchange is much slower for **[Eu.3.5]$^{3+}$** than it is for **[Yb.3.5]$^{3+}$**. This is thought to be due to Yb(III) being smaller than Eu(III) meaning that the ligand in the Yb(III) case is able to envelop the metal centre more completely thus speeding up the rate of dissociation of the axial ligand. This trend was

also observed by Aime et al. with a series of **[Ln.DOTA]**$^{-}$ complexes.[12] For our system, the rate of exchange is smaller than in the case of **[Yb.DTMA]**$^{3+}$ with the aromatic ligand substituents leading to a slower exchange rate, this phenomenon is also observed in water exchange with hydrophobic groups on the ligand scaffold reducing the exchange rate. [22]

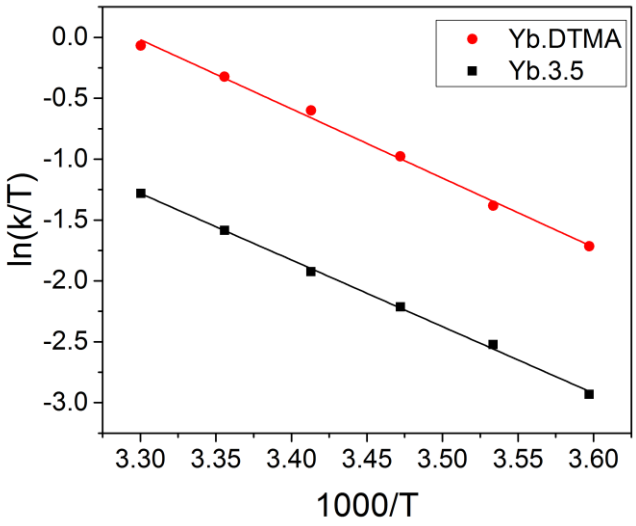


Figure 3. 13 Eyring plots for **[Yb.DTMA]**$^{3+}$ (Red, R^2 = 0.99) and **[Yb.3.5]**$^{3+}$ (Black, R^2 = 0.96) in D_2O for the exchange of fluoride bound and hydrated complexes.

The effect of the ligand on the fluoride exchange rate was explored by measuring k for **[Yb.DTMA]**$^{3+}$ and **[Yb.3.5]**$^{3+}$ at multiple temperatures in order to extract thermodynamic data. The Eyring plots (Figure 3. 13) show good linear fits, and the thermodynamic data extracted from the plots is shown in Table 3. 3. The values of $\Delta H^{\ddagger}$ are similar in each case which suggests that the electrostatic interaction between Yb(III) and fluoride is not influenced by the ligand scaffold. $\Delta S^{\ddagger}$ for **[Yb.3.5]**$^{3+}$ is more negative than for **[Yb.DTMA]**$^{3+}$, this implies that the nature of the ligand does affect the interaction between Yb(III) and fluoride. This difference in $\Delta S^{\ddagger}$ can be ascribed to the extent of rearrangement of solvent molecules in close proximity to the lanthanide

centre upon fluoride binding. The solvation sphere is significantly more disrupted in the fluoride binding process for **[Yb.3.5]$^{3+}$** (which contains large hydrophobic aromatic groups); this greater entropic penalty reduces the rate of exchange compared to **[Yb.DTMA]$^{3+}$**. The data reported corresponds to the transition states involved in the fluoride binding process which means the $\Delta G^{\ddagger}$ values obtained don't correspond to the overall fluoride affinity constants determined using NMR and luminescence techniques.

3.7 Conclusions

In this chapter it has been demonstrated that fluoride binding in lanthanide tetra-amide complexes causes substantial changes to their magnetic (NMR) and luminescence properties compared to solvent bound analogues. These changes are attributed to a change in the sign and magnitude of the second order crystal field parameter, B_0^2, though changes are also likely to be observed in higher order terms, B_q^k.[23] The change in sign of B_0^2 can be interpreted as a change in magnetic anisotropy around the lanthanide where in the case of Yb(III) and Eu(III) we go from a prolate electron distribution to an oblate one (Figure 3. 14). **[Yb.DTMA]$^{3+}$** has a significantly faster fluoride exchange rate than **[Yb.3.5]$^{3+}$** due to the less hydrophobic arm substituents. The nature of the ligand effect on exchange rate was probed using Eyring analysis and showed that the entropy of activation plays a substantial role in determining the free energy of activation for the fluoride binding process. It is clear that a variety of factors such as sterics, electrostatics and solvation affect the nature of the lanthanide fluoride interaction.

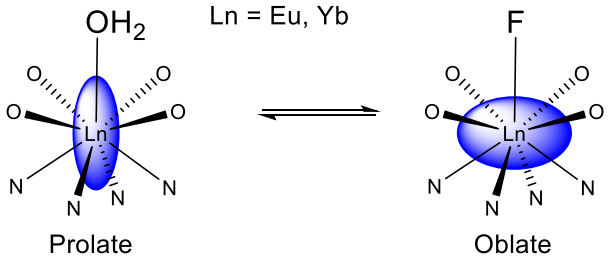


Figure 3. 14 Schematic representation showing the change in magnetic anisotropy upon fluoride binding.

3.8 References

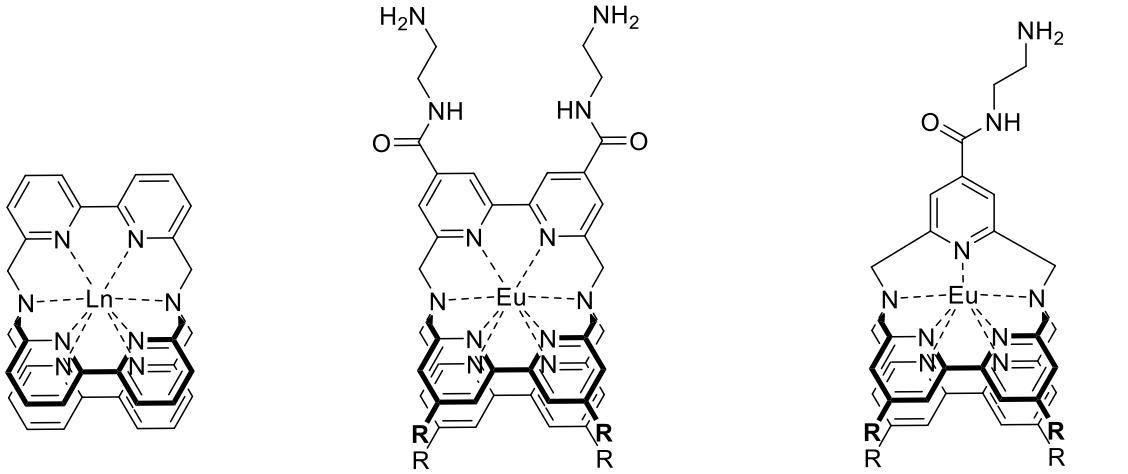
1. M. S. Frant and J. W. Ross, *Science*, 1966, **154**, 1553-&.
2. C. R. Wade, I.-S. Ke and F. P. Gabbai, *Angew. Chem., Int. Ed.*, 2012, **51**, 478-481.
3. J. F. Zhang, C. S. Lim, S. Bhuniya, B. R. Cho and J. S. Kim, *Org. Lett.*, 2011, **13**, 1190-1193.
4. S. Guha and S. Saha, *J. Am. Chem. Soc.*, 2010, **132**, 17674-17677.
5. S. J. M. Koskela, T. M. Fyles and T. D. James, *Chem. Commun.*, 2005, 945-947.
6. R. Tripier, C. Platas-Iglesias, A. Boos, J.-F. Morfin and L. Charbonniere, *Eur. J. Inorg. Chem.*, 2010, 2735-2745.
7. L. M. P. Lima, A. Lecointre, J.-F. Morfin, A. de Blas, D. Visvikis, L. J. Charbonniere, C. Platas-Iglesias and R. Tripier, *Inorg. Chem.*, 2011, **50**, 12508-12521.
8. S. J. Butler, *Chem. Commun.*, 2015, **51**, 10879-10882.
9. O. A. Blackburn, A. M. Kenwright, P. D. Beer and S. Faulkner, *Dalton Trans.*, 2015.
10. O. A. Blackburn, N. F. Chilton, K. Keller, C. E. Tait, W. K. Myers, E. J. L. McInnes, A. M. Kenwright, P. D. Beer, C. R. Timmel and S. Faulkner, *Angew. Chem., Int. Ed.*, 2015, **54**, 10783-10786.
11. T. Liu, A. Nonat, M. Beyler, M. Regueiro-Figueroa, K. N. Nono, O. Jeannin, F. Camerel, F. Debaene, S. Cianferani-Sanglier, R. Tripier, C. Platas-Iglesias and L. J. Charbonniere, *Angew. Chem., Int. Ed.*, 2014, **53**, 7259-7263.
12. S. Aime, M. Botta, M. Fasano, M. P. M. Marques, C. Geraldes, D. Pubanz and A. E. Merbach, *Inorg. Chem.*, 1997, **36**, 2059-2068.
13. T. Huynh, C. Valant, I. T. Crosby, P. M. Sexton, A. Christopoulos and B. Capuanot, *J. Med. Chem.*, 2013, **56**, 8196-8200.
14. G. Zucchi, R. Scopelliti and J. C. G. Bunzli, *J. Chem. Soc., Dalton Trans.*, 2001, 1975-1985.
15. B. Bleaney, *J. Magn. Reson.*, 1972, **8**, 91-&.
16. B. Bleaney, R. J. P. Williams, A. V. Xavier, R. B. Martin, B. A. Levine and C. M. Dobson, *Journal of the Chemical Society-Chemical Communications*, 1972, 791-+.
17. R. S. Dickins, J. A. K. Howard, C. W. Lehmann, J. Moloney, D. Parker and R. D. Peacock, *Angew. Chem., Int. Ed. Engl.*, 1997, **36**, 521-523.
18. C. N. Reilley and B. W. Good, *Anal. Chem.*, 1975, **47**, 2110-2116.
19. J. A. Peters, J. Huskens and D. J. Raber, *Prog. Nucl. Magn. Reson. Spectrosc.*, 1996, **28**, 283-350.
20. P. Kuzmic, *Anal. Biochem.*, 1996, **237**, 260-273.
21. A. D. Bain and J. A. Cramer, *J. Magn. Reson., Ser A*, 1996, **118**, 21-27.
22. S. Aime, A. Barge, A. S. Batsanov, M. Botta, D. Delli Castelli, F. Fedeli, A. Mortillaro, D. Parker and H. Puschmann, *Chem. Commun.*, 2002, 1120-1121.
23. A. M. Funk, K.-L. N. A. Finney, P. Harvey, A. M. Kenwright, E. R. Neil, N. J. Rogers, P. K. Senanayake and D. Parker, *Chem. Sci.*, 2015, **6**, 1655-1662.
24. B. Alpha, J. M. Lehn and G. Mathis, *Angew. Chem. Int. Ed.*, 1987, **26**, 266-267.
25. B. Alpha, V. Balzani, J. M. Lehn, S. Perathoner and N. Sabbatini, *Angew. Chem., Int. Ed. Engl.*, 1987, **26**, 1266-1267.

26. G. Blasse, G. J. Dirksen, D. Vandervoort, N. Sabbatini, S. Perathoner, J. M. Lehn and B. Alpha, *Chem. Phys. Lett.*, 1988, **146**, 347-351.
27. B. Alpha, R. Ballardini, V. Balzani, J. M. Lehn, S. Perathoner and N. Sabbatini, *Photochem. Photobiol.*, 1990, **52**, 299-306.
28. S. Faulkner, A. Beeby, M. C. Carrie, A. Dadabhoy, A. M. Kenwright and P. G. Sammes, *Inorg. Chem. Commun.*, 2001, **4**, 187-190.
29. US 5627074, 1997.
30. J. P. Cross, A. Dadabhoy and P. G. Sammes, *J. Lumin.*, 2004, **110**, 113-124.
31. J. C. Rodriguezubis, B. Alpha, D. Plancherel and J. M. Lehn, *Helv. Chim. Acta*, 1984, **67**, 2264-2269.
32. C. Bischof, J. Wahsner, J. Scholten, S. Trosien and M. Seitz, *J. Am. Chem. Soc.*, 2010, **132**, 14334-14335.
33. I. Bkouchewaksman, J. Guilhem, C. Pascard, B. Alpha, R. Deschenaux and J. M. Lehn, *Helv. Chim. Acta*, 1991, **74**, 1163-1170.
34. J. D. Rinehart and J. R. Long, *Chem. Sci.*, 2011, **2**, 2078-2085.
35. J. Sievers, *Z. Phys. B Con. Mat*, 1982, **45**, 289-296.
36. W. D. Horrocks, V. K. Arkle, F. J. Liotta and D. R. Sudnick, *J. Am. Chem. Soc.*, 1983, **105**, 3455-3459.

4 Investigating the interaction of fluoride with lanthanide complexes of Lehn's cryptand

4.1 Introduction

The Lehn cryptand represents one of the earliest effective approaches to form stable lanthanide complexes for use in assays; lanthanide complexes of the Lehn cryptand, **[Ln.4.7]$^{3+}$** and its derivatives have been widely used to sensitise emission of Eu(III) and Tb(III) in assays (Figure 4. 1).[24-27] There are many requirements to consider when designing lanthanide complexes for use in immunoassays, these include high absorptivity above 330 nm (to permit use in instruments with glass optics), high quantum yield and brightness (to give optimal detection limit), high kinetic and thermodynamic stability (to prevent lanthanide scrambling), high solubility in aqueous media and strong emission at ca. 620 nm. **[Eu.4.1]$^{3+}$** was one of the first lanthanide complexes to fulfil many of these requirements and was extensively used, however the absorption properties above 330 nm were not optimal and the addition of potassium fluoride was required to enhance signal in the assay. The absorption maximum was shifted through extending conjugation by incorporating carboxylate moieties on the pyridine backbone i.e. **[Eu.4.2]$^{3+}$**. **[Eu.4.3]$^{3+}$** was designed to have a smaller cavity to reduce the number of lanthanide bound solvent molecules and increase the luminescence quantum yield, removing the need to add fluoride.



[Ln.4.7]$^{3+}$ **[Eu.4.1]$^{3+}$: R = H** **[Eu.4.3]$^{3+}$: R = CO_2H**

[Eu.4.2]$^{3+}$: R = CO_2H

Figure 4. 1 Lanthanide complexes of the Lehn cryptand, **[Ln.4.7]$^{3+}$** and its derivatives.

Faulkner et al.[28] reported that Yb(III) and Nd(III) complexes of **[Ln.4.7]$^{3+}$** both exhibit sensitised luminescence in the near-IR upon excitation through the bipyridyl chromophore at 355 nm. The energy transfer mechanism for the Yb(III) complex was likely a double photoelectron transfer process; the overlap between the excited state of the bipyridyl chromophore (E_T = 21600 cm^{-1})[27] and the emissive $^2F_{5/2}$ state (ca. 10200 cm^{-1}) of Yb(III) is negligible. Time resolved luminescence showed a rise time of emission of < 5 ns and no triplet-triplet transient absorption was observed, supporting the double electron transfer mechanism. Inner sphere hydration numbers, *q*, were 1.53 for the Yb(III) complex whilst effective determination of *q* for Nd(III) complexes is broadly meaningless owing to the quenching effect of CH oscillators on the neodymium emissive state, and the long lifetimes observed for the neodymium complex are likely to reflect inefficient quenching by CH in the Lehn cryptand rather than a lower value of *q* for the Nd(III) complex. Given that the *q* value for Yb(III) was similar to values obtained for Eu(III) and Tb(III) complexes of the Lehn cryptand, it is

likely that the *q* value is very similar across the series (and that it approximates to two water molecules per lanthanide centre).

In the light of the observations made in chapter three regarding fluoride binding and its effect on the crystal field and magnetic anisotropy, we resolved to study a system where fluoride binding has also been inferred from previous work, but in which no discussion of the spectroscopic consequences of binding fluoride, or indeed the affinity of the complex for fluoride has been attempted. Mathis et al.[29] noticed that adding sodium fluoride to solutions containing lanthanide cryptands used in homogenous immunoassays resulted in the lifetimes of emission increasing. Sammes et al.[30] subsequently reported that upon adding potassium fluoride to the Eu(III) complex of the Lehn cryptand then significant changes were observed in both the intensity and form of the emission spectra though they did not rationalise these observations. Addition of fluoride resulted in longer Eu(III) emission lifetimes due to fluoride binding to the lanthanide centres and displacing inner sphere solvent molecules and reducing quenching. As such, we resolved to study fluoride binding in the lanthanide complexes of the Lehn cryptand, **[Ln.4.7]$^{3+}$** in detail using NMR and luminescence techniques. Furthermore the NMR spectra of lanthanide complexes of the Lehn cryptand do not lend themselves to straightforward Bleaney analysis.

4.2 Synthesis and characterisation

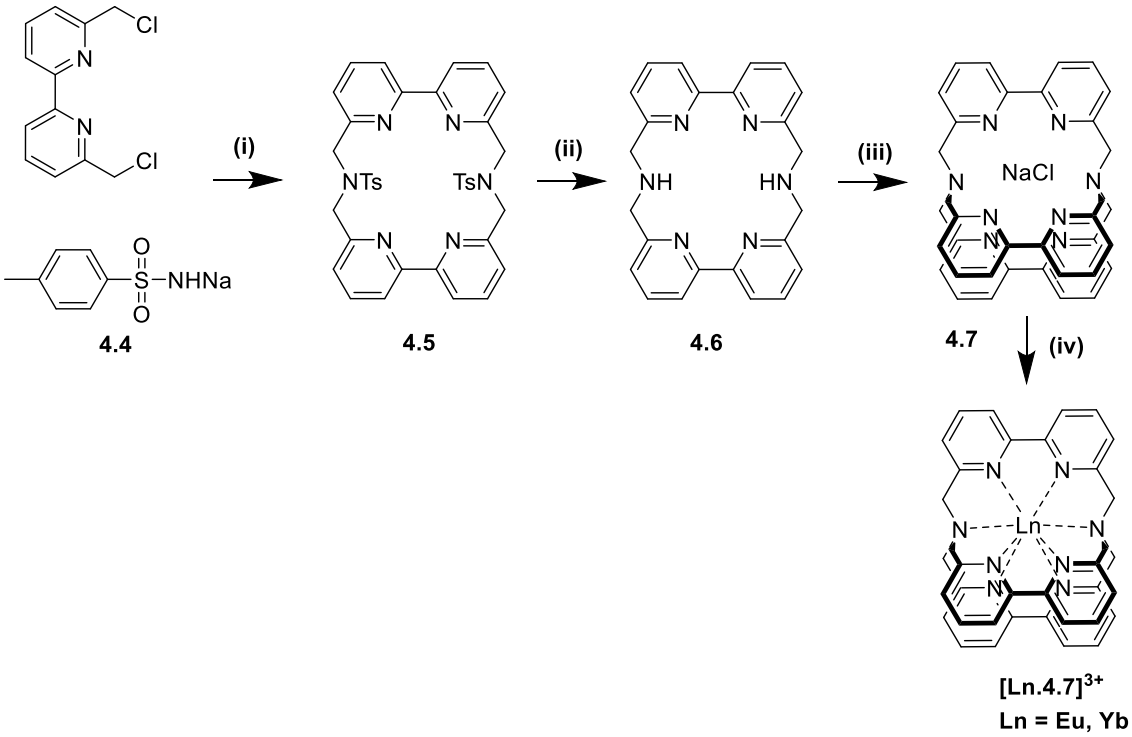


Figure 4. 2 Reaction scheme for the synthesis of lanthanide complexes of the Lehn cryptand. (i) EtOH, 90°C, 24h; (ii) c.H_2SO_4, 110°C, 2h; (iii); Na_2CO_3, 6,6'-bis(chloromethyl)-2,2'-bipyridyl, MeCN, reflux, 48h (iv) $Ln(OTf)_3$, MeCN, reflux, 2d.

[Ln.4.7]$^{3+}$ was synthesised essentially according to literature procedures (Figure 4. 2),[31, 32] though the procedure was modified in that 6,6'-bis(chloromethyl)-2,2'-bipyridyl was used instead of 6,6'-bis(bromomethyl)-2,2'-bipyridyl. *p*-Toluenesulfonamide monosodium salt was reacted with 6,6'-bis(chloromethyl)-2,2'-bipyridyl in acetonitrile to yield the macrobicycle, **4.5** in ca. 60% yield. This was subsequently deprotected using c.H_2SO_4 to yield **4.6** after neutralisation of the acidic solution and concomitant precipitation of the product. Since 6,6'-bis(chloromethyl)-2,2'-bipyridyl is not soluble in acetonitrile, further modification of the synthesis was required to access the cryptand. Instead of Lehn's method, the method used by Seitz et al.[32] was employed. This involved suspending all of the reagents in acetonitrile and heating this solution

under reflux. **4.7** was isolated as the NaCl salt after purification by silica gel column chromatography in ca. 20% yield.

Figure 4. 3 shows the ^{1}H NMR spectrum of **4.7:** the low number of observed resonances implies that the potential isomers of the cryptand ligand are in rapid exchange on the NMR timescale, or that the complex has high symmetry. The complexes, **[Ln.4.7]$^{3+}$** were obtained as colourless crystalline solids following reaction of the ligands with the corresponding lanthanide trifluoromethanesulfonate salt in acetonitrile for 2 days at reflux. All complexes where characterised by ^{1}H NMR and mass spectrometry.

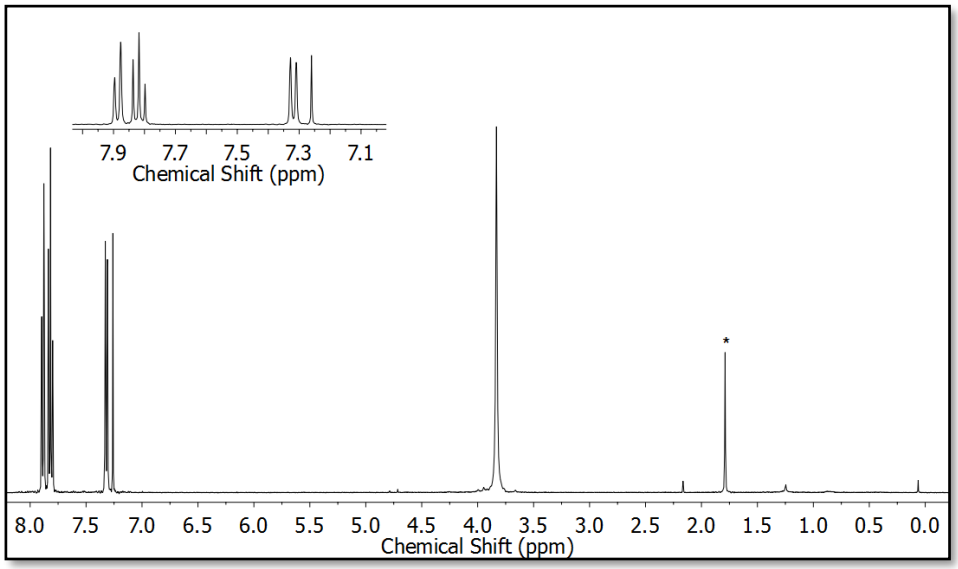


Figure 4. 3 ^{1}H NMR spectrum of **4.7** ($CDCl_3$, 298 K, 400 MHz). Inset: aromatic resonances.* indicates residual solvent signals.

4.3 NMR studies of lanthanide complexes

The ^{1}H NMR spectra of **[Eu.4.7]$^{3+}$** and **[Yb.4.7]$^{3+}$** were recorded in the presence and absence of fluoride (Figure 4. 5). In the absence of fluoride four peaks are observed which indicates that the crystallographically distinct environments observed in the crystal structure reported in literature[33] are in rapid equilibrium in solution - rendering the complex C_3 symmetric on the timescale of the NMR. In the case of **[Eu.4.7]$^{3+}$** the

resonances between 7 and 9 ppm correspond to the aromatic protons whilst the peak at 0.5 ppm corresponds to the NCH_2 resonances. Upon the addition of excess fluoride, a new species is evident for both Eu(III) and Yb(III) species in the ^1H NMR spectra with the complete loss of the original signals. The chemical shift range of the ^1H NMR resonances in **[Eu.4.7.F$_2$]$^+$** is significantly increased compared to that in **[Eu.4.7.(D$_2$O)$_2$]$^{3+}$** (18 ppm compared to 9 ppm). Correspondingly the chemical shift range in **[Yb.4.7.F$_2$]$^+$** is increased in compared to **[Yb.4.7.(D$_2$O)$_2$]$^{3+}$** (85 ppm compared to 6 ppm). The presence of more than four resonances upon the addition of fluoride suggests **[Eu.4.7.F$_2$]$^+$** and **[Yb.4.7.F$_2$]$^+$** are no longer C_3 symmetric on the timescale of the NMR experiment. The number of resonances suggests that two of the bipyridyl groups are equivalent on the NMR timescale with the other being inequivalent in each case. This suggests that binding of fluoride changes the rate of interconversion between isomers, suggesting that exchange of the monodentate ligands must form part of an interconversion mechanism that involves structural change and variable coordination at the lanthanide centre (summarised in Figure 4. 4).

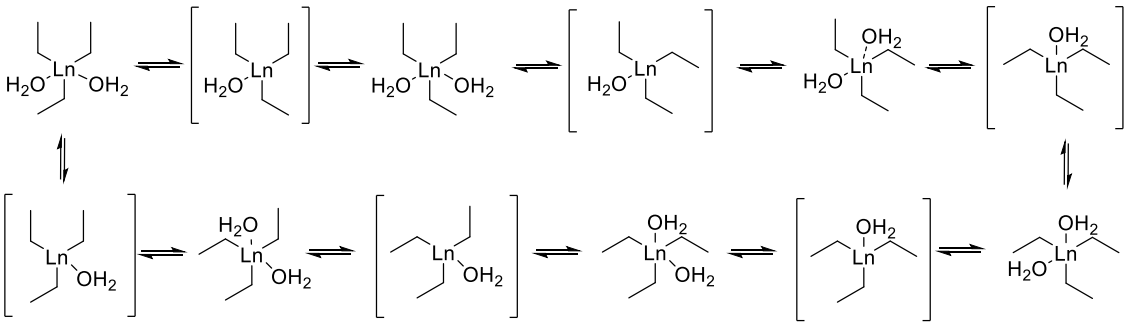


Figure 4. 4 Schematic showing water exchange and ligand rearrangement, with the approximate arrangement of the pyridyl rings defined in projection. Intermediate species in square brackets.

In the case of the hydrated Eu(III) and Yb(III) complexes then H_2O exchange and ligand rearrangement are both rapid on the NMR timescale, however fluoride exchange is significantly slower as a consequence of the electrostatic interaction between the

anion and the lanthanide, which reduces the speed of ligand rearrangement hence the apparent C_3 symmetry is lost.

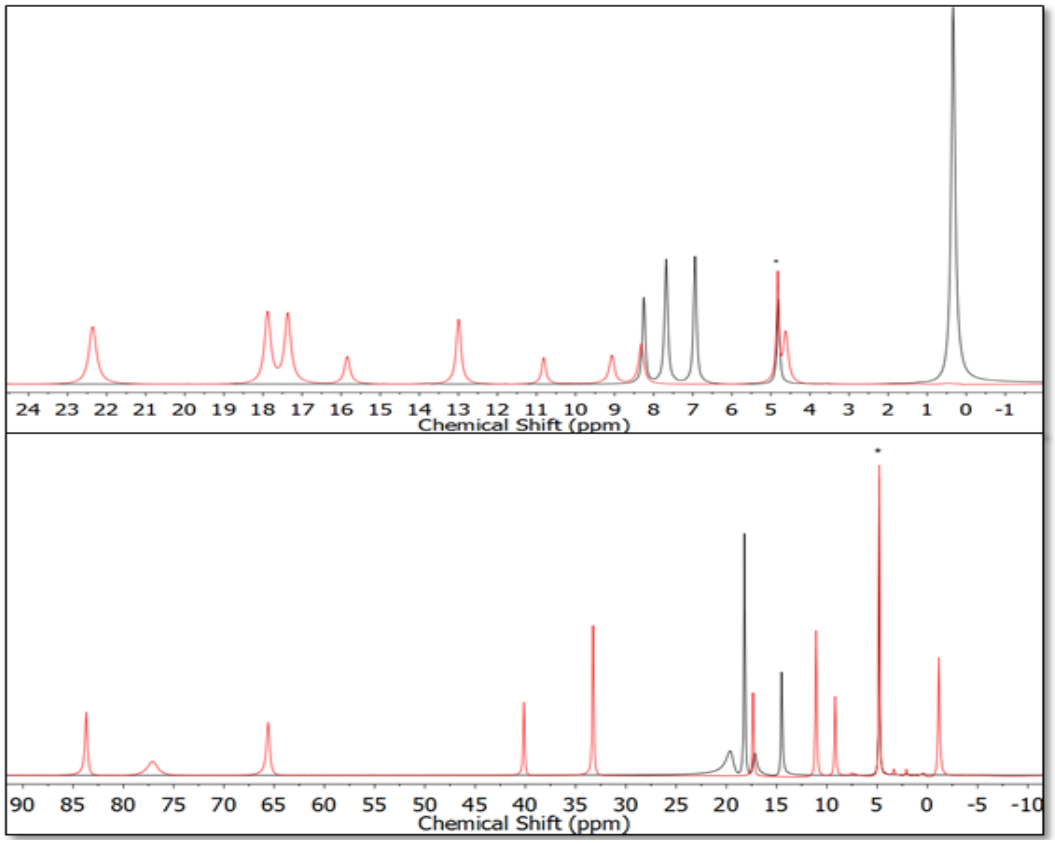


Figure 4. 5 Top: ^{1}H NMR spectrum of **[Eu.4.7]$^{3+}$** without fluoride (black) and with fluoride (red) (D_2O, 298 K, 400 MHz). * indicates residual solvent signal. Bottom: ^{1}H NMR spectrum of **[Yb.4.7]$^{3+}$** without fluoride (black) and with fluoride (red) (D_2O, 298 K, 400 MHz). * indicates residual solvent signal.

All of the chemical shifts in the ^{1}H NMR spectra of **[Eu.4.7]$^{3+}$** in the presence and absence of fluoride are positive which is unusual as in the ^{1}H NMR spectra of most Eu(III) complexes then both positive and negative shifts are observed (owing to the effect of geometric factors on the pseudocontact term). This suggests that both contact and pseudocontact terms are likely to be important in determining the shift; theoretical calculations would be required to fully explain this phenomenon. The bulk of the shifts go in the same direction upon addition of fluoride and there is a large expansion in the chemical shift range upon fluoride binding. In the case of **[Yb.4.7]$^{3+}$** then most of the chemical shifts are again positive and upon the addition of fluoride

there is a large increase in chemical shift range. Some of this increase in chemical shift range is a consequence of the exchange between ligand isomers with the spectra appearing more 'normal' for the fluoride bound species. It is also likely that fluoride binding has an effect on the lanthanide crystal field which will also affect the spectral range; Bleaney analysis is difficult in non-axial symmetry so the change in crystal field can't be easily quantified.

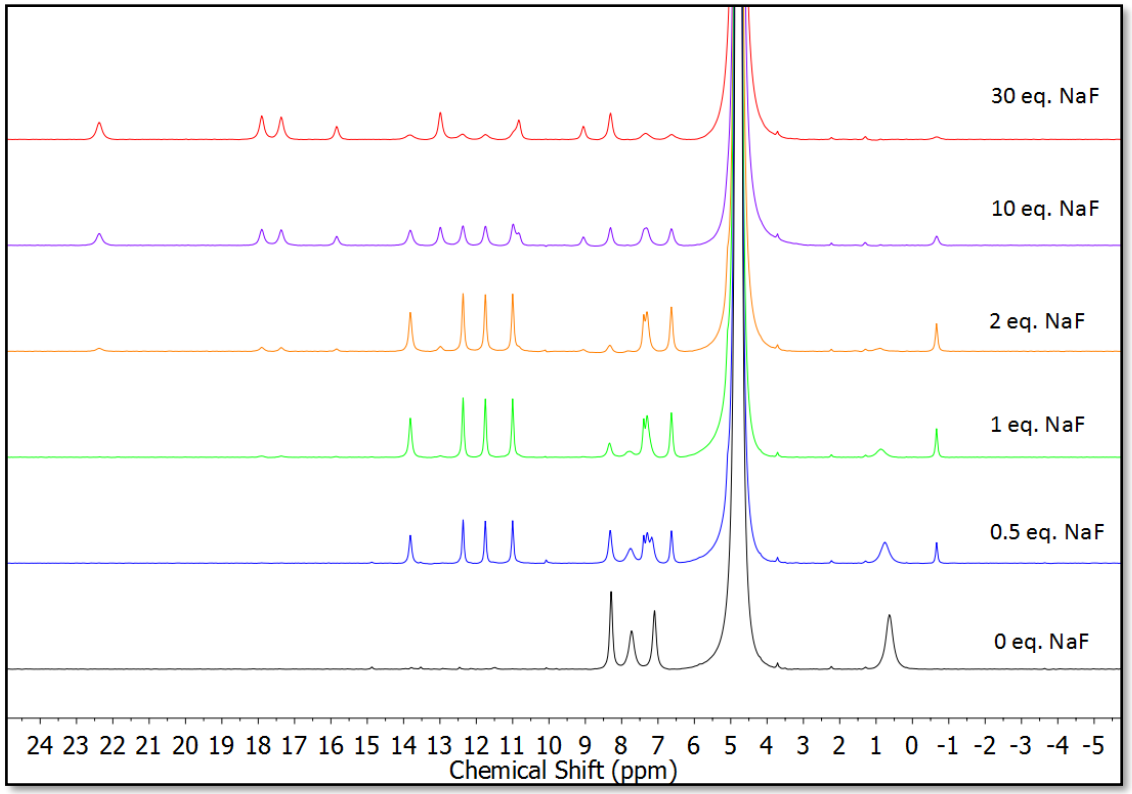


Figure 4. 6 ^{1}H NMR spectrum of **[Eu.4.7]$^{3+}$** upon addition of sodium fluoride in (D_2O, 298 K, 500 MHz).

The addition of 0.5 equivalents of sodium fluoride to **[Eu.4.7]$^{3+}$** resulted in the appearance of a new set of proton resonances corresponding to **[Eu.4.7.F.D_2O]$^{2+}$** in slow exchange with the original hydrated species, **[Eu.4.7.$(D_2O)_2$]$^{3+}$**, on the NMR timescale as well as an increase in spectral range (Figure 4. 6). In the presence of 1 equivalent of sodium fluoride there is an increase in the intensity of the resonances corresponding to the newly formed species with a decrease in the intensity of the

resonances corresponding to the original hydrated species. In the presence of 2 equivalents of sodium fluoride a third species, **[Eu.4.7.F$_2$]$^+$** is observed with a significant decrease in the intensity of the resonances corresponding to the original hydrated species, again an increase in spectral range is observed. After the addition of 10 equivalents of sodium fluoride then the original hydrated species is no longer observable whilst the **[Eu.4.7.F.D$_2$O]$^{2+}$** and **[Eu.4.7.F$_2$]$^+$** are in slow exchange on the NMR timescale. After addition of 30 equivalents of sodium fluoride, the dominant species in solution is **[Eu.4.7.F$_2$]$^+$**. The presence of three different species in solution supports a two-step fluoride binding process; this is also supported by luminescence titration data. Qualitatively the ^{1}H NMR titration shows that there is a high affinity for the first fluoride binding to the lanthanide centre with a lower affinity for the second fluoride binding.

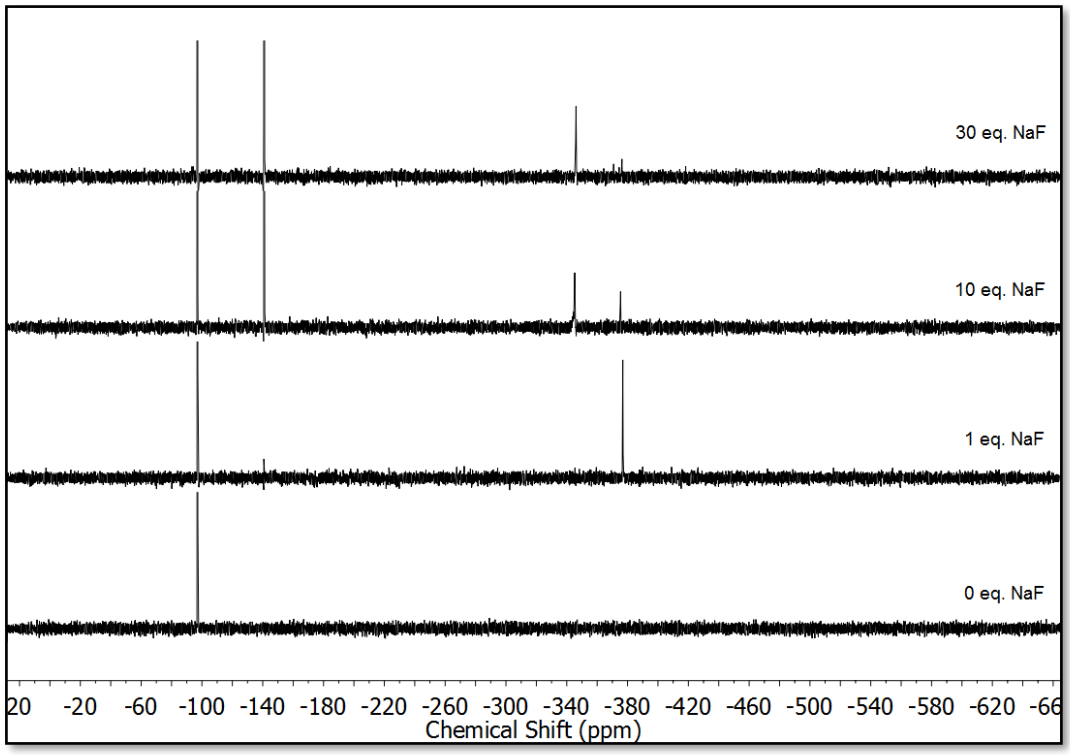


Figure 4. 7 ^{19}F NMR spectrum of **[Eu.4.7]$^{3+}$** upon addition of sodium fluoride in (D_2O, 298 K, 500 MHz).

^{19}F NMR data (Figure 4. 7) also supports a two-step fluoride binding process; after the addition of 1 equivalent of sodium fluoride a Eu(III) bound fluoride peak corresponding to the **[Eu.4.7.F.D$_2$O]$^{2+}$** species is apparent in the ^{19}F NMR spectra at -376 ppm with a peak at ca. -140 ppm corresponding to free sodium fluoride. At 10 equivalents of sodium fluoride another Eu(III) bound fluoride peak is present at -345 ppm which corresponds to the **[Eu.4.7.F$_2$]$^{+}$** species; a singlet is observed for this peak suggesting both bound fluorides are equivalent. At 30 equivalents of sodium fluoride, **[Eu.4.7.F$_2$]$^{+}$**, is the dominant species with only trace amounts of **[Eu.4.7.F.D$_2$O]$^{2+}$**. Upon addition of sodium fluoride to **[Yb.4.7]$^{3+}$** the Yb(III) bound fluoride could not be observed by ^{19}F NMR, however it is clear from the ^{1}H NMR spectra that fluoride is indeed binding to the lanthanide centre.

4.4 Photophysical properties

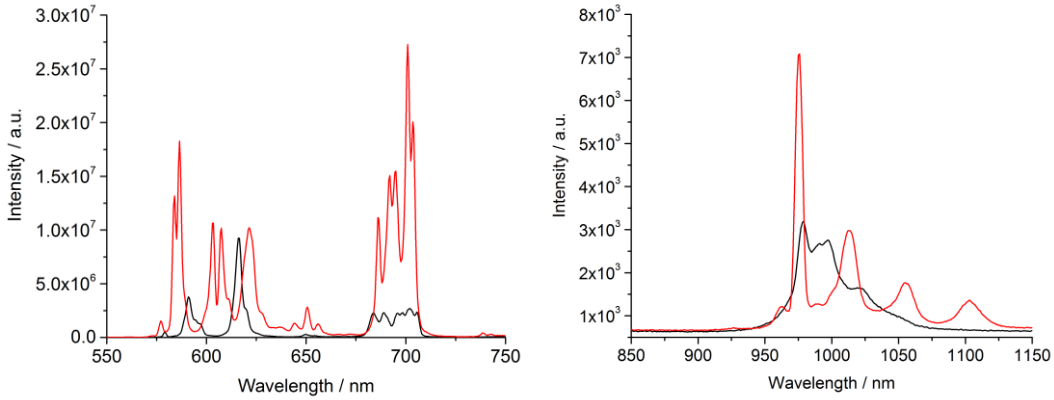


Figure 4. 8 Left: Change in form of emission spectra with fluoride. **[Eu.4.7]$^{3+}$** in D_2O (black) and with excess sodium fluoride (red), λ_{ex} = 327 nm, exit slits 1 nm. Right: **[Yb.4.7]$^{3+}$** in D_2O (black) and with excess sodium fluoride (red), λ_{ex} = 339 nm, exit slits 5 nm.

The emission spectra of **[Eu.4.7]$^{3+}$** and **[Yb.4.7]$^{3+}$** were recorded in the presence and absence of fluoride (Figure 4. 8) by excitation through the ligand at 327 and 339 nm respectively. Dramatic changes in the intensity, band position and form are observed upon addition of fluoride in both complexes. There is a significant increase in the

intensity of the $^5D_0$-$^7F_1$ and $^5D_0$-$^7F_4$ transitions, with both the $^5D_0$-$^7F_1$ and $^5D_0$-$^7F_2$ transitions experiencing significant splitting suggesting a large increase in the crystal field upon fluoride binding. Substantial m_J splitting was observed in the Yb(III) spectra upon the addition of fluoride. Long et al. [11] have pictorially represented the m_J states for the lowest J states of the Ln(III) ions using a method developed by Sievers'.[12] In the case of Yb(III) then these representations show that some of these states are prolate whilst others are oblate; the relative energy and the ordering of these states is determined by the nature of the ligand field with the relative populations of these showing a Boltzmann distribution. Changes in the ligand field experienced (i.e. replacing bound H_2O for bound F^-) can affect the energy, ordering and relative populations of the m_J states thus modulating the anisotropy and spectroscopic properties. Blackburn et al.[10] have shown through theoretical calculations that changing the Yb-F bond length in **[Yb.DTMA.F]$^{2+}$** alters the relative energy and populations of the m_J states. It is therefore reasonable that the substantial increase in the energy between the m_J states as estimated from the Yb(III) emission spectra (Figure 4. 8) will result in significant changes in the anisotropy and observed spectroscopic properties in these systems. Figure 4. 9 shows the energy differences of the $\pm$ 1/2, 3/2, 5/2, and 7/2 states with their relative Boltzmann populations; it is not possible to determine the ordering to specific m_J states without computational studies.

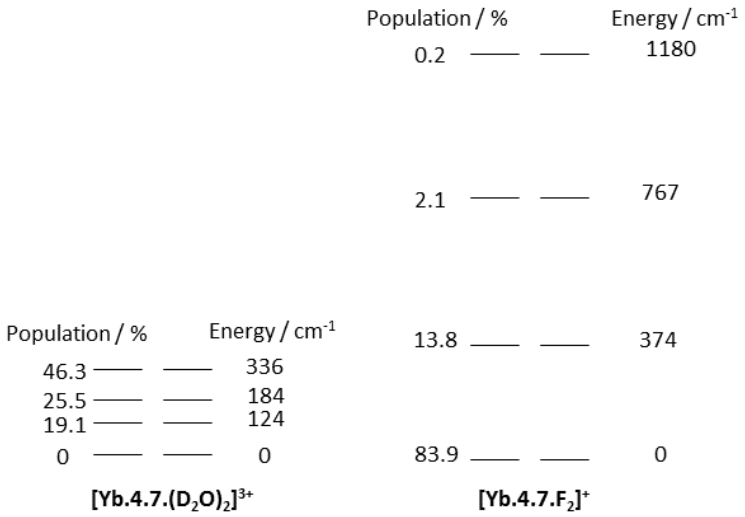


Figure 4. 9 Schematic showing the energy differences and normalised Boltzmann distribution for **[Yb.4.7.$(D_2O)_2$]$^{3+}$** and **[Yb.4.7.F_2]$^{+}$** of the ground Yb(III) m_J states.

The number of solvent molecules coordinated to the Eu(III) centre, *q*, in the presence and absence of fluoride are shown in Table 4. 1. In the absence of fluoride the *q* value was found to be 2.4 which is in line with literature values and suggests there is a mixture of doubly and triply hydrated species in solution. Lifetimes were also measured upon the addition of an excess of fluoride, there was a significant decrease in *q*, with the value being approximately 0 suggesting that fluoride has displaced the bound solvent molecules. Mono-exponential decay was observed for the luminescence of **[Eu.4.7]$^{3+}$** in the presence and absence of excess fluoride, this reflects the rapid exchange of water and fluoride.[36]

4.5 Fluoride binding

The affinity of fluoride with **[Eu.4.7]$^{3+}$** was determined by luminescence spectroscopy; Dynafit® was used to fit the observed changes. A two-step binding model was used as this gave less error upon fitting compared to a one-step (2:1) binding process. The association constants and confidence intervals are shown in Table 4. 1.

$$[LnL.2H_2O]^{3+} + F^- \rightleftharpoons [LnL.H_2O.F]^{2+} + H_2O$$

$$[LnL.H_2O.F]^{2+} + F^- \rightleftharpoons [LnL.F]^{+} + H_2O$$

The changes in intensity of regions of the emission spectra were monitored to assess the fluoride binding affinity. Fitted binding data is shown in Figure 4. 10.

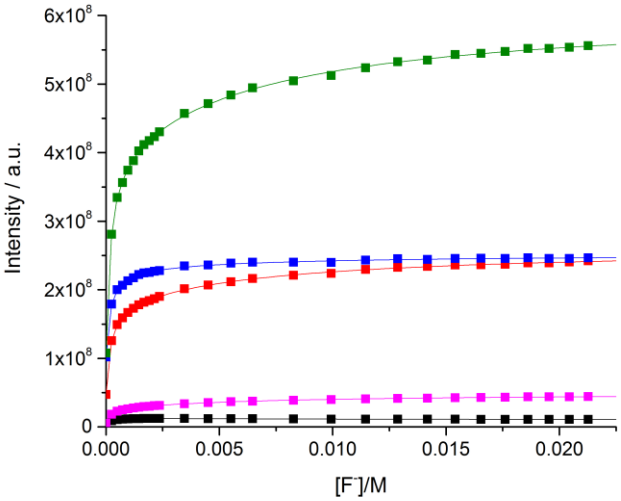


Figure 4. 10 Binding isotherm and line of best fit for titration of **[Eu.4.7]$^{3+}$** with NaF in H_2O. Black: 575-581 nm, purple: 640-662 nm, red: 682-605 nm, blue: 606-634 nm and green: 677-716 nm.

The two step fluoride binding process is supported by the NMR data. K_1 is significantly larger than K_2, it is likely that K_1 is the association constants for the formation of **[Eu.4.7.F.H$_2$O]$^{2+}$**, with K_2 corresponding to the formation of **[Eu.4.7.F$_2$]$^{+}$**. The decrease in the association constant for sequential fluoride binding is likely due to the fact that one of the two lanthanide binding sites already being taken up by a fluoride and the fact the intermediate species, **[Eu.4.7.F.H$_2$O]$^{2+}$**, has a 2+ charge reducing the electrostatic attraction between the complex and fluoride compared to **[Eu.4.7.(H$_2$O)$_2$]$^{3+}$**. Both of the association constants observed are larger than those observed in the lanthanide tetra-amide complexes in chapter three (ca. K = 40 M^{-1}) which could be due to the lanthanide being more exposed in the lanthanide complexes of the Lehn cryptand compared to the lanthanide in the tetra-amide complexes.

Furthermore, the residual charge on the lanthanide in the case of the complexes of the Lehn cryptand will likely be larger due to the bipyridyl being a less efficient donor than the amine and acetamide ketone donors in the case of the tetra-amide species.

Table 4. 1 Association constants, *K*, for **[Eu.4.7]$^{3+}$** with NaF in H_2O at 298K. 95% confidence intervals in square brackets, lifetimes and *q* values.

	***K*/M^{-1}**	**No NaF**			**+ NaF**		
	Luminescence	**τ_{H2O}[a]**	**τ_{D2O}[a]**	***q***	**τ_{H2O}[b]**	**τ_{D2O}[b]**	***q***
[Eu.4.7]$^{3+}$	K_1 = 5651 [5370 - 6250]	0.36	1.81	2.4	1.08	2.53	0.3
	K_2 = 148 [136 -160]						

[a] λ_{ex} = 327 nm, λ_{em} = 616 nm. [b] λ_{ex} = 327 nm, λ_{em} = 621 nm.

4.6 Conclusions

In this chapter the nature of the interaction between fluoride and lanthanide complexes of the Lehn cryptand has been explored in detail. It was shown by NMR spectroscopy that fluoride binding to the metal centre is a two-step process (Figure 4. 11) where the first binding event occurs more readily than the second. The binding of fluoride removes the apparent C_3 symmetry observed for the hydrated species which is due to the significantly slower fluoride exchange compared to H_2O exchange. Fluoride binding resulted in a significant increase in the crystal field which changes the magnetic anisotropy; this is observed directly through luminescence studies and indirectly through NMR studies.

These results complement those from the earlier chapters in this thesis, and reveal further subtleties in the effect of fluoride on the lanthanide crystal field. However, a complete understanding must wait until it becomes possible to model these systems effectively.

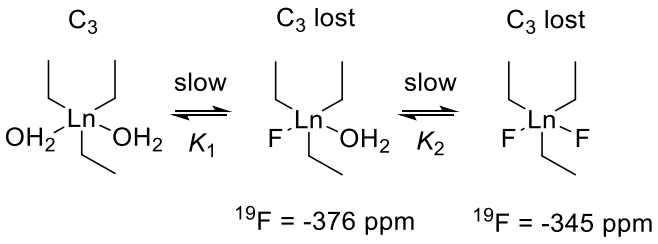


Figure 4. 11 Schematic of fluoride binding to lanthanide centre.

4.6 References

1. B. Alpha, J. M. Lehn and G. Mathis, *Angew. Chem. Int. Ed.*, 1987, **26**, 266-267.
2. B. Alpha, V. Balzani, J. M. Lehn, S. Perathoner and N. Sabbatini, *Angew. Chem., Int. Ed. Engl.*, 1987, **26**, 1266-1267.
3. G. Blasse, G. J. Dirksen, D. Vandervoort, N. Sabbatini, S. Perathoner, J. M. Lehn and B. Alpha, *Chem. Phys. Lett.*, 1988, **146**, 347-351.
4. B. Alpha, R. Ballardini, V. Balzani, J. M. Lehn, S. Perathoner and N. Sabbatini, *Photochem. Photobiol.*, 1990, **52**, 299-306.
5. S. Faulkner, A. Beeby, M. C. Carrie, A. Dadabhoy, A. M. Kenwright and P. G. Sammes, *Inorg. Chem. Commun.*, 2001, **4**, 187-190.
6. US 5627074, 1997.
7. J. P. Cross, A. Dadabhoy and P. G. Sammes, *J. Lumin.*, 2004, **110**, 113-124.
8. J. C. Rodriguezubis, B. Alpha, D. Plancherel and J. M. Lehn, *Helv. Chim. Acta*, 1984, **67**, 2264-2269.
9. C. Bischof, J. Wahsner, J. Scholten, S. Trosien and M. Seitz, *J. Am. Chem. Soc.*, 2010, **132**, 14334-14335.
10. I. Bkouchewaksman, J. Guilhem, C. Pascard, B. Alpha, R. Deschenaux and J. M. Lehn, *Helv. Chim. Acta*, 1991, **74**, 1163-1170.
11. J. D. Rinehart and J. R. Long, *Chem. Sci.*, 2011, **2**, 2078-2085.
12. J. Sievers, *Z. Phys. B Con. Mat*, 1982, **45**, 289-296.
13. O. A. Blackburn, N. F. Chilton, K. Keller, C. E. Tait, W. K. Myers, E. J. L. McInnes, A. M. Kenwright, P. D. Beer, C. R. Timmel and S. Faulkner, *Angew. Chem., Int. Ed.*, 2015, **54**, 10783-10786.
14. W. D. Horrocks, V. K. Arkle, F. J. Liotta and D. R. Sudnick, *J. Am. Chem. Soc.*, 1983, **105**, 3455-3459.

5 Synthesis and study of halogenated phenacylDO3A complexes

5.1 Introduction

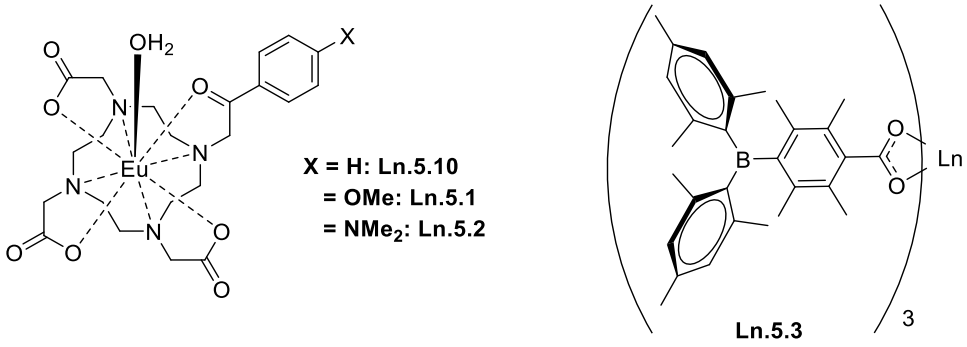


Figure 5. 1 Lanthanide compounds discussed in this section.

This chapter describes the synthesis and application of a range of halogenated phenacylDO3A derivatives, culminating in the demonstration of cyanide responsive behaviour by lanthanide complexes derived from such systems.

Bushby et al.[1] were the first to investigate the effects of changing the para substituent in phenacylDO3A lanthanide complexes (Figure 5. 1): unsubstituted (**5.10**) and methoxy-substituted (**5.1**) ligands were found to be capable of sensitising Eu(III) in aqueous media, while the dimethylamino-substituted ligand (**5.2**) showed solvent dependent behaviour with no emission in aqueous media.

In this chapter halogen substituents were chosen to explore the influence of their π electron-donating and σ electron-withdrawing properties on the photophysical properties of their lanthanide complexes. Furthermore, halogen substituents offered further utility; fluorine has the potential to be used as an internal standard in ^{19}F NMR fluoride binding studies whilst the iodo- and bromo-substituted species offer the potential to be utilised in 'Pd' cross coupling reactions with the aim to produce multimetallic lanthanide systems. This chapter also builds on the observations in chapter three and attempts to investigate the fluoride binding ability of eight

coordinate lanthanide complexes bearing arylacyl sensitising groups. We also resolved to study the effect of cyanide in aqueous solution on the spectroscopic properties of stable lanthanide complexes. There is very little information on the interaction between cyanide and lanthanide complexes in the literature; coordination of cyanide to a lanthanide ion in aqueous media is unlikely on thermodynamic grounds since coordination of cyanide would be unlikely to offset the loss of hydration energy. However, there are a number of non-lanthanide based cyanide probes based on triarylboron moieties.[2-4] Wang et al.[5] reported lanthanide based cyanide probes (**Ln.5.3**, Figure 5. 1) based on 1, 3-diketonato ligands bearing triarylboron moieties (it should be noted that these probes are often ineffective in water). Addition of cyanide or fluoride to **Eu.5.3** in THF caused a multi-stage colour change to occur. Addition of up to two equivalents of the anions resulted in an increase in Eu(III) emission intensity which is attributed to a lowering of the ligand triplet state upon anion binding resulting in more efficient energy transfer. Above two equivalents quenching of Eu(III) emission is observed due to the displacement of the ligand from the lanthanide centre by the anion. **Eu.5.3** and **Tb.5.3** were tested for sensing of fluoride and cyanide by loading onto filter paper; a significant response was observed upon addition of fluoride (TBAF in MeOH, with little response for aqueous sources of fluoride) whilst a less obvious colour change was observed upon cyanide addition (TBACN in MeOH). It is worth noting that these investigations were conducted in THF and even in this relatively uncompetitive media the complexes aren't stable in the presence of competitive anions which results in the displacement of the lanthanide from the diketonate. This, together with the complexity of speciation and the ambiguity of the

response to two different ions, makes Wang's probes unsatisfactory for practical purposes.

The importance of sensing, and indeed discriminating, both fluoride and cyanide in chemical weapons detection applications caused us to consider exploring the prospect of chemical reactivity of cyanide at a ligand site being rendered more likely by the proximity of a lanthanide ion acting as a Lewis acid. As will be seen, this approach has been used to show how lanthanide complexes can offer specificity for cyanide over fluoride, complementing the fluoride responsive probes described earlier in the thesis.

5.2 Synthesis and characterisation

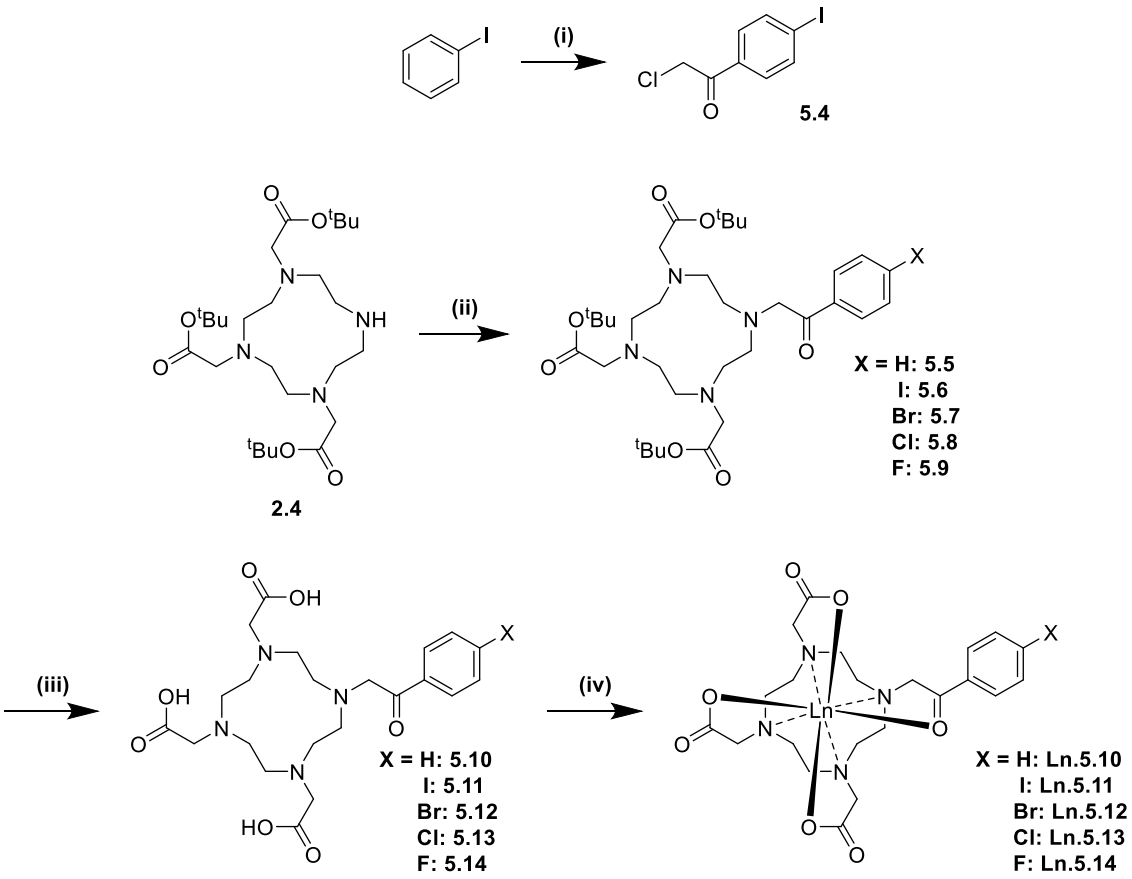


Figure 5. 2 Synthetic scheme for the preparation of lanthanide complexes containing acetophenones. (i) $AlCl_3$, 2-chloroacteylchloride, DCM, 0°C, 3h; (ii) dihaloacetophenone, KI, K_2CO_3, MeCN, 80°C, 48h; (iii) TFA, DCM, RT, 24h; (iv) $Ln(OTf)_3$, MeOH, 60°C, 2d.

As with the compounds described in chapter two, the targets chosen here all incorporate an aryl ketone that is directly coordinated to the lanthanide centre. As well as providing an octadentate ligand, this approach aids energy transfer from the chromophore to the metal by favouring a Dexter exchange pathway. Figure 5. 2 shows the synthetic route employed for the preparation of lanthanide complexes containing an acetophenone chromophore. **5.4** was synthesised *via* Friedel-Crafts acylation of iodobenzene using $AlCl_3$ as a Lewis acid catalyst, and purification by silica gel column chromatography gave the desired species as an off white solid. All the other acetophenones used were commercially available. Alkylation of the fourth nitrogen of triester (**2.4**) was conducted in the same manner for all acetophenone species using standard literature conditions. Purification by silica gel column chromatography afforded the protected ligands as pale yellow solids. The *t*-butyl groups were cleaved using TFA in DCM giving the ligands in quantitative yield. Lanthanide complexes were obtained by stirring the ligand and the corresponding lanthanide triflate salt in methanol at 60°C using a small excess of the lanthanide salt. Excess lanthanide was removed in the reaction work up by raising the pH to around 10 and precipitating the insoluble lanthanide hydroxide, which was removed by centrifuging and filtration. All complexes were found to be soluble in water and all characterisation was conducted in aqueous media. Figure 5. 3 shows high resolution ESMS of the **Eu.5.11**, **Tb.5.11** and **Gd.5.11**.

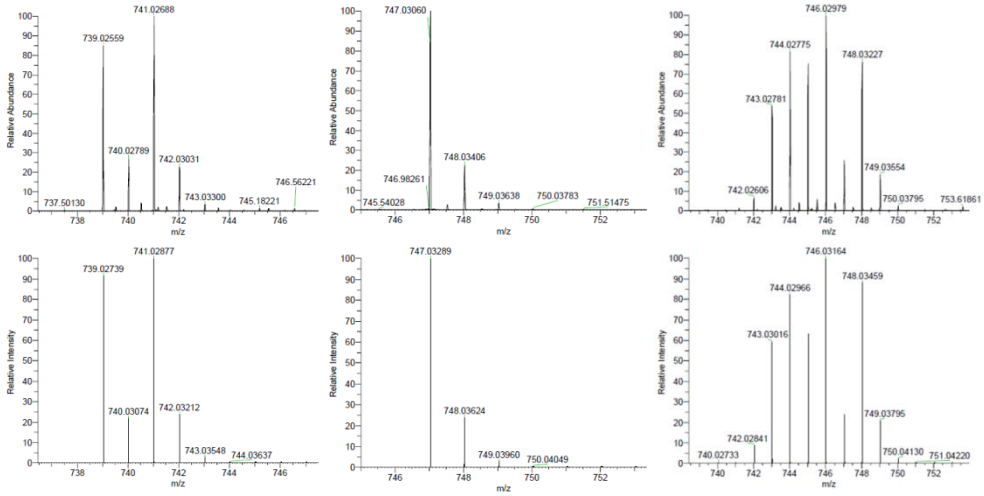


Figure 5. 3 Experimental (Top) and Theoretical (Bottom) high resolution mass spectra of **Eu.5.11** (left), **Tb.5.11** (middle) and **Gd.5.11** (right) as their $[M+H]^+$ adducts.

The ^{1}H NMR spectrum of **Eu.5.14** is shown in Figure 5. 4. In **Eu.5.14** the four axial ring proton signals between 25 and 40 ppm suggest that the square antiprismatic (SAP) geometry is predominant in solution, with the twisted square antiprismatic (TSAP) diasteroisomer present in a much lower abundance. From these spectra it is clear that the oxygen atom of the carbonyl group attached to the acetophenone is coordinated to the Ln(III) ion. This behaviour is exhibited in all other Eu(III) acetophenone variants discussed in this chapter suggesting that they have similar solution structures and Eu(III) environment. The spectra of **Eu.5.10-5.14** reveal similar chemical shifts, suggesting that the electron donating ability of the acetophenone ligand has little effect on the ability of the ketone oxygen to coordinate to the Ln(III) ion.

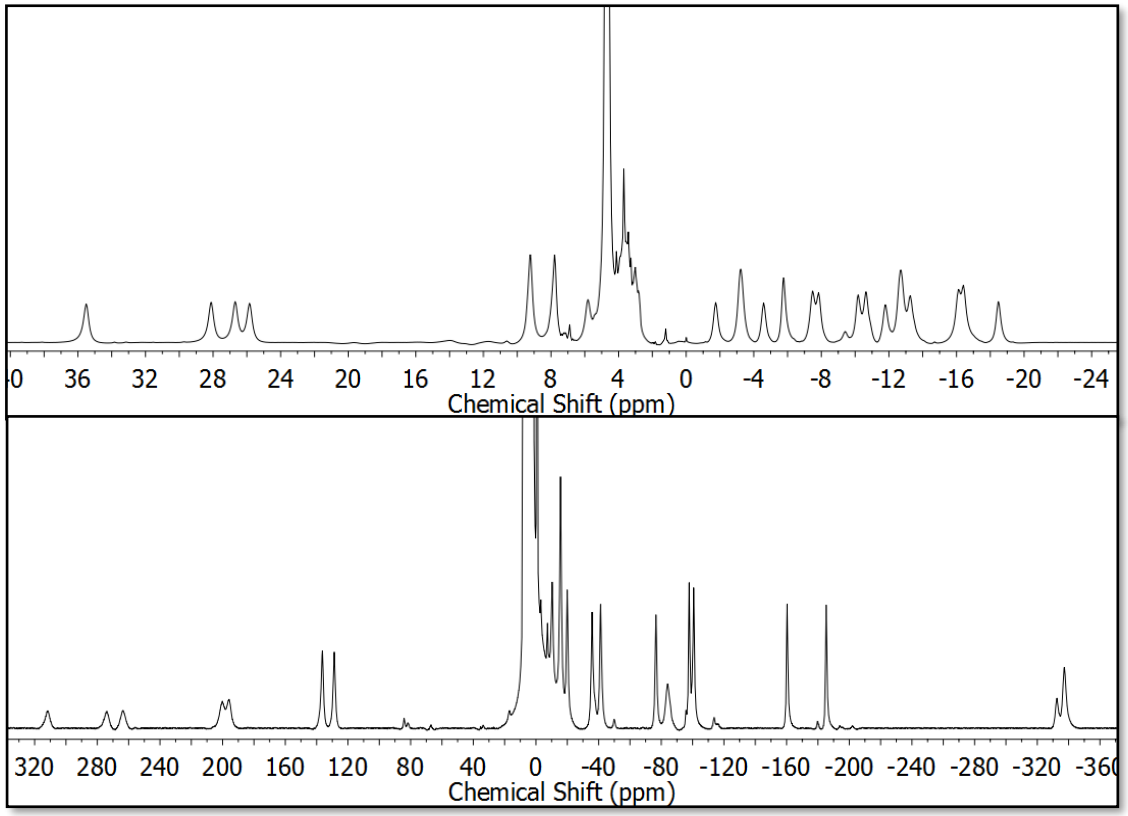


Figure 5. 4 Top: ^{1}H NMR spectrum of **Eu.5.14** (298 K, D_2O, pH 4). Bottom: ^{1}H NMR spectrum of **Tb.5.10** (298 K, D_2O, pH 4).

The NMR of the Tb(III) complexes reveals similar structural characteristics. It is worth noting that these Tb(III) complexes display a reduced contribution from the contact shift by comparison with their Eu(III) analogues, meaning that the shifts observed reflect the geometric pseudocontact contributions to a greater degree.

5.3 Photophysical properties

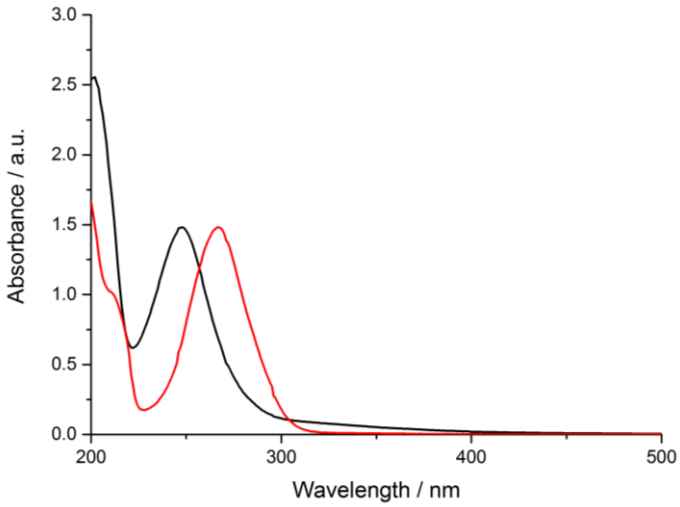


Figure 5. 5 Comparison of the UV-Vis absorption spectra of **5.14** (black) and **Eu.5.14** (red) in H_2O.

Figure 5. 5 shows the comparison of the UV-Vis spectra of **5.14** and **Eu.5.14**. The ligand absorption spectrum shows a ground state absorption maxima at 248 nm in aqueous solution which can be attributed to an ILCT transition centred on the aromatic chromophore. Upon complexation there is a red shift in the absorption maxima to 266 nm, this is indicative of a strong interaction between the lanthanide and the carbonyl group of the sensitiser supporting the fact that the ketone oxygen is coordinated to the lanthanide centre. The phenomenon was also observed in all other variants in this study suggesting also that these species have ILCT transitions. The difference in the absorption maxima for the ligands and their corresponding lanthanide complexes are ca. 18 nm in all cases which suggests the interaction between the ketone oxygen and the lanthanide centre are similar in all cases.

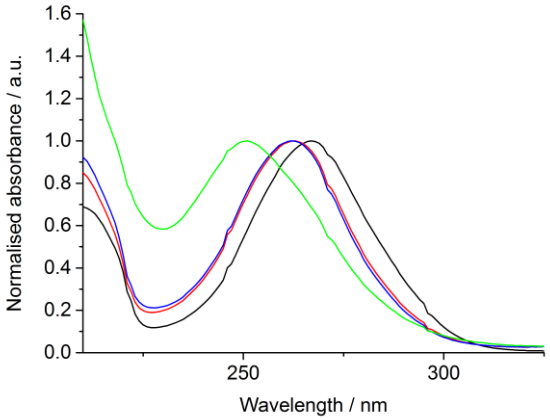


Figure 5. 6 UV-Vis absorption spectra of **Tb.5.14** in solvents of different polarity [H_2O (black), MeCN (green), MeOH (red), EtOH (blue)].

The charge transfer nature of the absorption bands was confirmed by recording the absorption spectra of **Tb.5.14** in solvents of different polarities (Figure 5. 6). The absorption band maximum is red shifted upon the increase in solvent polarity due to the excited state being stabilised more efficiently.

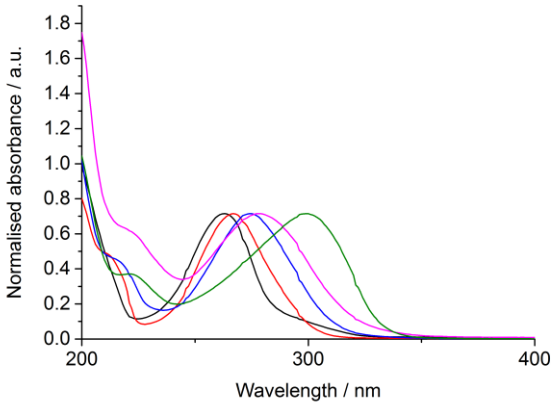


Figure 5. 7 Comparison of the UV-Vis absorption spectra of **Eu.5.10** (black), **Eu.5.11** (green), **Eu.5.12** (purple), **Eu.5.13** (blue) and **Eu.5.14** (red) in H_2O.

The UV-Vis spectra of the Eu(III) complexes of the substituted phenacylDO3A species are shown in Figure 5. 7. The absorption wavelength maxima increases as the electron donating capability of the ring substituent increases due to increased conjugation stabilising the excited state.

All the Eu(III) and Tb(III) compounds displayed characteristic emission upon excitation into the lowest energy absorption bands which confirms that sensitisation is occurring. The emission lifetimes of the complexes in H_2O and D_2O as well as the inner sphere hydration numbers, *q*, are shown in Table 5. 1. The modified Horrocks' equation used to determine inner sphere hydration numbers are shown below:

$$q_{Eu} = 1.2(k_H - k_D - 0.25)$$

$$q_{Tb} = 5(k_H - k_D - 0.06)$$

The values of *q* for all of the Eu(III) species synthesised are close to one which is consistent with the complexes being octadentate and that the sensitiser carbonyl is coordinated to the lanthanide. The *q* values for **Tb.5.10** and **Tb.5.14** are also consistent with the lanthanide having one bound water molecule. However for **Tb.5.11**, **Tb.5.12** and **Tb.5.13** the much shorter lifetimes suggest quenching pathways other than those offered by high frequency solvent oscillators are playing a role and thus the margins of error associated with Horrocks' equation are substantially greater in these cases, meaning that the values obtained need to be treated with caution.

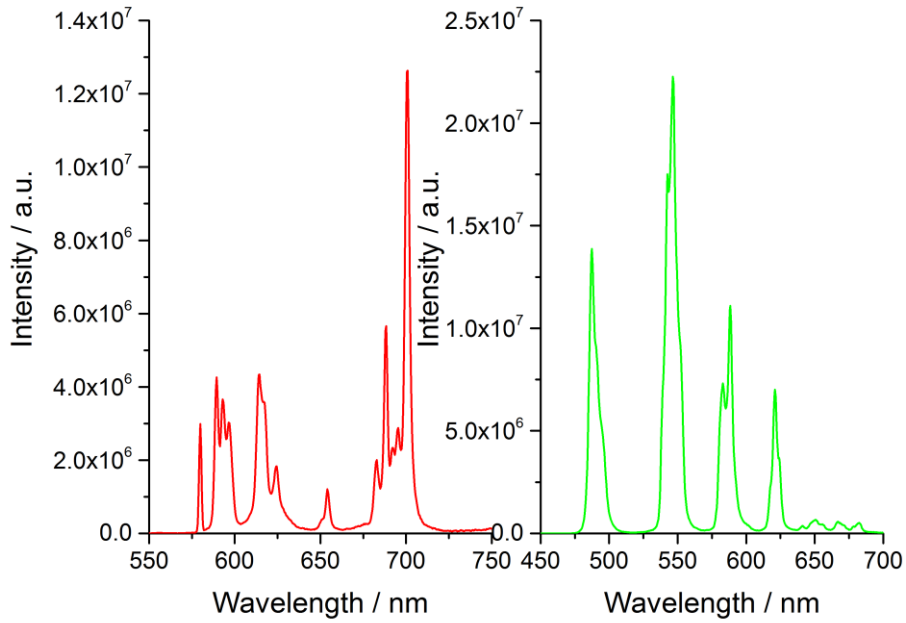


Figure 5. 8 Emission spectra of **Eu.5.13** (left) and **Tb.5.13** (right) in H_2O.

Eu.5.10-5.14 have very similar emission profiles in aqueous media (an example is shown in Figure 5. 8); all have a single sharp $^5D_0$-$^7F_0$ transition indicating one main species in solution in each case. The intensity and form of the other transitions are very similar for all the other bands with changes in intensity of the hypersensitive $^5D_0$-$^7F_2$ transition relative to the of $^5D_0$-$^7F_2$ transition of up to ca. 10%; the intensity of the $^5D_0$-$^7F_2$ transition increases as the electron donating ability of the aryl substituent increases which in turn enhances the polarisability of the ketone carbonyl. The similar emission profiles indicate that the complexes have very similar solution structures.

Tb.DO3A complexes typically have emission lifetimes in the order of 1-2 ms in H_2O and 2-3 ms on D_2O. **Tb.5.11**, **Tb.5.12** and **Tb.5.13** have significantly shorter lifetimes in H_2O and D_2O when compared to **Tb.5.10** and **Tb.5.14** which might suggest that in the former compounds back energy transfer which deactivates the Tb(III) $^5D_4$ emissive state is occurring. In order to investigate the origin of this deactivation then photophysical studies were conducted on **Tb.5.11** in H_2O under aerated and

deoxygenated conditions (Figure 5. 9). The form of the Tb(III) emission profile remains unchanged upon the deoxygenation of the sample; a small increase in the emission intensity was observed which suggests either a degree of triplet involvement in the energy transfer cascade, or a dual energy transfer mechanism in which a through space component of energy transfer from the triplet state is disrupted by competitive oxygen quenching. The absence of a significant change in lifetime upon deoxygenation suggests that this second pathway (in which oxygen and the lanthanide compete to quench the excited state) is responsible for the change in observed emission intensity. If the triplet is quenched competitively by the lanthanide and oxygen, and no significant equilibrium between the lanthanide state and the triplet donor can be achieved on the timescale of energy transfer/quenching, then the signal intensity will vary with the concentration of oxygen.[6]

The shorter than expected lifetimes of the Tb(III) complexes also need to be addressed. In this case, it is clear that another state must be quenching the Tb(III) centred emissive state. This quenching is likely to be due to low lying ILCT states deactivating the $^5D_4$ state and reducing the emissive state lifetimes. Once again, the degree of quenching appears to be determined by the nature of the halogen atom, suggesting that non-bonding electrons on the halogen play a role in this process: a hypothesis borne out by the effective quenching observed in the iodine substituted system (and by the relative lack of quenching in the fluorine substituted system). Shorter than expected lifetimes are also observed with the brominated and chlorinated analogues with the effectiveness of the ILCT quenching increasing with electron donating ability of the halide. If this hypothesis is valid, then the ILCT state of **Ln.5.11** must be higher in energy than the emissive state of Eu(III), but lower in energy

than the emissive state of Tb(III). Though the very short lifetimes of the Tb(III) complex suggest that this is likely to be the case (since energy transfer would be expected to be rapid), the transient absorption study that could confirm the hypothesis is beyond the scope of this work.

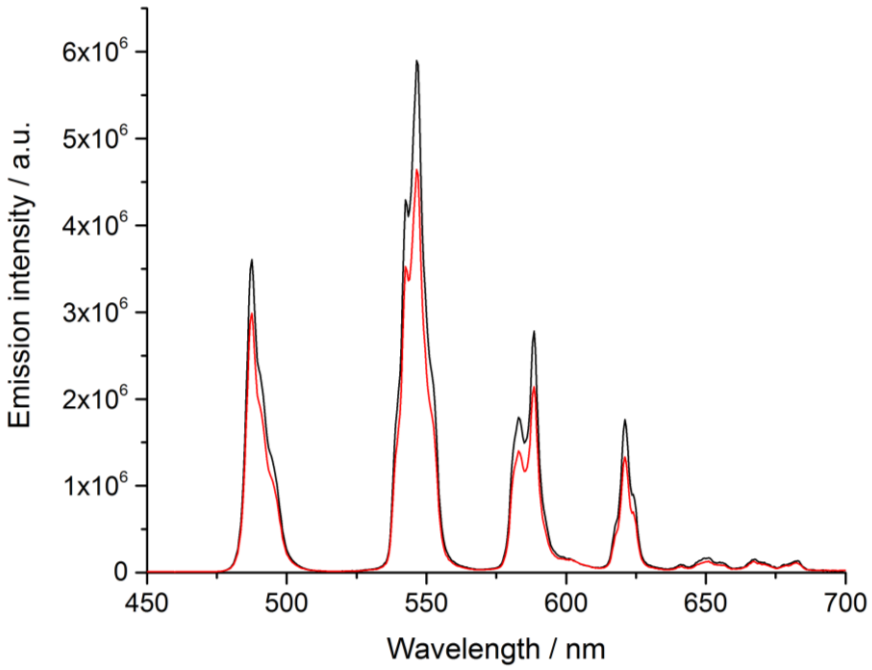


Figure 5. 9 Emission spectra of **Tb.5.11** before (red) and after (black) deoxygenation.

The triplet state energies obtained from EtOH glasses of **Gd.5.10-5.14** at 77 K are shown in Table 5. 1. The energy of the accepting states for Eu(III) and Tb(III) lanthanide ions are ($^5D_0$) 17200 cm^{-1} and ($^5D_4$) 20500 cm^{-1} respectively. The triplet state energy determined for **Eu.5.10** was in line with the value determined by Bushby et al,[1] while the others are broadly in line with expectations for a series of related structures.

Table 5. 1 Photophysical properties of the lanthanide complexes studied.

Complex	E_T/cm^{-1} [a]	λ_{abs}/nm	$\tau(H_2O)$/ms	$\tau(D_2O)$/ms	*q*
5.10	-	245	-	-	-
Eu.5.10	-	262	0.61	2.25	1.2
Tb.5.10	-	262	1.69	2.60	1.0
Gd.5.10	25000	262	-	-	-
5.11	-	273	-	-	-
Eu.5.11	-	300	0.61	2.28	1.2
Tb.5.11	-	300	0.13	0.14	[b]
Gd.5.11	23000	300	-	-	-
5.12	-	261	-	-	-
Eu.5.12	-	278	0.61	2.52	1.2
Tb.5.12	-	278	0.86	1.24	1.7
Gd.5.12	21800	278	-	-	-
5.13	-	255	-	-	-
Eu.5.13	-	275	0.60	2.27	1.2
Tb.5.13	-	275	1.05	1.59	1.6
Gd.5.13	22000	275	-	-	-
5.14	-	248	-	-	-
Eu.5.14	-	266	0.62	2.16	1.1
Tb.5.14	-	266	1.77	2.91	1.0
Gd.5.14	22500	266	-	-	-

[a]Triplet energy of the acetophenone chromophores, estimated from the phosphorescence spectra of the Gd(III) complexes at 77 K in an EtOH glass, ±200 cm^{-1}.

[b]*q* not determined, since the short lifetimes impart a significant error (>1) to the measurement.

5.4 Attempted synthesis of a tri-amide analogue of Ln.5.14

Compound **5.20** (Figure 5. 10) was chosen as a target ligand for the encapsulation of lanthanide salts and for the study of the interaction of these lanthanide complexes with fluoride. The ligand structure was designed with the excellent sensitising properties of aryl ketone groups and the ability of lanthanide tetra-amide derivatives bearing benzylacamide arms to successfully bind fluoride in aqueous media. The replacement of the acetate arms used in **DO3A** derivatives with benylacetamides would lead to the lanthanide ion having a larger residual charge which should aid fluoride binding to the lanthanide centre. The aryl ketone sensitiser was chosen as it has been shown that these groups can effectively sensitise lanthanide emission and coordinate to the lanthanide centre rendering the complex eight coordinate which will help ensure the stability of the complexes whilst leaving a vacant axial site for solvent or fluoride to bind to the lanthanide. The fluorine appended aryl ketone was chosen due to the potential of the fluorine to be used as a useful handle to assess fluoride binding using ^{19}F NMR techniques.

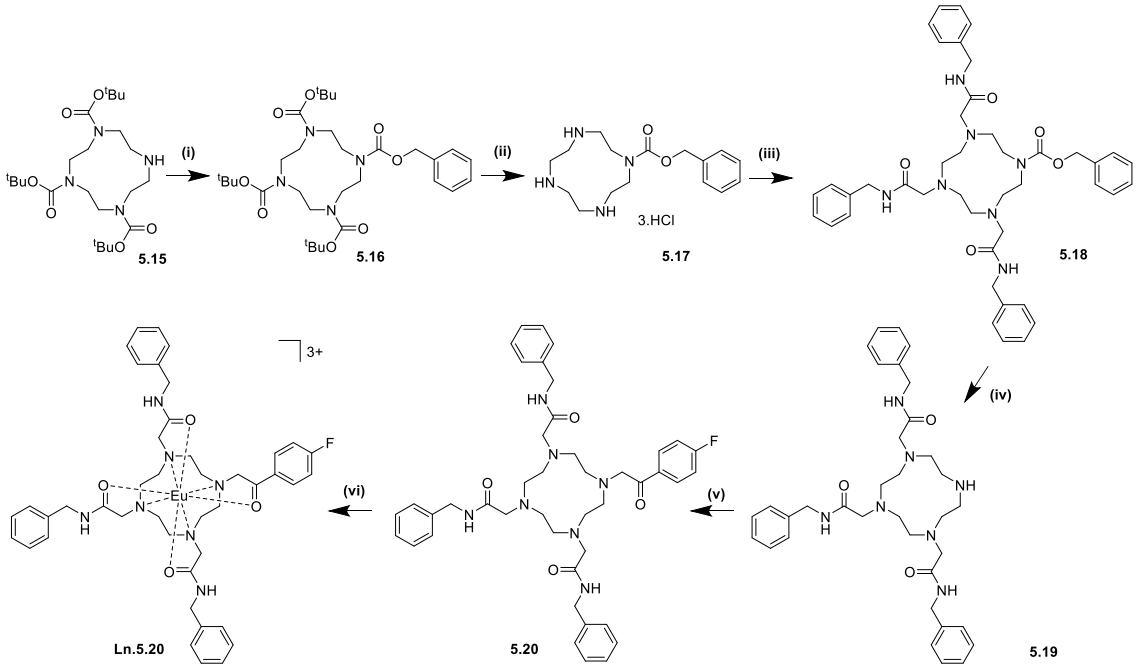


Figure 5. 10 Proposed synthetic scheme for the preparation of triamide lanthanide complexes containing acetophenones. (i) benzyl chloroformate, NEt_3, $CHCl_3$, RT, 8h; (ii) c.HCl, MeOH, RT, 8h; (iii) N-Benzyl-2-chloroacetamide, K_2CO_3, MeCN, 70°C, 18h; (iv) Pd/C/H_2, EtOH, RT, 2d; (v) 2-Chloro-4'-fluoroacetophenone, K_2CO_3, MeCN, 70°C, 18h; (vi) Ln(OTf)$_3$, MeOH, 60°C, 2d.

The proposed synthetic scheme for the target tri-amide lanthanide complexes (**Ln.5.20**) is shown in Figure 5. 10. **5.15**-**5.17** were synthesised according to literature procedures.[7] Initially three cyclen amines were protected as *tert*-butoxycarbamates using di-*tert*-butyl dicarbonate, after purification by silica gel column chromatography the fourth amine was orthogonally protected as a benzyloxycarbamate using benzyl chloroformate. **5.17** was then obtained by removal of the boc protecting groups using methanolic hydrochloric acid. **5.18** was synthesised but first forming the free base of **5.17** and then alkylating the three amines with N-benzyl-2-chloroacetamide using standard conditions (K_2CO_3, MeCN, 70°C, 18h). This was isolated as an oil after purification by silica gel column chromatography, hydrogenolysis of the benzyloxycarbamate using Pd/C/H_2 then gave **5.19**. Figure 5. 11 shows the ^{1}H NMR spectra of **5.18** and **5.19**.

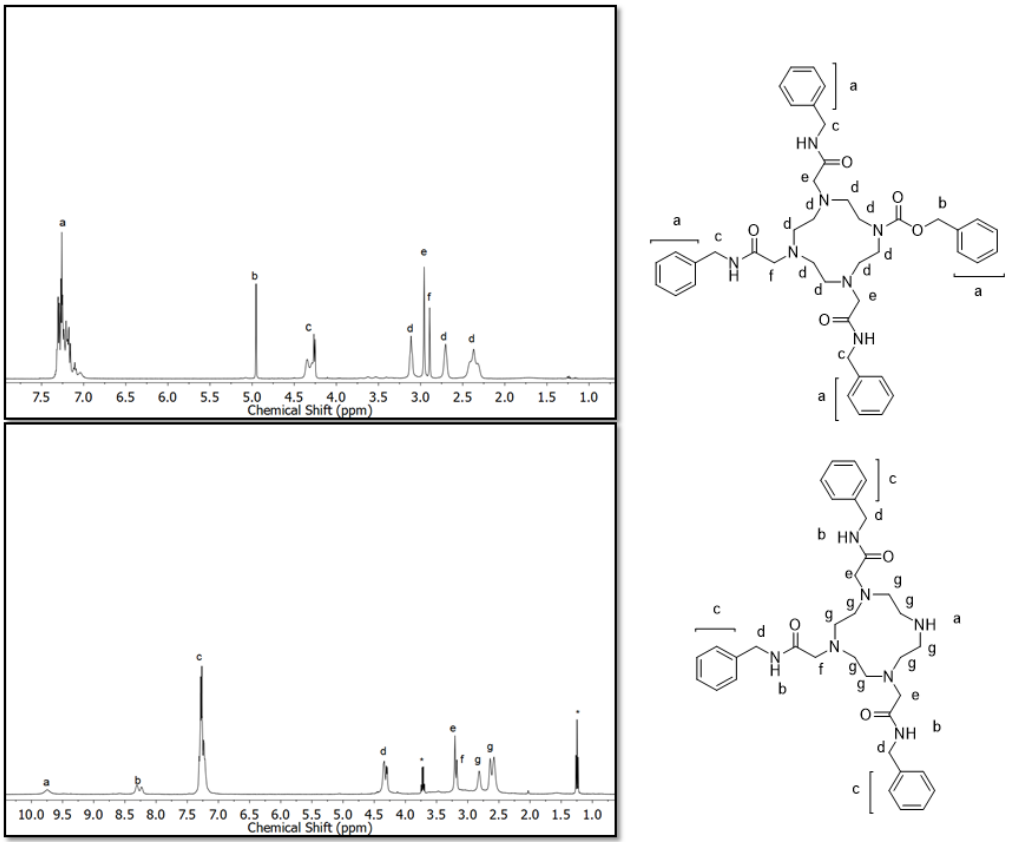


Figure 5. 11 Top: ^{1}H NMR of **5.18** ($CDCl_3$, 298K). Bottom: ^{1}H NMR of **5.19** ($CDCl_3$, 298K). * indicates residual solvent signals.

Alkylation of the fourth position in **5.19** using standard conditions (K_2CO_3, MeCN, 70°C, 18h) was attempted; the reaction was monitored by ESMS and TLC, neither of which showed evidence of the formation of the product **5.20** after 18h. The reaction was left for a further 48h under the same conditions again no sign of the product was observed by ESMS and TLC; significant peaks were observed in the ESMS which correspond to adducts of **5.19** indicating little reaction had occurred. Attempts to try and purify the crude material obtained during the reaction by chromatography or crystallisation to ascertain what happened were ultimately unsuccessful. It is plausible that the steric bulk and flexibility of the benzylacetamide arms effectively block the access of 2-chloro-4'-fluoroacetophenone to alkylate the fourth position.

Attempts to extend the absorption wavelength by incorporating an alkynyl moiety into the ligand scaffold as well as attempting palladium cross coupling with the **Eu.5.11** to produce multimetallic systems ultimately were unsuccessful.

5.5 Fluoride binding

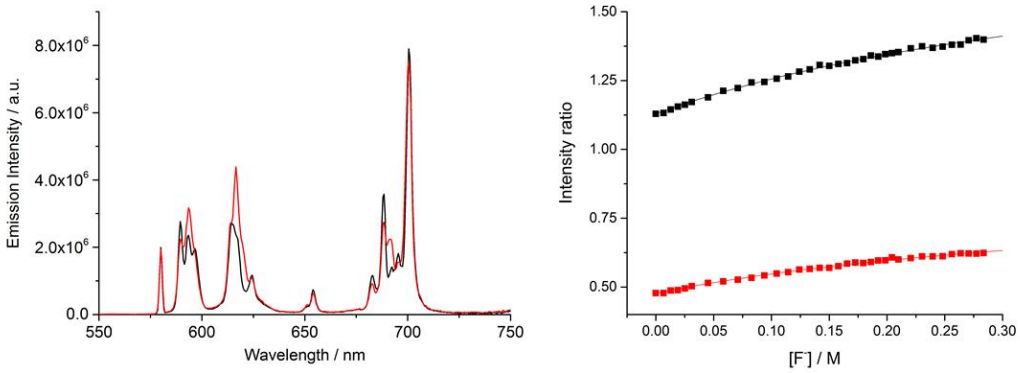


Figure 5. 12 Left: **Eu.5.14** in H_2O (black) and with excess sodium fluoride (red), λ_{ex} = 266 nm, exit slits 1 nm. Right: Binding isotherms and fits for titration of **Eu.5.14** with NaF using the intensity ratios ΔJ=2/ΔJ=1 and ΔJ=2/ΔJ=4.

The affinity of fluoride with **Eu.5.14** was determined using luminescence spectroscopy. Dynafit® was used to fit the changes observed during luminescence titrations with a 1:1 binding model being used. Association constants and confidence intervals are shown in Table 5. 2.

$$[LnL.H_2O] \quad + F^- \rightleftharpoons [LnL.F]^- + H_2O$$

The changes in the intensity of the hypersensitive ΔJ = 2 transition were monitored relative to those of the ΔJ = 1 and ΔJ = 4 transitions to follow the change in the Eu(III) local coordination environment and assess binding. The titration data shows that **Eu.5.14** has negligible fluoride affinity compared with the tetra-amides studied in chapter three (**Eu.3.5** and **Eu.3.6**). The dramatically smaller fluoride association constant observed for **Eu.5.14** compared to the tetra-amides is likely to be due to the low residual charge on the Eu(III) centre in the **DO3A** derivative, **Eu.5.14**, reducing the

electrostatic interaction. The UV-Vis spectra were also recorded in the absence and presence of fluoride with no change in the form of the absorption band indicating that the changes observed in the luminescence spectra aren't due to the interaction between fluoride and the sensitising moiety.

Lifetimes and *q* values in the absence and presence of fluoride are shown in Table 5. 2; it can be seen that, in the absence of fluoride, *q* was 1.1 - which implies on average that a single solvent molecule is directly coordinated to the lanthanide in its axial site. Lifetimes in D_2O and H_2O slightly increased upon the addition of fluoride, *q* was calculated to be approximately 0.8. This indicates that the water molecule in the averaged lanthanide inner coordination sphere has been partially displaced by fluoride; as *q* is still close to 1 then this suggests that the majority of Eu(III) centres have bound solvent with a small number of them having fluoride bound. This supports weak binding of fluoride to the lanthanide centre.

Table 5. 2 Association constant, *K*, for **Eu.5.14** with NaF in H_2O at 298K. 95% confidence intervals in square brackets, lifetimes and *q* values.

	***K*/M^{-1}**	**No NaF**			**+ NaF**		
	Luminescence	τ_{H2O}	τ_{D2O}	***q***	τ_{H2O}	τ_{D2O}	***q***
Eu.5.14	2.1 [1.9 – 2.3]	0.62	2.16	1.1	0.77	2.43	0.8

5.6 Cyanide binding studies

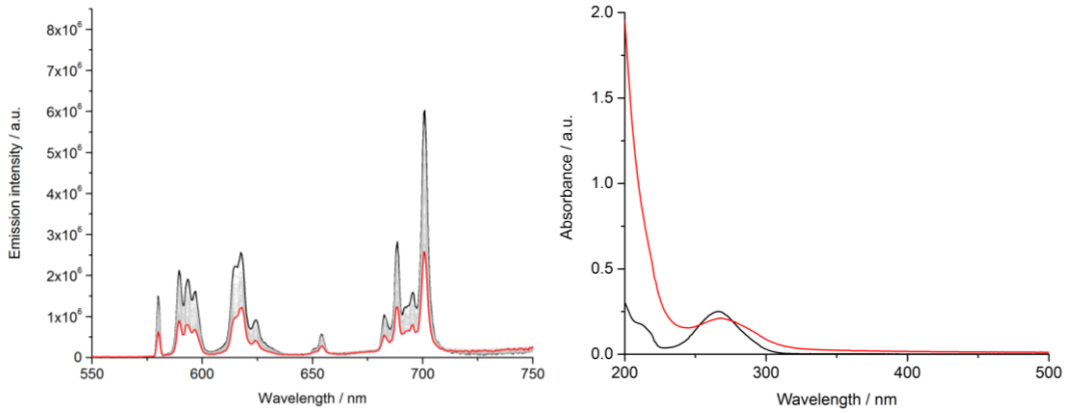


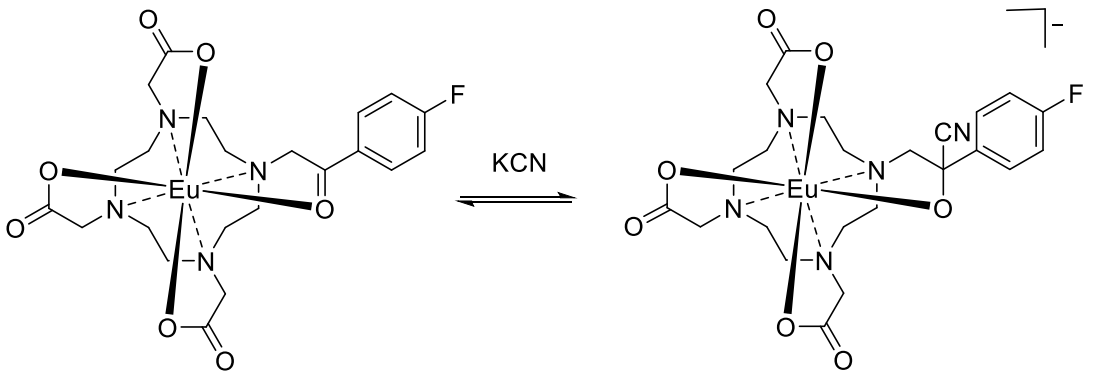
Figure 5. 13 Left: Changes in the **Eu.5.14** emission spectra in H_2O upon addition of KCN, λ_{ex} = 266 nm, exit slits 1 nm. Start of titration (black), end of titration (red) and intermediate concentrations (grey). Right: Changes in the **Eu.5.14** UV-Vis absorption spectra in H_2O upon addition of KCN. Start of titration (black) and end of titration (red).

The affinity of cyanide for **Eu.5.14** was determined using luminescence spectroscopy and the data was analysed using the same methods previously employed to determine fluoride affinity.

It is clear (from Figure 5. 13) that addition of cyanide results in a dramatic quenching of Eu(III) emission though the ratio of the peaks does not change significantly. The changes in peak ratio are likely to reflect the small changes in the donor state (i.e. ketone to alcohol) rather than the displacement of H_2O by cyanide. Furthermore, the affinity constant for cyanide (Table 5. 3) is considerably larger than that observed for fluoride, meaning that collisional quenching of the lanthanide emissive state by cyanide can be ruled out as an explanation of the observed data, since a collisional process would be expected to exhibit linear Stern-Volmer behaviour.

No significant change was observed in the Eu(III) lifetimes in the presence and absence of KCN, again suggesting that the quenching is occurring through an interaction with the ligand as direct binding to the lanthanide centre would result in the displacement of quenching solvent and should result in an increase in lifetime, as well as a dramatic

change in the local ligand field and emission band structure. The continuity of an N_4O_5 donor set at the lanthanide is also supported by the fact that no change in fine structure of the emission bands are observed, which suggests that there is minimal change in the local coordination environment of Eu(III).



Scheme 5. 1 Formation of cyanohydrin upon addition of KCN to **Eu.5.14**.

Changes in the UV-Vis spectra at the start and end of the titration (Figure 5. 13) support an interaction between the cyanide and the phenacyl chromophore. The coordination of a lanthanide centre to the carbonyl group in the phenacyl chromophore suggests one possibility: it is likely that the Lewis acidity of the lanthanide would favour formation of a cyanohydrin (Scheme 5. 1). No significant change in lifetime occurs upon cyanide addition suggesting that if a cyanohydrin is formed then the oxygen remains coordinated to the lanthanide centre (in the manner of known ligands such as **HP-DO3A**). Changes to the ligand structure are confirmed by changes to the ^{1}H NMR spectrum. Figure 5. 14 shows the spectrum before and after addition of an excess of cyanide: from this it is clear that a new set of peaks forms in slow exchange with the original peaks. Furthermore, addition of cyanide to other complexes that lack a phenacyl group (e.g. **[Yb.DTMA]$^{3+}$** and **[Eu.3.6]$^{3+}$**) did not give rise to any detectable change in NMR or luminescence spectra, adding additional weight to the hypothesis of nucleophilic attack by cyanide on the carbonyl.

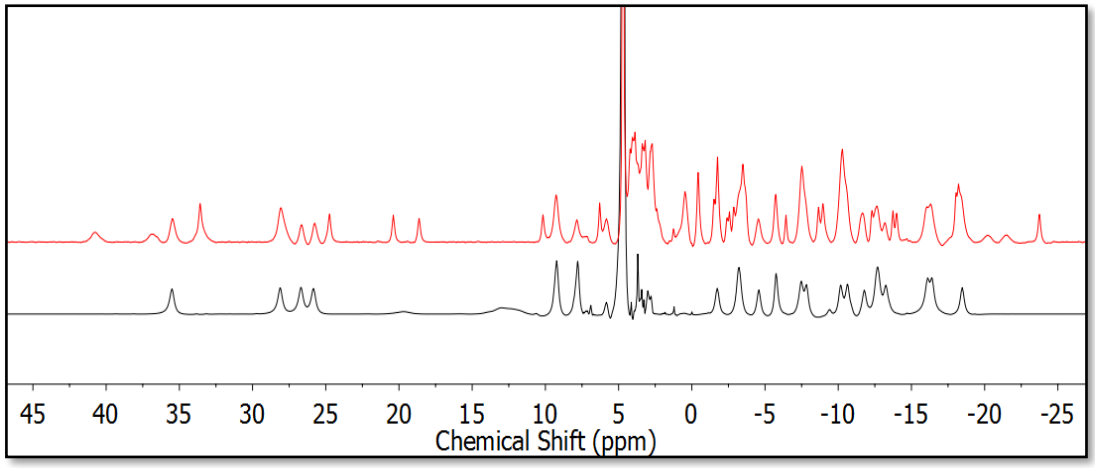


Figure 5. 14 ^{1}H NMR spectra of **Eu.5.14** without cyanide (black) and with cyanide (red) (D_2O, 298 K, 400 MHz).

In the light of this hypothesis, we return to considering the diminished signal observed following cyanide addition. In Scheme 5. 1, it is clear that the phenacyl chromophore is directly conjugated to the lanthanide, and that this conjugation is disrupted by cyanohydrin formation. This disruption will preclude sensitisation of lanthanide luminescence *via* a Dexter exchange mechanism,[8] meaning that less-efficient energy transfer *via* a Förster energy transfer mechanism will play a major role in energy transfer. Owing to the limited spectral overlap between the sharp lines of the lanthanide absorption spectrum and the broad triplet state of the chromophore, this ineffective Förster transfer gives rise to a reduction in intensity of emission in the presence of cyanide. It is likely that the Förster mechanism will give such a great reduction in intensity that the cyanohydrin will only make a small contribution to the emission spectrum.

Table 5. 3 Association constant, *K*, for **Eu.5.14** with KCN in H_2O at 298K (95% confidence intervals in square brackets) and lifetimes.

	***K*/M^{-1}**	**No KCN**	**+ KCN**
	Luminescence	**τ_{H2O}**	**τ_{H2O}**
Eu.5.14	94.2 [80.3 – 110.7]	0.62	0.66

5.7 Conclusions

The work in this chapter extends the utility of phenacyl chromophores for sensitising lanthanide emission and it has been shown that changes in the ring substituents can have profound effects on the photophysical properties of such systems. Very weak fluoride binding was observed as a consequence of the low residual charge on the lanthanide centre, meaning that, unlike the tetra-amides studied earlier (chapter three), the complexes exhibit very limited response to fluoride. By contrast, **Eu.5.14** exhibited affinity for cyanide that is not observed for tetra-amide complexes, and that is a direct consequence of the structure of the phenacyl chromophore. The chemical reactivity of the phenacyl carbonyl when bound to a lanthanide ion offers a wholly new route to sensing cyanide. Moreover, unlike existing cyanide responsive systems (which only respond to cyanide in non-competitive solvent systems), **Eu.5.14** exhibits an excellent response in water. As such, this opens up a new range of possibilities for sensing cyanide (both optically and by NMR methods).

Furthermore, it is now clear that the systems described in this thesis exhibit specificity between cyanide and fluoride - the two most common markers for chemical warfare agents. **Eu.5.14** responds only to cyanide, while the tetra-amide systems described in earlier chapters do not respond to cyanide but deliver a response to fluoride. Taken together, these complexes offer a potential route to new and effective chemical weapons sensors.

5.8 References

1. A. Beeby, L. M. Bushby, D. Maffeo and J. A. G. Williams, *J. Chem. Soc., Dalton Trans.*, 2002, 48-54.
2. A. E. J. Broomsgrove, D. A. Addy, C. Bresner, I. A. Fallis, A. L. Thompson and S. Aldridge, *Chem. Eur. J.*, 2008, **14**, 7525-7529.
3. C. A. P. Swamy, S. Mukherjee and P. Thilagar, *Chem. Commun.*, 2013, **49**, 993-995.
4. G.-L. Fu, H. Pan, Y.-H. Zhao and C.-H. Zhao, *Org. Biomol. Chem.*, 2011, **9**, 8141-8146.
5. L. F. Smith, B. A. Blight, H.-J. Park and S. Wang, *Inorg. Chem.*, 2014, **53**, 8036-8044.
6. R. Hueting, M. Tropiano and S. Faulkner, *RSC Adv.*, 2014, **4**, 44162-44165.
7. M. Woods, G. E. Kiefer, S. Bott, A. Castillo-Muzquiz, C. Eshelbrenner, L. Michaudet, K. McMillan, S. D. K. Mudigunda, D. Grin, G. Tircso, S. R. Zhang, P. Zhao and A. D. Sherry, *J. Am. Chem. Soc.*, 2004, **126**, 9248-9256.
8. T. Lazarides, D. Sykes, S. Faulkner, A. Barbieri and M. D. Ward, *Chem. Eur. J.*, 2008, **14**, 9389-9399.

6 Conclusions and future perspectives

Perhaps the most important aspect of the work described in this thesis is the realisation that the nature of ligands bound to the lanthanide centre can have a profound effect on the crystal field experienced by the lanthanide ion. This changes the relative energies of the m_J states in the lanthanide: even at room temperature, the Boltzmann population of these states can influence the form of both the NMR and luminescence spectra. In the case of NMR, the observed reversal of spectra upon fluoride binding seems surprising at first glance, but is in line with the effectiveness of fluoride as an axial ligand.

These studies clearly show that it is essential to take the coordination sphere as a whole into account when attempting to understand and predict spectroscopic behaviour. Bleaney's theories of paramagnetism in open shell lanthanide complexes are almost half a century old, but still represent the core of current understanding. The approximations inherent to these theories work well for the **DOTA**-tetraamide complexes studied in this thesis. However, the case of the Lehn cryptand is much more complex, not only as a result of isomerism in the system studied, but also because Bleaney's approximations are beginning to break down. It is clear that a proper understanding of such systems is long overdue: obviously it is beyond the scope of this thesis, but such studies must take priority if we are to have a true predictive understanding of lanthanide complexes. The methods outlined in this thesis can be developed further to understand the role of higher order crystal field terms, but a new approach will be required to test the validity of J itself as a quantum number.

The second strand to this thesis has employed phenacylDO3A derivatives: these have been shown to be highly effective sensitisers for a range of lanthanides, giving rise to

bright emission and tuneable behaviour. Here too, subtleties are observed as a consequence of ligand structure, including pH dependent behaviour as a consequence of ligand deprotonation to control of the emission spectra. Future work in this project could focus on investigating the importance of the conjugation between the light harvesting chromophore and the lanthanide centre on the efficiency of the energy transfer cascade. This could be achieved by replacing the ketone functionality (as in the complexes studied in chapter two) connecting the chromophore to the macrocyclic cavity with and amide linking group. Structures of the desired species to be studied are show in Figure 6. 1.

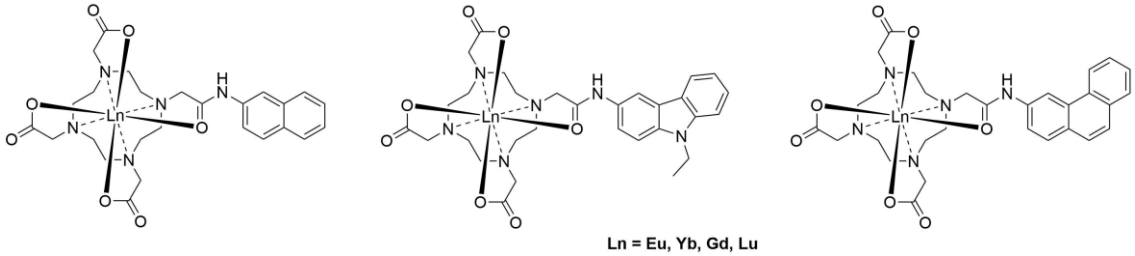


Figure 6. 1 Amide derivatives to be studied.

In the course of these studies, we have also shown that **DOTA**-tetraamide complexes exhibit a ratiometric response to fluoride ions in water as a consequence of binding at the metal centre. By contrast, the phenacylDO3A derivatives described in chapter five do not bind fluoride to any significant degree. However, they do exhibit a response to cyanide which appears to result from reaction of cyanide at the phenacyl carbonyl group. Since the tetra-amides are specific to fluoride while the phenacyl systems are specific to cyanide, it is clear that this study has moved detection of these species in water to a much higher level than had previously been achieved - not least because this specificity is available in aqueous solution. Much is still to be done here: detection limits need to be determined and fluoride affinity enhanced, while the fluoride

responsive systems would benefit greatly from incorporation of more effective sensitising chromophores. The conjugated aromatic nature of effective sensitisers typically precludes the study of tetra-substituted **DOTA** species bearing such chromophores due to poor solubility in aqueous media. The tetra-amide species studied in chapter three are readily water soluble in aqueous media however the simple aromatic chromophores were incapable of lanthanide sensitisation. With this in mind future work regarding fluoride binding at the lanthanide centre in aqueous media could focus on the study of C_2 symmetric lanthanide complexes bearing effective sensitising groups. Figure 6. 2 shows possible target lanthanide complexes; these incorporate aryl ketone sensitisers which have been shown to be efficient sensitising groups. The charge of the overall complex can be varied by utilising either amide of acid moieties, whilst the absorption wavelength can be varied by extending conjugation. The fluoride substituted ligand offers the possibility of studying fluoride binding utilising ^{19}F NMR. The stability of such complexes is unknown so it is vital that this is determined before fluoride binding studies occurs.

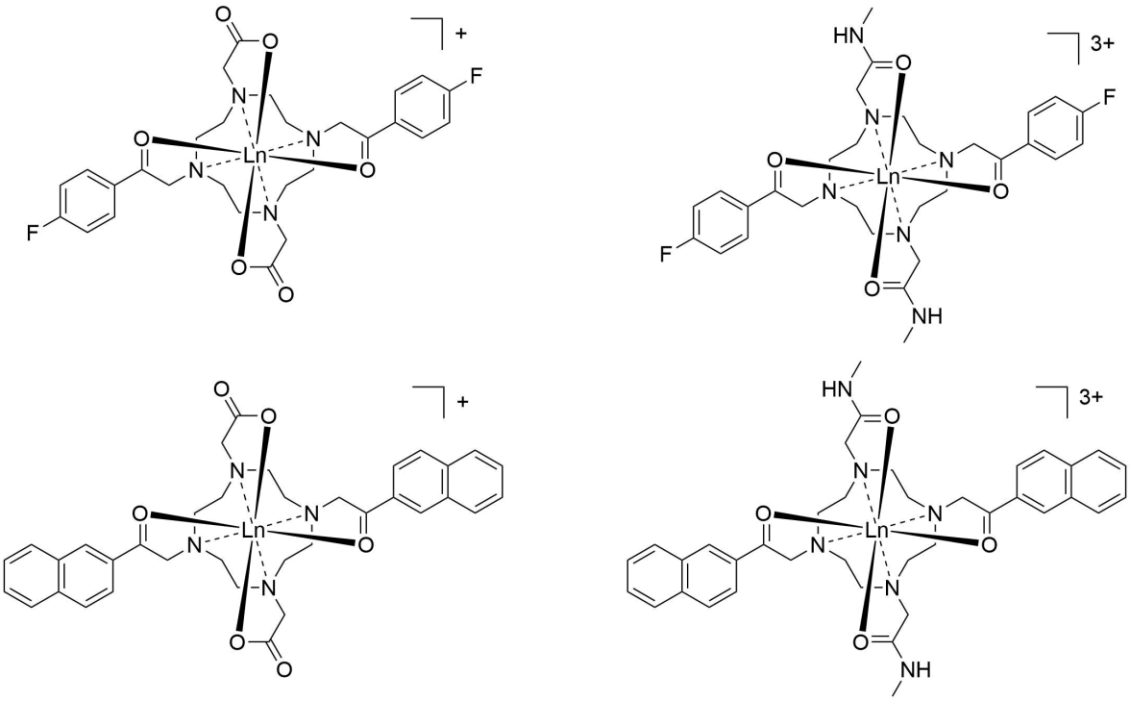


Figure 6. 2 C_2 symmetric target compounds.

The investigation of cyanide binding in phenacylDO3A derivatives as discussed in chapter five would benefit from the use of infrared spectroscopy to study the proposed reaction of cyanide at the phenacyl carbonyl group. It would also be interesting to study the effect of varying the aromatic substituent on the cyanide binding affinity; in the first instance the remaining phenacylDO3A derivatives discussed in chapter five (were X = H, Cl, Br and I) would be investigated. Finally, it is vital to study the selectivity of phenacylDO3A complexes to cyanide; fluorescence response to cyanide would be tested in the presence of a variety of anions such as fluoride, hydrogen sulphide and thiocyanate.

Overall, it is clear that the road to application of lanthanide complexes can be smoothed by an improved understanding of their fundamental properties.

7 Experimental

7.1 General procedures

Commercially available solvents and reagents were used without further purification. Anhydrous solvents were obtained by passing through a MBraun MPSP-800 column (degassed with nitrogen) and then used immediately. Water was deionised and microfiltered using a Milli-Q Millipore machine. Silica TLC plates used were purchased from Merck (TLC Silica gel 60). Alumina TLC plates used were purchased from Sigma-Aldrich (aluminum oxide, pore size 60 Å, 254 nm indicator). Silica gel for column chromatography was purchased from Merck (Geduran, pore size 60 Å, 230 - 400 mesh, 40 - 63 μm) and neutral alumina was purchased from Sigma-Aldrich (aluminum oxide activated, neutral, Brockmann I, pore size 58 Å, 150 mesh); the neutral alumina was soaked in ethyl acetate before use. Dialysis of lanthanide complexes was performed using a dialysis chamber purchased from Sigma Aldrich and using cellulose membrane (MWCO = 100, 500 or 1000 were used). The complex was dissolved in deionised water, placed in the chamber with the appropriate membrane and the chamber was placed in a large conical flask filled with deionised water. Dialysis occurred under stirring and typically ran for two days; the water was changed at least three times a day.

NMR spectra were recorded at 298 K unless otherwise stated. 400 MHz ^{1}H NMR, 101 MHz ^{13}C NMR and 376 MHz ^{19}F NMR were recorded on a Bruker Avance III HD nanobay 400 MHz spectrometer. 500 MHz ^{1}H NMR, 470 MHz ^{19}F NMR, EXSY spectra, COSY spectra, variable temperature (VT) measurements, inversion recovery experiments and NMR titrations were recorded on a Bruker Avance III 500MHz spectrometer. All

coupling constants are quotes in Hz with all chemical shifts (δ) quoted in parts per million (ppm) and referenced to the residual solvent peak. Abbreviations when quoting NMR data are as follows: singlet (s), doublet (d), triplet (t), quartet (q), multiplet (m) and broad (br).

Mass spectra were obtained using either an Agilent Technology 1260 Infinity or a Waters LCT Premier XS. Accurate mass spectra were recorded to four decimal places using Bruker µTOF and Micromass GCT spectrometers.

UV-Visible spectroscopy was performed using a PG instruments T60u UV-Vis spectrophotometer. Luminescence spectroscopy measurements were obtained using a HORIBA Jobin Yvon FluoroLog3 fluorimeter equipped with a Hamamatsu R928 detector and a double-grating emission monochromator; emission and excitation spectra were recorded at room temperature and in steady state mode unless otherwise stated. Emission lifetimes were obtained using the HORIBA Jobin Yvon FluoroLog3 fluorimeter system equipped with a Xenon flash lamp. Luminescence lifetimes were obtained by tail fit for Eu(III) and Tb(III) complexes using Fluoressence™ software. All lifetimes gave satisfactory fitting using a mono-exponential decay function; attempted fitting to a double exponential decay did not improve the fit unless otherwise stated. Near-infrared luminescence spectra from Yb(III) complexes were measured on the HORIBA Jobin Yvon FluoroLog3 fluorimeter system equipped with a Hamamatsu R5509-42 NIR PMT InGaAs detector cooled to -80 °C. Luminescence lifetimes of Yb(III) complexes were obtained by exciting the sample using a pulsed nitrogen laser (PTI-3301-337nm). Light emitted at right angles to the excitation beam was focused onto the slits of a monochromator (PTI120), which was used to select the appropriate Yb(III) emission wavelength (980 nm). The growth and decay of the

luminescence at selected wavelengths was detected using a germanium photodiode (Edinburgh Instruments, EI-P) and recorded using a digital oscilloscope (Tektronix TDS220) before being transferred to the computer for analysis using Microsoft Excel. Luminescence lifetimes were obtained by iterative deconvolution of the detector response (obtained by using a scatter). Triplet state emission spectra were measured on samples prepared in ethanol at 77 K on a Perkin Elmer LS55 spectrophotometer equipped with an Oxford Instrument cryostat. Quantum yield for Eu(III) complexes were recorded relative to cresyl violet in methanol and the compound reported by Bünzli et al. using the conditions reported.[1, 2] Where molar absorption coefficient were measured the complexes were further purified by semipreparative HPLC.

A Hannah pH meter was used for pH measurements of solution of complexes in water and deuterium oxide. In the case of deuterium oxide, the values reported here is the pH value given by the instrument with pD = pH + 0.45 as reported in the literature.[3] pH dependent studies of the photophysical properties of lanthanide compounds were carried out using 0.1 M NaOH or HCl for pH adjustments; the dilution at the end of the titration was kept to less than 5% of the initial volume.

7.2 X-ray crystallography

For single crystal X-ray analysis of compound **2.6**, the crystal was mounted using the oil drop technique, in perfluoropolyether oil at 150(2) K using a Cryostream N_2 open-flow cooling device.[4] Diffraction data were collected using graphite monochromatic Mo-Kα radiation (λ = 0.71073 Å) on a Nonius Kappa CCD diffractometer. For all data collections, series of ω-scans were performed in such a way as to collect a complete data set to a maximum resolution of 0.77 Å. Data reduction including unit cell

refinement and inter-frame scaling was carried out using DENZO-SMN/SCALEPACK.[5] Intensity data were processed and corrected for absorption effects by the multi-scan method, based on repeat measurements of identical and Laue equivalent reflections. Structure solution was carried out with direct methods using the program SIR92[6] within the CRYSTALS software suite.[7] Coordinates and anisotropic displacement parameters of all non-hydrogen atoms were refined freely. Hydrogen atoms were generally visible in the difference map and refined with soft restraints prior to inclusion in the final refinement using a riding model.[8] A summary of the X-ray crystallographic data is provided in Table 7. 3. and the ORTEP depiction of the single crystal X-ray structure is in chapter two (Figure 2.4). Crystallographic data (excluding structure factors) for the structure has been deposited with the Cambridge Crystallographic Data Centre (CCDC 1040048). Conducted by Dr Jones.

7.3 Titration methodology

A non-dilution method was used for luminescence and NMR anion binding titrations. To ensure that the luminescence intensity was not altered by dilution, the titrant solutions were made using the complex stock solution as the solvent. The concentrations used for each titration are shown in Table 7. 1. The anion concentrations were typically more than one hundred times more concentrated than the lanthanide complex concentration. 1.5 mL of stock lanthanide solution was transferred to a quartz cuvette with a lid and then initial photophysical data was recorded. Successive emission spectra were recorded upon addition of known amounts of the titrant solution using an Eppendorf pipette.

Table 7. 1 Concentrations of solutions used for titrations.

	λ_{ex} / nm	[Ln] / mM	[Anion] / M	Solvent	Method
Eu.3.5 + NaF	395	0.52	0.80	D_2O	Luminescence
Eu.3.5 + NaF	-	1.0	0.79	D_2O	^{19}F NMR
Eu.3.6 + NaF	395	0.52	0.79	D_2O	Luminescence
Eu.3.6 + NaF	-	1.1	0.78	D_2O	^{19}F NMR
Eu.4.7 + NaF	327	0.11	0.050	D_2O	Luminescence
Eu.4.7 + NaF	-	0.70	0.056	D_2O	^{1}H NMR
Eu.4.7 + NaF	-	0.67	0.053	D_2O	^{19}F NMR
Eu.5.14 + NaF	266	0.053	0.50	H_2O	Luminescence
Eu.5.14 + KCN	266	0.051	0.11	H_2O	Luminescence

7.4 Dynafit

Dynafit® was used to fit observed binding isotherms using procedures already developed in the group and discussed in detail in the literature.[9-11]

Example dynafit scripts

one event binding – peak ratio

[task]

data = equil

task = fit

[mechanism]

Eu + F <==> complex1 : K1 assoc

[constants]

K1 = 500??

[concentrations]

Eu = 5.18e-4

[responses]

intensive

[equil]

variable F

file ./Binding/EuDOTAMBnD2O/RATIO1.txt |response Eu = 0.83289 , complex1 = 1.59334?

file ./Binding/EuDOTAMBnD2O/RATIO2.txt |response Eu = 0.38704 , complex1 = 0.85043?

[output]

directory ./output/EuDOTAMBnD2Oratio

[end]

one event binding – peak sum

[task]

data = equil

task = fit

[mechanism]

Eu + F <==> complex1 : K1 assoc

[constants]

K1 = 500??

[concentrations]

Eu = 5.18e-4

[responses]

[equil]

variable F

file ./Binding/EuDOTAMBnD2O/SUMJ=1.txt |response Eu = 3.14e9 , complex1 = 2.93e9?

file ./Binding/EuDOTAMBnD2O/SUMJ=2.txt |response Eu = 2.62e9 , complex1 = 4.68e9?

file ./Binding/EuDOTAMBnD2O/SUMJ=4.txt |response Eu = 6.76e9 , complex1 = 5.50e9?

[output]

directory ./output/EuDOTAMBnD2OSUM

[end]

Two event binding – peak sum

[task]

data = equil

task = fit

[mechanism]

Eu + F <==> complex1 : K1 assoc

complex1 + F <==> complex2 : K2 assoc

[constants]

K1 = 1000??

K2 = 100??

[concentrations]

Eu = 1.12e-4?

[responses]

[equil]

variable F

file ./Binding/EuLehn1/J=0.txt |response Eu = 2.06e10? , complex1 = 9.69e10?, complex2= 9.69e10?

file ./Binding/EuLehn1/J=1.txt |response Eu = 4.23e11? , complex1 = 2.16e12?, complex2= 2.16E12?

file ./Binding/EuLehn1/J=2.txt |response Eu = 9.10e11? , complex1 = 2.20e12?, complex2= 2.20E12?

file ./Binding/EuLehn1/J=3.txt |response Eu = 4.52e10? , complex1 = 3.95e11?, complex2= 3.95e11?

file ./Binding/EuLehn1/J=4.txt |response Eu = 9.62e11? , complex1 = 4.96e12?, complex2= 4.96E12?

[output]

directory ./output/Eulehnsum1

[end]

7.5 Rate determination

Rates of exchange and T_1 measurements were conducted on a Bruker Avance III 500MHz spectrometer using inversion recovery.

7.6 HPLC

HPLC traces were measured on a Gilson analytical HPLC equipped with a Gilson 322 dual pump and a Gilson 152 UV-Vis detector; the stationary phase used was a Discovery Cyano analytical HPLC column. Samples were monitored at λ = 350 nm. Solvent gradient conditions used are described in the Table 7. 2**.**

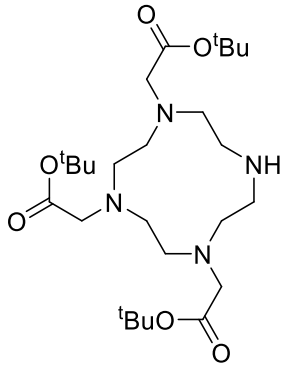
Table 7. 2 Solvent gradient conditions.

Time / min	Acetonitrile % (0.1% formic acid)	Water % (0.1% formic acid)	Flow rate (mL/min)
0-3	5	95	1
15-20	95	5	1
22-25	5	95	1

7.7 Synthesis

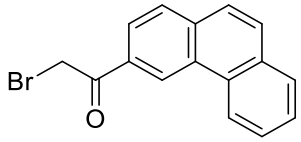
7.8 Achieving high luminescence quantum yields with arylacylDO3A complexes

1,4,7-Tris(*tert*-butoxycarbonylmethyl)-1,4,7,10-tetraazacyclododecane, hydrobromide salt, 2.4[12]



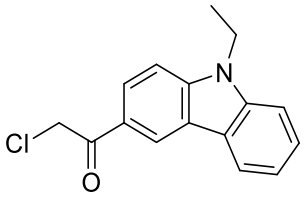
1,4,7,10-Tetraazacyclododecane (5.341 g, 31.0 mmol) and $NaHCO_3$ (8.341 g, 99.3 mmol) were stirred in anhydrous MeCN (180 mL) cooled to 0 °C, whilst *tert*-butylbromoacetate (14.55 mL, 98.5 mmol) in anhydrous MeCN (30 mL) was added dropwise over 30 min. After the addition the reaction mixture was allowed to reach room temperature and was stirred under nitrogen for a further 48h. Inorganic solids were removed by filtration and the filtrate evaporated under reduced pressure to yield a beige solid. Recrystallization from toluene gave the *title compound* as a white solid (8.698 g, 47%). ^{1}H NMR (400 MHz, $CDCl_3$) δ_H 10.0 (br. s, 1H, N*H*), 3.36 (s, 4H, 1,7-C*H*$_2$CO$_2$), 3.30 (s, 2H, 4-C*H*$_2$CO$_2$), 3.10 (s, 4H, 9,11-C*H*$_2$NH), 2.94 (s, 8H, 2,3,5,6-C*H*$_2$), 2.88 (s, 4H, 8,12-C*H*$_2$), 1.45 (s, 27H, C(C*H*$_3$)$_3$) ppm. ESMS found *m/z* 537.3 for $[M+Na]^+$.

2-Bromo-3'- acetophenanthrone, 2.5



3-Acetylphenanthrene (0.410 g, 1.86 mmol) was dissolved in Et_2O (10 mL) and dioxane (5 mL) and the mixture stirred in an ice bath while Br_2 was added dropwise (0.1 mL, 1.86 mmol). The reaction was left stirring at RT and its progress monitored by TLC. Typically after 3 h all starting material was consumed. H_2O (30 mL) was added to the organic mixture and the aqueous layer was extracted with Et_2O (3 x 30 mL). The organic solvent was washed with brine, dried ($MgSO_4$) and solvent removed. Purification by silica gel column chromatography (petroleum ether:DCM, 1:1) gave the *title compound* as a yellow oil (0.313 g, 56%). ^{1}H NMR (400 MHz, $CDCl_3$) δ_H 9.33 (s, 1H, Ar*H*), 8.74 (d, 1H, Ar*H*, J = 8.0 Hz), 8.11 (d, 1H, Ar*H*, J = 8.0 Hz), 7.92 (m, 2H, Ar*H*), 7.86 (d, 1H, Ar*H*, J = 8.0 Hz), 7.73 (m, 2H, Ar*H*), 7.66 (t, 1H, Ar*H*, J = 8.0 Hz), 4.62 (s, 2H, C*H*$_2$Cl) ppm. ^{13}C{^{1}H} NMR (101 MHz, $CDCl_3$) δ_c 191.4, 135.5, 132.2, 131.5, 130.5, 130.3, 129.9, 129.1, 128.9, 127.5, 127.4, 126.2, 125.6, 124.8, 122.7, 31.1 ppm. ESMS found *m/z* 323.0 for $[M+Na]^+$.

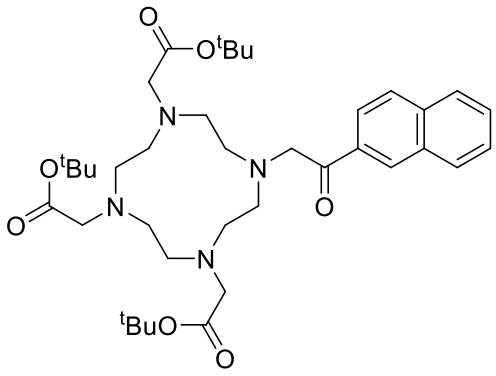
2-Chloro-1-(9-ethyl-9H-carbazol-3-yl)ethan-1-one, 2.6[13]



$AlCl_3$ (0.75 g, 5.62 mmol) was added portion wise to 9-ethylcarbazole (1.00 g, 5.12 mmol) and 2-chloroacetylchloride (0.50 mL, 6.15 mmol) in benzene at 0°C. The mixture was allowed to reach RT and then stirred for 5h, poured onto ice and

extracted with DCM (3 x 50 mL). The organic layer was washed H_2O (50 mL), dried (Na_2SO_4), filtered and the solvent removed. Purification by silica gel column chromatography (hexane to hexane:EtOAc, 9:1) gave the *title compound* as an off white solid (0.100 g, 7%). ^{1}H NMR (400 MHz, $CDCl_3$) δ_H 8.75 (s, 1H, Ar*H*), 8.17 (d, 1H, Ar*H*, J = 8.0 Hz), 8.12 (d, 1H, Ar*H*, J = 8.0 Hz), 7.55 (t, 1H, Ar*H*, J = 8.0 Hz), 7.46 (t, 2H, Ar*H*, J = 8.0 Hz), 7.34 (t, 1H, Ar*H*, J = 8.0 Hz), 4.85 (s, 2H, CH_2Cl), 4.41 (q, 2H, NCH_2, J = 8.0 Hz), 1.48 (t, 3H, CH_3, J = 8.0 Hz). ESMS found *m/z* 272.1 for $[M+H]^+$. Crystals were formed upon slow evaporation of a hexane:ethyl acetate solution.

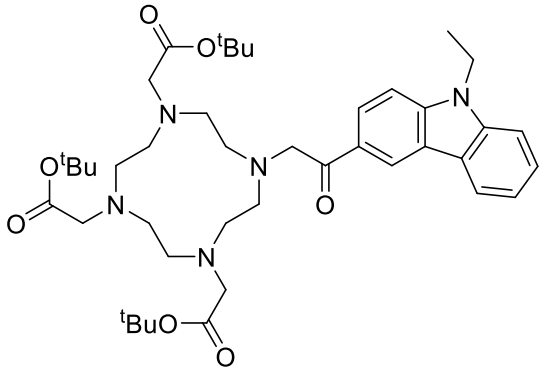
1-(2-Acetonapthone)-4,7,10-tris(*tert*-butoxycarboxymethyl)-1,4,7,10-tetraazacyclododecane, 2.7



To a solution of **2.4** (0.979 g, 1.65 mmol) in anhydrous MeCN (50 mL), K_2CO_3 was added (0.455 g, 3.29 mmol) followed by 2-bromo-2'-acetonaphthone (0.410 g, 1.65 mmol). This suspension was left stirring at RT for 16 h, monitoring the reaction using TLC (DCM:MeOH, 9:1). Purification by silica gel column chromatography (DCM to DCM:MeOH, 96:4) gave the *title compound* as a light yellow glassy solid (0.790 g, 70%). ^{1}H NMR (400 MHz, $CDCl_3$) δ_H 8.09 (s, 1H, Ar*H*), 7.99 (d, 1H, J = 4.0, Ar*H*), 7.94-7.86 (m, 3H, Ar*H*), 7.64-7.56 (m, 2H, Ar*H*), 4.17 (s, br, 2H, NCH_2CO), 3.73-2.18 (m, br, 22H, CH_2 ring and arms), 1.47 (s, 27H, C(CH_3)$_3$). ^{13}C{^{1}H} NMR (101 MHz, $CDCl_3$) δ_c 199.5, 172.8,

135.7, 133.0, 132.3, 129.6, 129.4, 128.7, 128.5, 127.7, 126.9, 123.1, 81.94, 81.87, 60.3, 55.6, 52.9 (br), 50.6, 48.6 (br), 27.9. ESMS found *m/z* 683.5 for $[M+H]^+$. HR-ESMS found *m/z* 683.4356, calculated *m/z* 683.4378 for $[C_{38}H_{59}O_7N_4]^+$.

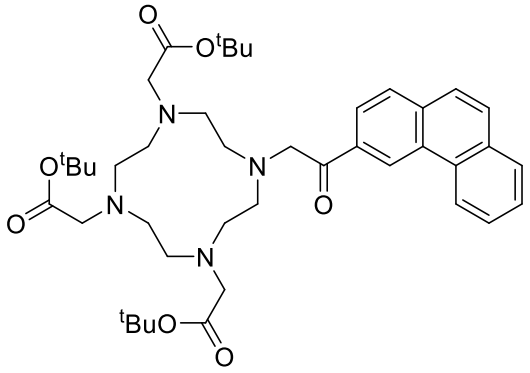
1-(1-(9-Ethyl-9H-carbazol-3-yl)ethan-1-one)-4,7,10-tris(*tert*-butoxycarboxymethyl)-1,4,7,10-tetraazacyclododecane, 2.8



To a solution of **2.4** (0.180 g, 0.30 mmol) in anhydrous MeCN (25 mL), K_2CO_3 was added (0.084 g, 0.61 mmol) followed by **2.6** (0.080 g, 0.30 mmol). This suspension was left stirring at RT under nitrogen for 18 h, monitoring the reaction using TLC (DCM/MeOH 9:1). The reaction mixture was filtered and the solvent removed under reduced pressure. Purification by silica gel column chromatography (DCM to DCM:MeOH, 96:4) gave the *title compound* as a light yellow solid (0.155 g, 69%). ^{1}H NMR (400 MHz, $CDCl_3$) δ_H 8.67 (s, 1H, Ar*H*), 8.11 (d, 1H, J = 4.0 Hz, Ar*H*), 8.05 (d, 1H, J = 8.0 Hz, Ar*H*), 7.55-7.50 (m, 1H, Ar*H*), 7.46 (d, 1H, J = 8.0 Hz, Ar*H*), 7.42 (d, 1H, J = 8.0 Hz, Ar*H*), 7.31 (t, 1H, J = 8.0 Hz, Ar*H*), 4.41 (m, 3H, CH_2CH_3), 4.14-2.20 (m, br, 26 H, CH_2 ring, arms and CH_2CH_3), 1.46 (s, 18H, $C(CH_3)_3$), 1.38 (s, 9H, $C(CH_3)_3$). $^{13}C\{^1H\}$ NMR (101 MHz, $CDCl_3$) δ_c 198.3, 172.8, 169.8, 143.0, 140.7, 121.2, 126.7, 125.7, 123.1, 122.7, 121.0, 120.5, 120.1, 109.2, 108.3, 81.9, 60.0, 55.8, 55.7, 53.5, 52.7 (br), 49.0 (br), 37.9,

27.9, 27.8, 13.8. ESMS found *m/z* 772.5 for $[M+Na]^+$. HR-ESMS found *m/z* 772.4598, calculated *m/z* 772.4620 for $[C_{42}H_{63}N_5O_7{}^{23}Na]^+$.

1-(3-Acetophenanthrene)-4,7,10-tris(tert-butoxycarboxymethyl)-4,7,10-tetraazacyclododecane, 2.9

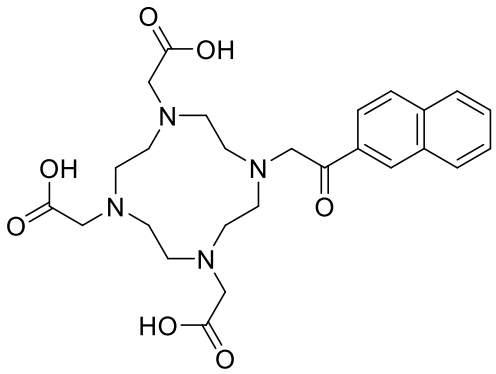


To a solution of **2.4** (0.211 g, 0.35 mmol) in anhydrous MeCN (25 mL), K_2CO_3 was added (0.100 g, 0.70 mmol) followed by **2.5** (0.106 g, 0.35 mmol). This suspension was left stirring at RT under nitrogen for 18 h, monitoring the reaction using TLC (DCM/MeOH 9:1). The reaction mixture was filtered and the solvent removed under reduced pressure. Purification by silica gel column chromatography (DCM to DCM:MeOH, 96:4) gave the *title compound* as a light yellow solid (85.0 mg, 33%). ^{1}H NMR (400 MHz, $CDCl_3$) δ_H 9.28 (s, 1H, Ar*H*), 8.76 (d, 1H, Ar*H*, J = 8.0 Hz), 8.06 (d, 1H, Ar*H*, J = 8.0 Hz), 7.94 (d, 2H, Ar*H*, J = 8.0 Hz), 7.88 (d, 1H, Ar*H*, J = 8.0 Hz), 7.77-7.72 (m, 2H, Ar*H*), 7.67 (t, 1H, Ar*H*, J = 8.0 Hz), 4.25 (s, br, 2H, NCH_2CO), 3.40-2.22 (m, br, 22H, CH_2 ring and arms), 1.47 (s, 18H, C(CH_3)$_3$), 1.26 (s, 9H, C(CH_3)$_3$). ^{13}C{^{1}H} NMR (101 MHz, $CDCl_3$) δ_c 199.8, 173.1, 172.9, 135.3, 133.5, 132.2, 130.5, 130.0, 129.8, 129.1, 128.9, 127.4, 126.2, 124.6, 123.2, 122.6, 82.0, 81.9, 60.6, 55.9, 55.7, 53.4, 52.6 (br), 49.1 (br), 27.9, 27.8. ESMS found *m/z* 755.4 for $[M+Na]^+$. HR-ESMS found *m/z* 755.4347, calculated *m/z* 755.4354 for $[C_{42}H_{60}N_4O_7{}^{23}Na]^+$.

General procedure for the deprotection of DO3A based pro-ligands

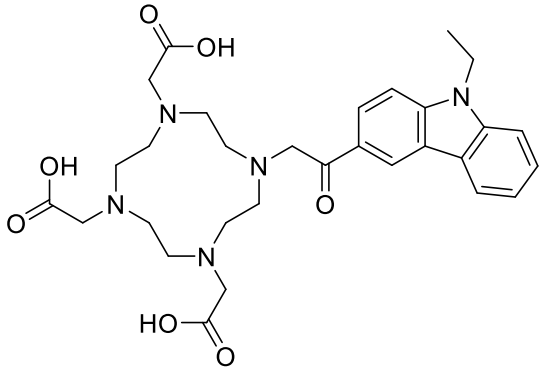
The appropriate pro-ligand was dissolved in DCM (3 mL) and TFA (3 mL) was added dropwise. The solution was stirred at RT for 24h and the solvent was removed under reduced pressure. DCM (3 x 5 mL) was added and the solvent removed followed by a similar treatment with MeOH (3 X 5 mL), the residue was dissolved in a minimum amount of MeOH and precipitated with Et_2O. Trituration with Et_2O gave the *title compound* in quantitative yield as an off white solid.

1-(2-Acetonapthone)-4,7,10-tris(carboxymethyl)-1,4,7,10-tetraazacyclododecane, 2.10



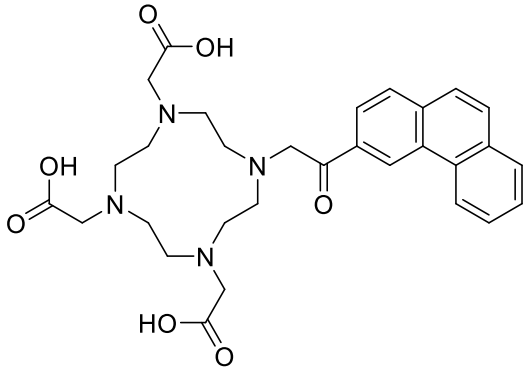
2.7 (0.480 g, 0.70 mmol). ^{1}H NMR (400 MHz, D_2O) δ_H 8.54 (s, 1H, Ar*H*), 8.06 (d, 2H, *J* = 8.0 Hz, Ar*H*), 8.02-7.92 (m, 2H, Ar*H*), 7.70 (t, 1H, *J* = 8.0 Hz, Ar*H*), 7.63 (t, 1H, *J* = 8.0 Hz, Ar*H*), 5.08 (s, br, 2H, NCH_2CO), 3.96-1.97 (m, br, 22H, CH_2 ring and arms). ^{13}C{^{1}H} NMR (101 MHz, D_2O) δ_c 163.3, 163.0, 162.6, 162.3, 135.8, 131.9, 129.7, 128.7, 127.8, 127.5, 123.0, 120.7, 117.8, 114.9, 112.0, 66.0, 58.7 (br), 53.5 (br), 51.4 (br), 48.4 (br). ESMS found *m/z* 515.3 for $[M+H]^+$. HR-ESMS found *m/z* 515.2487, calculated *m/z* 515.2500 for $[C_{26}H_{35}O_7N_4]^+$. UV-Vis (H_2O) λ_{max}/nm: 206, 249, 286 nm, 335 nm.

1-(1-(9-Ethyl-9H-carbazol-3-yl)ethan-1-one)-4,7,10-tris(tert-butoxycarboxymethyl)-1,4,7,10-tetraazacyclododecane, 2.11



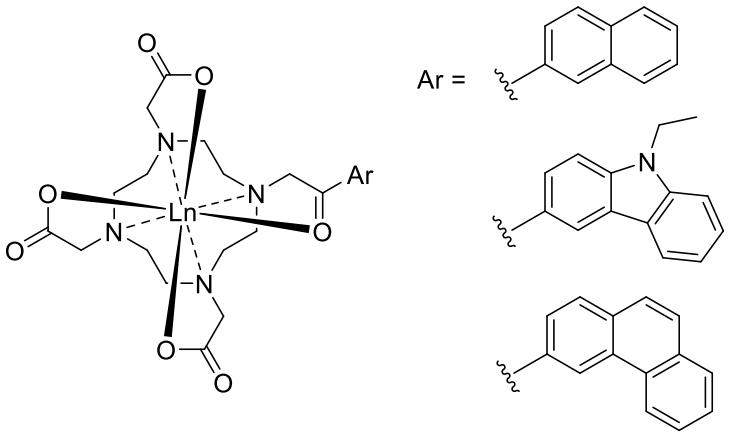
2.8 (0.150 g, 0.20 mmol). ^{1}H NMR (400 MHz, D_2O) δ_H 8.49 (s, 1H, Ar*H*), 8.02 (s, br, 1H, Ar*H*), 7.85 (s, br, 1H, Ar*H*), 7.40 (m, br, 3H, Ar*H*), 7.23 (s, br, 1H, Ar*H*), 4.18-3.19 (m, br, 29H, C*H*$_2$ ring, arms and C*H*$_2$CH$_3$). ^{13}C{^{1}H} NMR (101 MHz, D_2O) δ_c 190.4 (br), 174.6, 174.1 (br), 169.1 (br), 140.0 (br), 140.1, 126.6, 125.8, 123.9 (br), 122.3, 122.0, 121.5, 120.5, 109.3 108.9, 59.5 (br), 55.1 (br), 53.6 (br), 53.2, 51.7 (br), 49.3, 48.1 (br), 47.8, 42.4, 37.4 (br), 34.4, 31.7, 13.2. ESMS found *m/z* 582.3 for $[M+H]^+$. HR-ESMS found *m/z* 582.2913, calculated *m/z* 582.2922 for $[C_{30}H_{40}O_7N_5]^+$. UV-Vis (H_2O) λ_{max}/nm: 235, 243, 276, 292, 334.

1-(3-Acetophenanthrene)-4,7,10-tris(carboxymethyl)-1,4,7,10-tetraazacyclododecane, 2.12



2.9 (0.53 g, 0.07 mmol). ^{1}H NMR (400 MHz, D_2O) δ_H 8.71 (s, br, 1H, Ar*H*), 8.40 (s, br, 1H, Ar*H*), 7.90-7.18 (m, br, 7H, Ar*H*), 4.15-2.70 (m, br, 24H, CH_2 ring and arms). ^{13}C{^{1}H} NMR (101 MHz, D_2O) δ_c 174.3, 169.0 (br), 165.7, 135.3 (br), 131.6, 129.7, 128.8, 127.6, 126.0, 124.5, 122.6, 71.7, 69.6, 69.5, 69.4, 60.3, 55.1 (br), 53.4 (br), 53.1, 51.80, 51.4 (br), 48.8, 48.0 (br), 42.2. ESMS found *m/z* 565.3 for $[M+H]^+$. HR-ESMS found *m/z* 587.2455, calculated *m/z* 587.2476 for $[C_{30}H_{36}O_7N_4{}^{23}Na]^+$. UV-Vis ($H_2O$) λ_{max}/nm: 243, 252, 320.

General procedure for the synthesis of arylacylDO3A lanthanide complexes



To a solution of the ligand in MeOH the appropriate $Ln(OTf)_3$ was added (1.05 eq.) and the reaction mixture was stirred at 60°C for 30 min. The pH was adjusted to 4 by dropwise addition of an aqueous NaOH (1 M) solution. The reaction was left to stir at 60°C for 48 h. The methanol was removed under reduced pressure leaving an oil that was dissolved in water. The pH of this solution was adjusted to 10 by addition of aqueous NaOH (1 M) to remove excess of lanthanide as its insoluble hydroxide. The resulting precipitate was centrifuged and the supernatant filtered. The solvent was neutralised by addition of 1 M HCl. The solvent was removed, the residue dissolved in a minimum amount of MeOH and precipitated with Et_2O. Trituration with Et_2O gave the desired lanthanide containing product as an off white solid

Eu.2.10. Yield: 89 %. ^{1}H NMR (500 MHz, D_2O, pH = 7) δ_H 37.6 (s), 29.8 (s), 28.4 (s), 27.5 (s), 10.4 (s), 8.7 (s), 8.2 (s), 8.0 (s), 7.8 (s), 7.6 (s), 5.6 (s), 4.2 (s), -1.9 (s), -3.3 (s), -3.9 (s), -4.7 (s), -5.9 (s), -8.1 (s), -10.6 (s), -11.2 (s), -13.2 (s), -13.6 (s), -14.1 (s), -14.6 (s), -17.4 (s), -17.6 (s), -19.7 (s). ESMS found *m/z* 665.1 for $[M+H]^+$. HR-ESMS found *m/z* 661.1324, calculated *m/z* 661.1308 for $[C_{26}H_{30}O_7N_4{}^{151}Eu]^+$. UV-Vis ($H_2O$) λ_{max}/nm (ε/$M^{-1}cm^{-1}$): 207 (42,000), 260 (66,300), 305 (28,200), 362 (5,100). HPLC t_r : 10.2 min.

Yb.2.10. Yield: 95 %. ^{1}H NMR (500 MHz, D_2O, pH = 5) δ_H 134.1 (s), 105.8 (s), 99.5 (s), 93.0 (s), 48.1 (s), 37.2 (s), 19.4 (s), 18.4 (s), 15.2 (s), 14.8 (s), 11.6 (s), 9.9 (s), 9.5 (s), 9.1 (s), 8.6 (s), 8.5 (s), 8.1 (s), 5.6 (s), 3.3 (s), 0.3 (s), -5.3 (s), -20.7 (s), -22.2 (s), -42.1 (s), -48.1 (s), -61.7 (s), -62.0 (s), -62.7 (s), -63.2 (s), -65.6 (s), -74.0 (s). ESMS found *m/z* 708.2 for $[M+Na]^+$. HR-ESMS found *m/z* 684.1514, calculated *m/z* 684.1509 for $[C_{26}H_{30}O_7N_4{}^{174}Yb]^+$. UV-Vis ($H_2O$) λ_{max}/nm: 207, 260, 305, 363.

Gd.2.10. Yield: 91 %. ESMS found *m/z* 670.2 for $[M+H]^+$. HR-ESMS found *m/z* 692.1325, calculated *m/z* 692.1326 for $[C_{30}H_{31}O_7N_4{}^{158}Gd^{23}Na]^+$. UV-Vis ($H_2O$) λ_{max}/nm: 207, 260, 305, 362. $E_T \approx 19900$ cm^{-1}.

Lu.2.10. Yield: 92 %. ^{1}H NMR (500 MHz, D_2O, pH = 6) δ_H 8.77 (s, 1H, Ar*H*), 7.99 (m, 4H, Ar*H*), 7.72 (t, 1H, J = 8.0 Hz, Ar*H*), 7.62 (t, 1H, J = 8.0 Hz, Ar*H*), 4.95 (d, 1H, J = 16.0 Hz, Ar*H*), 4.47 (d, 1H, J = 16.0 Hz, Ar*H*), 3.66-3.24 (m, br, 10H, CH_2 ring and arms), 2.96-2.39 (m, br, 12H, CH_2 ring and arms). ESMS found *m/z* 687.2 for $[M+H]^+$. HR-ESMS found *m/z* 687.1658, calculated *m/z* 687.1673 for $[C_{26}H_{30}O_7N_4{}^{175}Lu]^+$. UV-Vis ($H_2O$) λ_{max}/nm: 207, 227, 260, 305, 362.

Eu.2.11. Yield: 95 %. ^{1}H NMR (500 MHz, D_2O, pH = 7) δ_H 34.9 (s), 28.7 (s), 27.9 (s), 27.4 (s), 6.9 (s), 1.4 (s), 0.5 (s), -2.0 (s), -4.1 (s), -4.8 (s), -7.8 (s), -8.9 (s), -10.1 (s), -12.0 (s), -12.8 (s), -13.2 (s),-14.4 (s), -14.9 (s), -16.1 (s), -17.9 (s). ESMS found *m/z* 732.3 for $[M+H]^+$. HR-ESMS found *m/z* 730.1765, calculated *m/z* 730.1754 for $[C_{30}H_{35}O_7N_5{}^{153}Eu]^+$. UV-Vis ($H_2O$) λ_{max}/nm (ε/M^{-1}cm^{-1}): 233 (21,700), 279 (22,600), 309 (16,800), 369 (15,600). HPLC t_r : 11.4 min.

Yb.2.11. Yield: 95 %. ^{1}H NMR (500 MHz, D_2O, pH = 4) δ_H 135.9 (s), 112.5 (s), 108.1 (s), 102.7 (s), 43.4 (s), 33.8 (s), 24.4 (s), 19.4 (s), 17.2 (s), 14.2 (s), 12.6 (s), 10.4 (s), -12.6 (s), -27.5 (s), -37.7 (s), -41.1 (s), -45.3 (s), -57.4 (s), -66.4 (s), -67.2 (s), -68.7 (s), -70.0 (s), -82.5 (s) ppm. Only resolved peaks outside the 0 to 10 ppm region are reported. ESMS found *m/z* 753.3 for $[M+H]^+$. HR-ESMS found *m/z* 775.1890, calculated *m/z* 775.1896 for $[C_{30}H_{36}O_7N_5{}^{23}Na{}^{174}Yb]^+$. UV-Vis ($H_2O$) λ_{max}/nm: 233, 279, 308, 368.

Gd.2.11. Yield: 94 %. ESMS found *m/z* 737.3 for $[M+H]^+$. HR-ESMS found *m/z* 759.1746, calculated *m/z* 759.1748 for $[C_{30}H_{36}O_7N_5{}^{158}Gd{}^{23}Na]^+$. UV-Vis ($H_2O$) λ_{max}/nm: 234, 277, 296, 365. $E_T \approx 21300$ cm^{-1}.

Lu.2.11. Yield: 95 %. ^{1}H NMR (500 MHz, D_2O, pH = 4) δ_H 8.63 (s, br, 1H, Ar*H*), 8.02 (s, br, 1H, Ar*H*), 7.94 (s, br, 1H, Ar*H*), 7.28 (s, br, 1H, Ar*H*), 7.24 (s, br, 1H, Ar*H*), 7.09 (s, br, 2H, Ar*H*), 4.05-1.25 (m, br, 24H, CH_2 ring and arms), 1.30 (s, br, 2H, NCH_2CH$_3$), 1.09 (s, br, 3H, NCH$_2$CH_3). ESMS found *m/z* 754.2 for $[M+H]^+$. HR-ESMS found *m/z* 754.2083, calculated *m/z* 754.2095 for $[C_{30}H_{37}O_7N_5{}^{175}Lu]^+$. UV-Vis ($H_2O$) λ_{max}/nm: 234, 279, 308, 368.

Eu.2.12. Yield: 95 %. ^{1}H NMR (500 MHz, D_2O, pH = 7) δ_H 35.4 (s), 28.2 (s), 26.8 (s), 26.0 (s), 9.7 (s), 8.1-7.8 (m), 3.3 (s), 1.1 (s), -1.7 (s), -3.2 (s), -4.5 (s), -5.6 (s), -7.5 (s), -10.4 (s), -11.8 (s), -12.5 (s),-15.8 (s), -16.3 (s), -18.3 (s). ESMS found *m/z* 715.2 for $[M+H]^+$. HR-ESMS found *m/z* 715.1628, calculated *m/z* 715.1634 for $[C_{30}H_{34}O_7N_4{}^{153}Eu]^+$. UV-Vis ($H_2O$) λ_{max}/nm (ε/M^{-1}cm^{-1}): 242 (58,800), 254 (45,600), 267 (42,600), 346 (19,600). HPLC t_r : 11.2 min.

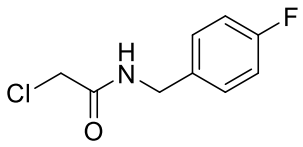
Yb.2.12. Yield: 95. ^{1}H NMR (500 MHz, D_2O, pH = 7) δ_H 138.4 (s), 105.0 (s), 98.7 (s), 92.9 (s), 48.1 (s), 37.2 (s), 18.0 (s), 15.9 (s), 11.2 (s), 10.5 (s), 9.7 (s), 9.1 (s), 8.5 (s), 8.1 (s), 7.7 (s), 5.3 (s), 0.5 (s), -4.7 (s), -20.8 (s), -42.3 (s), -48.1 (s), -61.2 (s), -62.2 (s), -62.5 (s), -65.0 (s), -74.2 (s). ESMS found *m/z* 736.2 for $[M+H]^+$. HR-ESMS found *m/z* 758.1622, calculated *m/z* 758.1630 for $[C_{30}H_{33}O_7N_4{}^{23}Na^{174}Yb]^+$. UV-Vis ($H_2O$) λ_{max}/nm: 242, 256, 266, 346.

Gd.2.12. Yield: 95 %. ESMS found *m/z* 720.3 for $[M+H]^+$. HR-ESMS found *m/z* 742.1477, calculated *m/z* 742.1483 for $[C_{30}H_{33}O_7N_4{}^{158}Gd^{23}Na]^+$. UV-Vis ($H_2O$) λ_{max}/nm: 242, 254, 267, 346. $E_T \approx 19500\ cm^{-1}$.

Lu.2.12. Yield: 94 %. ^{1}H NMR (500 MHz, D_2O, pH = 4) δ_H 9.12 (s, br, 1H, Ar*H*), 8.57 (s, br, 1H, Ar*H*), 8.01 (s, br, 1H, Ar*H*), 7.76 (s, br, 2H, Ar*H*), 7.67 (s, br, 2H, Ar*H*), 7.59 (s, br, 1H, Ar*H*), 7.51 (s, br, 1H, Ar*H*), 3.81-2.12 (m, br, 24H, CH_2 ring and arms). ESMS found *m/z* 737.2 for $[M+H]^+$. HR-ESMS found *m/z* 759.1635, calculated *m/z* 759.1649 for $[C_{30}H_{33}O_7N_4{}^{175}Lu^{23}Na]^+$. UV-Vis ($H_2O$) λ_{max}/nm: 242, 254, 267, 346.

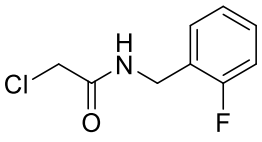
7.9 Studying the effect of fluoride on lanthanide tetra-amide complexes

N-(4-fluorobenzyl)-chloroacetamide, 3.3[14]



4-Fluorobenzylamine (2.0 mL, 17.5 mmol) and Et_3N (3.0 mL, 21.0 mmol) were dissolved in DCM (20 mL) and cooled to -2 to -5°C in an ice/acetone bath. 2-chloroacetylchloride (1.67 mL, 21.0 mmol) dissolved in DCM (10 mL) was added dropwise to the mixture. The mixture was allowed to stir for 30 min at 0°C and was then returned to room temperature and stirred overnight. The precipitate was then filtered off and washed with DCM. The filtrate was washed with 2 M HCl (2 x 10 mL) and brine (2 x 30 mL), dried (Na_2SO_4), filtered and solvent removed. The crude material was recrystallised from DCM/petroleum ether to give the *title compound* as a beige crystals (1.791 g, 51%). ^{1}H NMR (400 MHz, $CDCl_3$) δ_H 7.30-7.25 (m, 2H, Ar*H*), 7.07-7.01 (m, 2H, Ar*H*), 6.85 (br, s, 1H, N*H*), 4.47 (d, 2H, ArCH_2, J = 5.6 Hz), 4.41 (s, 2H, ClCH_2) ppm. ^{19}F{^{1}H} (376 MHz, $CDCl_3$) δ_F -114.9 (s). ESMS found *m/z* 202.1 for $[M+H]^+$.

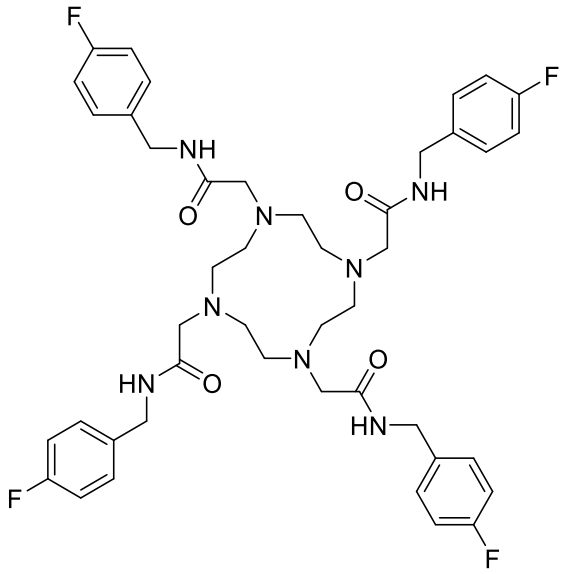
N-(2-fluorobenzyl)-chloroacetamide, 3.4[14]



2-Fluorobenzylamine (0.95 mL, 8.31 mmol) and Et_3N (1.30 mL, 9.35 mmol) were dissolved in DCM (10 mL) and cooled to -2 to -5°C in an ice/acetone bath. 2-chloroacetylchloride (0.75 mL, 9.42 mmol) dissolved in DCM (5 mL) was added dropwise to the mixture. The mixture was allowed to stir for 30 min at 0°C and was

then returned to room temperature and stirred overnight. The precipitate was then filtered and washed with DCM. The filtrate was washed with 2 M HCl (2 x 5 mL) and brine (2 x 15 mL), dried (Na_2SO_4), filtered and solvent removed. The crude material was recrystallised from DCM/petroleum ether to give the *title compound* as a beige crystals (0.954 g, 57%). ^{1}H NMR (400 MHz, $CDCl_3$) δ_H 7.35-7.31 (m, 1H, Ar*H*), 7.30-7.26 (m, 1H, Ar*H*), 7.14-7.10 (m, 1H, Ar*H*), 7.09-7.04 (m, 1H, Ar*H*), 6.98 (br, s, 1H, N*H*), 4.54 (d, 2H, ArCH_2, J = 5.9 Hz), 4.07 (s, 2H, ClCH_2) ppm. ^{19}F{^{1}H} (376 MHz, $CDCl_3$) δ_F -119.3 (s). ESMS found *m/z* 202.1 for $[M+H]^+$.

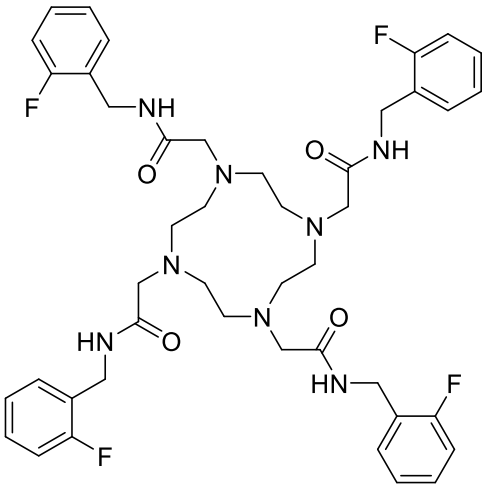
1,4,7,10-Tetrakis[*N*-(4-fluorobenzyl)carbamoylmethyl]-1,4,7,10-tetraazacyclododecane, 3.5



Cyclen (0.203 g, 1.18 mmol), N-(4-fluorobenzyl)-chloroacetamide (1.002 g, 4.97 mmol) and Et_3N (1.4 mL, 10.0 mmol) in DMF (50 mL) was heated overnight at 85°C. Water (170 mL) was added and the solution was heated at 100°C for 30 min. After cooling, the beige precipitate was filtered, washed with H_2O (30 mL) and dried. The solid was suspended in DMF (12 mL) and water (8 mL) and the mixture heated at 100°C for 30

min. After cooling, the solid was filtered and dried to give the *title compound* as a beige solid (0.261 g, 27%). ^{1}H NMR (400 MHz, DMSO-d_6) δ_H 8.46 (t, 4H, N*H*, J = 6.1 Hz), 7.25-7.22 (m, 8H, Ar*H*), 7.11-7.07 (m, 8H, Ar*H*), 4.22 (d, 8H, NCH_2Ar, J = 5.9 Hz), 2.97 (s, 8H, NCH_2CO), 2.52 (s, 16H, NCH_2) ppm. ^{13}C{^{1}H} NMR (101 MHz, DMSO-d_6) δ_C 170.3, 161.1 (d, $^{1}J_{CF}$ = 242.2 Hz, C), 135.7 (d, $^{4}J_{CF}$ = 3.2 Hz, C), 129.1 (d, $^{3}J_{CF}$ = 8.1 Hz, CH), 114.9 (d, $^{2}J_{CF}$ = 21.1 Hz, CH), 57.8, 53.6, 41.1 ppm.^{19}F{^{1}H} (376 MHz, DMSO-d_6) δ_F -116.7 (s). ESMS found *m/z* 833.4 for $[M+H]^+$. HR-ESMS found *m/z* 833.4124, calculated *m/z* 833.4120 for $[C_{44}H_{53}O_4N_8F_4]^+$. Found: C, 63.32; H, 6.24; N, 13.37. Calc. for $C_{44}H_{52}F_4N_8O_4$: C, 63.45; H, 6.29; N, 13.45%.

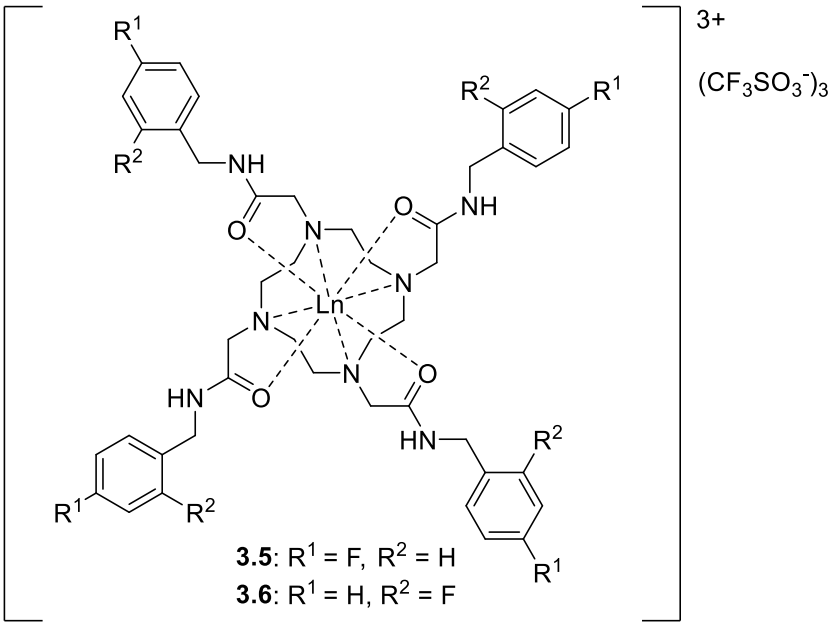
1,4,7,10-Tetrakis[*N*-(2-fluorobenzyl)carbamoylmethyl]-1,4,7,10-tetraazacyclododecane, 3.6



Cyclen (0.203 g, 1.18 mmol), N-(2-fluorobenzyl)-chloroacetamide (0.948 g, 4.72 mmol) and Et_3N (1.3 mL, 9.35 mmol) in DMF (50 mL) was heated overnight at 85°C. Water (170 mL) was added and the solution was heated at 100°C for 30 min. After cooling, the beige precipitate was filtered, washed with H_2O (30 mL) and dried. The solid was suspended in DMF (12 mL) and water (8 mL) and the mixture heated at 100°C for 30

min. After cooling, the solid was filtered and dried to give the *title compound* as a beige solid (0.469 g, 48%). ^{1}H NMR (400 MHz, DMSO-d_6) δ_H 8.45 (t, 4H, N*H*, J = 5.8 Hz), 7.32-7.25 (m, 8H, Ar*H*), 7.16-7.10 (m, 8H, Ar*H*), 4.29 (d, 8H, NCH_2Ar, J = 5.7 Hz), 3.01 (s, 8H, NCH_2CO), 2.55 (s, 16H, NCH_2) ppm. ^{13}C{^{1}H} NMR (101 MHz, DMSO-d_6) δ_C 170.4, 160.0 (d, $^{1}J_{CF}$ = 244.7 Hz, C), 129.4 (d, $^{3}J_{CF}$ = 4.1 Hz, CH), 128.8 (d, $^{3}J_{CF}$ = 8.3 Hz, CH), 126.0 (d, $^{2}J_{CF}$ = 14.9 Hz, C), 124.2 (d, $^{4}J_{CF}$ = 3.3 Hz, CH), 115.0 (d, $^{2}J_{CF}$ = 21.3 Hz, CH), 57.6, 53.7, 35.8 ppm. ^{19}F{^{1}H} (376 MHz, DMSO-d_6) δ_F -119.5 (s). ESMS found *m/z* 833.4 for $[M+H]^+$. HR-ESMS found *m/z* 833.4113, calculated *m/z* 833.4120 for $[C_{44}H_{53}O_4N_8F_4]^+$. Found: C, 63.37; H, 6.17; N, 13.34. Calc. for $C_{44}H_{52}F_4N_8O_4$: C, 63.45; H, 6.29; N, 13.45%.

General method for the synthesis of lanthanide tetra-amide complexes



$Ln(OTf)_3$/ $Y(OTf)_3$ (1 equiv.) and **3.5**/**3.6** (1 eq.) in anhydrous MeCN were heated under reflux overnight. After cooling, the solution was filtered and concentrated, DCM was added and the resulting solution kept overnight at 0°C. The deposited solid was recovered by filtration, washed with DCM and dried to obtain the product as a white solid.

Eu.3.5. Yield: 51.4 mg, 59%. ^{1}H NMR (400 MHz, D_2O) δ_H 25.9 (s), 6.7 (s), 6.3 (s), 3.7 (s), 3.1 (s), 2.5 (s), -2.6 (s), -6.0 (s), -8.0 (s), -12.5 (s), -13.4 (s) ppm. ^{19}F{^{1}H} (376 MHz, D_2O) δ_F -115.9 (s). ESMS found *m/z* 567.3 for $[M^{3+} + CF_3SO_3^-]^{2+}$. HR-ESMS found *m/z* 328.4415, calculated *m/z* 328.4415 for $[C_{44}H_{52}O_4N_8{}^{153}EuF_4]^{3+}$. Found: C, 39.54; H, 3.54; N, 7.75. Calc. for $C_{47}H_{52}EuF_{13}N_8O_{13}S_3$: C, 39.42; H, 3.66; N, 7.82%.

Yb.3.5. Yield: 54.1 mg, 61%. ^{1}H NMR (400 MHz, D_2O) δ_H 94.9 (s), 17.6 (s), 14.7 (s), 4.5 (s), 3.7 (s), -0.2 (s), -4.2 (s), -25.5 (s), -31.0 (s), -59.1 (s) ppm. ^{19}F{^{1}H} (376 MHz, D_2O) δ_F -118.6 (s). ESMS found *m/z* 577.7 for $[M^{3+} + CF_3SO_3^-]^{2+}$. HR-ESMS found *m/z* 1302.2487, calculated *m/z* 1302.2446 for $[C_{46}H_{52}O_{10}N_8F_{10}{}^{32}S_2{}^{172}Yb]^+$. Found: C, 38.66; H, 3.52; N, 7.62. Calc. for $C_{47}H_{52}YbF_{13}N_8O_{13}S_3$: C, 38.85; H, 3.61; N, 7.71%.

Lu.3.5. Yield: 63.2, 79%. ^{1}H NMR (400 MHz, D_2O) δ_H 7.40-7.36 (m, 8H, Ar*H*), 7.11 (t, 8H, Ar*H*, J = 8.7 Hz), 4.48-4.40 (m, 8H, ArCH_2), 3.23 (t, br, 4H, ax ring C*H*, J = 14.3 Hz), 3.13 (d, 4H, NCH_2CO, J = 16.6 Hz), 2.62 (d, br, 4H, eq ring C*H*, J = 14.3 Hz), 2.35 (d, br, 4H, eq ring C*H*, J = 14.2 Hz), 2.27 (d, 4H, NCH_2CO, J = 16.6 Hz), 2.02 (t, br, 4H, ax ring C*H*, J = 14.3 Hz) ppm. ^{19}F{^{1}H} (376 MHz, D_2O) δ_F -114.9 (s). ESMS found *m/z* 578.1 for $[M^{3+} + CF_3SO_3^-]^{2+}$. HR-ESMS found *m/z* 335.7811, calculated *m/z* 335.7813 for

$[C_{44}H_{52}O_4N_8F_4{}^{175}Lu]^{3+}$. Found: C, 38.69; H, 3.46; N, 7.81. Calc. for $C_{47}H_{52}LuF_{13}N_8O_{13}S_3$: C, 38.80; H, 3.60; N, 7.70%.

Y.3.5. Yield: 47.5 mg, 65%. ^{1}H NMR (400 MHz, D_2O) δ_H 7.40-7.37 (m, 8H, Ar*H*), 7.10 (t, 8H, Ar*H*, J = 8.7 Hz), 4.48-4.39 (m, 8H, ArCH_2), 3.25 (t, br, 4H, ax ring C*H*, J = 14.3 Hz), 3.08 (d, 4H, NCH_2CO, J = 16.5 Hz), 2.57 (d, br, 4H, eq ring C*H*, J = 14.3 Hz), 2.33-2.23 (m, 8H, eq ring C*H* and NCH_2CO), 2.03 (t, br, 4H, ax ring C*H*, J = 14.3 Hz) ppm. ^{19}F{^{1}H} (376 MHz, D_2O) δ_F -114.9 (s). ESMS found *m/z* 535.1 for $[M^{3+} + CF_3SO_3^-]^{2+}$. HR-ESMS found *m/z* 307.1029, calculated *m/z* 307.1030 for $[C_{44}H_{52}O_4N_8F_4{}^{89}Y]^{3+}$. Found: C, 41.06; H, 3.71; N, 8.66. Calc. for $C_{47}H_{52}YF_{13}N_8O_{13}S_3$: C, 41.23; H, 3.83; N, 8.18%.

Tb.3.5. Yield: 33.2 mg, 64%. ^{1}H NMR (400 MHz, D_2O) δ_H 205.1 (s), 104.0 (s), 55.5 (s), 38.7 (s), 28.7 (s), 18.5 (s), 17.0 (s), -83.3 (s), -84.1 (s), -312.6 (s) ppm. ^{19}F{^{1}H} (376 MHz, D_2O) δ_F -101.6 (s). ESMS found *m/z* 570.3 for $[M^{3+} + CF_3SO_3^-]^{2+}$. HR-ESMS found *m/z* 1289.2288, calculated *m/z* 1289.2336 for $[C_{46}H_{52}O_{10}N_8F_{10}{}^{32}S_2{}^{159}Tb]^+$. Found: C, 39.35; H, 3.61; N, 7.85. Calc. for $C_{47}H_{52}TbF_{13}N_8O_{13}S_3$: C, 39.23; H, 3.64; N, 7.79%.

Dy.3.5. Yield: 32.3 mg, 67%. ^{1}H NMR (400 MHz, D_2O) δ_H 248.0 (s), 126.2 (s), 79.5 (s), 44.8 (s), 31.5 (s), 20.6 (s), 18.3 (s), -85.8 (s), -88.1 (s), -371.5 (s) ppm. ^{19}F{^{1}H} (376 MHz, D_2O) δ_F -99.2 (s). ESMS found *m/z* 572.3 for $[M^{3+} + CF_3SO_3^-]^{2+}$. HR-ESMS found *m/z* 1294.2341, calculated *m/z* 1294.2374 for $[C_{46}H_{52}O_{10}N_8F_{10}{}^{32}S_2{}^{163}Dy]^+$. Found: C, 39.30; H, 3.53; N, 7.83. Calc. for $C_{47}H_{52}DyF_{13}N_8O_{13}S_3$: C, 39.13; H, 3.63; N, 7.77%.

Ho.3.5. Yield: 31.1 mg, 57%. ^{1}H NMR (400 MHz, D_2O) δ_H 127.2 (s), 66.0 (s), 36.1 (s), 25.1 (s), 13.7 (s), 12.6 (s), -46.4 (s), -48.9 (s), -186.9 (s) ppm. $^{19}F\{^{1}H\}$ (376 MHz, D_2O) δ_F -107.2 (s). ESMS found *m/z* 573.3 for $[M^{3+} + CF_3SO_3^-]^{2+}$. HR-ESMS found *m/z* 1295.2343, calculated *m/z* 1295.2386 for $[C_{46}H_{52}O_{10}N_8F_{10}{}^{32}S_2{}^{165}Ho]^+$. Found: C, 37.70; H, 3.47; N, 7.84. Calc. for $C_{47}H_{52}HoF_{13}N_8O_{13}S_3$: C, 39.07; H, 3.63; N, 7.75%.

Er.3.5. Yield: 37.8 mg, 67%. ^{1}H NMR (400 MHz, D_2O) δ_H 103.8 (s), 11.9 (s), 3.6 (s), 0.0 (s), -4.0 (s), -33.5 (s), -38.3 (s), -62.5 (s) ppm. $^{19}F\{^{1}H\}$ (376 MHz, D_2O) δ_F -119.1 (s). ESMS found *m/z* 573.8 for $[M^{3+} + CF_3SO_3^-]^{2+}$. HR-ESMS found *m/z* 1296.2347, calculated *m/z* 1296.2386 for $[C_{46}H_{52}O_{10}N_8F_{10}{}^{32}S_2{}^{167}Er]^+$. Found: C, 39.48; H, 3.53; N, 7.83. Calc. for $C_{47}H_{52}ErF_{13}N_8O_{13}S_3$: C, 39.00; H, 3.62; N, 7.74%.

Tm.3.5. Yield: 41.3 mg, 71%. ^{1}H NMR (400 MHz, D_2O) δ_H 248.3 (s), 41.8 (s), 31.8 (s), 1.0 (s), -1.4 (s), -7.3(s), -17.4 (s), -73.4 (s), -84.3 (s), -160.7 (s) ppm. $^{19}F\{^{1}H\}$ (376 MHz, D_2O) δ_F -124.7 (s). ESMS found *m/z* 575.3 for $[M^{3+} + CF_3SO_3^-]^{2+}$. HR-ESMS found *m/z* 1299.2380, calculated *m/z* 1299.2425 for $[C_{46}H_{52}O_{10}N_8F_{10}{}^{32}S_2{}^{172}Yb]^+$. Found: C, 39.17; H, 3.52; N, 7.84. Calc. for $C_{47}H_{52}TmF_{13}N_8O_{13}S_3$: C, 38.96; H, 3.62; N, 7.73%.

Eu.3.6. Yield: 70.5 mg, 66%. ^{1}H NMR (400 MHz, D_2O) δ_H 26.0 (s), 6.9 (s), 6.2 (s), 3.7 (s), 3.3 (s), 2.6 (s), -2.6 (s), -6.0 (s), -8.0 (s), -12.5 (s), -13.5 (s) ppm. $^{19}F\{^{1}H\}$ (376 MHz, D_2O) δ_F -119.9 (s). ESMS found *m/z* 567.2 for $[M^{3+} + CF_3SO_3^-]^{2+}$. HR-ESMS found *m/z* 328.4416, calculated *m/z* 328.4415 for $[C_{44}H_{52}O_4N_8{}^{153}EuF_4]^{3+}$. Found: C, 39.30; H, 3.53; N, 7.81. Calc. for $C_{47}H_{52}EuF_{13}N_8O_{13}S_3$: C, 39.42; H, 3.66; N, 7.82%.

Yb.3.6. Yield: 69.5 mg, 80%. ^{1}H NMR (400 MHz, D_2O) δ_H 96.1 (s), 18.1 (s), 15.1 (s), 5.8 (s), 3.6 (s), 0.5 (s), -3.5 (s), -25.5 (s), -31.1 (s), -59.1 (s) ppm. ^{19}F{^{1}H} (376 MHz, D_2O) δ_F -122.9 (s). ESMS found *m/z* 577.4 for $[M^{3+} + CF_3SO_3^-]^{2+}$. HR-ESMS found *m/z* 577.6472, calculated *m/z* 577.6473 for $[C_{45}H_{52}O_7N_8F_7{}^{32}S^{174}Yb]^{2+}$. Found: C, 39.02; H, 3.58; N, 7.84. Calc. for $C_{47}H_{52}YbF_{13}N_8O_{13}S_3$: C, 38.85; H, 3.61; N, 7.71%.

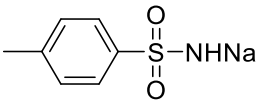
Lu.3.6. Yield: 56.7 mg, 64%. ^{1}H NMR (400 MHz, D_2O) δ_H 7.37-7.33 (m, 8H, Ar*H*), 7.14-7.07 (m, 8H, Ar*H*), 4.56 (d, 4H, ArCH_2, J = 14.6 Hz), 4.39 (d, 4H, ArCH_2, J = 14.6 Hz), 3.14 (t, br, 4H, ax ring C*H*, J = 14.4 Hz), 3.03 (d, 4H, NCH_2CO, J = 16.7 Hz), 2.54 (d, br, 4H, eq ring C*H*, J = 14.5 Hz), 2.30-2.16 (m, 8H, eq ring C*H* and NCH_2CO), 1.92 (t, br, 4H, ax ring C*H*, J = 14.0 Hz) ppm. ^{19}F{^{1}H} (376 MHz, D_2O) δ_F -118.9 (s). ESMS found *m/z* 578.3 for $[M^{3+} + CF_3SO_3^-]^{2+}$. HR-ESMS found *m/z* 1305.2443, calculated *m/z* 1305.2490 for $[C_{46}H_{52}F_{10}N_8O_{10}S_2{}^{175}Lu]^+$. Found: C, 38.64; H, 3.48; N, 7.66. Calc. for $C_{47}H_{52}LuF_{13}N_8O_{13}S_3$: C, 38.80; H, 3.60; N, 7.70%.

Y.3.6. Yield: 58.4 mg, 74%. ^{1}H NMR (400 MHz, D_2O) δ_H 7.48-7.35 (m, 8H, Ar*H*), 7.25-7.13 (m, 8H, Ar*H*), 4.63 (d, 4H, ArCH_2, J = 14.6 Hz), 4.48 (d, 4H, ArCH_2, J = 14.8 Hz), 3.24 (t, br, 4H, ax ring C*H*, J = 14.9 Hz), 3.05 (d, 4H, NCH_2CO, J = 16.7 Hz), 2.57 (d, br, 4H, eq ring C*H*, J = 14.5 Hz), 2.35-2.22 (m, 8H, eq ring C*H* and NCH_2CO), 2.01 (t, br, 4H, ax ring C*H*, J = 14.5 Hz) ppm. ^{19}F{^{1}H} (376 MHz, D_2O) δ_F -118.9 (s). ESMS found *m/z* 535.2 for $[M^{3+} + CF_3SO_3^-]^{2+}$. HR-ESMS found *m/z* 307.1030, calculated *m/z* 307.1030 for $[C_{44}H_{52}O_4N_8F_4{}^{89}Y]^{3+}$. Found: C, 40.94; H, 3.69; N, 8.75. Calc. for $C_{47}H_{52}YF_{13}N_8O_{13}S_3$: C, 41.23; H, 3.83; N, 8.18%.

7.10 Investigating the interaction of fluoride with lanthanide complexes of Lehn's cryptand

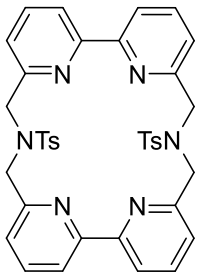
4.5, **4.6** and **4.7** synthesised according to reference.[15] In a modification to the literature procedure 6,6'-bis(chloromethyl)-2,2'-bipyridyl was used instead of 6,6'-bis(bromomethyl)-2,2'-bipyridyl.

p-Toluenesulfonamide monosodium salt, 4.4[16]



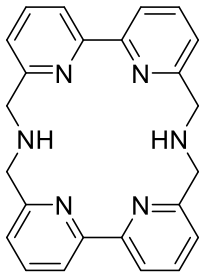
p-Toluenesulfonamide (2.005 g, 11.71 mmol) and NaOEt (0.798 g, 11.72 mmol) in anhydrous EtOH (20 mL) was refluxed for 2 h. The reaction mixture was cooled to RT, filtered and washed with EtOH to give the *title compound* as an off white solid (1.591 g, 71%). This compound was used without further purification for the following step.

4.5



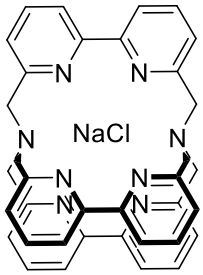
4.4 (0.547 g, 2.83 mmol) and 6,6'-bis(chloromethyl)-2,2'-bipyridyl (0.358 g, 1.41 mmol) in anhydrous EtOH (40 mL) was refluxed for 24 h. The reaction mixture was cooled to -5°C, filtered and the insoluble solid formed was washed with H_2O and EtOH to give the *title compound* as an off white solid (0.276 g, 56%). This compound was used without further purification for the following step.

4.6



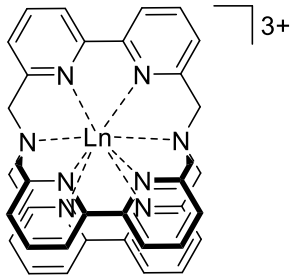
4.5 (0.276 g, 0.39 mmol) was dissolved in conc. H_2SO_4 (5 mL) and heated at 110°C for 2 h. The reaction mixture was allowed to cool to RT, H_2O (4 mL) added and the pH of the solution brought to 10 using NaOH solution (2M). The product precipitated and the aqueous layer was extracted with $CHCl_3$ (3 x 30 mL), the organic layer dried ($MgSO_4$) filtered and the solvent removed to give the *title compound* as a colourless solid (151.2 g, 97%). This compound was used without further purification for the following step.

4.7



4.6 (0.151 g, 0.38 mmol), Na_2CO_3 (0.408 g, 3.80 mmol) and 6,6'-bis(chloromethyl)-2,2'-bipyridyl (98.8 mg, 0.39 mmol) were suspended in anhydrous MeCN (200 mL). The mixture heated at reflux for 48 h, cooled to RT, filtered and solvent removed. Purification by silica gel column chromatography (15:1 to 9:1, $CHCl_3$:MeOH) gave the *title compound* as a colourless solid (40.8 mg, 17%). ^{1}H NMR (400 MHz, $CDCl_3$) δ_H 7.89 (d, 4H, Ar*H*, J = 7.7 Hz), 7.82 (t, 6H, Ar*H*, J = 7.7 Hz), 7.32 (d, 4H, Ar*H*, J = 7.5 Hz), 3.83 (s, 12H, NCH_2) ppm. ESMS found *m/z* 597.3 for $[M+Na]^+$.

General method for the synthesis of lanthanide complexes of the Lehn cryptand



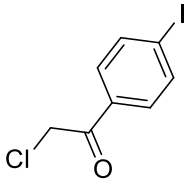
$Ln(OTf)_3$ (1 eq.) and **4.7** (1 eq.) in anhydrous MeCN were heated under reflux for 48 h. After cooling, the solution was filtered and the solvent removed. The residue was dissolved in a minimum amount of MeOH and Et_2O added until the solution just became cloudy, the resulting solution kept overnight at 0°C. The deposited solid was recovered by filtration, washed with Et_2O and dried to obtain the product as a colourless solid. Data obtained was consistent with that found in the literature.[15, 17, 18]

Eu.4.7. Yield: 38.1 mg, 65%. ^{1}H NMR (400 MHz, D_2O) δ_H 8.2 (s), 7.7 (s), 6.9 (s), 0.3 (s) ppm. ESMS found *m/z* 1025.2 for $[M^{3+} + 2CF_3SO_3^-]^+$. UV-Vis (H_2O) λ_{max}/nm: 245, 303.

Yb.4.7. Yield: 8.9 mg, 72%. ^{1}H NMR (400 MHz, D_2O) δ_H 19.6 (s), 18.2 (s), 17.2 (s), 14.5 (s) ppm. ESMS found *m/z* 1046.0 for $[M^{3+} + 2CF_3SO_3^-]^+$. UV-Vis (H_2O) λ_{max}/nm: 245, 304.

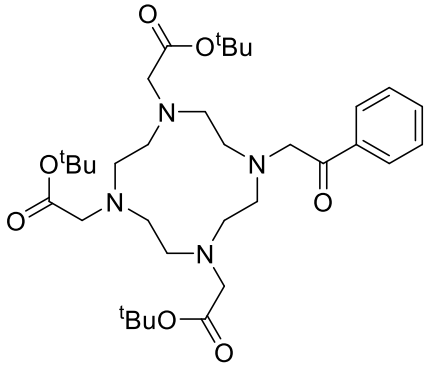
7.11 Synthesis and study of halogenated phenacylDO3A complexes

2-Chloro-4'-iodoacetophenone, 5.4



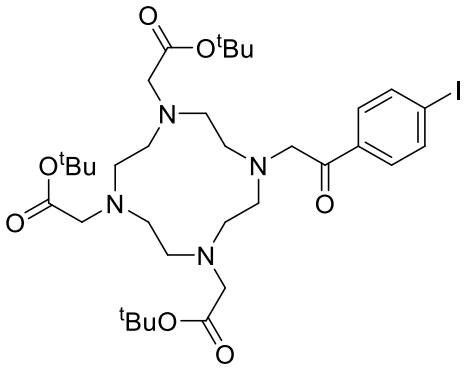
2-Chloroacetylchloride (4.00 mL, 50.3 mmol) was added dropwise over 30m to $AlCl_3$ (6.851 g, 51.4 mmol) in anhydrous DCM (50 mL) at 0°C. The mixture was stirred at 0°C for 30m. Iodobenzene (5.60 mL, 50.0 mmol) was added dropwise over 1h to the solution at 0°C. The mixture was allowed to reach RT and then stirred for 2h, poured onto a concentrated HCl/ice slurry and extracted with DCM (3 x 50 mL). The organic layer was washed with saturated $NaHCO_3$ (50 mL), brine (50 mL), dried (Na_2SO_4), filtered and the solvent removed. Purification by silica gel column chromatography (petroleum ether:EtOAc, 4:1) gave the *title compound* as an off white solid (6.448 g, 46%). ^{1}H NMR (400 MHz, $CDCl_3$) δ_H 7.88 (d, 2H, Ar*H*, J = 8.6 Hz), 7.68 (d, 2H, Ar*H*, J = 8.6 Hz), 4.65 (s, 2H, CH_2) ppm. FIMS found *m/z* 279.9151, calculated *m/z* 279.9152 for $[M]^+$.

1-(2-Acetophenone)-4,7,10-tris(*tert*-butoxycarboxymethyl)-1,4,7,10-tetraazacyclododecane, 5.5[19]



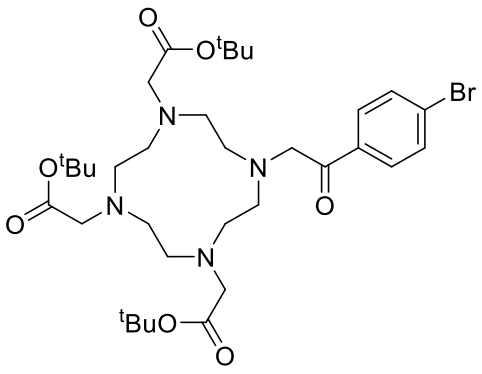
A solution of 2-bromoacetophenone (0.372 g, 1.87 mmol), **2.4** (1.008 g, 1.69 mmol), K_2CO_3 (0.515 g, 3.72 mmol) and a catalytic amount of KI in anhydrous MeCN (30 mL) was heated at 80°C for 48h. The mixture was allowed to cool to RT, filtered and solvent removed. Purification by silica gel column chromatography (DCM to DCM:MeOH, 97:3, 0.1 mL per 100 mL) gave the *title compound* as a yellow solid (0.456 g, 43%). ^{1}H NMR (400 MHz, $CDCl_3$) δ_H 7.90 (d, 2H, Ar*H*, J = 7.2 Hz), 7.58 (t, 1H, Ar*H*, J = 7.5 Hz), 7.46 (t, 2H, Ar*H*, J = 7.7 Hz), 3.61-2.10 (m, 24H, CH_2 ring and arms), 1.46 (s, 27H, C(CH_3)$_3$) ppm. ESMS found *m/z* 655.3 for $[M+Na]^+$.

1-(4'-Iodo-2-acetophenone)-4,7,10-tris(*tert*-butoxycarboxymethyl)-1,4,7,10-tetraazacyclododecane, 5.6



A solution of 2-chloro-4'-iodoacetophenone (0.528 g, 1.88 mmol), **2.4** (1.021 g, 1.71 mmol), K_2CO_3 (0.506 g, 3.66 mmol) and a catalytic amount of KI in anhydrous MeCN (30 mL) were heated at 80°C for 48h. The mixture was allowed to cool to RT, filtered and solvent removed. Purification by silica gel column chromatography (DCM to DCM:MeOH, 97:3, 0.1 mL per 100 mL) gave the *title compound* as a yellow solid (0.548 g, 42%). ^{1}H NMR (400 MHz, $CDCl_3$) δ_H 7.77 (d, 2H, Ar*H*, J = 8.6 Hz), 7.58 (d, 2H, Ar*H*, J = 8.6 Hz), 3.40-2.01 (m, 24H, CH_2 ring and arms), 1.39 (s, 27H, C(CH_3)$_3$) ppm. ^{13}C{^{1}H} NMR (101 MHz, $CDCl_3$) δ_c 199.1, 172.9, 172.6, 137.8, 134.7, 128.9, 101.4, 81.9, 60.0, 55.6, 55.4, 52.7 (br), 48.4 (br), 27.7, 27.6 ppm. ESMS found *m/z* 781.3 for $[M+Na]^+$. HR-ESMS found *m/z* 781.2984, calculated *m/z* 781.3008 for $[C_{34}H_{55}{}^{127}IN_4O_7{}^{23}Na]^+$.

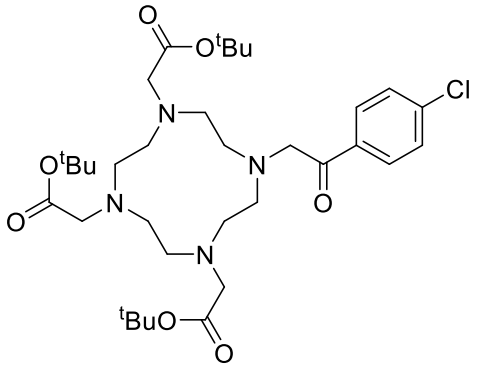
1-(4'-Bromo-2-acetophenone)-4,7,10-tris(*tert*-butoxycarboxymethyl)-1,4,7,10-tetraazacyclododecane, 5.7



A solution of 2,4'-dibromoacetophenone (0.526 g, 1.89 mmol), **2.4** (1.019 g, 1.71 mmol), K_2CO_3 (0.527 g, 3.81 mmol) and a catalytic amount of KI in anhydrous MeCN (30 mL) were heated at 80°C for 48h. The mixture was allowed to cool to RT, filtered and solvent removed. Purification by silica gel column chromatography (DCM to DCM:MeOH, 97:3, 0.1 mL per 100 mL) gave the *title compound* as a yellow solid (0.699

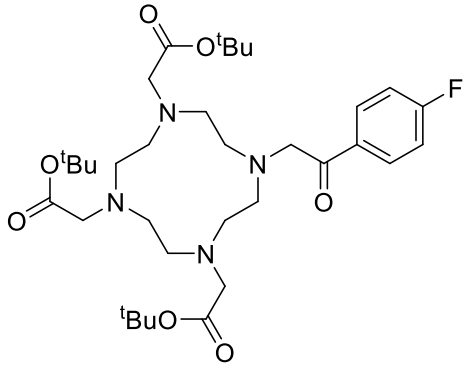
g, 57%). ^{1}H NMR (400 MHz, $CDCl_3$) δ_H 7.79 (d, 2H, Ar*H*, J = 8.4 Hz), 7.56 (d, 2H, Ar*H*, J = 8.4 Hz), 3.53-2.00 (m, 24H, CH_2 ring and arms), 1.40 (s, 27H, C(CH_3)$_3$) ppm. ^{13}C{^{1}H} NMR (101 MHz, $CDCl_3$) δ_c 198.4, 172.3, 172.1, 135.7, 131.3, 128.7, 127.9, 81.4, 59.6, 55.1, 54.8, 52.3 (br), 47.7 (br), 27.2, 27.1 ppm. ESMS found *m/z* 733.2 for $[M+Na]^+$. HR-ESMS found *m/z* 733.3127, calculated *m/z* 733.3146 for $[C_{34}H_{55}{}^{79}BrN_4O_7{}^{23}Na]^+$.

1-(4'-Chloro-2-acetophenone)-4,7,10-tris(*tert*-butoxycarboxymethyl)-1,4,7,10-tetraazacyclododecane, 5.8



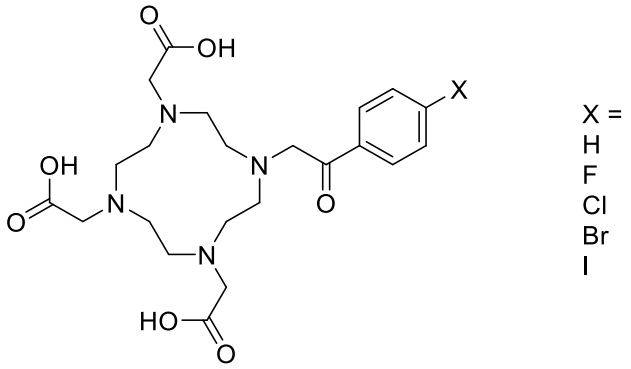
A solution of 2,4'-dichloroacetophenone (0.358 g, 1.89 mmol), **2.4** (1.028 g, 1.73 mmol), K_2CO_3 (0.5274 g, 3.82 mmol) and a catalytic amount of KI in anhydrous MeCN (30 mL) were heated at 80°C for 48h. The mixture was allowed to cool to RT, filtered and solvent removed. Purification by silica gel column chromatography (DCM to DCM:MeOH, 97:3, 0.1 mL per 100 mL) gave the *title compound* as a yellow solid (0.707 g, 61%). ^{1}H NMR (400 MHz, $CDCl_3$) δ_H 7.89 (d, 2H, Ar*H*, J = 8.7 Hz), 7.44 (d, 2H, Ar*H*, J = 8.6 Hz), 3.55-2.08 (m, 24H, CH_2 ring and arms), 1.46 (s, 27H, C(CH_3)$_3$) ppm. ^{13}C{^{1}H} NMR (101 MHz, $CDCl_3$) δ_c 198.5, 172.7, 172.5, 139.7, 133.6, 128.9, 128.7, 81.8, 60.0, 55.5, 55.3, 52.4 (br), 48.3 (br), 27.6, 27.5 ppm. ESMS found *m/z* 689.2 for $[M+Na]^+$. HR-ESMS found *m/z* 689.3633, calculated *m/z* 689.3652 for $[C_{34}H_{55}{}^{35}ClN_4O_7{}^{23}Na]^+$.

1-(4'-Fluoro-2-acetophenone)-4,7,10-tris(*tert*-butoxycarboxymethyl)-1,4,7,10-tetraazacyclododecane, 5.9



A solution of 2-chloro-4'-fluoroacetophenone (0.334 g, 1.93 mmol), **2.4** (1.045 g, 1.75 mmol), K_2CO_3 (0.537 g, 3.88 mmol) and a catalytic amount of KI in anhydrous MeCN (30 mL) were heated at 80°C for 48h. The mixture was allowed to cool to RT, filtered and solvent removed. Purification by silica gel column chromatography (DCM to DCM:MeOH, 97:3, 0.1 mL per 100 mL) gave the *title compound* as a yellow solid (0.588 g, 51%). ^{1}H NMR (400 MHz, $CDCl_3$) δ_H 7.96 (dd, 2H, Ar*H*, J = 8.7, 5.5 Hz), 7.12 (t, 2H, Ar*H*, J = 8.6 Hz), 3.59-2.04 (m, 24H, CH_2 ring and arms), 1.44 (s, 27H, C(CH_3)$_3$) ppm. ^{13}C{^{1}H} NMR (101 MHz, $CDCl_3$) δ_C 198.0, 172.8, 172.5, 165.7 (d, $^1J_{CF}$ = 255.3 Hz), 131.8, 131.2 (d, $^3J_{CF}$ = 9.8 Hz), 115.6 (d, $^2J_{CF}$ = 22.5 Hz), 81.83, 81.79, 60.0, 55.6, 55.3, 52.4 (br), 48.5 (br), 27.7, 27.6 ppm. ^{19}F{^{1}H} (376 MHz, $CDCl_3$) δ_F -104.5 (s). ESMS found *m/z* 673.3 for $[M+Na]^+$. HR-ESMS found *m/z* 673.3928, calculated *m/z* 673.3947 for $[C_{34}H_{55}{}^{19}FN_4O_7{}^{23}Na]^+$.

General procedure for the deprotection of ligands



The pro-ligands were deprotected according to the 'General procedure for the deprotection of DO3A based pro-ligands' (section 7.8).

1-(2-Acetophenone)-4,7,10-tris(carboxymethyl)-1,4,7,10-tetraazacyclododecane, 5.10[19]

2.3 (0.433 g, 0.68 mmol). ^{1}H NMR (400 MHz, D_2O) δ_H 7.97 (d, 2H, Ar*H*, J = 8.0 Hz), 7.74 (t, 1H, Ar*H*, J = 7.8 Hz), 7.58 (t, 1H, Ar*H*, J = 7.8 Hz), 4.09 – 2.93 (m, br, 24H, CH_2 ring and arms) ppm. ESMS found *m/z* 465.1 for $[M+H]^+$. UV-Vis (H_2O): λ_{max} 245 nm.

1-(4'-Iodo-2-acetophenone)-4,7,10-tris(carboxymethyl)-1,4,7,10-tetraazacyclododecane, 5.11

2.4 (0.508 mg, 0.67 mmol). ^{1}H NMR (400 MHz, D_2O) δ_H 7.99 (d, 2H, Ar*H*, J = 8.2 Hz), 7.72 (d, 2H, Ar*H*, J = 8.5 Hz), 4.02 – 2.92 (m, br, 24H, CH_2 ring and arms) ppm. ESMS found *m/z* 591.1 for $[M+H]^+$. HR-ESMS found *m/z* 591.1302, calculated *m/z* 591.1310 for $[C_{22}H_{32}{}^{127}IN_4O_7]^+$. UV-Vis ($H_2O$): λ_{max} 273 nm.

1-(4'-Bromo-2-acetophenone)-4,7,10-tris(carboxymethyl)-1,4,7,10-tetraazacyclododecane, 5.12

2.5 (0.662 g, 0.87 mmol). ^{1}H NMR (400 MHz, D_2O) δ_H 7.86 (d, 2H, Ar*H*, J = 7.9 Hz), 7.76 (d, 2H, Ar*H*, J = 7.7 Hz), 3.91 – 2.72 (m, br, 24H, C*H*$_2$ ring and arms) ppm. ESMS found *m/z* 543.1 for $[M+H]^+$. HR-ESMS found *m/z* 565.1264, calculated *m/z* 565.1268 for $[C_{22}H_{32}{}^{79}BrN_4O_7{}^{23}Na]^+$ UV-Vis (H_2O): λ_{max} 261 nm.

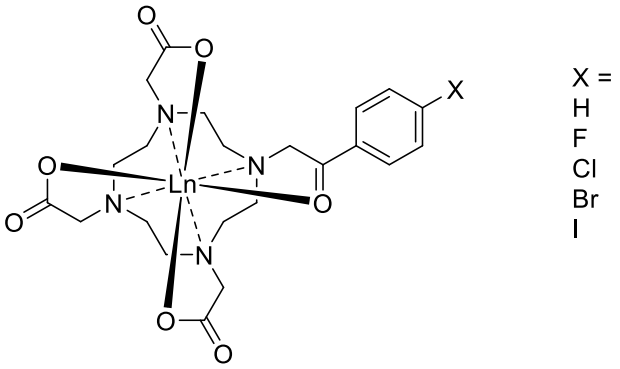
1-(4'-Chloro-2-acetophenone)-4,7,10-tris(carboxymethyl)-1,4,7,10-tetraazacyclododecane, 5.13

2.6 (0.675 g, 1.01 mmol). ^{1}H NMR (400 MHz, D_2O) δ_H 7.93 (d, 2H, Ar*H*, J = 7.9 Hz), 7.58 (d, 2H, Ar*H*, J = 7.6 Hz), 4.06 – 2.82 (m, br, 24H, C*H*$_2$ ring and arms) ppm. ESMS found *m/z* 499.1 for $[M+H]^+$. HR-ESMS found *m/z* 499.1943, calculated *m/z* 499.1954 for $[C_{22}H_{32}{}^{35}ClN_4O_7]^+$. UV-Vis ($H_2O$): λ_{max} 255 nm.

1-(4'-Fluoro-2-acetophenone)-4,7,10-tris(carboxymethyl)-1,4,7,10-tetraazacyclododecane, 5.14

2.7 (0.567 g, 0.87 mmol). ^{1}H NMR (400 MHz, D_2O) δ_H 8.04 (dd, 2H, Ar*H*, J = 8.2, 5.4 Hz), 7.29 (d, 2H, Ar*H*, J = 8.4 Hz), 4.11 – 2.94 (m, 24H, C C*H*$_2$ ring and arms) ppm. ^{19}F{^{1}H} (376 MHz, $CDCl_3$) δ_F – 102.5 (s, major species), - 105.0 (s, minor species) ppm. ESMS found *m/z* 483.1 for $[M+H]^+$. HR-ESMS found *m/z* 505.2056, calculated *m/z* 505.2069 for $[C_{22}H_{32}{}^{19}FN_4O_7{}^{23}Na]^+$. UV-Vis ($H_2O$): λ_{max} 248 nm.

General procedure for the synthesis of phenacylDO3A lanthanide complexes



The lanthanide complexes were synthesised according to the 'General procedure for the synthesis of arylacylDO3A lanthanide complexes' (section 7.8).

Eu.5.10.[19] Yield: 83%. ^{1}H NMR (500 MHz, D_2O, pH = 4) δ_H 35.7 (s), 28.1 (s), 26.8 (s), 25.9 (s), 9.1 (s), 8.03 (s), 7.95 (s), 7.5 (s), 6.9 (s), -1.8 (s), -3.3 (s), -4.6 (s), -5.7 (s), -7.5 (s), -7.8 (s), -10.2 (s), -10.7 (s), -11.8 (s), -12.8 (s), -13.3 (s), -16.2 (s), -16.4 (s), -18.5 (s) ppm. Only resolved peaks outside the 0 to 5 ppm region are reported. ESMS found *m/z* 615.0 for $[M+H]^+$. HR-ESMS found *m/z* 637.1144, calculated *m/z* 637.1141 for $[C_{22}H_{29}O_7N_4{}^{153}Eu{}^{23}Na]^+$. UV-Vis ($H_2O$): λ_{max} 262 nm. Luminescence lifetimes: H_2O: 0.61 ms, D_2O: 2.25 ms, *q* = 1.2.

Tb.5.10.[19] Yield: 94%. ^{1}H NMR (500 MHz, D_2O, pH = 4) δ_H 311.5 (s), 273.5 (s), 263.4 (s), 200.2 (s), 196.0 (s), 136.3 (s), 128.7 (s), -10.3 (s), -15.7 (s), -19.8 (s), -35.7 (s), -41.3 (s), -76.1 (s), -83.8 (s), -97.8 (s), -100.7 (s), -160.3 (s), -185.2 (s), -332.2 (s), -337.1 (s) ppm. Only resolved peaks outside the 10 to -10 ppm region are reported. ESMS found *m/z* 621.0 for $[M+H]^+$. HR-ESMS found *m/z* 643.1182, calculated *m/z* 643.1182 for $[C_{22}H_{29}O_7N_4{}^{23}Na{}^{159}Tb]^+$. UV-Vis ($H_2O$): λ_{max} 262 nm. Luminescence lifetimes: H_2O: 0.69 ms, D_2O: 2.65 ms, *q* = 1.0.

Gd.5.10.[19] Yield: 73%. ESMS found *m/z* 620.0 for $[M+H]^+$. HR-ESMS found *m/z* 642.1174, calculated *m/z* 642.1170 for $[C_{22}H_{29}O_7N_4{}^{158}Gd^{23}Na]^+$. UV-Vis ($H_2O$): λ_{max} 262 nm. $E_T \approx 25000$ cm^{-1}.

Eu.5.11. Yield: 72%. ^1H NMR (500 MHz, D_2O, pH = 4) δ_H 35.6 (s), 28.0 (s), 26.5 (s), 25.6 (s), 9.2 (s), 8.7 (s), 7.9 (s), 7.7 (s), 6.5 (s), -1.6 (s), -3.0 (s), -4.6 (s), -5.9 (s), -7.1 (s), -7.8 (s), -10.1 (s), -10.7 (s), -11.5 (s), -12.7 (s), -13.1 (s), -16.2 (s), -16.4 (s), -18.5 (s) ppm. Only resolved peaks outside the 0 to 5 ppm region are reported. ESMS found *m/z* 763.07 for $[M+Na]^+$. HR-ESMS found *m/z* 739.0256, calculated *m/z* 739.0274 for $[C_{22}H_{29}N_4O_7{}^{151}Eu^{127}I]^+$. UV-Vis ($H_2O$): λ_{max} 300 nm. Luminescence lifetimes: H_2O: 0.61 ms, D_2O: 2.28 ms, q = 1.2.

Tb.5.11. Yield: 88%. ^1H NMR (500 MHz, D_2O, pH = 4) δ_H 314.6 (s), 278.7 (s), 260.3(s), 200.4(s), 195.7 (s), 139.8(s), 131.3(s), -15.4 (s), -19.5 (s), -32.1 (s), -39.5 (s), -75.5 (s), -91.7 (s), -100.0 (s), -162.3 (s), -188.3 (s), -328.0 (s), -334.5 (s) ppm. Only resolved peaks outside the 10 to -10 ppm region are reported. ESMS found *m/z* 747.09 for $[M+H]^+$. HR-ESMS found *m/z* 747.0306, calculated *m/z* 747.0329 for $[C_{22}H_{29}N_4O_7{}^{159}Tb^{127}I]^+$. UV-Vis ($H_2O$): λ_{max} 300 nm. Luminescence lifetimes: H_2O: 0.13 ms, D_2O: 0.14 ms.

Gd.5.11. Yield: 81%. ESMS found *m/z* 768.07 for $[M+Na]^+$. HR-ESMS found *m/z* 746.0298, calculated *m/z* 746.0316 for $[C_{22}H_{29}N_4O_7{}^{158}Gd^{127}I]^+$. UV-Vis ($H_2O$): λ_{max} 300 nm. $E_T \approx 23000$ cm^{-1}.

Eu.5.12. Yield: 82%. ^{1}H NMR (500 MHz, D_2O, pH = 4) δ_H 35.6 (s), 27.9 (s), 26.4 (s), 25.6 (s), 9.3 (s), 8.4 (s), 7.65 (s), 7.60 (s), 6.4 (s), -1.7 (s), -3.0 (s), -4.7 (s), -6.0 (s), -7.2 (s), -7.9 (s), -10.3 (s), -10.8 (s), -11.6 (s), -12.8 (s), -13.2 (s), -16.5 (s), -18.7 (s) ppm. Only resolved peaks outside the 0 to 5 ppm region are reported. ESMS found *m/z* 693.1 for $[M+H]^+$. HR-ESMS found *m/z* 713.0219, calculated *m/z* 713.0232 for $[C_{22}H_{28}N_4O_7{}^{151}Eu^{79}Br^{23}Na]^+$. UV-Vis ($H_2O$): λ_{max} 278 nm. Luminescence lifetimes: H_2O: 0.61 ms, D_2O: 2.52 ms, q = 1.2.

Tb.5.12. Yield: 78%. ^{1}H NMR (500 MHz, D_2O, pH = 4) δ_H 314.5 (s), 278.9 (s), 260.0 (s), 200.4 (s), 196.0 (s), 140.0 (s), 131.1 (s), -15.0 (s), -19.3 (s), -31.8 (s), -39.5 (s), -75.2 (s), -92.0 (s), -98.9 (s), -99.7 (s), -162.4 (s), -188.4 (s), -327.9 (s), -335.0 (s) ESMS found *m/z* 699.1 for $[M+H]^+$. HR-ESMS found *m/z* 721.0269, calculated *m/z* 721.0287 for $[C_{22}H_{28}N_4O_7{}^{159}Tb^{79}Br^{23}Na]^+$. UV-Vis ($H_2O$): λ_{max} 278 nm. Luminescence lifetimes: H_2O: 0.86 ms, D_2O: 1.24 ms, q = 1.7.

Gd.5.12. Yield: 87%. ESMS found *m/z* 698.1 for $[M+H]^+$. HR-ESMS found *m/z* 696.0425, calculated *m/z* 696.0435 for $[C_{22}H_{28}N_4O_7{}^{158}Gd^{79}Br^{23}Na]^+$. UV-Vis ($H_2O$): λ_{max} 278 nm. E_T ≈ 21800 cm^{-1}.

Eu.5.13. Yield: 83%. ^{1}H NMR (500 MHz, D_2O, pH = 4) δ_H 35.6 (s), 28.0 (s), 26.5 (s), 25.6 (s), 9.3 (s), 8.2 (s), 7.9 (s), 7.56 (s), 7.46 (s), 6.3 (s), -1.8 (s), -3.1 (s), -4.7 (s), -6.0 (s), -7.2 (s), -7.9 (s), -10.3 (s), -10.8 (s), -11.6 (s), -12.8 (s), -13.2 (s), -16.5 (s), -18.7 (s) ppm. Only resolved peaks outside the 0 to 5 ppm region are reported. ESMS found *m/z* 647.0 for $[M+H]^+$. HR-ESMS found *m/z* 647.0904, calculated *m/z* 647.0918 for

$[C_{22}H_{29}N_4O_7{}^{151}Eu^{35}Cl]^+$. UV-Vis ($H_2O$): λ_{max} 275 nm. Luminescence lifetimes: H_2O: 0.60 ms, D_2O: 2.27 ms, *q* = 1.2.

Tb.5.13. Yield: 83%. ^1H NMR (500 MHz, D_2O, pH = 4) δ_H 315.0 (s), 278.8 (s), 260.9 (s), 200.4 (s), 196.2 (s), 139.9 (s), 131.3 (s), -14.3 (s), -19.0 (s), -32.2 (s), -39.7 (s), -75.4 (s), -90.2 (s), -98.9 (s), -99.9 (s), -162.0 (s), -182.5 (s), 197.9 (s), -329.1 (s), -335.8 (s) ppm. Only resolved peaks outside the 10 to -10 ppm region are reported. ESMS found *m/z* 655.0 for $[M+H]^+$. HR-ESMS found *m/z* 655.0961, calculated *m/z* 655.0973 for $[C_{22}H_{29}N_4O_7{}^{159}Tb^{35}Cl]^+$. UV-Vis ($H_2O$): λ_{max} 275 nm. Luminescence lifetimes: H_2O: 1.05 ms, D_2O: 1.59 ms, *q* = 1.6.

Gd.5.13. Yield: 87%. ESMS found *m/z* 654.0 for $[M+H]^+$. HR-ESMS found *m/z* 654.0949, calculated *m/z* 654.0960 for $[C_{22}H_{29}N_4O_7{}^{158}Gd^{35}Cl]^+$. UV-Vis ($H_2O$): λ_{max} 275 nm. $E_T \approx$ 22000 cm^{-1}.

Eu.5.14. Yield: 89%. ^1H NMR (500 MHz, D_2O, pH = 4) δ_H 35.5 (s), 28.1 (s), 26.7 (s), 25.9 (s), 9.2 (s), 7.8 (s), 5.8 (s), -1.8 (s), -3.2 (s), -4.6 (s), -5.8 (s), -7.5 (s), -7.9 (s), -10.2 (s), -10.7 (s), -10.7 (s), -11.8 (s), -12.7 (s), -13.3 (s), -16.1 (s), -16.4 (s), -18.5 (s) ppm. Only resolved peaks outside the 0 to 5 ppm region are reported. $^{19}F\{^1H\}$ (470 MHz, D_2O) δ_F -98.0 (s) ppm. ESMS found *m/z* 633.0 for $[M+H]^+$. HR-ESMS found *m/z* 633.1215, calculated *m/z* 633.1227 for $[C_{22}H_{29}N_4O_7{}^{151}Eu^{19}F]^+$. UV-Vis ($H_2O$): λ_{max} 266 nm. Luminescence lifetimes: H_2O: 0.60 ms, D_2O: 2.16 ms, *q* = 1.2. This species was dialysed to remove salts.

Tb.5.14. Yield: 74%. ^{1}H NMR (500 MHz, D_2O, pH = 4) δ_H 311.1 (s), 275.0 (s), 263.5 (s), 201.1 (s), 197.1 (s), 137.3 (s), 129.1 (s), -10.4 (s), -20.6 (s), -35.1 (s), -41.7 (s), -76.1 (s), -84.2 (s), -98.2 (s), -100.3 (s), -160.4 (s), -185.2 (s), -332.1 (s), -338.0 (s) ppm. Only resolved peaks outside the 10 to -10 ppm region are reported. $^{19}F\{^{1}H\}$ (470 MHz, D_2O) δ_F -102.7 (s) ppm. ESMS found *m/z* 639.0 for $[M+H]^+$. HR-ESMS found *m/z* 639.1257, calculated *m/z* 639.1268 for $[C_{22}H_{29}N_4O_7{}^{159}Tb^{19}F]^+$. UV-Vis ($H_2O$): λ_{max} 266 nm. Luminescence lifetimes: H_2O: 1.77 ms, D_2O: 2.91 ms, *q* = 1.1.

Gd.5.14. Yield: 84%. ESMS found *m/z* 638.2 for $[M+H]^+$. HR-ESMS found *m/z* 638.1252, calculated *m/z* 638.1256 for $[C_{22}H_{29}N_4O_7{}^{158}Gd^{19}F]^+$. UV-Vis ($H_2O$): λ_{max} 266 nm. $E_T \approx$ 22500 cm^{-1}.

7.12 X-ray Crystallography data

Single crystals of compound **2.6** suitable for X-ray diffraction studies were grown by slow evaporation of ethyl acetate:hexane 1:1. The crystals and refinement data are shown in Table 7. 3.

Table 7. 3 Crystal data and structure refinement parameters.

Compound	**2.6**
Empirical formula	$C_{16}H_{14}ClNO$
Formula weight	271.74
Temperature/K	150
Crystal system	Orthorhombic
Space group	P 21 21 21
Unit cell dimensions	
a/Å	6.9474(10)
b/Å	13.2522(2)
c/Å	14.1927(2)
α/°	90
β/°	90
γ/°	90
Volume/Å^3	1306.70 (3)
Z	4
Calculated density/Mg m^{-3}	1.381
Absorption coefficient/ mm^{-1}	0.282

F(000)	568
Crystal size/mm	0.18 x 0.28 x 0.28
ϑ range from data collection/°	5.0≤ϑ≤27.5
Index ranges, *hkl*	0≤*h*≤9, 0≤*k*≤17, 0≤*l*≤18
Reflections collected/unique	24029/1714
Absorption correction	0.92, 0.95
Data/restraints/parameters	1714/0/173
Goodness-of-fit on F^2	1.0005
Final R indices [I > 2σ(I)]	0.0362
R indices (all data)	0.0461
Largest diff. peak and hole/e $Å^{-3}$	-0.32, 0.28
CCDC number	1040048

7.14 References

1. A. S. Chauvin, F. Gumy, D. Imbert and J. C. G. Bunzli, *Spectrosc. Lett.*, 2004, **37**, 517-532.
2. A.-S. Chauvin, F. Gumy, D. Imbert and J.-C. G. Bunzli, *Spectrosc. Lett.*, 2007, **40**, 193-193.
3. A. Krezel and W. Bal, *J. Inorg. Biochem.*, 2004, **98**, 161-166.
4. J. Cosier and A. M. Glazer, *J. Appl. Crystallogr.*, 1986, **19**, 105-107.
5. Z. Otwinowski and W. Minor, *Macromol Crystallography Part A* 1997, 307-326.
6. A. Altomare, G. Cascarano, C. Giacovazzo and A. Guagliardi, *J. Appl. Crystallogr.*, 1994, **27**, 1045-1050.
7. D. Watkin, R. Cooper and C. K. Prout, *zkri*, 2002, **217**, 429.
8. R. I. Cooper, A. L. Thompson and D. J. Watkin, *J. Appl. Crystallogr.*, 2010, **43**, 1100-1107.
9. P. Kuzmic, *Analytical Biochemistry*, 1996, **237**, 260-273.
10. J. A. Tilney, T. J. Sorensen, B. P. Burton-Pye and S. Faulkner, *Dalton Trans.*, 2011, **40**, 12063-12066.
11. M. Tropiano, O. A. Blackburn, J. A. Tilney, L. R. Hill, M. P. Placidi, R. J. Aarons, D. Sykes, M. W. Jones, A. M. Kenwright, J. S. Snaith, T. J. Sorensen and S. Faulkner, *Chem. Eur. J.*, 2013, **19**, 16566-16571.
12. A. Dadabhoy, S. Faulkner and P. G. Sammes, *J. Chem. Soc., Perkin Trans. 2*, 2002, 348-357.
13. N. P. Buu-Hoï and R. Royer, *J. Org. Chem.*, 1950, **15**, 123-130.
14. T. Huynh, C. Valant, I. T. Crosby, P. M. Sexton, A. Christopoulos and B. Capuanot, *J. Med. Chem.*, 2013, **56**, 8196-8200.
15. J. C. Rodriguezubis, B. Alpha, D. Plancherel and J. M. Lehn, *Helv. Chim. Acta*, 1984, **67**, 2264-2269.
16. F. Bottino, M. Digrazia, P. Finocchiaro, F. R. Fronczek, A. Mamo and S. Pappalardo, *J. Org. Chem.*, 1988, **53**, 3521-3529.
17. S. Faulkner, A. Beeby, M. C. Carrie, A. Dadabhoy, A. M. Kenwright and P. G. Sammes, *Inorg. Chem. Commun.*, 2001, **4**, 187-190.
18. B. Alpha, V. Balzani, J. M. Lehn, S. Perathoner and N. Sabbatini, *Angew. Chem., Int. Ed. Engl.*, 1987, **26**, 1266-1267.
19. A. Beeby, L. M. Bushby, D. Maffeo and J. A. G. Williams, *J. Chem. Soc., Dalton Trans.*, 2002, 48-54.